# Study of STAT3 interactions with DNA as a target for anticancer drug discovery

Yiwen Yang

Supervisor: Dr. Andy Wilderspin

UCL

PhD Thesis

I, Yiwen Yang, confirm that the work presented in this thesis is my own. Where information has been derived from other sources, I confirm that this has been indicated in the thesis.

## Impact statement

This research proved that the STAT3 protein can bind to dsDNA without the present of the SH2 domain. This novel discovery suggests that inhibitors targeting STAT3 SH2 domain may not completely inhibit STAT3 transcription activity. Therefore, we suggest the DNA binding domain as a better target for anti-STAT3 drug development.

The developed *in vitro* assays can be used for screening small molecules that target STAT3. The *in vitro* assays are more efficient and economical compared to the *in vivo* assays of testing small molecule inhibitors. The method of using E.coli cells to express and ion exchange to purify STAT3 can be scaled up for massive production of purified STAT3 proteins. The purified proteins can be used in different types of *in vitro* assays.

The developed PEMSA assay can test protein precipitation and small molecule inhibition at the same time. The developed STAT3 $_{127\text{-}497}$ FP assay can be used as a high-throughput method to test inhibitors targeting STAT3 DNA binding domain more specifically. The developed FRET assay is also high-throughput and can be used to detect both STAT3 dimerisation and DNA binding activity.

## Abstract

STAT3 is a transcription factor involved in the regulation of many cellular functions including proliferation, differentiation, apoptosis, migration and immune response. It has great biological value in understanding the regulation system from genes to cellular activities. STAT3, is one transcriptional activator, but is involved in multiple cellular activities in different cells. It is regarded as an important anti-cancer drug target and a biomarker for tumour growth. Understanding the detailed biological activity of STAT3 can lead to the discovery of mechanisms of regulation of different cellular functions. In this thesis, we reveal more detailed biological activities of STAT3 with three different *in vitro* methods: protein electrophoresis mobility shift assay (PEMSA), fluorescent polarization (FP) and fluorescent resonance energy transfer (FRET). The development of *in vitro* methods not only provide more direct visualization of STAT3 biological functions such as DNA binding activity, dimerization, and aggregation, but also can be easily developed into inhibitor screening methods. We successfully created and purified different STAT3 mutations that provide different STAT3 functional domains to detect detailed STAT3 domain functions. Both PEMSA assay and FP assay suggest that STAT3 binds to dsDNA without a requirement for the SH2 domain, which emphasis the possibility of STAT3 binding to dsDNA as a monomer. The PEMSA assay provided an intuitive and orthogonal method to detect STAT3 DNA binding activity while the FP assay is very high-throughput. The developed FRET assay can not only be used to study the DNA binding activity of STAT3 but also be used to detect STAT3 dimerization.

**Acknowledgement**

First, I want to thank my principle supervisor Dr. Andy Wilderspin and my second supervisor Dr. Gary Parkinson. Thanks for their support with patience, motivation, and immense knowledge. I also want to thank Dr. Geoffrey Wells and Dr. Coline James for their support.

Next, I want to thank my parents. They supported me financially and mentally.

I also want to thank my colleges and friends who helped me and accompanied me through my PhD life. Their companion helped me through many difficult times.

# Contents

# Chapter 1, Introduction

## 1.1 STAT family and STAT3

Signal transducer and activator of transcriptions (STAT) are a group of proteins that regulate intracellular transcription and therefore control many cellular activities including cell proliferation, cell apoptosis, inflammation, differentiation, and cell migration. The STATs play an essential role during embryo development, immune response and tumour growth [1-3]. Therefore the STATs are regarded as valuable targets in cancer studies and diseases caused by inflammatory disorders such as inflammatory bowel disease [4]. The STAT family is composed of 7 members in mammalian cells: STAT1, STAT2, STAT3, STAT4, STAT5a, STAT5b and STAT6. They share similar activities while having different properties as well. For example, STAT1, STAT2 and STAT3 are involved in IFN induced transcription [5-7]. STAT3, STAT4, STAT5 and STAT6 play an important role in IL induced CD4+ T cell differentiation [8-10]. The STAT3 protein has the most complex set of functions among the STAT family and is therefore particularly interesting to study. The genomic location of the STATs is as variable as the functions of this protein family. The gene encoding for STAT1 and STAT4 locate in chromosome 1 while STAT2 and STAT6 locate in chromosome 10 and STAT3, STAT5a and STAT5b are mapped in chromosome 11 in human cells [11]. STAT5a and STAT5b are transcribed from different genes but share over 90% similarities in amino acid sequences [12]. The genomic study of the STAT members may also contribute to the understanding the STATs' functions and mechanisms. The complex functions of STATs can also be revealed by the differences of the protein structure of each STAT family.

The STATs share similar domain structures consisting of several functional domains: an N-terminal domain, a coiled-coil domain, a DNA binding domain, a Src homologous domain and a transactivation domain.

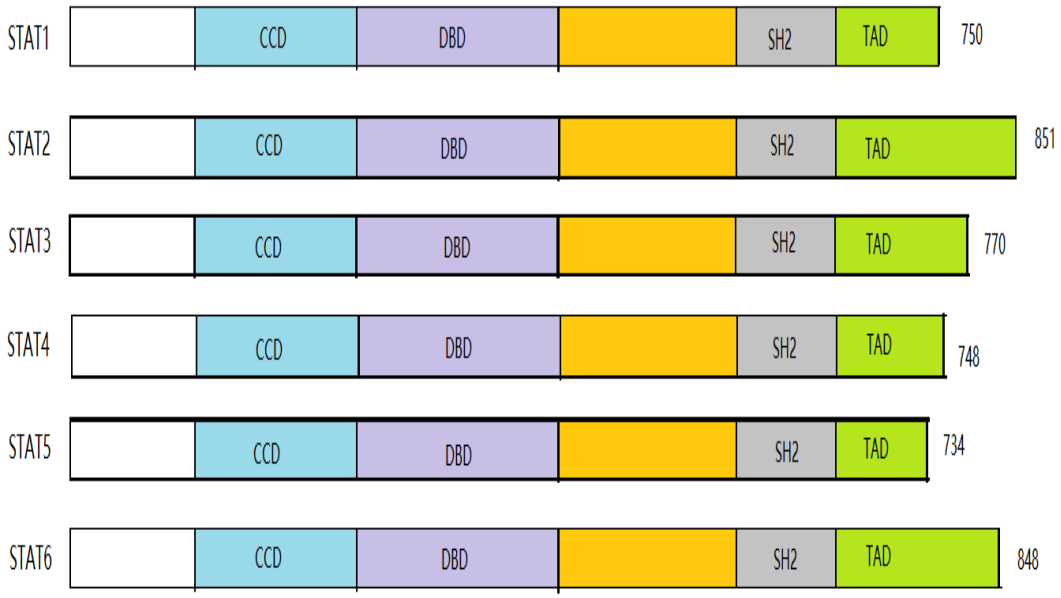


Figure 1.1. Domain structure of the STAT family members. All STAT family members consist of seven domains.

The N-terminal domain of the STATs contribute to the formation of the transcriptional complexes involving the STAT proteins. It is also responsible for the tetramerisation of the STAT3 and STAT5 proteins [13, 14]. The SH2 domain is responsible for the formation homo- and hetero- dimers of the STAT proteins. However, the mechanisms of the formation of the STAT dimers are still unknown. The formation of the different STAT homo- and hetero- dimers may be related to the complex functions of the STAT family.

The involvement of STATs in different stages of cell development and activities emphasized their biological importance. The study of the STAT family, especially STAT3, can lead to the development of potential cancer treatments and diagnosis since abnormal expression and activation of STATs is often involved in different diseases and cancers. For example, STAT1 null mice are more susceptible for bacterial and viral infections [15].

| Cancer type | Activated STATs | References |
|---|---|---|
| ***Breast*** | *STAT1, STAT3, STAT5* | [16] |
| ***Head and neck*** | *STAT1, STAT3, STAT6* | [17] |
| ***Lung*** | *STAT3, STAT5* | [18] |
| ***Prostate*** | *STAT3, STAT5* | [19] |
| ***Ovarian*** | *STAT3* | [20] |
| ***Pancreatic*** | *STAT3* | [21] |
| ***Lymphoma and Leukemia*** | *STAT1, STAT3, STAT5* | [20] |
| ***Carcinoma*** | *STAT3* | [22] |
| ***Melanoma*** | *STAT3* | [22] |
| ***Renal*** | *STAT3* | [23] |
| ***Glioma*** | *STAT3* | [24] |
| ***Colon*** | *STAT3* | [25] |

Table 1.1. Activated STATs in different types of cancer. Different STAT family member is shown to be over-activated in different types of cancer. STAT3 is over activated in all of the cancers with disordered STAT activity.

Table 1.1 summarises the overexpressed STAT family detected in different types of cancers. Among all STAT family members, STAT3 is the most widely involved protein in many cellular processes. Therefore the study of STAT3 may reveal the detailed control mechanisms of many signalling control pathways and contribute to the development of treatment methods of many studies. Later in the following chapters, I will describe the activation pathway of STAT3, the protein structure of STAT3 and its role in cancer and other diseases in detail. In this thesis, several *in vitro* assays were designed to study detailed STAT3 biological activities. The developed *in vitro* assays were used to investigate the mechanisms of STAT3 protein at the molecular level and to optimise the STAT3 inhibitor screening methods for use in anti-cancer drug design.

## 1.2 STAT3 regulation pathways

STAT3 activation refers to the initiation of STAT3's transcription activity. Activated STAT3 is able to promote the transcription of many genes related to cell proliferation, cell survival, differentiation, immune response and stem cell self-renew [26, 27]. Normally, STAT3 stays in a non-activated form in the cells. The activity of STAT3 is controlled by 'activators' and 'suppressors'. The activity of STAT3 can be regarded as self-regulated since it can both enhance the expression of itself and a STAT3 'suppressor'. Both receptor kinases and non-receptor kinases can act as a STAT3 'activator'. Common receptor kinases include epidermal growth factor receptor (EGFR), vesicular endothelial growth factor receptor (VEGFR), platelet-derived growth factor receptor (PDGFR) and colony stimulating factor-1 (CSF-1). Non-receptor kinases include Abl and Src kinases. These activators may activate STAT3 in different ways. The most typical STAT3 activator is JAK. JAK phosphorylates STAT3 on Tyr705 after being phosphorylated by the cytokine stimulated receptors. The phosphorylated STAT3 proteins form dimers and translocate into cell nucleus and initiate transcription. That is the most well-known STAT3 activation pathway, however another two STAT3 activation methods were also reported and there may be more. STAT3 can be activated by Serine727 phosphorylation triggered by CDK5, protein-kinase C (PKC) and mitogen-activated protein kinases (MAPK) [28]. And the regulation of acetylation of STAT3 Lysine685 by histone acetyltransferase was also described as a STAT3 activation method[29]. The discovery of different activation mechanisms revealed the complexity of STAT3 as a transcriptional activator. Other STAT3 activation pathway may yet be discovered. The suppressors can inhibit STAT3 activation by binding to the upstream tyrosine kinase, by binding to STAT3 itself and by promoting STAT3 degradation.

### 1.2.1 The JAK-STAT pathway

The most 'popular' and well-studied STAT3 activation mechanism is called the JAK-STAT pathway since the main upstream STAT3 activators are the Janus Kinases (JAK). JAK is a kinase family consists of 4 members: JAK1, JAK2, JAK3 and Tyrosine Kinase 2 (TYK2). The cellular expression of JAK1, JAK2 and TYK2 is ubiquitous while the expression of JAK3 is restricted in

hepatic cells since it is essential for hepatic cell development [30]. This family of non-receptor tyrosine kinases work as intracellular mediators that translate cytokine signals into transcriptional signals through the JAK-STAT pathway. This pathway is familiar with most cancer researchers since it is widely involved in tumour development. In gastric tumorigenesis, a disordered JAK-STAT pathway was reported to contribute to cancer progression [31-33]. Aberrant level of STAT3 was discovered in various gastric cancer cell lines and inhibition of the JAK-STAT pathway with a JAK or STAT inhibitor promotes cell apoptosis. JAK-STAT pathway is also reported to be essential for the immune response and metastasis in breast cancer [34]. Over-activation of the JAK-STAT pathway is also reported in neck squamous cell carcinoma as a result of the increased production of IL6 [35]. Regulation of the JAK-STAT pathway is essential for maintaining cellular homeostasis in normal cells. Abnormal JAK-STAT regulation usually results in various pathologies, cancers and immune diseases [36]. The consequent diseases related to STAT3 disorder is described in section 1.3 in more detail. There is no specific description about which JAK family is controlling which STAT family in literature due to the cross-talk between JAK and STAT family members. JAK1 and JAK2 are reported to mediate the type II interferon (IFN-γ) signalling while JAK1 and TYK2 contribute to type I interferon (IFN-α , IFN-β, IFN-γ) signalling.

The JAK-STAT pathway is initiated by the immune modulators including cytokines, growth factors and hormones binding to their target receptors which then phosphorylate the receptor-associated JAK [37, 38]. Type I and type II cytokine receptors lack catalytic kinase activity thus recruit JAK family to phosphorylate their downstream proteins. The JAK proteins associated with the cytokine receptors locate a proline-rich region in the intracellular domain of the receptor named the box1/box2 region. The morphology change of the cytokine receptor upon cytokine activation results in the phosphorylation of the associated JAK. The phosphorylated JAK then phosphorylates the tail of the cytokine receptor, which in turn phosphorylates the recruited STAT proteins. By interacting with the kinases, STATs usually get phosphorylated at a specific tyrosine residue near the C-terminus. For

example, STAT1 will get phosphorylated at Tyrosine 701 and STAT3 get phosphorylated at Tyrosine 705. Before phosphorylation, the un-phosphorylated STAT proteins are constantly presented in cytoplasm. The un-phosphorylated STAT3 proteins are constantly expressed and the cytoplasmic concentration is down-regulated by proteasome degradation. The phosphorylated STATs are released from the cytokine receptor tail and form hetro/homodimers. The STAT dimers are able to translocate into the cell nucleus. Different STAT dimers recognize different target sequences. In the nucleus, the STAT3 dimers are able to bind to its targeted sequence known as the GAS sequence and then promote transcription. The phosphorylated STAT3 proteins have been reported to up regulate genes including IL-6, IL-10, VEGF, EGF, SOCS, and p53

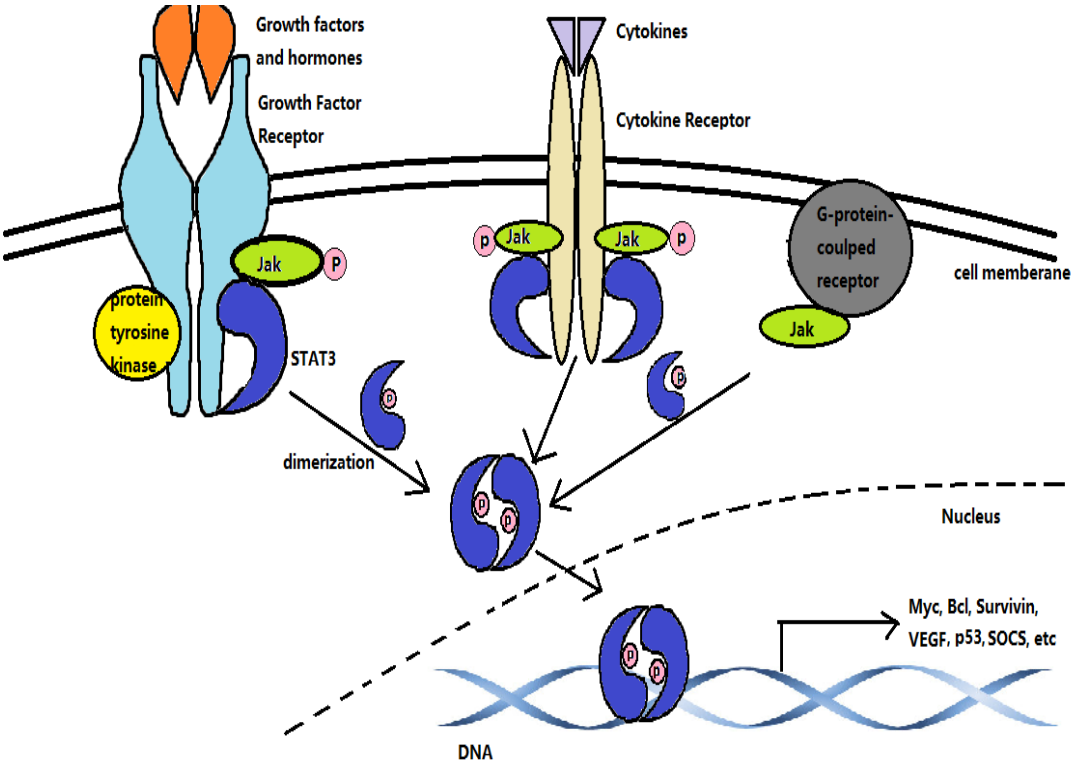


Figure 1.2. JAK-STAT activation pathway of STAT3. In this pathway, the growth factor receptor, the cytokine receptor and the G-protein coupled receptor receives extracellular signals (cytokines, growth factors and hormones) and phosphorylates the attached JAK. The phosphorylated JAK

transfer a phosphate group to the nearby STAT3 monomer. The phosphorylated STAT3 monomer dispatches from the receptor and form dimers. The STAT3 dimers transport into cell nucleus, bind to the dsDNA and initiate the transcription.

As the most typical STAT3 activation pathway, the inhibition of the JAK-STAT pathway is believed to supress the STAT3-regulated oncogene expression. The observation of un-regulated JAK-STAT pathway in solid tumours added further evidences that the JAK-STAT pathway can be an anticancer drug target. A JAK2 mutation (V617F somatic mutation) resulting in the constitutive activation of JAK-STAT pathway has been reported in various types of leukaemia and lung cancer.

Besides the phosphorylated STAT3, un-phosphorylated STAT3 is also reported to perform transcriptional activity. It is reported that un-phosphorylated STAT3 can form complex with nuclear factor κB (NFκB) therefore express NFκB targeted genes [39]. The mechanisms of un-phosphorylated STAT3 transcriptional activities may relate to other STAT3 modifications described below.

### 1.2.2 Other STAT3 post-translational modifications

STATs can also be phosphorylated at Ser727 by PKC, MAPK (e.g. ERK, JNK) and CDK5 independent of Tyr705 phosphorylation. Extracellular regulated protein kinase (ERK) was found to promote STAT3 Ser727 phosphorylation in response to epidermal growth factor (EGF) [40]. C-Jun N-terminal kinase (JNK) phosphorylates STAT3 Ser727 in response to the stress signal [41]. It not only regulates cell survival and nuclear translocation but also affect the de-phosphorylation level of Tyr705 phosphorylated STAT3. Ser727 phosphorylated STAT3 regulates 12-O-tetradecanoylphorbol-13-acetate-mediated cell survival and nuclear translocation [42]. The phosphorylation of STAT3 Ser727 results in the enhanced expression of endonuclease involved in DNA damage repair called EME1 [43]. Furthermore, Wakahara *et al.* suggested that the phosphorylation at Ser727 accelerates the de-phosphorylation process of the Tyr705 and

thus shortens the duration of STAT3 activity [44]. Ser727 phosphorylation-mediate Tyr705 de-phosphorylation through the activity of nuclear TC45 phosphatase activity [44]. Significantly high levels of Ser727 phosphorylated STAT3 were observed in cervical intraepithelial neoplasia suggesting that it can be used as a biomarker for cervical cancer diagnosis [45]. Constitutive phosphorylation of Ser727 regulated by the B-Raf-MEK-ERK1/2 pathway was observed in all melanoma cell lines [42]. The same phenomenon was also detected in chronic lymphocytic leukaemia [46].

A reversible acetylation of STAT3 Lysine685 contributes to STAT3 dimerization and transcriptional activity [29]. Lys685 was found to be essential for the formation of stable STAT3 dimers [47]. The STAT3 Lys685 acetylation is regulated by histone acetyltransferase p300 in response to IL6 simulation while the de-acetylation was regulated by type I histone deacetylase (HDAC) [29]. This modification was prerequisite for STAT3 dimers binding to the specific DNA target and conduct transcription activity in HepG2 and HEK297 cell lines [48]. P300 modulated constant STAT3 Lys685 acetylation contributes to STAT3 transcription in chronic lymphocytic leukaemia cells [49]. Lys685 acetylation supports the STAT3 transcriptional activity mostly independent of STAT3 phosphorylation [50]. The transcriptional activity of un-phosphorylated STAT3 is highly related to the Lys685 acetylation [51]. Lys685 acetylated STAT3 mediates the transcription of cylclinD1 with application of CCD4 and p300 independent of phosphorylation [52].

The STAT3 Lys685 acetylation regulates gene expression independent of STAT3 phosphorylation. The acetylation of STAT3 Lys685 is highly involved in gene expression resulted in the high concentration of the intracellular un-phosphorylated STAT3 [52]. Acetylated STAT3 is found to regulate the expression of indoleamine 2, 3-dioxidase in dendritic cells [53]. Besides, it is also involved in the methylation of tumour suppressor genes in company with DNA methyltransferase 1 (DNMT1), a key factor for CpG methylation [54]. Inhibition of STAT3 acetylation results in the enhanced activity of tumour suppressor genes including detected in lung and oesophageal 1 (DLEC1), cyclin-dependent kinase inhibitor 2A (CDKN2A) and STAT1 [55].

Other important STAT3 modulations were also discovered in literature but these STAT3 modifications was not reported to be sufficient for supporting STAT3 transcriptional activity. Lysine 49 and Lysine 87 was also acetylated in response to p300 activity. The Lys49 and Lys87 acetylation is reported to be essential for gene transcription induced by IL6 [56]. Furthermore, Lysine 97 acetylation has been reported to be influenced in bromodomain containing protein 4 (BRD4)-dependent anti-apoptotic and pro-proliferation gene expression [57]. Mono-ubiquitination of STAT3 was observed on Lys97 and results in the enhanced BRD4 involved positive transcriptional elongation factor (P-TEFb) complex formation thus regulate to anti-apoptosis and cell proliferation [57]. Furthermore, STAT3 acetylation was identified at multiple points involving Lys685, Lys796, Lys707 and Lys709 in a liver cell line. The acetylation was found to be related to STAT3 phosphorylation [58].

Reversible methylation on STAT3 Lysine140, Lysine49 and Lysine180 was also reported to regulate STAT3 activities. The methylation of Lys140 is mediated by histone methyl transferase SET9 (SET domain containing methyl transferase 9) and reversed by lysine specific demethylase 1 (LSD1) [59]. Lys140 methylation may relate to the selectivity of STAT3 binding to promoters since the inhibited Lys140 methylation results in the enhanced expression of certain STAT3 activated genes (i.e.SOCS3) [59]. SOCS3 is one of the STAT3 suppressors whose transcription is activated by STAT3 itself. The regulation of SOCS3 expression by Lys140 methylation may reveal the mechanism of STAT3 self-regulation. The methylation of Lys180 is resulted from the activity of the Enhancer of Zeste Homolog 2 (EZH2) [60]. Lys180 methylation leads to the enhanced activity of tyrosine phosphorylated STAT3 [60]. EZH2 is also reported to be involved in the Lysine49 methylation, which contributes to the expression of major STAT3 regulated genes [61].

The activity of the different STAT3 modifications are generally independent but related to each other. STAT3 Tyr705is the most commonly observed STAT3 post-translational modifications. Tyr705 phosphorylation is required for Lys49 methylation [61]. The activity of STAT3 Tyr705 was believed to dominate STAT3 dimerization and nuclear translocation. Both Ser727

phosphorylation and Lys47 de-methylation require STAT3 nuclear translocation and DNA binding [46, 62]. However, STAT3 Ser727 phosphorylation is independent of STAT3 Tyr705 phosphorylation. Ser727 phosphorylation is still observed in cells when Tyr705 phosphorylation is inhibited by Magnolol [63]. Therefore, there are other mechanisms leads to STAT3 nuclear translocation and DNA binding except for Tyr705 phosphorylation. Many STAT3 modifications have been reported to relate to un-phosphorylated STAT3 nuclear translocation and transcriptional activity including Lys685 acetylation. Ser727 phosphorylation reduces the duration of Tyr705 phosphorylation [64]. Phosphorylation on both sites of the STAT3 proteins can optimize DNA binding and transcriptional activity [65]. Phosphorylated STAT3 up-regulates the expression of un-phosphorylated STAT3 and therefore enhances Lys685 acetylated STAT3 transcriptional activity [58]. The STAT3 phosphorylation is reported to be influenced by SirT1 mediated STAT3 acetylation state [58].

### 1.2.3 Down-regulation of STAT3

The activity of STATs is down-regulated by three types of proteins: suppressor of cytokine signalling (SOCS), namely protein tyrosine phosphate (PTP) and protein inhibitor of activated STAT (PIAS) [66]. PTP inhibits the JAK-STAT pathway by dephosphorylating the JAK, STAT and related receptors. PIAS is able to bind to the downstream gene of the STAT target genes therefore restrict the movement of the transcriptional activator and stop transcription [67]. SOCS proteins is able to bind to the STAT and interfere with JAK-STAT interaction. SOCS is a self-negative regulator of STAT since its production is promoted by the STAT's transcriptional activity. Furthermore, STAT3 degradation mediated by ubiquitin also terminates STAT3 activation. A nuclear ubiquitin E3 ligase, PDLIM2, mediates STAT3 proteasomal degradation and poly-ubiquitination through its LIM domain [68]. STAT3 can also be modified by small ubiquitin-like modifier (SUMO) and thus lose the ability to be phosphorylated and form dimers [69]. Furthermore, a Golgi resident protein, TMF/ARA160 was also reported to drive the proteasomal degradation of STAT3 [70]. STAT3 is also down-regulated by

miRNAs. In bone marrow derived mesenchymal stem cells, miR-127 directly interacts and inhibits the translation of STAT3 mRAN [71]. Other miRNA discovered to inhibit STAT3 include miR-1181 in pancreatic cancer [72] and miR-7 in breast cancer [73].

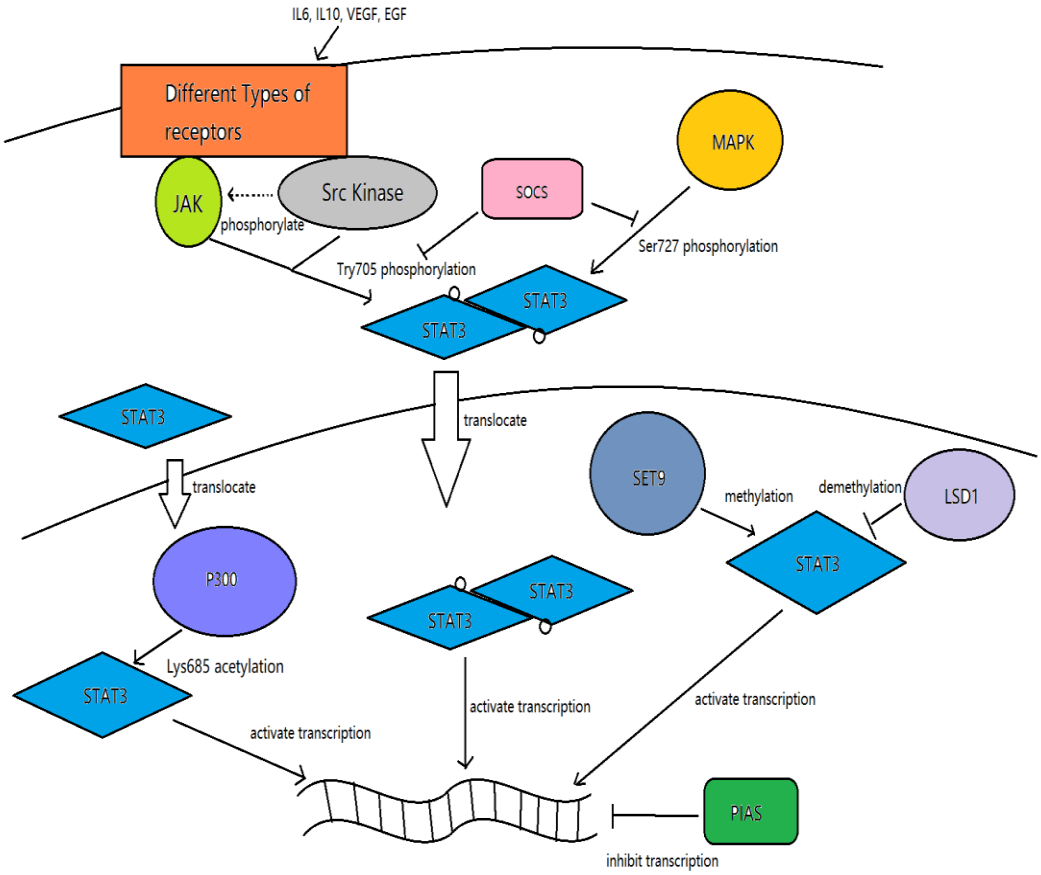


Figure 1.3. A summary of currently discovered STAT3 regulation pathways. STAT3 Try705 can be phosphorylated by JAK and Src kinase. STAT3 Ser727 can be phosphorylated by MAPK. The phosphorylated STAT3 can form dimers and translocate into nuclear and conduct transcription. Unphosphorylate STAT3 can be acetylated in cell nuclear by P300 or methylated by SET9. All these modifications can activate STAT3 transcription activity.

The importance of the JAK-STAT pathway is signified by the application of the JAK inhibitors in the medical treatment of cancer and inflammatory diseases. Jak inhibitors, Jakinibs, are the main class of drugs targeting the JAK-STAT pathway on market. Jakinibs have been widely used to regulate

cytokine induced inflammatory pathologies including psoriasis, arthritis, immune and homological disorders (and inflammatory bowel diseases [74]. For example, Tofacinibs, the first JAK inhibitor tested in human, has been used to treat rheumatoid arthritis and psoriatic arthritis. Furthermore, Jakinibs can supress the cytokine induced immune response through inhibition of the JAK-STAT pathway. The JAK-STAT pathway is essential for proliferation, anti-apoptosis and immune escape in tumour cells. Therefore inhibition of the JAK-STAT pathway is a potential method for tumour inhibition. Ruxolitinib, selectively targeting JAK1 and JAK2, may have the potential to regulate myelofibrosis and therefore affect cancer development [75]. However there is no direct application of Jakinibs in cancer treatment yet. The JAK/STAT pathway is still regarded as a therapeutic target of cancer treatment although the Jakinibs cannot be used as a treatment method for cancer without combination with other medicines. The reason why Jakinibs are not widely used in cancer treatment may relate to the complex activation mechanisms of STAT3. STAT3 phosphorylation resulted from JAK activity may not be the single way to activate STAT3 transcription. Cancer cells may develop another pathway to activate STAT3 controlled genes when the JAK-STAT pathway is blocked. Various STAT3 activation mechanisms including Tyr705 phosphorylation, Ser727 phosphorylation and Lysine 685 acetylation have been observed in cancer cells. Un-phosphorylated STAT3 has been proved to bind to the GAS sequence and certain DNA structures including Holiday Junctions and act as a chromatin organizer [76]. The activity of un-phosphorylated STAT3 may be regulated by other post translational modifications. Different post translational modification of STAT3 results in different level of STAT3 regulated gene expression. STAT3, as a transcriptional regulator, is not a simple on/off switch. The complexity of STAT3 regulation underlines its unique function in gene transcription. Improved understanding of STAT3 activation and transcriptional mechanism is required for the future therapeutic method development. Therefore, we suggest STAT3 as a better target compared to its upstream regulators. STAT3 nuclear translocation can be independent of STAT3 Tyr705 phosphorylation. Un-phosphorylated STAT3 can translocate into cell nucleus with the help of CCD4, a type I transmembrane glycoprotein. CCD4 forms a

complex together with STAT3 and p300 resulting in the acetylation of STAT3 lysine 685 and promote the formation of STAT3 dimers independent of cytokine and growth factor stimulation. The complex promotes transcription of cyclinD1 thus promotes cell proliferation [52].

## 1.3 The role of STAT3 in cancer

STAT3 is involved in the transcription of many genes related to cell proliferation, differentiation, and anti-apoptosis. Therefore it plays an important role in both normal cells and tumour cells. Genes regulated by STAT3 including interlukin-6 (IL-6), IL-10, EGF, VEGF, Her/Neu, p30 contributes to the regulation of cell cycle, apoptosis, and immune response. The activity of STAT3 is tightly regulated in normal cells while highly over-activated in tumour cells. The un-regulated STAT3 activity is detected in most human cancers and during different cancer stages from malignant potential to metastasis. In cancer cells, STAT3 contributes to tumour cell self-renewal, evasion, migration and immune escape. STAT3 activities in cancer cell lines are controlled by several STAT3 post translational modifications including Tyr705 phosphorylation, Ser727 phosphorylation, and Lys695 acetylation. The detailed activation mechanism is discussed in Chapter 1.2. This chapter reviews the discoveries of un-regulated STAT3 activity in cancer and relates the abnormal STAT3 activity and its downstream expressed genes to different types of cancer. Although STAT3 is proved to be over-activated in most cancer cell lines, how STAT3 activity influences cancer development seems to be different from each cancer type. STAT3 enhances tumour growth in breast, prostate and skin cancer [77] while it is also reported to act as a tumour suppressor in mouse astrocytes [78]. The differences of STAT3 function in different cancer cell lines may relate to the different STAT3 modifications, different level of STAT3 expression, different upstream signalling or the activity of different STAT3 isoforms. The aim of this chapter is to clarify the relationship between the abnormal STAT3 activity and tumour progression, tumour cell survival and immune escape, and therefore point out the therapeutic value of STAT3

research. Furthermore, we also describe the differences on gene regulation between different STAT3 isoforms.

### 1.3.1 STAT3 contributes to tumour cell proliferation

STAT3 modulates cell proliferation by transcribing genes that regulate cell cycle. One of the cell cycle regulatory gene is cyclin D1. Cyclin D proteins mediate G1 to S phase transition by activating cyclin-dependent kinases 4/6 (CDK4/6). The activated CDK4/6 phosphorylates retinoblastoma (Rb) therefore allows the cell cycle to enter S phase. STAT3 is proved to bind to the promoter and to enhance the expression of cyclin D1 [79]. STAT3 is also reported to mediate IL-17 induced cell proliferation in B16 melanoma and MB49 bladder carcinoma [80]. Furthermore, inhibition of STAT3 reduces glioblastoma stem cell proliferation [81]. IL-6 induced constant STAT3 activation in colorectal carcinoma and is positively related to cancer cell multiplication while the inhibition of STAT3 leads to a reduced cell growth [82]. Haviland *et.al.* suggested that STAT3 can bind to Necdin promoter but the binding inhibits Necdin expression [83]. Necdin is coded by human NGN gene and function as a growth suppressor that arrests cell cycle. The STAT3 activity downregulates the expression of Necdin therefore induces cell proliferation [83].

### 1.3.2 STAT3 supports the anti-apoptosis activity of cancer cells

STAT3 supports tumour cell survival by interfering with the apoptosis pathways. Cell apoptosis is usually regulated by two types of pathways: 1) intrinsic pathway regulated by the balance of the anti-apoptotic proteins and pro-apoptotic proteins in mitochondria and 2) extrinsic pathway directed by ligand recognition of the death receptors. The pro-apoptotic proteins involved in the intrinsic apoptosis pathway include: Bax, Bad, Bak, Bim, PUMA and NOXA. The anti-apoptotic proteins involved in the intrinsic apoptosis pathway include: Bcl-2, Bcl-xL, Bcl-w and Mcl-1 in which, Bcl-2, Bcl-xL and Mcl-1 have been detected to be directly regulated by STAT3.

The intrinsic apoptosis initiates from the accumulation of the pro-apoptotic protein-induced mitochondria outer membrane permeabilization and release of cytochrome C. The released cytochrome C forms an apoptosome and

triggers caspase regulated apoptosis. The transcription of anti-apoptotic proteins resulted from the activation of STAT3 interact with the Bax proteins therefore reduces their pore-forming activity. STAT3 directly binds to the Bcl-2 and Mcl-1 promoter and activates the transcription of the Bcl-2 [84] and Mcl-1 genes [85]. Inhibition of STAT3 activity results in reduced Mcl-1 expression in peripheral leukocytes [86]. The expression of another Bcl protein, Bcl-xl, is also reported to be enhanced by STAT3 transcriptional activity in melanoma [87]. STAT3 induced Bcl-xl expression contributes to the anti-apoptosis activity in colorectal cancer with oncogenic GTPase Kras mutation [88]. Furthermore, STAT3 also directly promotes the expression of survivine, which inhibits the activity of the caspase therefore reducing cell apoptosis [89].

Besides the intrinsic apoptosis pathways, STAT3 is also shown to be involved in the extrinsic apoptosis pathways. Increased Fas expression was observed in a dominant negative STAT3 mutation melanoma cell line resulting in enhanced Fas-ligand induced apoptosis [90]. STAT3 cooperates with c-Jun to bind to the Fas gene and suppress the Fas transcription [90]. The increased STAT3 activity in tumour cells supresses the expression of Fas and therefore resists apoptosis.

### 1.3.3 STAT3 regulates immune evasion

STAT3 has been widely described to be involved in the immune evasion and anti-inflammation in tumour cells. STAT3 regulate immune response in cancer cells by both a direct influence on the expression immune regulatory cytokines and an in-direct effect on immunity by regulating genes that modulate antigen presentation. The STAT3 activity in cancer cells suppress immune mediators while producing immune suppressive genes. For example, constant phosphorylation of STAT3 is reported to contribute to the immune suppressive microenvironment in glioblastoma multiforme [91]. Enhanced anti-inflammatory cytokine expression was observed with STAT3 phosphorylation, while inhibition of STAT3 up-regulated dendritic cell activity [91].

STAT3 activity enhances the expression of immune suppressive factors while down regulating pro-inflammatory factors. The major immunosuppressive cytokine regulated by STAT3 transcriptional activity is Interleukin-10 (IL10). IL10 inhibits the immune response by inhibiting pro-inflammatory cytokines including IL1 and TNF-α and reducing antigen presentation on the cell surface. Overexpressed IL10 can result in serious immune suppressive diseases such as Epstein-Barr virus associated lymphomas and chronic inflammatory bowel diseases [92]. STAT3 binds directly to the IL10 promoter and initiates the transcription of IL10 in B cells [93].

Other immune suppressive cytokine directly regulated by STAT3 include IL-23, transforming growth factor β1 (TGF-β1) and VEGF. IL-23 reduces $CD8^+$ T cell activity and contributes to tumour angiogenesis [94]. The expression of IL-23 is enhanced with constitutive STAT3 activity in tumour cells while the knock-down of STAT3 results in decreased IL23 level [95]. IL-23 is regarded as a key factor for Th17 cell proliferation [96]. Th17 cells are T cells that secrete IL17 that supress inflammation. TGF-β1 is a polypeptide that suppresses the activity of autoreactive T cells and regulatory T cells. STAT3 can also initiate the transcription of VEGF. VEGF is a growth factor that induces angiogenesis. It also plays an important role in regulating immunity. VEGF is involved in early stage T cell development and maturation of dendritic cells. [97, 98].

Interestingly, both the immune inducer such as IL-6 and the immune suppressor IL-10 can stimulate the activation of STAT3 and are directly activated by STAT3. These cytokines have opposite functions in response to the STAT3 activity and are reported to be involved in different stages of dendritic cell development as a consequence of the SOCS3 activity [99]. In early stages, STAT3 is stimulated by IL-6 and contributes to the immune microenvironment in tumour cells while with activation of STAT3, increased SOCS3 resulting the suppression of pro-inflammatory effects of IL-6 but not IL-10. Although STAT3 activates IL-6 expression directly, decreased levels of IL-6 with the increased STAT3 concentration was observed in murine microphages [100]. Therefore, STAT3 contributes to both early stage

immune microenvironment development and the following immune evasion in tumour cells.

Besides anti- and pro- inflammatory cytokines, STAT3 also affects immunity through other factors including cyclooxygenase-2 (COX-2). COX-2 is an enzyme that converts arachidonic acid into prostaglandins. It is involved in many inflammatory diseases and carcinogenesis [101]. The expression of COX-2 in regulatory T cells (Treg) is correlated with forkhead box P3 (FOXP3), which is essential for Treg development. Inhibition of the COX-2 reduced the activity of effector T cells suppressed by Treg cells [102]. COX-2 inhibitors has been widely used as non-steroid anti-inflammatory drugs in the clinic indicating that COX-2 also enhances the inflammatory effect. Inhibition of COX-2 with COX-2 inhibitors can enhance the activity of natural killer cells [103]. In tumour cells, over expressed COX-2 contributes to the immune evasion in gastric carcinogenesis [101]. STAT3 binding site has been identified to the COX-2 promoter [104]. Therefore, STAT3 may contribute to immunosuppression in gastric carcinogenesis through regulation of COX-2 expression.

STAT3 contributes to tumour progression by suppressing anti-tumour immune activity conducted by immune cells including dendritic cells, T cells, natural killer cells, and neutrophils. The immune cell regulation of STAT3 indirectly contributes to the immune suppression during tumour growth. STAT3 is involved in immune regulation in a number of ways.

Firstly, STAT3 is involved in regulation of T cell activity. T cells play an essential role in the development of anti-tumour response. It has been an important target of cancer treatment immune therapies. T cells affected by STAT3 activity include helper T cells (Th), regulatory T cells (Treg), and $CD8^+$ T cells. STAT3 expression supresses Th1 activity while inhibition of STAT3 results in enhanced Th1 induced immune response in chronic enterocolitis [105]. Th17 cells can also be influenced by STAT3 activity as described before. Th17 immune activity is mediated by TGF-β, IL-17, IL-23 and IL-21, in which TGF-β and IL-23 can be activated by STAT3 activity. STAT3 regulates Treg cells via transcription of IL-10 and TGF-β. STAT3

regulated Treg inhibits the activity of $CD8^+$ T cells with application of TGF-β and IL-10 while expression of IFNγ in CD8+ T cells also supress Treg cell activity [106].

Secondly, STAT3 regulates the maturation of dendritic cells (DC). Dendritic cells mediate the antigen presentation in the immune process. STAT3 activity leads to the expression of IL-6, IL-10 and VEGF. Those factors were reported to suppress DC maturation in human cells [107]. IL-6 expression regulated by phosphorylated STAT3 inhibits bone-marrow derived DC maturation [108]. IL-10 regulates Bruton's tyrosine kinase in DC therefore influences the activity of DC [109].

STAT3 also regulates the activity of all types of macrophages. The two types of macrophages are divided according to their different functions: M1 cells regulate Th1 activity and M2 cells express cytokines and growth factors including IL-10, TGF-β, VEGF and EGF. The activity of M1 cells is mediated by IL-12 expression, which is influenced by STAT3 expressed IL-23 [110]. The gene expression of M2 cells is directly mediated by STAT3 transcription.

### 1.3.4 STAT3 contributes to cancer invasion and metastasis

Metastasis is the process of cancer cells spreading from where they developed from into other parts of the body. Replicated cancer cells invade into the nearby tissues and spread around via the bloodstream during metastasis. The spread tumour cells can develop adhesion later and attach to other tissues and then grow into another tumour. It is one of the essential causes of cancer's morbidity and mortality. Compelling research indicates that STAT3 plays an essential role in the process of metastasis. STAT3 contributes to cancer metastasis through regulating cell morphology change, malignant transformation, migration, evasion, proliferation and anti-apoptosis, angiogenesis and immune suppression. The way STAT3 contributes to cell proliferation, anti-apoptosis and immune suppression have been described before.

Epithelial-mesenchymal transition (EMT) initiates the process of metastasis. EMT is the process of an epithelial cell transform into a mesenchymal cell therefore increase cell migration, invasion and anti-apoptosis ability. STAT3

regulates the process of EMT through transcription of genes including Twist, and ZEB1 [111]. STAT3 was first found to be involved in Twist modulated EMT in hepatocellular carcinoma (HCC) [112]. Knockdown of STAT3 in oesophageal squamous cell carcinoma result in decreased hypoxia induced EMT and reduced Hypoxia-induced factor 1α (HIF-1α) expression, which is a transcription factor controlling cell response of hypoxia [113]. The same study also proved that STAT3 directly interacts with HIF-1α promoter and activate HIF-1α transcription [113]. Furthermore, STAT3 up-regulates the activity of Snail, an EMT inducer that supresses the expression of E-cadherin [114].

STAT3 mediates malignant transformation in skin cancer. STAT3 is reported to mediate the transformation in multiple stages of mouse skin cell carcinogenesis [115]. Turkson et.al. suggested that STAT3 mediates the Src-induced malignant transformation in NIH3T3 cells, a type of mouse embryo cell used to cultivate skin cells that secrete keratins [116].

The overexpression of phosphorylated STAT3 is positively related to matrix metalloproteinase (MMPs) induced cell invasion in cutaneous squamous cell carcinoma [117]. MMP is an extracellular endopeptidase which is usually secreted in malignancies and damaged tissues and regulate the extracellular matrix. The activity of MMP is usually related to cell invasion and metastasis. Knockout of STAT3 results in reduced MMP-7 expression which thus inhibited pancreatic cancer invasion in nude mice [118]. Direct interaction between STAT3 and MMP promoters has been detected and STAT3 has been proved to transcribe the genes of MMP1 [119], MMP2 [120] and MMP9 [121]. STAT3 also induces the expression of neutrophil gelatinase associated lipocalin (NGAL), which mediates the activity of MMP9 and promotes cell invasion and metastasis [122].

STAT3 activity is involved in tumour cell migration. Inhibition of STAT3 was reported to reduce cell migration in SKOV3 cells [123]. STAT3 has been proven to interact with stathmin and therefore mediate microtube depolymerization [124]. Microtube polymerization facilitates regulated cell migration. Furthermore, STAT3 is also involved in Rac1 mediated cell

migration [125]. Moreover, the expression of COX-2 enhanced by STAT3 activity reduces E-cadherin induced cell adhesion and therefore contributes to tumour invasion and metastasis [101]. Decreased cell adhesion results in enhanced un-directed cell mortality which favours cancer metastasis.

### 1.3.5 STAT3 contributes to tumour angiogenesis

Angiogenesis is the process of blood vessel generation in tumours. It is essential for supporting tumour growth. The most important signalling factor involved in angiogenesis is VEGF, which is directly regulated by STAT3 activity [126]. Constant activation of STAT3 in melanoma cells results in VEGF overexpression which therefore initiates angiogenesis [127]. Similar effects of STAT3 were observed in human pancreatic cancers too [128]. Besides VEGF, STAT3 also regulates other angiogenesis factors such as hypoxia-inducible factor 1α (HIF1α) [129]. STAT3 induces HIF1α expression in Human HepG2 hepatoma cells [130].

### 1.3.6 Other important oncogenes regulated by STAT3

STAT3 activity is also related to the expression of heat shock proteins (Hsps). Heat shock proteins maintain the structure of cellular proteins. It is usually overexpressed in tumour cells and prevents the degradation of the oncogenic proteins. In vascular smooth muscle cells, the thrombin induced expression of Hsp70 and Hsp90β is suppressed with STAT3 inhibition [131]. STAT3 has been proved to bind directly to the promoter of both Hsp70 and Hsp90β with EMSA assays [131]. STAT3 may also bind to the Hsp90α promoter since it has the GAS sequence. Heat shock can increase STAT3 binding to the GAS sequence on the promoter and induce Hsp90α transcription [132]. Therefore, STAT3 can mediate the preservation of the structure and function of other oncogenic proteins in cancer cells through regulation of Hsps expression.

### 1.3.6 STAT3 as a tumour suppressor

Although abundant evidence exists to suggest that STAT3 is the ‘accomplice’ of tumour development, some researchers also pointed out that STAT3 can act as a tumour suppressor. STAT3 can activate transcriptional factors that suppress tumour development and regulate several tumour suppressive genes.

STAT3 regulates the expression of growth factors that function as tumour suppressors, include FOXO1, FOXO3A, and FOXP3. FOX refers to forkhead box, FOXP3 is also named scurfin. FOX transcription factors contain the forkhead box domain that binds to DNA. FOXO transcription factors bind to DNA and suppress the targeted gene transcription and thus interfere with tumour cell proliferation. STAT3 can upregulate the expression of FOXO1 and FOXO3A in CD4+ T cells [133]. STAT3 binding sites have been discovered in both FOXO1 and FOXO3A promoters. No direct interaction between STAT3 and FOXOP3 promoter has been reported but Zorn *et.al*. proved that the expression of FOXOP3 is upregulated by STAT3 activity in cells.

Although STAT3 was described to contribute to cell proliferation and anti-apoptosis previously, it is also shown to have pro-apoptosis function in certain types of tissues. STAT3 is involved in expression of regulation subunits of the PI3K complex: p50α and p55α, which suppresses cell proliferation and promote autophagy [134]. The activity of p50α and p55α interferes with PI3K/Akt mediated cell survival pathway. The PI3K complex forms in response to receptor tyrosine kinase activity and regulates the activity of other kinases to assist entry into cell cycle and cell survival. STAT3 activity leads to increased expression of p50α and p55α therefore limited PI3K activity and results in increased cell apoptosis has only been reported in mammary glands [135, 136]. This suggests that STAT3 activity may be different in different tissues.

STAT3 can not only activate genes promote cell proliferation, suppress immune response, contribute to tumour malignance transformation and metastasis, initiate angiogenesis, but also support tumour suppressor gene expression. Different functions of STAT3 was detected in different types of tissues. The differences in the STAT3 function may result from different cytokine signalling or the expression of different STAT3 isoforms. STAT3β has been shown as a dominant negative effector of STAT3 transcription. The differences of STAT3 isoforms is described in chapter 1.4.

### 1.3.7 STAT3 in solid tumours

STAT3 transcribes many important genes regulating cell proliferation, differentiation, immune response, and cell migration. The STAT3 activity is usually under strict control by different regulators and by self-regulation. STAT3 activity can be induced by various cytokines and the activity of STAT3 also enhance cytokine expression (e.g. IL6, IL10, VEGF, and EGF). STAT3 suppresser SOCS3 transcription is also enhanced by STAT3 and therefore creates a negative feedback loop to prevent STAT3 over activation. However, STAT3 transcription and activity still lose control in various cancers including breast cancer, pancreatic cancer, lung cancer and blood cancer. The abnormal STAT3 activity can be induced by abnormal cytokine activity, mutation of upstream regulators and dominant negative mutation of STAT3 suppressors. STAT3 activity has been proved to be relate to the development of 70% of solid tumours [137]. The activity of STAT3 is also involved in different development processes of cancers. There is no single way of how STAT3 contributes to the cancer development. In addition, STAT3 activity is reported to behave differently in different cancers. Although most research papers reviewed here support STAT3's contribution to tumour development, several papers also pointed out the potential tumour suppressor function of STAT3. The reason why STAT3 behaves differently in different cancer may relate to the different activation pathway of STAT3 and different STAT3 isoforms expressed in the tumour cells. Understanding STAT3 activity in cancer can help develop better treatment methods targeting STAT3 and reveal detailed mechanisms of cancer development. The activity of STAT3 is often related to many important regulators in different cancers and other diseases therefore the development of STAT3 inhibitor may also be used as a supportive treatment method. The genes regulated by STAT3 is summarised in the following table (Table 1.2), which also classifies how STAT3 contribute to tumour development.

| Functions | Gene name | up/down regulation | Reference |
|---|---|---|---|
| Cell proliferation | p53 | ↓ | [138] |
| | Cyclin-D1 | ↑ | [139] |
| Apoptosis | BCL-XL | ↑ | [140] |
| | cMYC | ↑ | [141] |
| | survivine | ↑ | [142] |
| Angiogenesis | VEGF | ↑ | [143] |
| | HGF | ↑ | [144] |
| | IFNβ | ↓ | [145] |
| | IFNγ | ↓ | [146] |
| Metastasis | MMP2 | ↑ | [147] |
| | MMP9 | ↑ | [148] |
| Immune evasion | IL-6 | ↑ | [149, 150] |
| | IL-10 | ↑ | [151] |
| | TGF-β | ↑ | [152] |
| | VEGF | ↑ | [153] |
| | IFNβ | ↓ | [154] |
| | IFNγ | ↓ | [146] |

Table 1.2. A summary of STAT3 regulated genes. This table shows how the genes are controlled by STAT3 and gene related functions.

### 1.3.8 STAT3 and other diseases

Biological, and chemical evaluation of STAT3, and drug design targeting STAT3, should not only benefit cancer treatment but also bring novel treatment methods to other diseases. Apart from its important role in tumour development, STAT3 is also involved in many other diseases. Since one of the functions of STAT3 is to regulate the immune response and apoptosis, the abnormal STAT3 activities can result in diseases related to abnormal immune functions.

Diseases caused by genetically inherited abnormal STAT3 activities that lead to increased transcriptional activities are classified as STAT3 gain of function diseases (STAT3 Gof). The symptoms of the STAT3 Gof are usually related to autoimmune diseases. For example, STAT3 Gof can lead to the development of autoimmune lymphoproliferative syndrome (ALPS), rheumatic disease [155] and myelodysplastic syndrome [156, 157]. This paragraph is using ALPS as an example to describe how increased STAT3 activity relate to autoimmune disease. ALPS, also called the Canale-Smith

syndrome, is resulted from dysregulation of cell apoptosis [158]. Over 70% of the ALPS patients were identified to have gene mutations related to Fas receptor (FAS), caspase-10 (CASP10) and Fas ligand (FASLG). While STAT3 activity can enhance Fas-mediated cell apoptosis with normal Fas receptor expression [159]. Therefore the mutation of STAT3 affect the pathology of ALPS independent of Fas related mutations. Furthermore, STAT3 Gof is reported to cause multi-organ autoimmune disorders [160], hypogammaglobulinemia [161] and other ALPS related symptoms. Therefore, STAT3 activity plays an important role in ALPS and it can be a potential target for drug design and in more detailed pathology studies.

On the other hand, diseases caused by gene mutation resulting in decreased STAT3 activity are regarded as STAT3 dominant negative disease (STAT3 DN). Loss or reduced STAT3 activity results in hyper-IgE syndrome (HIES). HIES was first identified as the Job's syndrome in 1966 with symptoms of skin and lung infection [162]. Later, this disease was found to be related to an elevated serum IgE level [163]. In HIES patients, STAT3 mutations were identified specifically in SH2 domain and DNA-binding domain, which did not affect STAT3's phosphorylation and nuclear translocation [164]. The specific mechanisms that relate the STAT3 mutation and HIES is not fully understood, but is related to IL-6 mediated responses [165]. Therefore, understanding the detailed mechanisms of STAT3 and its role in immunity is important for the pathological study of HIES.

## 1.4 Different isoforms of STAT3

Previously in section 1.3, we described the different influence of STAT3 activity in different types of cancer. One of the reasons leading to the functionality variance of STAT3 may be the different STAT3 isoforms. Several STAT3 isoforms have been reported in literature including: STAT3α, STAT3β, STAT3$\gamma$ and STAT3$\delta$, of which, STAT3α and STAT3β are the most well studied two isoforms. Both of these two STAT3 isoforms have complete transcriptional function and may regulate different genes. However, most

STAT3 studies do not specify the STAT3 isoforms detected in their assays. Therefore the relationship between the STAT3 isoforms and STAT3 function in cancer is still not clear. The next sections describe the structural and functional differences of the STAT3 isoforms and conclude current discoveries in the functions of different STAT3 isoforms.

### 1.4.1 The relationship between STAT3$\alpha$ and STAT3$\beta$

STAT3$\alpha$ is a 92kDa STAT3 protein compromised of 770 amino acids. The STAT3 tumour progression function is mostly related to the function of the STAT3$\alpha$ isoform. Most STAT3 research that does not define the specific STAT3 isoform generally refers to STAT3α since this is the most abundant STAT3 isoform in cells. The over-expression of STAT3$\alpha$ is always related to tumour cell growth, apoptosis resistance or the oncogenic behaviour of cells. For example, over-expressed STAT3$\alpha$ results in increased cell proliferation and promoted epithelial mesenchymal transition and invasion of endometrial carcinoma cells [166].

While STAT3β is an 83kDa STAT3 isoform with 722 amino acids and was regarded as a negative regulator of STAT3α when STAT3β was first discovered by Caldenhoven *et.al*. [167]. Thanks to Bharadwaj *et.al.*, antibodies targeting the STAT3β unique sequences provided more convenient identification of STAT3β isoform by immunoblotting [168]. The two isoforms of STAT3, STAT3$\alpha$ and STAT3$\beta$ are created from alternative splicing: [169]. STAT3$\alpha$ is usually regarded as the complete STAT3 while STAT3$\beta$ was thought to be a negative regulator of STAT3$\alpha$ but later proved to have its own specific transcriptional function. The reason why STAT3$\beta$ was regarded as a negative mutant of STAT3$\alpha$ is that in its amino acid sequence, STAT3$\beta$ has an incomplete transcriptional activation domain. In the amino acid sequence of STAT3$\beta$, the transcriptional activation domain (the last 55aa) is replaced with 7 amino acids compared to STAT3$\alpha$. The creation of STAT3$\beta$ is due to a frameshift caused by the stimulation of the acceptor site in exon 23. The frameshift results in the deletion of the C-terminal end sequences and introduced a new sequence (FIDAVWK) with stop codons to the C-terminal end.

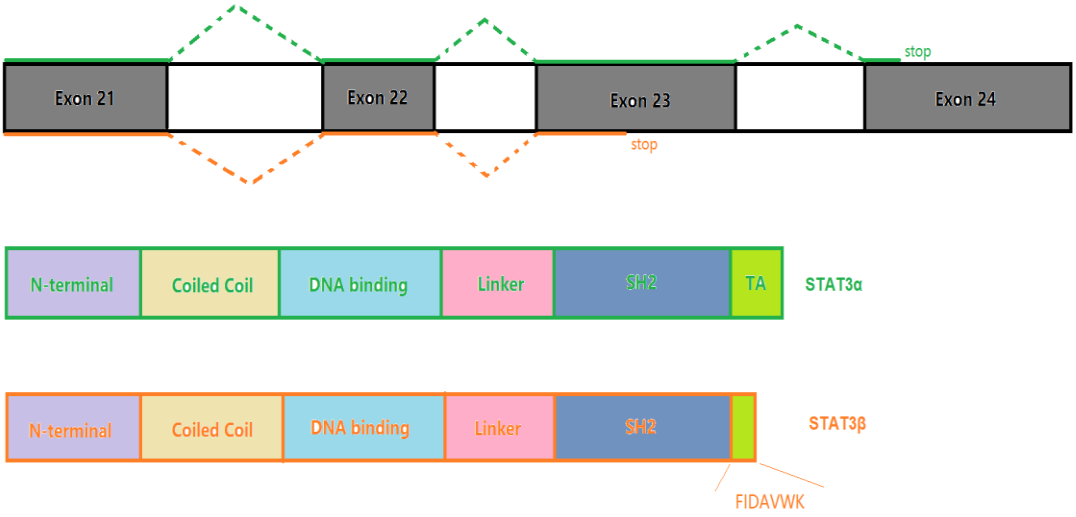


Figure 1.4. STAT3$\alpha$ and STAT3$\beta$ created from alternative splicing. In the STAT3β isoform, the transactivation domain in the STAT3α isoform is replaced by amino acids FIDAVWK.

STAT3$\alpha$ and STAT3$\beta$ co-exists in all types of normal cells. The concentration of STAT3α can be 4 to 10 times higher than the STAT3β concentration in different cell types [170]. The expression of STAT3$\alpha$ is higher in most cells [171]however the level of STAT3$\beta$ expression can be higher than the $\alpha$ isoform under certain conditions. For example, the concentration of STAT3β is higher than STAT3α during myeloid differentiation [171, 172]. STAT3β concentration can be induced by endotoxic shock in liver cells and therefore change the domination of STAT3α [173]. The variant of the STAT3α:STAT3β ratio during cell differentiation, cytokine stimulation and endotoxic shock may contribute to the complexity of STAT3 function in different cells. In order to understand the relationship between the expression of different STAT3 isoforms and STAT3 regulation of cellular functions, more detailed STAT3 function correlated with the specified isoform is required.

Both isoforms have transcriptional functions and their regulation of genes have similarities and differences. For example, embryonic lethality is observed in mice with complete knock out of STAT3, but the expression of either isoform can stop embryonic death [174]. This indicates that both isoforms have sufficient functionality to support embryo development.

Maritano *et.al.* conducted research to screen downstream genes regulated by a single STAT3 isoform [175]. In their research, STAT3 null mutation cells were inserted with a plasmid that produce either STAT3 isoform to create the cell line that produce only one STAT3 isoform. Their research indicated that IL-10 mediated inflammation can be controlled by both STAT3$\alpha$ and STAT3$\beta$. The expression of STAT3β rescued the lethality of STAT3α deleted embryo cells. But STAT3$\alpha$ and STAT3$\beta$ also have unique downstream genes although the fundamental biochemical mechanisms is still unknown. For example, STAT3α is response for IL-6 induced IFN-γ expression. But STAT3β is also reported to mediate IL-6 dependent myeloid cell apoptosis [176]. Knock out of single isoform will result in significant gene expression changes [175].

STAT3$\alpha$ and STAT3$\beta$ have different nuclear retention ability after phosphorylation [176]. STAT3$\beta$ is found to generate faster nuclear translocation and longer nuclear retention compared to STAT3$\alpha$.The STAT3$\beta$ homodimer is also a tighter binder to DNA compared to STAT3$\alpha$ homodimers [177]. According to Ng *et.al.*, the DNA binding stability and fast nuclear translocation of STAT3$\beta$ is due to the C-term deletion rather than the 7 unique amino acid sequences since the C-terminal truncated STAT3$\alpha$ has similar DNA binding stability and nuclear translocation speed as the STAT3$\beta$ isoform [178]. Zhang *et.al.* also revealed STAT3$\beta$ expression prolonged the phosphorylation and nuclear retention of STAT3$\alpha$ [179]. Therefore, although STAT3α expression is higher than STAT3β isoform in most cells, the activity of STAT3β may still have a significant influence on the STAT3 activities.

### 1.4.2 Unique functions of STAT3β isoform

With accumulating evidence showing that STAT3β has its own unique transcriptional activity, STAT3β is no longer just regarded as a dominant negative regulator of STAT3 activity. However, STAT3β overexpression can contribute to opposing effect of STAT3α in cells. STAT3β activity is usually related to STAT3's tumour suppressor activity. The expression of STAT3β in gastric cancer reduces chemoresistance and cancer invasion [180]. STAT3β activity also inhibits Bcl-XL, p21 and cycline D1 expression which can be induced by STAT3α, and therefore control cell proliferation [174, 181]. On the

other hand, STAT3β activity also seems to be independent of the function of STAT3α. Maritano *et.al*. suggested the expression of STAT3β does not interfere with STAT3α's function in embryo and adult mice [175].

STAT3β activity is not only related to tumour suppression but also to tumour progression. Continuous overexpression and over activation of STAT3β isoform in breast cancer suggested that STAT3β may contribute to breast cancer progression [176]. The level of STAT3β was also significantly positively related to acute myeloid leukaemia (AML) relapse in a clinical study [182]. This suggests that STAT3β may be used as an additional diagnostic factor in the future.

STAT3$\beta$ activity is highly related to inflammation response. Deletion of STAT3$\beta$ in mice result in macrophages hypersensitive to endo-toxic shock [173]. However, Matiano *et.al.* revealed acute-phase response to LPS simulation also present in STAT3$\beta$ deleted liver cells [175]. This finding suggests that STAT3$\beta$ is not the only isoform that can activate those genes. Therefore, the present of STAT3$\beta$ reduces the inflammation response simulated by endo-toxic in macrophages and liver cells. Since inflammation has been long associated with the development of tumours, it is obvious that STAT3$\beta$ activity is related to cancer. With the presence of STAT3$\beta$, tumour cells are more resistant to inflammation response therefore have a higher chance to go through the early stage of tumour growth [183]. On the other hand, STAT3$\beta$ was regarded as a dominant negative version of STAT3$\alpha$ with its own transcriptional function. Its expression was found to reduce gastric cancer cells invasion and make the cancer cells more susceptible for chemotherapies [174]. STAT3$\beta$ was found to inhibit the constitutive activation of STAT3$\alpha$ and reduce tumour growth in several in vivo assays [184]. The inhibition of STAT3$\alpha$ activation maybe due to the formation of STAT3$\alpha$/STAT3$\beta$ heterodimers. The heterodimer reduces STAT3$\alpha$ binding to a cytokine phosphatase called PTP-MEG2, hence reducing the phosphorylation and nuclear translocation of STAT3$\alpha$. However, STAT3$\beta$'s suppression in tumour development can only be observed when the expression level of STAT3$\beta$ is much higher than STAT3$\alpha$. The influence of

STAT3$\beta$ to cancer is highly related to the balance between the two STAT3 isoforms.

### 1.4.3 Other STAT3 isoforms: STAT3$\gamma$ and STAT3$\delta$

Another two isoforms: STAT3$\gamma$ and STAT3$\delta$, can be generated through a proteolytic process. STAT3$\gamma$ is a C-terminal truncated isoform created by proteolytic cleavage of STAT3$\alpha$ [185]. It has a full deletion of the transactivation domain without any additional amino acid sequences. Therefore STAT3$\gamma$ is the true dominant negative variant of STAT3. Proteolytic cleavage creating the $\gamma$ isoform with deleted transcriptional activation domain is also observed in other STAT family members (e.g. STAT5) [186]. The expression of STAT5$\gamma$ was detected in CD4+ T cells from HIV patients and found to be accompanied by positive responses to the treatment therapy [187]. The constitutive expression of STAT3$\gamma$ in AML is also significantly related to pathology [174, 188]. However, there is no study revealing the reason for STAT3$\gamma$'s formation yet.

Diane et.al described a 64kDa STAT3 isoform in 2002 and defined the novel isoform as STAT3$\delta$ [172]. The new STAT3 variant was found to be expressed during granulocytic differentiation. The information about this isoform is very limited.

In general, the different function of different STAT3 isoforms may reveal the diversity of STAT3 functions in cancer and normal cells. STAT3α and STAT3β are the two well-studied STAT3 isoforms. They have been reported to contribute to similar functions but also regulate different gene expressions. STAT3β is generated from alternative splicing and able to conduct transcription independently. The activity of STAT3β can not only be a negative regulator of STAT3α but also support STAT3α or enhance transcription of its own targeted genes. The creation of STAT3β is not a random result, it can be regarded as a self-regulation mechanism of STAT3 activity. Understanding the relationship and functions of different STAT3 isoforms may reveal many more unknown regulation systems in tumour cells. The described differences between STAT3α and STAT3β functions are all generated by the differences in the transactivation domain therefore

understanding STAT3 structure is also important for STAT3 related cancer research.

## 1.5 The domain structure of STAT3

Understanding STAT3 structure not only helps to understand STAT3 activity but also contributes to structural based drug design targeting STAT3 as a cancer treatment. In this section we describe the domain structure and discuss the functions of each STAT3 domain related to specific STAT3 activities. The STAT3 protein shown in figure 1.5 consists of 6 domains including: N-terminal domain (ND), Coiled-coil domain (CCD), DNA binding domain (DBD), linking domain (LD), Src homologous 2 domain (SH2) and Transactivation domain (TAD). Each domain has its unique function and all contributes to the stability of STAT3 structure.

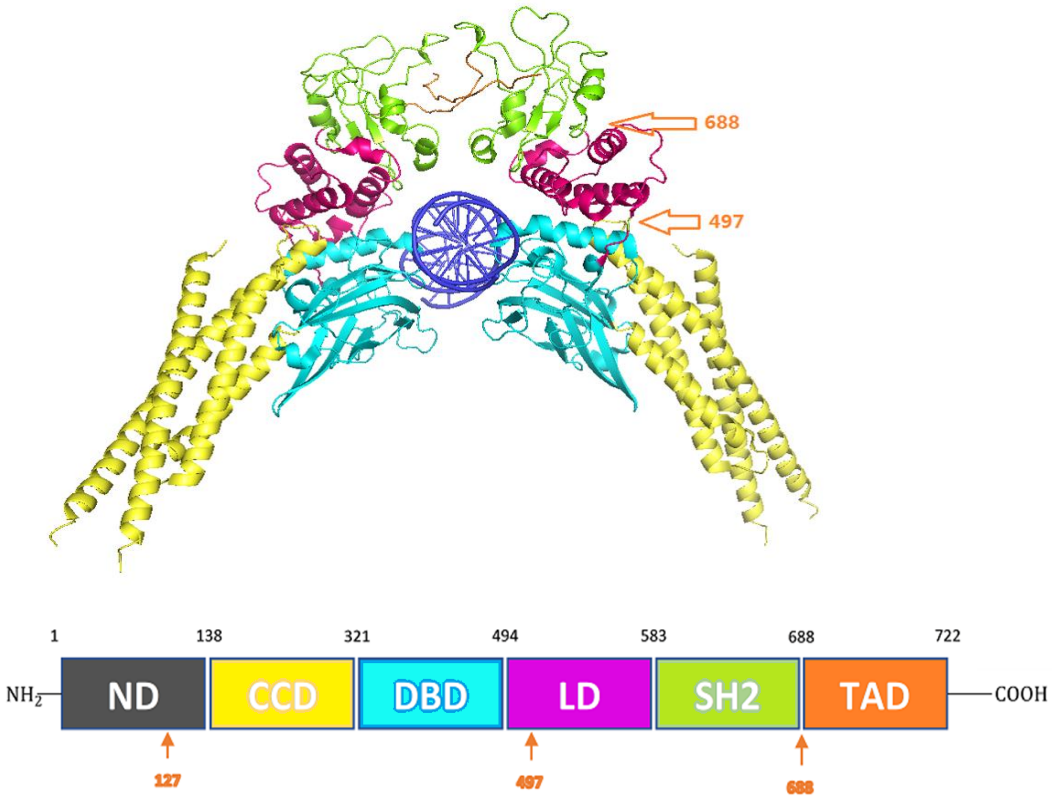


Figure 1.5. The crystal structure of STAT3β lacking N-terminal domain binding to dsDNA and the domain structure of STAT3β. N-terminal domain labelled in grey, CCD labelled in yellow, DBD labelled in light blue, LD

labelled in pink, SH2 domain labelled in green and TAD labelled in orange. The dsDNA is labelled in dark blue. [PDB 1BG1]

### 1.5.1 N-terminal domain

The N-terminal domain of STAT3 (absent from figure 1.5, but shown separately in Figure 1.6) is comprised of an 8 α-helix structure. Alpha helical structures are involved in a wide range of protein-protein interactions and is regarded as a potential target for inhibitor design (Edwards and Wilson, 2011). The N-terminal domain structure is analysed separately from the other domains using x-ray crystallization since full length STAT3 forms insoluble aggregates very easily. The first N-terminal domain structure was revealed by Hu *et.al.* [189].

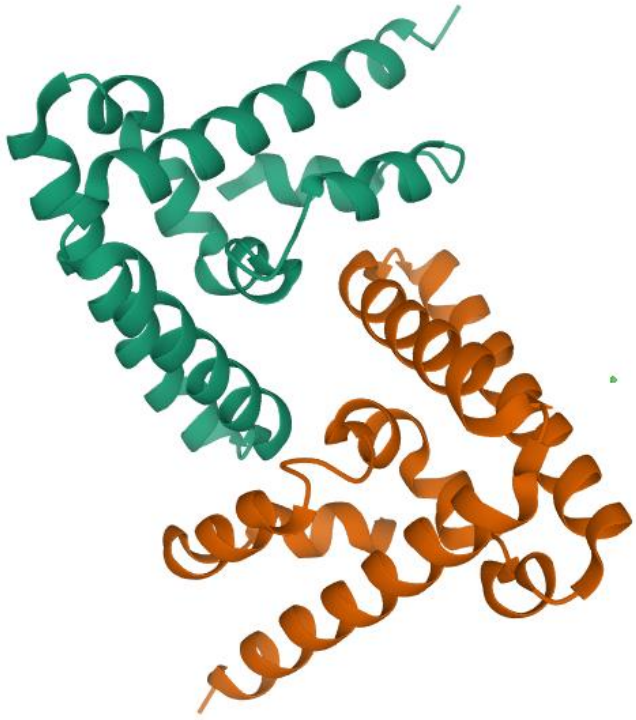

Figure 1.6. The crystal structure of the STAT3 N-terminal domain dimer. The green dot to the right side of the protein is $Ni^{2+}$ [pdb: 4ZIA] [190]. This figure shows the α-helix structure of the STAT3 N-terminal domains interacting with each other. The α-helix structure is important for STAT3 protein-protein interactions.

The ND is reported to be involved in multiple functions including: protein-protein interaction, nuclear translocation and DNA binding. Figure 1.6 shows

the crystal structure of a STAT3 N-terminal domain dimer. Firstly, ND is responsible for teramerization of Tyr705 phosphorylation induced STAT3 dimers [14]. The interaction between the ND of the nearby STAT3 dimers enhance the stability of the STAT3 binding to the dsDNA [191]. The tetramerization is essential for the interaction between STAT3 dimers and weak binding promoters. A dimer interface was observed in crystal structure of STAT3 ND which cooperates DNA binding [189]. Deletion of ND results in decrease of STAT3 DNA binding activity *in vivo* [192]. Furthermore, the activity of un-phosphorylated STAT3 monomers (uSTAT3) is also influenced by the ND [193]. ND contributes to the stability of un-phosphorylated STAT3 dimers and promotes un-phosphorylated STAT3 translocation [193]. N-terminal point mutations decreased the formation of stable un-phosphorylated dimers in inflammatory hepatocellular adenoma (IHCA) [194]. The activity of ND is also essential for un-phosphorylated STAT3 nuclear accumulation [195]. Moreover, ND is involved in chromatin remodelling mediated transcriptional activity of un-phosphorylated STAT3 and therefore influences gene expression resulting from STAT3 transcription [196]. Post-translational modifications of ND were identified during a STAT3 mediated antiviral response which interferes with STAT3 transcriptional regulation [56]. N-terminal deletion of STAT3 results in the decreased expression of STAT3 targeted genes specifically when the STAT3 phosphorylation is low [189]. Since ND is involved in general functions of STAT3, it has potential to be developed into a drug target for regulating STAT3 activities.

### 1.5.2 Coiled-coil domain

The coiled-coil domain (CCD) is another α-helical composed domain of STAT3 which is related to protein-protein interactions (PPI). CCD is involved in the regulation of SH2 domain mediated cytokine interaction, STAT3 phosphorylation and transcription [197]. Understanding the activity of the STAT3 CCD in molecular level is essential for understanding STAT3 activity and its regulation. Zhang *et.al.* reported that the deletion of CCD results in the loss of STAT3 function (inhibited tyrosine phosphorylation of STAT3) and therefore reduced the downstream STAT3 activities. They also pointed out

the most essential residue involved in the CCD activity is Asp170 [197]. Another important function of the CCD domain is that it supports STAT3 nuclear retention [198]. Mutation in the CCD domain reduced IL-6 and EGF induced nuclear translocation and retention of STAT3 [199]. In their study they also pointed out the important residue involved in this activity is Arg214/215 [199]. Later, Sato *et.al.* supported Ma *et.al.*'s discovery. Sato *et.al.* showed that mutation in Arg214/215 can speed up the nuclear exportation of STAT3 [198]. Although more detailed mechanism of STAT3 nuclear translocation and nuclear retention is still unclear, the importance of CCD domain in nuclear retention suggests that protein-protein interaction is involved in this process. Furthermore, the inhibition of STAT3 nuclear retention may also be a possible way to inhibit STAT3 transcriptional activity.

### 1.5.3 SH2 domain

The Src homologous 2 (SH2) domain present in many proteins relate to tyrosine phosphorylation signalling pathways and they function as a phosphotyrosine binding site [200]. The STAT3 SH2 domain is the most popular target for STAT3 inhibitor drug development. The SH2 domain contributes to the dimerization of phosphorylated STAT3. Figure 1.7 shows a cartoon crystal structure of a STAT3 SH2 domain dimer with the binding pocket labelled. Targeting the SH2 domain with small molecule inhibitors has disrupted the formation of stable STAT3 dimers [201]. SH2 also facilitates phosphorylation on Tyr705 by JAKs and non-receptor tyrosine kinases. Most STAT3 inhibitors targeting the SH2 domain interrupt the STAT-STAT dimer interaction and STAT-receptor interactions [202].

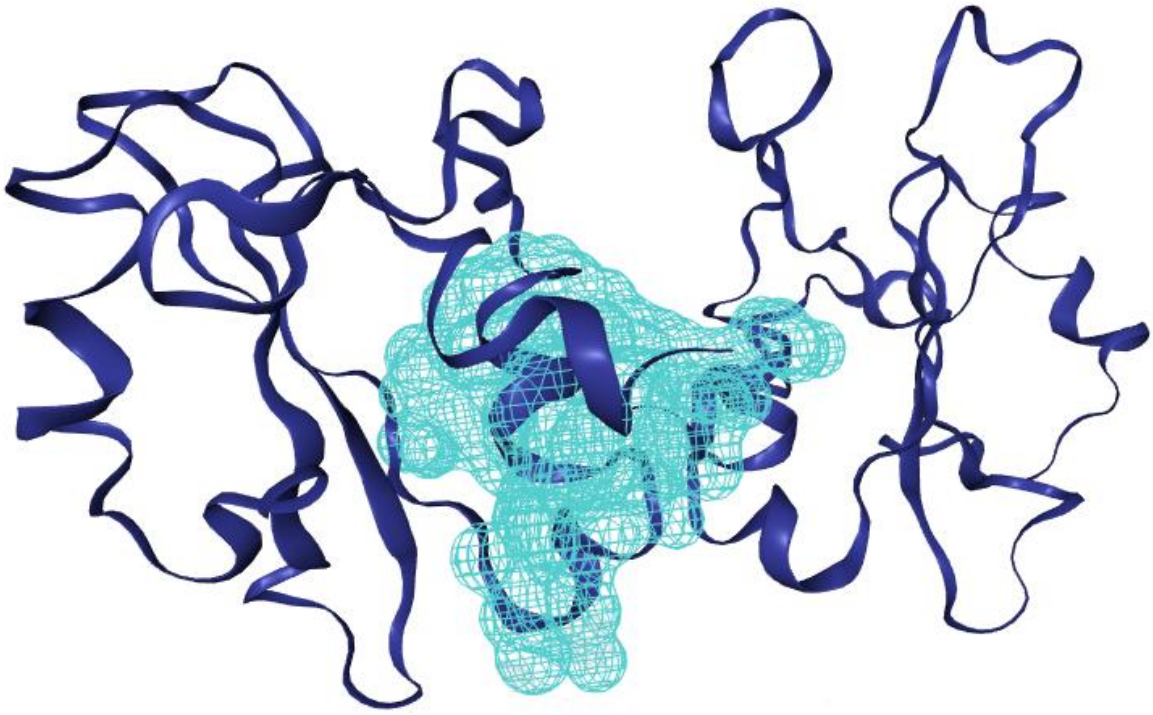

Figure 1.7. The crystal structure of two STAT3 SH2 domains in a crystallized STAT3β homodimer [PDB: 1BG1] [190]. The light blue part labels the binding pocket of a STAT3 SH2 domain monomer. This binding pocket image is conducted by ezCADD. The ezCADD program is published by Tao *et.al.* [203].

### 1.5.4 DNA binding domain

The DNA binding domain (DBD) of STAT3 contributes to the recognition and binding to the target DNA-GAS sequence (TTCCGGGAA). The antiparallel α-helix structure of the DBD domain is essential for the hydrophilic interactions between STAT3 and other proteins while the DNA contacting pocket is supported by a small β-sheet structue [204]. The crystal structure of the DBD domain binding to dsDNA is shown in figure 1.8. Although the DBD is dominant for DNA binding ability of STAT3, the connection with the SH2 domain through the linking domain is also important for binding stability [205]. The DNA binding domain is another ‘drugable’ domain in STAT3. Interfering with DBD activity can directly inhibit the STAT3 interaction with the targeted dsDNA. In this thesis, we suggest that the STAT3 DBD domain is the best domain to target for STAT3 inhibitor design based on the complexity of STAT3 activation pathways. The linker domain is between DBD and SH2 but its function is not well studied. It has been reported that

the LD is crucial for STAT3's DNA binding activity and may also be involved in nuclear transportation [206].

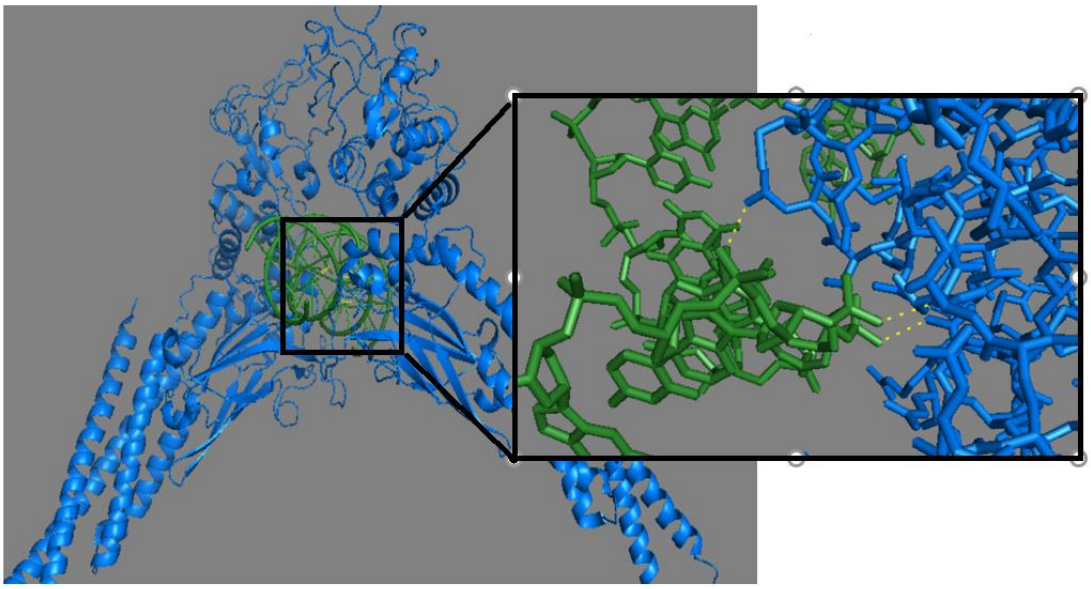

Figure 1.8. Two STAT3 DNA binding domain interacting with dsDNA as a dimer [PDB: 4E68] [207]. The picture is generated by Pymol, a molecular modelling software used to visualise the molecular structure of proteins. The green color shows the dsDNA, the blue color shows the STAT3 protein and the yellow dash line shows the polar interaction between one STAT3 monomer and one DNA chain.

### 1.5.5 TAD domain

TAD is the transcriptional activation domain that is only present in the STAT3α isoform. However, the seven amino acid (FIDAVWK) in STAT3β isoform can also support STAT3 transcriptional activity. This indicates that the 7 amino acid peptide should be able to form complex with other transcription factors and mRNA to enhance transcription. A structural study of the CT7 may lead to the discovery of novel STAT3 inhibitors interfering with STAT3 transcriptional activity directly.

Analysing the structural of STAT3 in detail contributed to structural based drug discovery targeting STAT3. The range of potential small molecule drugs

is highly specified with binding pockets identified in each domain. Furthermore, with the help of deletion studies, STAT3's biological functions can be related to single or several amino acids. These studies specified the target therefore help increase the specificity and sensitivity of future developed drugs. In this thesis, we selected our target and designed our mutated STAT3 based on the crystal structural information of STAT3.

### 1.6 Current STAT3 inhibitors

The final aim of studying STAT3 is to use STAT3 as a target to treat cancer and other related diseases. The knockout of STAT3 has shown the reduction of tumour cell proliferation and improved apoptosis and immune sensitivity in breast cancer, lung cancer, and leukaemia. Drugs inhibit STAT3 activities by either directly interacting with STAT3 or by interfering with upstream targets in STAT3 pathways. The targeted STAT3 upstream pathway can include JAK2, EGFR and Src. Two of the STAT3 domains appear to be the most popular targets and are highlighted in Table 1.3 below for published STAT3 inhibitors: these are the SH2 domain and the DNA binding domain.

As stated before, the STAT3 SH2 domain is reported to be essential for STAT3 dimerization and for protein-protein interactions. Inhibition of the STAT3 SH2 domain interferes with the interaction between STAT3 and its upstream tyrosine kinases and therefore prevents STAT3 phosphorylation and the subsequent transcriptional activities. It has been considered the most 'druggable' STAT3 domain target since several STAT3 inhibitors targeting the SH2 domain have reached clinical trials including: C188-9 (TTI-101), Napabucasin, OPB-111077, and AZD9150.

Another anti-cancer drug target in the STAT3 structure is the DNA binding domain. Due to the complexity of STAT3 activation pathway and accumulating evidences showing the un-phosphorylated has transcriptional activity, the importance of inhibiting direct interaction between the STAT3 proteins with the dsDNA is emphasized. However, the development of STAT3 inhibitors targeting the DNA binding domain is slow. Table 1.3 summarise current STAT3 inhibitors under development. In this thesis, we

developed several *in vitro* assays that can be used in the screening of STAT3 inhibitors that target the DNA binding domain specifically.

| Inhibitor name | STAT3 target domain | Tested cancer | Test phase | Substrate | Reference |
|---|---|---|---|---|---|
| Bruceantinol (BOL) | unknown | Colorectal cancer | *In vivo* | Natural product | [208] |
| WP1066 | JAK/STAT inhibitor | Melanoma | Phase 1 | Small molecule | [209] |
| Cpd188 | SH2 domain | Glioblastoma | *In vivo* | Small molecule | [210] |
| Stattic | SH2 domain | Breast cancer | *In vivo* | Small molecule | [211] |
| S31-201 | SH2 domain | Chronic kidney disease Liver fibrosis | *In vivo* | Small molecule | [212, 213] |
| C188-9 | SH2 domain | Leukaemia Also inhibit STAT5 | Phase 1 | Small molecule | [188, 214] |
| 5,15-DPP | SH2 domain | Nerve sheath tumours | *In vitro* | Small molecule | [215] |
| STX-0119 | SH2 domain | Liver fibrosis | *In vivo* | Small molecule | [216] |
| LLL12 | SH2 domain | Breast cancer | *In vivo* | Small molecule | [217] |
| BP-1-102 | SH2 domain | Breast cancer Lung cancer | *In vivo* | Small molecule | [218] |
| Cryptotanshinone | SH2 domain | Colorectal cancer Prostate cancer | *In vivo* | Nature product | [219] |
| KYZ3 | SH2 domain | Breast cancer | *In vivo* | Small molecule | [220] |
| STA-21 | SH2 domain | Breast cancer | *In vivo* | Small molecule | [221] |
| Niclosamide | DNA binding domain | Lung cancer | *In vivo* | Small molecule | [222] |
| S3-54A18 | DNA binding domain | Not reported | *In vitro* | Small molecule | [223] |
| IS3 295 | Unknown | Breast cancer | *In vivo* | Small molecule | [224] |
| Bt354 | SH2 domain | Breast cancer | *In vivo* | Small molecule | [225] |
| Arctigenin | SH2 domain | Lung, liver | *In vivo* | Small molecule | [226] |

| | | | | | |
|---|---|---|---|---|---|
| Alantolactone | SH2 domain | Breast cancer | *In vivo* | Nature product | [227] |
| OPB-51602 | unknown | Solid tumours | Phase 1 | Small molecule | [228] |
| Napabucasin | SH2 domain | Pancreatic cancer, Colon cancer | Phase 3 | Small molecule | [229] |
| OPB-111077 | unknown | B-cell lymphoma | Phase 1 | Small molecule | [230] |
| Silibinin | Both SH2 and DNA binding domain | Prostate cancer | *In vivo* | Naturalproduct | [231] |
| AZD9150 | SH2 domain | Lung cancer, Overian cancer, GIC | Phase 2 | Small molecule | [232] |

Table 1.3 A summary of STAT3 small molecule inhibitors that directly interact with STAT3. This table shows the novel STAT3 inhibitors and their targeted domain and their current stage in drug development.

## 1. 7 Protein aggregation *in vitro* and the impact on pharmacy

In this thesis, three different types of in vitro assay were designed to test STAT3 DNA binding activity and screen STAT3 inhibitors. During the experiments, protein aggregation has been the priority problem to solve. The phenomenon of protein aggregation and protein precipitation is directly related to the success of assays. It is also an important result we found in the inhibition tests.

Protein aggregation *in vitro* usually refers to the phenomenon that two or more protein molecules form a stable complex that influence the monomeric protein's tertiary structure, toxicity or biological activities [233]. This process is also called non-native protein aggregation. Protein aggregation starts from nucleation and polymerization [234]. Aggregated proteins either form soluble agglomerated aggregates or particles. The study of protein aggregation is essential in pharmacy since protein-based pharmaceuticals play an important role in treatment methods of auto-immune diseases, some metabolic disorder diseases and various cancers [235]. Protein aggregation is often confused with protein precipitation and polymerization. The protein aggregation process mentioned in this project refers to the process of

polymerization and the polymer either remain soluble or form insoluble precipitates. Protein precipitation brings difficulty in STAT3 production, purification and storage while proteins forming soluble polymers are hard to detect and may affect STAT3 functionality.

There are four ways that proteins can initiate precipitation: 1) precipitation caused by misfolding or unfolding proteins; 2) self-association without changing the morphology of the monomeric protein molecules; 3) chemical reaction creating covalent bonds between protein molecules; and 4) precipatation caused by protein degradation. Generally, protein aggregations can be separated into two types: the physical aggregation and the chemical aggregation based on whether there is formation of covalent bonds between two protein molecules. Physical aggregation is based on the Van der Wal forces, hydrogen bonds, hydrophobic and electrostatic interactions between the protein molecules [236]. The formation of physical aggregation and chemical aggregation can happen to the same protein. For example, insulin can form soluble and insoluble aggregates through both physical and chemical aggregation [237, 238]. One protein type can also generate different forms of polymers based on the differences of misfolding, such as monoclonal antibodies (mAbs) [239].

The process of protein aggregation brings advantages and disadvantages to pharmacy. Protein aggregation is a challenge for the production of recombinant proteins with bacteria, protein purification, formulation and storage. Normally, compared to natural proteins, truncated proteins are more likely to aggregate. Due to natural evolution, the chemical characteristics (including structure, stability, and solubility) of the cellular proteins usually exhibit in favour of the protein's function [240]. The aggregation of proteins expressed in bacteria cells is affected by complex conditions including protein structure, cellular environment, and extracellular environment [241]. Control and analysis of protein aggregation of the synthesized protein has always been challenging in *in vivo* studies. The application of recombinant proteins in therapeutic treatment methods has been developed since 1970s, and has been a great success [242]. On the other hand, protein aggregation can also bring benefits to pharmacy. For example, aggregated protein

polymers can increase the immune response compared to soluble protein monomers [243]. However, during industrial production of the therapeutic proteins, protein precipitation also reduces the quality and quantity of the purified protein [244].

In this thesis, protein precipitation is a major problem to be studied and solved during STAT3 production, purification, buffer exchange and the storage of the purified STAT3. The protein pricipitation that occurred during the production of the recombinant protein could have been caused by protein misfolding within in the bacteria. The designed protein overexpression mechanism intransformed bacteria causes a burden to cell functions such as transcription, translation, and protein folding[245][245][245][245][245][245][245][245][245] [241][240][243]. Protein degradation, oxidation during purification and buffer exchange also induce the process of protein precipitation. The protein concentration created during purification can also cause protein aggregation hence result in the precipitation. We observed irreversible precipitates during our studies of STAT3. However, soluble or irreversible STAT3 aggregates may also be formed during the production processes. Various techniques have been used to detect protein aggregation however none of them can be used to detect all types of aggregation. One of the reason for this is that no single detection methods covers the size range of the protein aggregates. Techniques used to detect protein aggregation include: HPLC, SDS-PAGE, dynamic light scattering, and microscopy. Size exclusion chromatography can be used to separate molecules with different molecular weights. It can be used to separate and quantify soluble protein and soluble aggregates but not precipitates [246]. Dynamic light scattering measures soluble protein aggregates in the range of 1-100nm. It is also a method that can be used to measure protein aggregation kinetics [247]. Large insoluble protein aggregates are usually detected through light microscopy and visualization.

The introduction pointed out the importance of STAT3 in cancer research and described current knowledge about STAT3's biological activities. It also introduced the protein aggregation, which was found to be the major difficulty in the experiments. The following chapters will discuss these points in the

production and characterization of truncated recombinant STAT3 proteins of various lengths, the biophysical observations including PEMSA assays, and the development and application of fluorescence polarization assays for cancer drug discovery.

In summary, based on current knowledge of STAT3, it is widely believed to be a potential anticancer drug target. Its essential role in cell differentiation, immune response, and tumour development, suggest that STAT3 is an important protein in the pathology of cancer and immune diseases. However, the detailed regulation and activation mechanisms of STAT3 is not well understood. In the classical STAT3 activation pathway, STAT3 requires phosphorylation and dimerisation to enter the cell nucleus and start transcription. However, it has been proved that unphosphorylated STAT3 can also transport into nucleus and bind to dsDNA as dimers. Therefore we hypothesis that unphosphorylated STAT3 may also have transcription activity as long as they bind tight enough to the dsDNA. There are other modulation pathways of STAT3 including acetylation and methylation that can stable the binding of STAT3 to the dsDNA. Understanding the mechanism of STAT3 activation is essential for make entirely use of STAT3 and avoid side effects in drug research. The mystery of STAT3 not only lay on its complicated activation and regulation pathway, but also its diverse function in the two different isoforms: STAT3α and STAT3β. The two isoforms with only N-terminal differences have varied regulation in transcription. The activation of the two isoforms result differently in immune response and tumour development. Since the distribution and the regulation of the formation of the two STAT3 isoforms are not well studied, the consequences of inhibiting STAT3 in different types of cells is not ensured. An inhibitor that completely inhibit STAT3 transcription activity is required in the research of detecting different STAT3 functions. Current testing drugs targeting STAT3 are mainly target SH2 domain, and there are a few drugs reaching clinical trial now. However, we recommend DNA binding domain as a better target to complete inhibit STAT3 transcription activity since phosphorylation of STAT3 in the SH2 domain may not be the only modification that control STAT3

transcription. With STAT3 SH2 domain inhibited, STAT3 may still get acetylated or methylated, thus the transcription of STAT3 may be influenced but may not be completely inhibited. To study the relationship between STAT3 SH2 domain and its DNA binding activity, we produced different length of truncated STAT3 protein and designed different in vitro assays. The in vitro assays can also be applied in STAT3 inhibitor screening.

# Chapter 2- Protein production, extraction and purification

All STAT3 mutants applied to the project were expressed in Rosetta2 (DE3) cells with IPTG induction. The methods of producing human STAT3 protein in *E. coli* cells were developed from previous protocols developed by Dr. Wilderspin. The structure and biological activities (DNA binding activity and peptide binding activity) of the *E. coli* produced STAT3$_{127\text{-}722}$ have been checked in previous research [248]. Comparing to extracting STAT3 proteins from mammalian cell lines, producing STAT3 proteins in *E. coli* cells is much more cost effective, and the truncated form was not so insoluble. Furthermore, producing STAT3 proteins in *E. coli* cells provides a simple way to produce large amount of purified STAT3 proteins for study.

In this project, three STAT3 truncated proteins were used to detect the influence of different STAT3 domains on STAT3's DNA binding activity. They are STAT3 $_{127\text{-}722}$, STAT3 $_{127\text{-}688}$ and STAT3 $_{127\text{-}497}$. STAT3 $_{127\text{-}722}$ consists of all domains of STAT3β isoform except for the N-terminal domain. STAT3 $_{127\text{-}688}$ is a shorter truncated STAT3 protein made from the STAT3 $_{127\text{-}722}$ with deletion of the important Tyrosine 705. STAT3 $_{127\text{-}497}$ is a very short truncated STAT3 protein with only two integrated domains: the CCD and the DBD. Fluorescent protein labels were attached to either N-terminal or C-terminal of the STAT3 mutants to perform different types of assays.

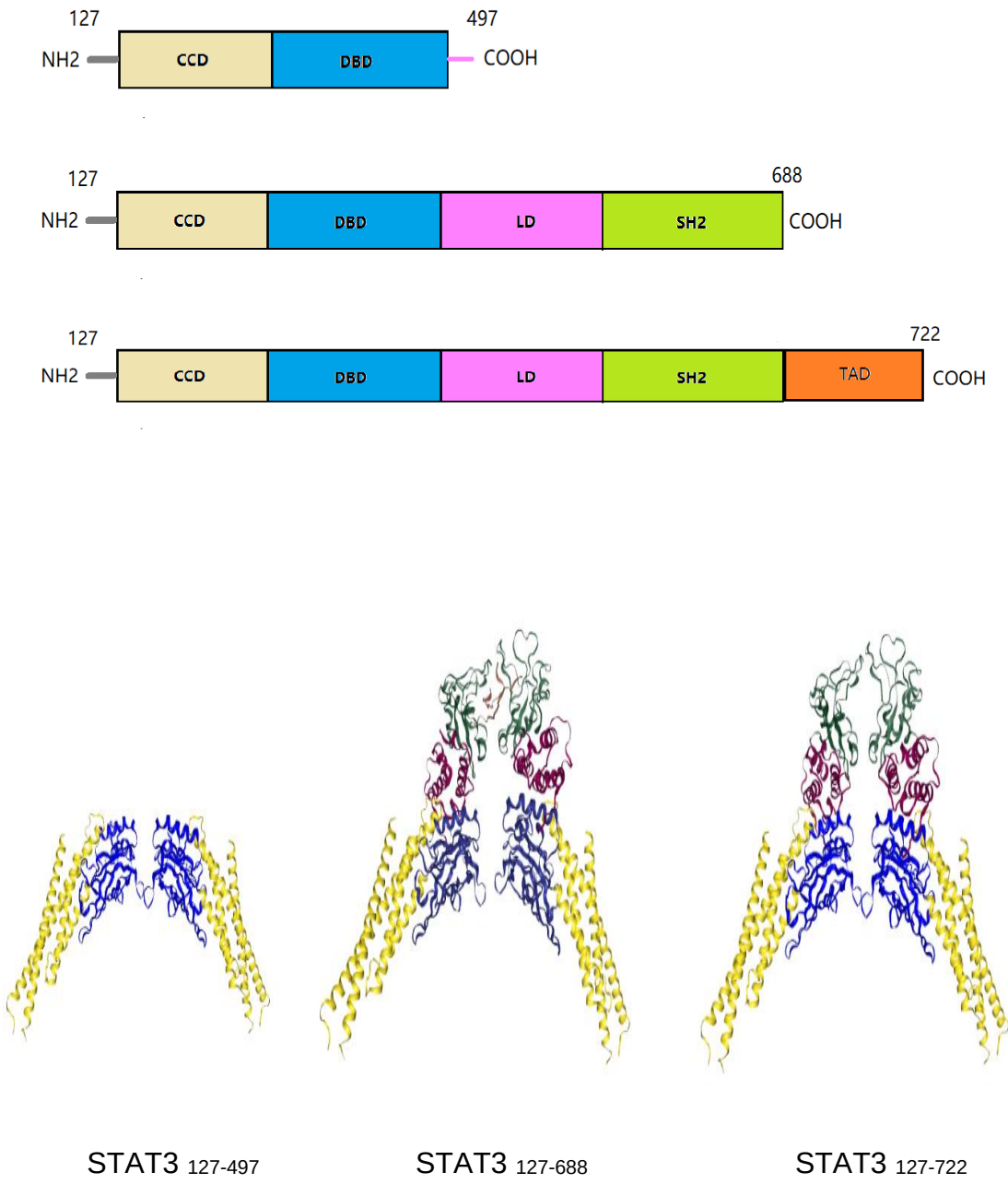


Figure 2.1 shows the domain structure and the molecular structure of three STAT3 truncated proteins: STAT3 $_{127\text{-}497}$, STAT3 $_{127\text{-}688}$ and STAT3 $_{127\text{-}722}$ in dimers. The CCD domain was labelled in yellow. The DBD domain is in blue. The LD domain is in pink and the SH2 domain in green. The TAD domain is in orange.

The molecular weight (MW) of the STAT3 $_{127\text{-}722}$ truncated protein is about 68kDa by calculation according to the published protein sequence while about 64kDa according to the SDS gels. The extinction coefficient (E.C.)

calculated according to the protein sequence for STAT3 $_{127\text{-}722}$ is 89x10$^{3}$ M$^{-1}$cm$^{-1}$. For the STAT3 $_{127\text{-}688}$ protein, the MW is about 64kDa and the E.C. is 82x10$^{3}$ M$^{-1}$cm$^{-1}$. The shortest STAT3 truncated protein STAT3 $_{127\text{-}497}$ has lowest MW of 42.5kDa and the E.C. is 31x10$^{3}$ M$^{-1}$cm$^{-1}$. The above parameters were used to calculate the concentrations of the extracted STAT3 proteins when combined with the $A_{280}$ readings.

## 2.1 A brief introduction of using genetically modified microorganisms to produce eukaryotic proteins

Genetically modified microorganisms (GMOs) have been used to produce human protein in medical research. Microbial systems were the first genetically modified living systems in the history [249]. Microorganisms, especially prokaryotic bacteria, contain relatively simple gene information compared to other prokaryotic cells. The *E. coli* gene was first completely sequenced in 1997 containing 6.4 million base pairs (bp) while the human genome contains more than 3000 million bp per haploid. Therefore, the mutations and modifications in the *E. coli* genes are easier to be monitored. Furthermore, the structure of the *E. coli* gene is a single circle while the human gene contains 23 pairs of chromosomes. The complexity of the human gene added more difficulty on gene modification processes. The use of *E. coli* cells also benefits from fast proliferation speed, which results in higher protein production level compared to human cells incubated for the same length of time. With the advantages of fast replication, easy transformation, ordinary energy requirement, relatively simple genomic content, bacteria culture comparing to animal cell culture are very cheap to grow, easier to be monitored. Therefore, GMOs are widely applied in many fields including the food industry, medical research, energy production and waste treatment. The method of using GMOs to produce synthetic proteins was first created by Herbert Boyer. He successfully produced synthetic insulin in *Escherichia coli* (*E. coli*) in 1978. The capacity for producing high quantities of the protein in a relatively short time speeds up the process of biochemical characterisation, medical research on protein targets and industrial production. In this thesis, we use genetically modified *E. coli* cells to produce truncated human STAT3 proteins and their derivatives. With the

application of the produced STAT3 recombinant proteins, we can analyse the biological activity of STAT3 *in vitro*, learn about the molecular structural of STAT3 and test STAT3 inhibitors that have potential to be developed into anticancer drugs.

Nowadays, production and purification of recombinant proteins in bacteria is almost the imperative skill in the field of biochemistry. Research using GMOs to produce human proteins usually start with host selection, plasmid selection, strain selection and other trouble-shooting questions.

Host microorganisms can be bacteria, yeast or filamentous fungi (moulds). The advantages of choosing *E. coli* as the host include rapid proliferation, high protein yield, cheap and cost-effective, easy to culture and to modify [250]. However, the *E. coli* as host also have some disadvantages. The *E. coli* system produces protein without glycosylation and therefore sometimes produces protein without its desired biological function [251]. Another disadvantage of the *E. coli* host is that the produced protein may aggregate to form inclusion bodies in the bacterial cells. The aggregated proteins in the inclusion bodies are usually misfolded, insoluble and require re-folding. In this thesis, the first problem was eliminated by using the results of previous research. The STAT3 $_{127\text{-}722}$ protein has been successfully produced in the *E. coli* cells with the biological activity analysed by FP assay and PEMSA assay (peptide binding and DNA binding) and structurally analysed by X-ray crystallisation [248]. The second disadvantage is still unsolvable in this thesis since the efforts made to decrease inclusion bodies (induction at low temperature, adding glucose during expression and changing different culture) did not work. However, the disadvantage did not completely outweigh the advantages of using *E. coli* as a host. In general, producing the STAT3 protein in *E. coli* cells is still the best choice.

The plasmid selection is based on the following factors: replication, promoters, cloning site, antibiotic resistant gene and affinity tags for protein purification [250].A good replicon leads to the suitable copy number of the plasmids that produced high yield of the recombinant protein without causing metabolic burden to the bacteria cell. The role of the promoter is like a switch

to the gene transcription and protein expression in the bacteria cell. A multiple cloning site allows the easy insertion of the desired gene sequence or antibiotic resistant gene for selection. The antibiotic resistant gene is crucial for colony selection and incubation. The antibiotics make sure that only successfully transformed bacteria can be selected and avoid plasmid loss during incubation. Finally, affinity tags are often fused to the recombinant protein with an enzyme digestion site as a linker that allows the tag to be removed after purification.

## 2.2 pET32a(+) plasmid as a vector

In this thesis, we use the pET32a(+) as our vector plasmid. The pET32a(+) plasmid map is shown in Figure 2.2.

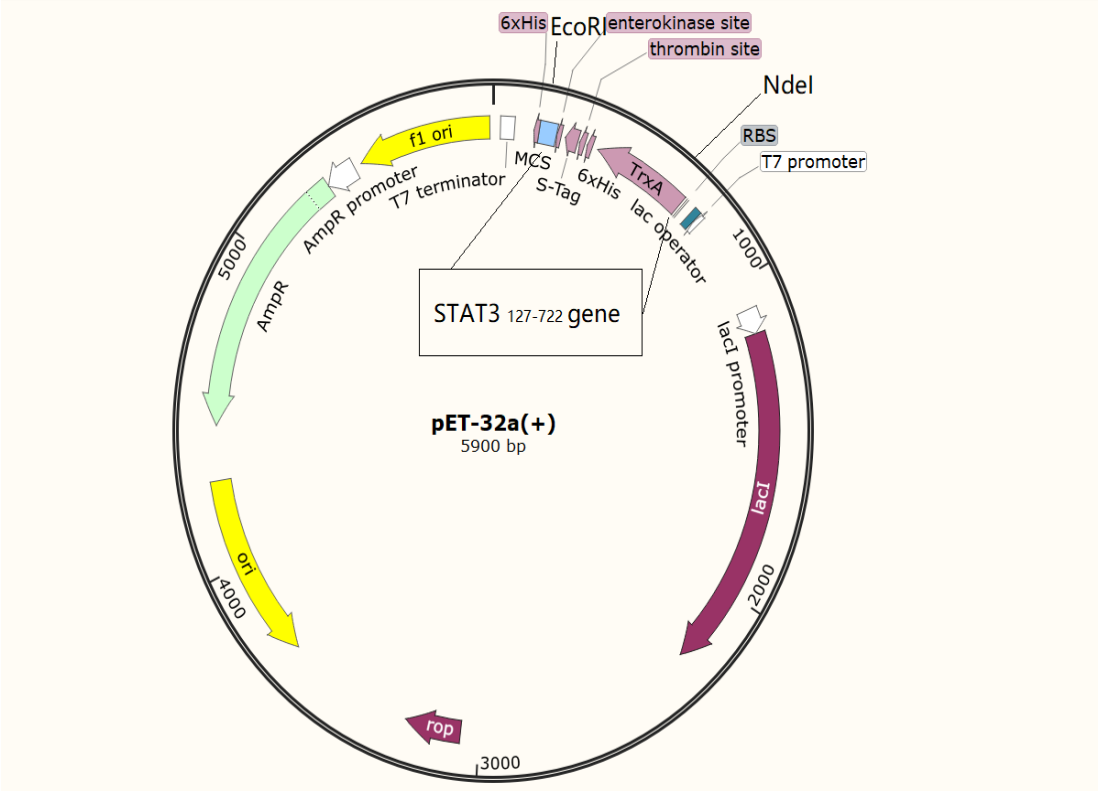


Figure 2.2. The pET-32a (+) plasmid map obtained from SnapGene. The STAT3 $_{127\text{-}722}$ gene was inserted between the *Eco*R1 and *Nde*1 restriction site labelled in the picture.

The pET32 plasmid series contains pET32a pET32b and pET32c. The system was designed in 1993 by Edward et.al. in order to achieve high protein expression level with limited formation of inclusion bodies in *E. coli*

[252]. The system contains gene coding for a thioredoxin protein (TrxA) that can be fused to the recombinant protein inserted into the multiple cloning site and increase the solubility of the fused protein [252]. Apart from the TrxA tag, it also contains S-tags and His-tags that can be removed by cleavage in the plasmid map. However, none of the tags was used in this thesis.

The pET32a(+) plasmid coding for the STAT3 $_{127\text{-}722}$, YFP-STAT3 $_{127\text{-}722}$ and CFP-STAT3 $_{127\text{-}722}$ was created by Dr. Nkansah. The STAT3 genes were cloned into the multiple cloning site (MCS) of the pET32a(+) between the *Eco*R1 and the *Nde*1 restriction site shown on figure 2.2. The expression of the inserted STAT3 sequence was controlled by the T7 promoter. The sequence between the *Nde*1 after the ribosome binding site (RBS) and the *Eco*R1 in the MCS was deleted. That includes the TrxA-tag, S-tag and the N-terminal His-tag. The stop codon was added after the STAT3 codon for amino acid 722 therefore the C-terminal His-tag was not expressed. The inserted sequence for the STAT3 $_{127\text{-}722}$ gene was 1803bp and the eYFP coding sequence was 720bp. Hence the total plasmid of the success insertion for the STAT3 $_{127\text{-}722}$ pET32a(+) was 7925bp and the YFP-STAT3 $_{127\text{-}722}$ was 8645bp. The success of the bacteria transformation can be confirmed Ampicillin resistance.

## 2.3 Rosetta2 (DE3) were applied for STAT3 protein production

The host strain employed for protein production in this thesis was Rosetta2 (DE3) manufactured by Novagen and sold by Merck. Rosetta2 (DE3) is a BL21(DE3) derivative that contains genes encoding tRNAs with anti-codons to compensate for the differences in eukaryotic codon usage, and therefore improves eukaryotic protein expression. The BL21 strain was developed form an *E. coli* B strain to remove the Lon protease which can cleave the recombinant proteins [253]. DE3 indicates that the bacteria strain contains a λDE3 lysogen that expresses T7 polymerase under the control of the lacUV5 promoter. The lacUV5 promoter can be switched on by Isopropyl β-D-1-thiogalactopyranoside (IPTG) induction and therefore turns on the expression of the T7 polymerase. The T7 polymerase can then transcribe the genes controlled by the T7 promoter.

## 2.4 Method:

### 2.4.1 Creation of N-terminal fluorescent labelled STAT3 truncated proteins

Four N-terminal fluorescent labelled STAT3 truncated proteins were produced through point-directed mutagenesis: YFP-STAT3 $_{127\text{-}688}$, YFP-STAT3 $_{127\text{-}497}$, CFP-STAT3 $_{127\text{-}688}$ and CFP-STAT3 $_{127\text{-}497}$. The yellow fluorescent protein (YFP) labelled STAT3s were constructed for application in the protein mobility electrophoresis shift assays (PEMSA) while the cyan fluorescent protein (CFP) labelled STAT3s were used in the fluorescent resonance energy transfer (FRET) assays. Both PEMSA and FRET assays were developed to detect STAT3's DNA binding activity and STAT3 inhibitor screening.

All mutants were generated with Qiagen Quick Change Lightning point directed mutagenesis kit. The original plasmids YFP-STAT3 $_{127\text{-}722}$ and CFP-STAT3 $_{127\text{-}722}$ were provided by Dr. Wilderspin. The original plasmids were made from pET32a(+) plasmid with insertion of YFP/CFP gene sequence followed by human STAT3 gene sequence coding for amino acid (aa) 127-722 between *Eco*R1 and *Nde*1 restriction sites. Two pairs of primers were designed to insert stop codons after the codons coding for aa688 and aa497 respectively.

Primers designed for the STAT3 $_{127\text{-}497}$ and the STAT3 $_{127\text{-}688}$ truncated proteins are:

497stop Forward: 5'-CTT CTT CAC TAA GCC GCC ATA ATG AAC CTG GGA CCA AGT GGC C-3'

497stop Reverse: 5'-GGC CAC TTG GTC CCA GGT TCA TTA TGG CGG CTT AGT GAA GAA G-3'

688stop Forward: 5'-CAT TTG GAA AGT ACT GTA GGT GAT CAG CCA GGA GCA CCC CG-3'

688stop Reverse: 5'-CGG GGT GCT CCT GGC TGA TCA CCT ACA GTA CTT TCC AAA TG-3'

50ul of the polymerase chain reaction (PCR) cocktails consists of 50ng plasmid template (YFP-STAT3 $_{127-722}$ or CFP-STAT3 $_{127-722}$), 125ng of both primers (forward and reverse), 1µl dNTPs, 1 µl enzyme, Quick Change Lightning buffer and Quick solution. All materials except for the primers and templates were provide in the Qiagen Quick Change Lightning kit. The content of Quick Change Lightning and Quick solution were not specified. The PCR cycles were processed according to the following form:

| Stage | Cycles | Temperature | Time |
|---|---|---|---|
| 1 | 1 | 60 | 2mins |
| 2 | 18 | 95 | 20s |
| | | 60 | 10s |
| | | 68 | 240s |
| 3 | 1 | 68 | 5mins |
| 4 | 1 | 4 | 10mins |

After the PCR cycles were finished, 5 µl of the PCR products mixed with 50 µl of the XL10-Gold cells and heated in a PCR machine at 42 ℃ for 90 s. 100 µl of the transformed *E. coli* cells were spread onto LB agar plates with ampicillin (Amp), chloramphenicol (Chl) and tetracycline (Tet) followed by overnight incubation at 37 ℃. Only successfully transformed *E. coli* cells were able to form colonies on the plates. Single colonies were selected to incubate in 5 ml autoclaved LB culture with Amp, Chl and Tet at 37 ℃, shaking at 180 rpm. When the $OD_{600}$ of the inoculated 5 ml bacteria culture reached about 0.6, 1 ml of the bacteria culture was transferred into 500 ml autoclaved LB culture with Amp (1mg/ml), Chl (0.35 mg/ml) and Tet (1 mg/ml). The 500 ml bacteria culture was continuous incubated at 37 ℃, 180 rpm until the $OD_{600}$ reached 0.6. The 500ml cloudy bacteria culture were centrifuged at 12,450 g, 4 ℃ for 30 mins to harvest the bacteria pellets. After carefully discard of the supernatant, the bacteria pellets were incubated in ice for 10 mins.

The resuspension of the bacteria pellets, column equilibrate, purification of the plasmids steps were performed according to the Qiagen Maxiprep Kit. The plasmids were eluted with 500 µl of $dH_2O$ (HPLC grade) and stored in -20 ℃. Sequence of the stop codons were confirmed by Eurofins Tube Sequencing Service.

### 2.4.2 Result- Success creation of N-terminal fluorescent labelled STAT3 mutants

The sequencing results are shown in figure 2.3.

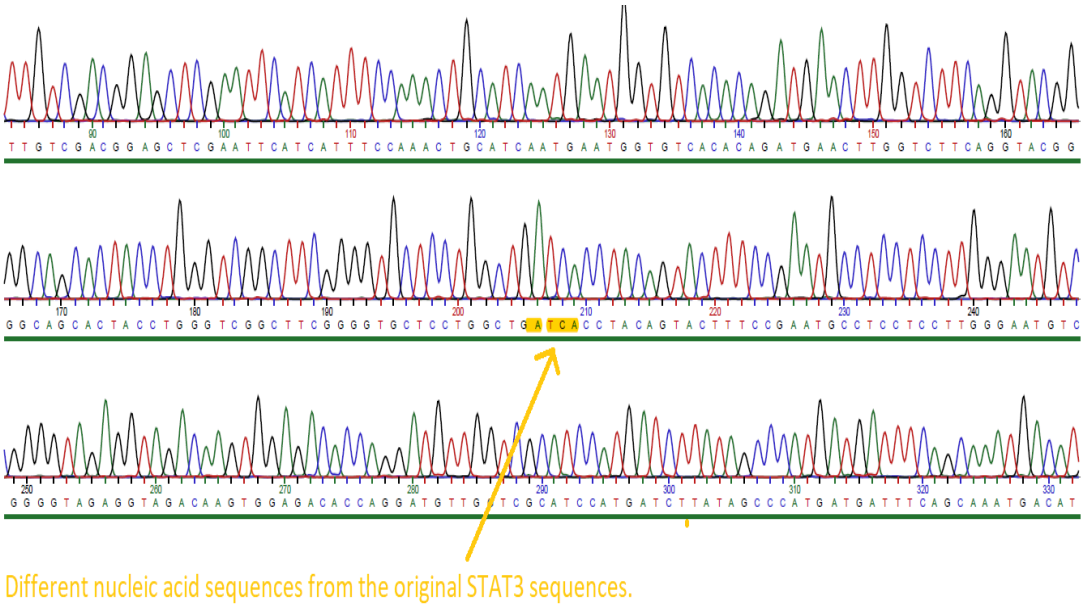


Figure 2.3. Part of the DNA sequencing result received from Eurofins for 688 stop codon insertion. The primer chose for this sequencing was T7 term. The mutagenesis site is completely covered in the sequencing result.

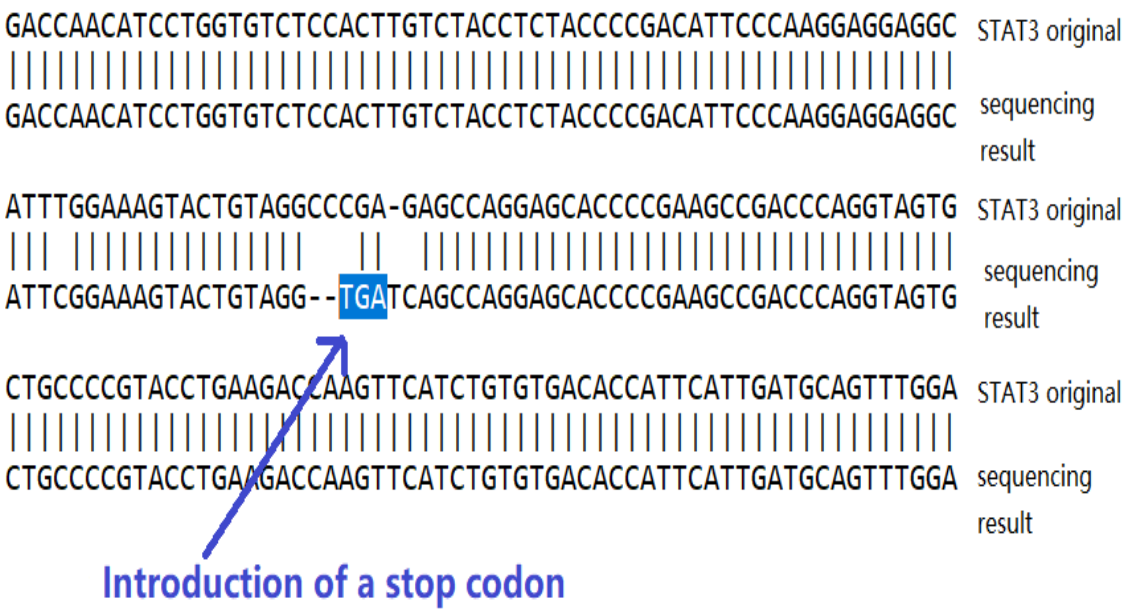


Figure 2.4. Alignment of the sequencing result with the GenBank database STAT3 sequence NM_011486. The upper-strand is the original STAT3 DNA sequence and the bottom-strand is the sequencing result. The CCCGAG was clearly replaced with TGATC. There was one already presented nucleic acid mutation present in the Wilderspin lab clones just before the stop codon, a T to C mutation results in a TTT to TTC change for the codon which is a silent mutation. Both TTT and TTC code for Phenylalanine (F).

The sequencing results confirmed the successful introduction of the 688 stop codon. Besides, an unpublished single nucleic acid mutation before the stop codon was confirmed in the sequencing alignment. This mutation was inherited from the YFP-STAT3 $_{127\text{-}722}$ and CFP-STAT3 $_{127\text{-}722}$ plasmids and was present in the original STAT3btc clone obtained from Becker *et al*. The single nucleic acid from TTT to TCT does not change the amino acid sequence therefore does not influence the STAT3's structure and biological activities.

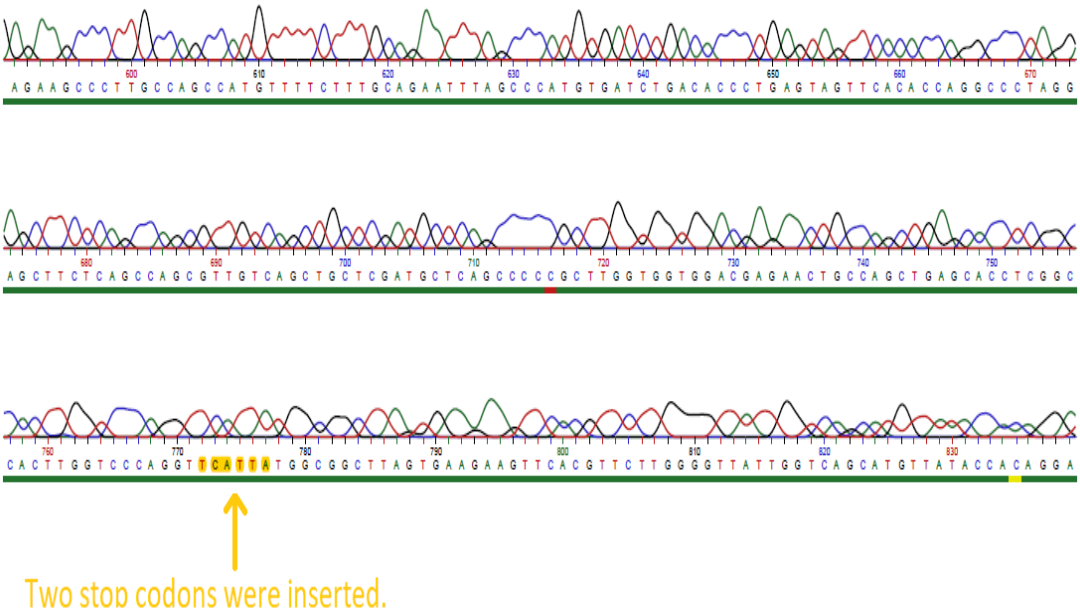


Figure 2.5. There are two stop codons inserted after the codons coding for aa497. This sequence started from T7 term primer and covers 156bp until the 497 stop codons were covered.

According to figure 2.5, 497 stop codons were successfully inserted into the YFP-STAT3 $_{127\text{-}722}$ and CFP-STAT3 $_{127\text{-}722}$ plasmids. The signal of the sequencing is weaker compared to the 688 stop codon sequencing results because 497 stop codons are further from the T7 term primer compared to the 688 stop codons. But the sequences of the stop codons are still within the ‘confident sequencing region’.

In conclusion, four plasmids expressing YFP and CFP-STAT3 $_{127\text{-}688}$ and YFP and CFP-STAT3 $_{127\text{-}497}$ were successfully created. The created plasmids were able to produce YPF and CFP fused STAT3 proteins in bacteria cells under the control of the T7 promoter.

### 2.4.3 Materials preparation

Buffers used during the protein production, extraction and purification are listed in the following form.

| | |
|---|---|
| Extraction buffer | 100mM Tris pH 8.5, 200mM NaCl, 10mM $MgCl_2$, 25% glycerol |
| $CaCl_2$ buffer with glycerol | 100mM $CaCl_2$, 20% glycerol |
| LB media | 25mg/ml Miller or Lennox LB??? |
| IEx buffer A | 25mM Tris pH 8.5 |
| IEx buffer B | 25mM Tris pH 8.5, 1M NaCl |
| 10xSDS tank buffer | 250mM Tris pH8.3, 1.92M Glycine, 10%SDS |
| 1000x Amp | 100mg/ml dissolved in 70% ethanol |
| 1000x Chl | 35mg/ml dissolved in 100% ethanol |
| 1000x Tet | 10mg/ml dissolved in $ddH_2O$ |

The extraction buffer and the $CaCl_2$ buffer with glycerol was autoclaved and stored at -20 ℃ overnight before use. The LB culture were autoclaved and stored at 4℃ before use. The IEx buffers were filtered with 0.2 μM membrane before application. The antibiotic stocks were stored in -20 ℃.

### 2.4.4 The preparation of the Rosetta2 (DE3) competent cells and the XL10-Gold competent cells：

The original stock of Rosetta2 (DE3) competent cells were purchased from Merck and then we produce the second generation from the original Rosetta as our working stocks. The methods of the competent cell preparation are similar for the Rosetta2 (DE3) and the XL10-Gold. One single difference is that in terms of XL10-Gold incubation, we also added tetracycline. The original Rosetta2 (DE3) competent cells were plated on chloramphenicol plate and incubated overnight. Single colonies were selected and incubated in 5ml of the autoclaved LB with chloramphenicol at 37 ℃ overnight. The overnight culture were transferred into 500 ml autoclaved LB with chloramphenicol and incubated again at 37℃ until the $OD_{600}$ of the bacteria culture is about 0.6. The bacteria cells were harvested by centrifuging at 12,450 g for 20 mins. The bacteria pellets were re-suspended in 250 ml of the ice-cold 100 mM $CaCl_2$ solution and incubated on ice for 45 mins. After incubation, the re-suspended bacteria culture were centrifuged again at 12,450 g for 20 mins. The supernatant were discarded and the pellets were re-suspended in 20 ml 100m M CaCl2 with 20% glycerol. The re-suspended

bacteria were aliquoted into small tubes and snap frozen in liquid nitrogen. The frozen competent cells were stored in -80 ℃ freezer.

### 2.4.5 The preparation of the pET32a (+) plasmids expressing the STAT3 truncated proteins

The stock of pET32a (+) STAT3 plasmid DNA was prepared with a Qiagen Maxi prep kit. 5μl of the constructed plasmid (0.5 mg/ml) or 2μl of the previous plasmid stock were mixed with 50μl of the Rosetta2 (DE3) competent cell stock and incubated on ice for 30mins. The incubated mixture was heat-shocked in a PCR machine at 42℃ for 90s and then rested on ice for 2mins. 200μl of the autoclaved LB were added into the heat-shocked mixture and incubated at 37℃ for 45mins. 100μl of the incubated bacteria culture were spread onto the Ampicillin and Chloramphenicol agar plate and incubated at 37℃ overnight. Single colonies from the overnight agar plate were selected and incubated in 5ml autoclaved LB with Amp and Chl at 37℃. Then the 5ml LB was transferred into 500ml autoclaved LB with Amp and Chl and incubated at 37℃ until the $OD_{600}$ of the bacteria culture reached about 0.6. The bacteria culture were harvested by centrifuging at 4500rpm for 20mins. The plasmid purification steps were conducted according to the Qiagen Maxi prep kit. The plasmids were finally eluted in dd$H_2O$ and stored at -20℃.

### 2.4.6 STAT3 mutations were expressed in Rosetta2 (DE3) competent cells

The plasmids coding for each STAT3 mutants were inserted into Rosetta2 (DE3) competent cells through heat shock of the plasmid and the competent cells mixture at 42 ℃ for 90 s in 500 µl thin wall PCR tubes. Before heat shock, the plasmid and the competent cells mixture was incubated on ice for 30 mins. After heat shock, the mixture was incubated on ice again for 2 mins. The ice incubation steps were applied to avoid a sustained elevated temperature which causes competent cell death. After incubation on ice for 2 mins, 200 µl of autoclaved LB was mixed with the cells gently and the tube was incubated at 37℃ for 45mins, shaking at 180rpm. 100 µl of the incubated bacteria culture from the thin wall PCR tube was spread onto LB agar plate with Amp and Chl followed by the incubation. The plates plated with transformed *E. coli* cells were then incubated at 37℃ overnight.

One single colony from the overnight LB agar plate was inoculated into one 5ml autoclaved LB culture. The 5 ml LB culture was incubated at 37 ℃ until OD600 reached about 0.6, 1 ml of the bacteria culture was then transferred into a 500ml autoclaved LB culture for overnight incubation at 27 ℃, 180rpm. During the incubation, both Amp and Chl were added throughout.

The induction of the STAT3 protein production in the *E. coli* cells was started after adding IPTG. 1ml of 1M IPTG was pre-mixed with 500 µl of 1000x Amp, 500µl of 1000x Chl and 500ml of pre-chilled autoclaved LB. The LB, antibiotics and IPTG mixture was then added into the 500 ml overnight bacteria culture to start induction. The induction culture was incubated at 21℃, 180rpm for 8 hrs. After induction, the bacteria culture were harvested by centrifuging at 4500 g, 4℃, 30 mins. The supernatants were carefully discarded and the bacteria pellets were stored at -20 ℃ overnight.

### 2.4.7 The STAT3 proteins were extracted from the Rosetta2 (DE3) competent cells

The overnight frozen bacteria pellets were first thaw on ice for about 30 mins and then re-suspended in 20 ml Extraction buffer A (100 mM Tris pH 8.5, 200 mM NaCl, 10 mM $MgCl_2$, 25% glycerol, 20 mM PMSF, 10 mM benzamidine, 10 mM DTT and 1x HALT protease inhibitor cocktail) and then mixed with 20 ml Extraction buffer B (100 mM Tris pH 8.5, 200 mM NaCl, 10 mM $MgCl_2$, 25% glycerol, 1 mg/ml Lysozyme). Buffer A contains protease inhibitors and reducing reagent while buffer B contains lysozyme that helps breaking the bacteria cells. The re-suspended mixture was then incubated at room temperature of 5 mins to allow lysozyme to interact with the bacteria. Sonication was applied to further break up the bacteria cells. The re-suspended bacteria solution was sonicated at 16 unit for 1 min with 1 min pause for 5 times after incubation. Next, the sonicated bacteria culture was centrifuged at 21000 rpm, 4 ℃ for 1 hr to separate the soluble protein and insoluble cell components. The soluble STAT3 proteins in the supernatant was then precipitated by adding 4℃ saturated ammonium sulphate solution. For non-labelled STAT3 proteins, 35% of saturation of the ammonium sulphate solution was used to precipitate out the STAT3 proteins while for fluorescent protein labelled STAT3 proteins, 40% of saturation of the

ammonium sulphate solution was applied. The precipitated STAT3 proteins were stored in -20 ℃ freezer for future purification.

### 2.4.8 The STAT3 proteins were purified with Ion Exchange chromatography

A simple one-step ion exchange chromatography was applied to purify the truncated STAT3 proteins. The purified STAT3 proteins were suitable to use in most of the assays mentioned in this project. The frozen protein pellets were first thawed on ice and dissolved into 50-100 ml the loading buffer (25 mM Tris pH8.5, 3 mM DTT). The re-dissolved protein solution were loaded to HiTrapQFF columns (5ml) with 1ml/min speed at 4℃. The HiTrapQFF columns were pre-washed according to its provided protocol with 1M NaOH and 2M NaCl and equilibrated with 25mM Tris pH8.5. Since the HiTrapQFF columns were re-used, each column was only used for one STAT3 truncated protein to avoid cross contamination. Two liquid phases were prepared to create the salt gradient in the ion exchange chromatography: elution buffer A (25 mM Tris pH 8.5, 1 mM DTT) and elution buffer B (25 mM Tris pH 8.5, 1 M NaCl, 1 mM DTT). The STAT3 proteins usually started to elute when the liquid phase contains 90 mM NaCl and kept eluting in the next 10 ml (1 ml/min). The eluted STAT3 proteins were collected in 96 well sample collectors with 1 ml of the protein solution in each well. The fractions containing purified STAT3 proteins were either stored at 4℃ or precipitated with 50% of the saturated ammonium sulphate solution and then stored at -20℃.

### 2.4.9 The IEx purified STAT3 proteins were further purified with size exclusion chromatography

Size exclusion chromatography (also called gel filtration) were applied to increase the purity of the protein product to 99.99%. The column used in this thesis were Hiload 16/60 Superdex 200 (240ml). The concentration of the loaded protein needs to be higher than 1 mg/ml in order to insure the $A_{280}$ signal of the STAT3 protein is easily detected during size exclusion chromatography. The STAT3 protein was eluted with 25 mM Tris pH 8.5, 100 mM NaCl, 10 mM $MgCl_2$. The size exclusion was conducted at 0.6 ml/min.

### 2.4.10 SDS-PAGE gel

10% (w/v) polyacrylamide gel (pH 8.8) was used as resolving gel and on top of it is 5% (w/v) polyacrylamide gel (pH 6.8) as stacking gel. 22.5μl of each sample was mixed with 7.5 μl of the 4x NuStain ready-made sample buffer. The mixture were heated at 90℃ for 10mins before loading. 15 μl of the heated sample were loaded into each well. The gel was run at 40 volts for 45mins until the protein reach the resolving gel and then run at 100 volts for 1 hour. After running, the gels were stained by commasive blue stain buffer (45% Methanol, 10% Acetic Acid Glacial, 1g coomassie blue) and destained with destain buffer (10% Methanol, 7% Acetic Acid Glacial).

## 2.6 Result- Protein production and extraction

### 2.6.1 Extraction of the STAT3 truncated proteins:

The extraction and purification of STAT3 proteins were analysed by SDS polyacrylamide gel electrophoresis (SDS-PAGE). Seven STAT3 truncated proteins were produced and purified: STAT3 $_{127\text{-}497}$, YFP-STAT3 $_{127\text{-}688}$, YFP-STAT3 $_{127\text{-}497}$, CFP-STAT3 $_{127\text{-}688}$, CFP-STAT3 $_{127\text{-}497}$, CFP-STAT3 $_{127\text{-}722}$ and CFP-STAT3 $_{127\text{-}722}$.

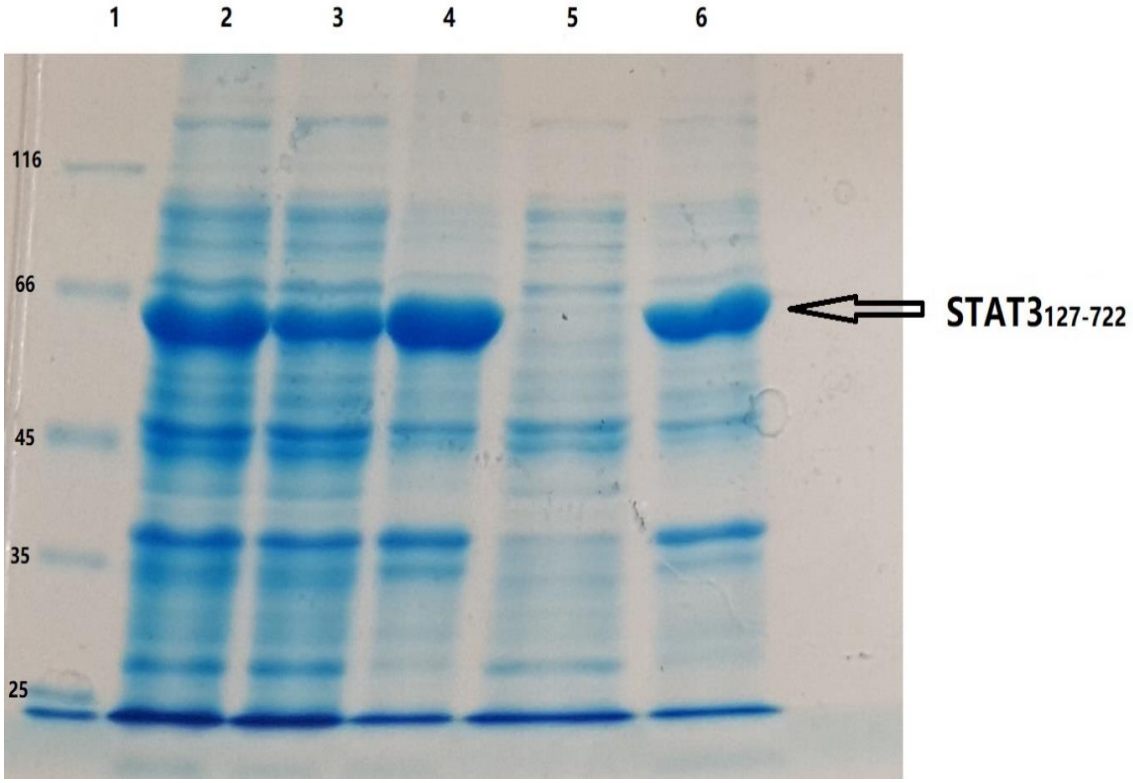


Figure 2.6. Extraction of STAT3 $_{127\text{-}722}$ protein from Rosetta2 (DE3) cells. Well 1 is the protein molecular weight marker. Well 2 contains the sample of bacteria culture after sonication. Well 3 contains the sample of supernatant containing soluble proteins from the bacteria culture. Well 4 contains the pellets containing unsoluble materials of the broken bacteria cells. Well 5 is the supernatant from the centrifuged protein solution after adding ammonium sulphate solution and well 6 contains the pellets containing precipitated protein.

Figure 2.6 indicates that the STAT3 127-722 protein was successfully produced in the Rosetta2 (DE3) competent cells. About 20% of the produced STAT3 protein were soluble in the bacteria supernatant while 80% of the STAT3 protein precipitated with un-soluble bacteria protein. This maybe caused by the low solubility of the STAT3 truncated protein or the bacteria cell produced a certain amount of missfolded protein that didn't dissovel in the Tris buffer. After incubation with 35% of the saturated ammonium sulphate, 90% of the soluble STAT3 proteins were precipitated. Comparing to the bacteria supernatant, the purity of the precipitated STAT3 protein increased about 20%. Furthermore, the precipitated STAT3 proteins can be

stored at -20℃ and preserved for a month while the STAT3 protein in bacteria supernatant would lose their biological activity within three days. Therefore, 35% of the ammonium sulphate not only increased STAT3 purity after extration but also provided a longer preservation method for the purified STAT3 protein.

The STAT3 $_{127\text{-}688}$ protein was extracted with the same method. Although the concentration of the STAT3 $_{127\text{-}688}$ protein in the *E. coli* cells are lower than the STAT3 $_{127\text{-}722}$ protein, the STAT3 protein band on the SDS-PAGE is still the most intense band comparing to other bacteria proteins.

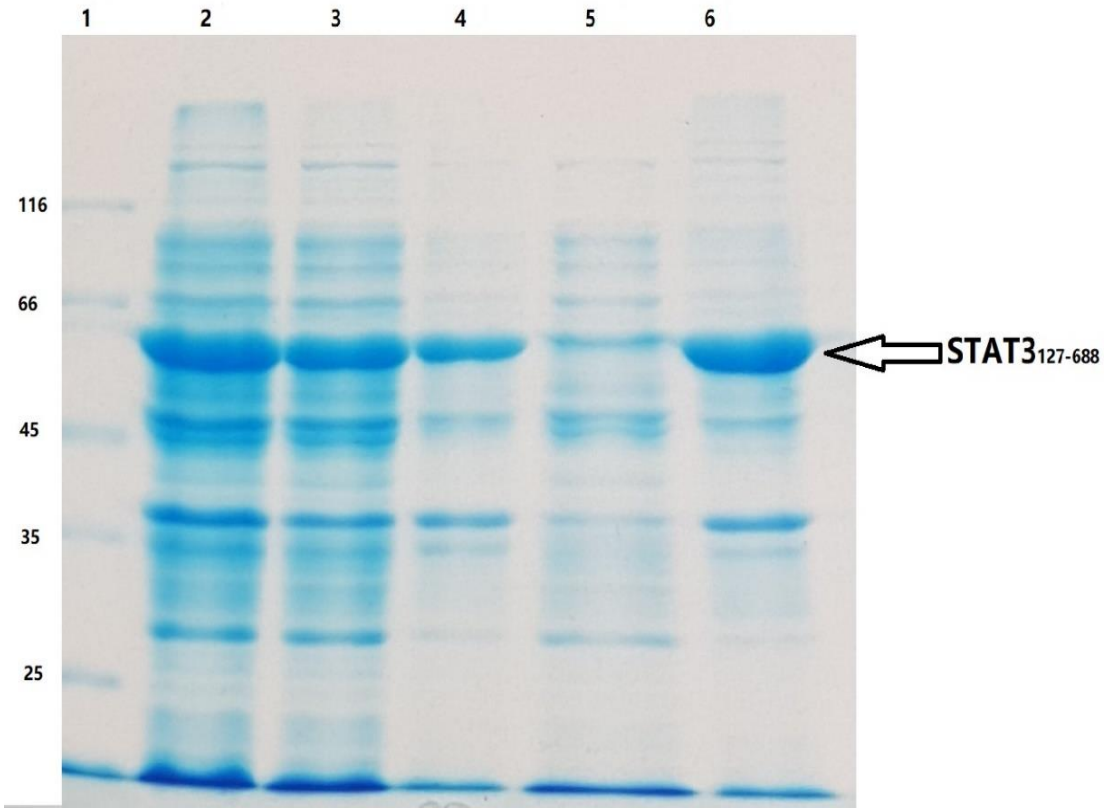


Figure 2.7. SDS-PAGE gel shows that STAT3 127-688 portein was succesfully produced extracted. Well 1 to 6 contains: unstained protein molecular weight marker, sample taken after sonication, supernatant of the broken bacteria, pellet of the broken bacteria, supernatant after the protein precipitated with ammonium sulphate and pellets of the protein precipitated by ammonium sulphate respectively.

The STAT3 $_{127\text{-}688}$ protein was successfully produced in the Rosetta2 (DE3) competent cells. According to figuer 2.6.1-2, over 60% of the STAT3 $_{127\text{-}688}$ protein was soluble in the bacteria supernatant. 90% of the soluble STAT3 proteins were precipitated by 35% of the saturated ammonium sulphate. The total amount of the STAT3 $_{127\text{-}688}$ protein extracted in the ammonium sulphate precipitation is similar to the amount of the STAT3 $_{127\text{-}722}$.

However, the amount of the shortest construct STAT3 $_{127\text{-}497}$ produced in the Rosetta2 (DE3) competent cells was dramatically decreased comparing to the other two STAT3 truncated proteins. The production of the STAT3 $_{127\text{-}497}$ protein band is not very obvious in the SDS-PAGE gel.

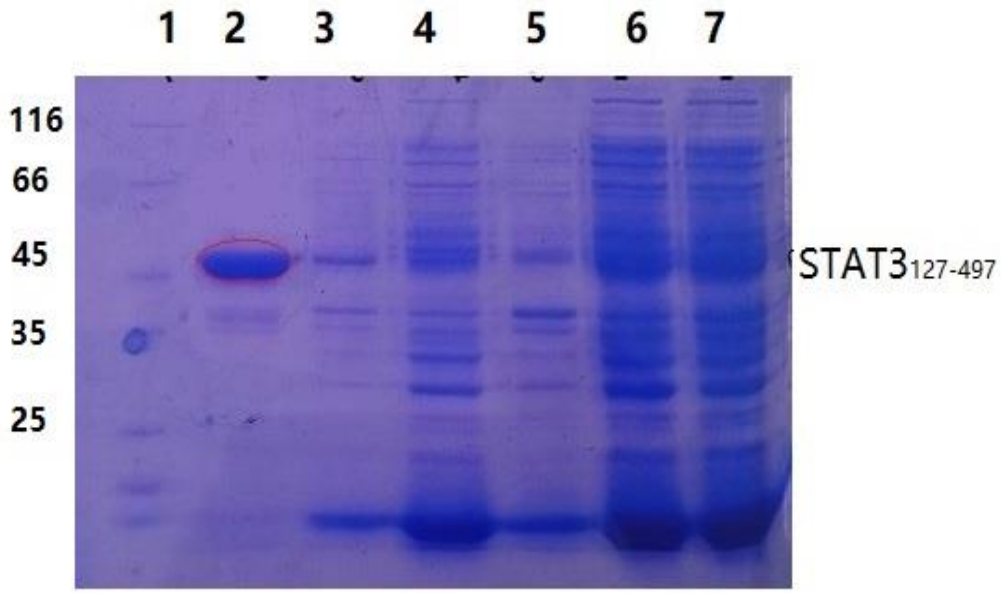


Figure 2.8. SDS-PAGE gel analysing samples taken from STAT3 $_{127\text{-}497}$ extraction processes. Well 1 is the unstained protein molecular weight marker. Well 2 is a marker of purified and concentrated STAT3 $_{127\text{-}497}$ protein. Well 3 is the STAT3 $_{127\text{-}497}$ protein precipitated with 35% of the saturated ammonium sulphate. Well 4 is the supernatant after the ammonium sulphate precipitation centrifugation. Well 5 contains the sample of the insoluble bacteria components. Well 6 contains the supernatant from centrifuging the sonicated bacteria culture. Well 7 contains the sample of the sonicated bacteria culture.

It is very hard to calculate the percentage of the soluble STAT3 $_{127\text{-}497}$ protein produced in the Rosetta2 (DE3) competent cell according to figure 2.8 since the STAT3 127-497 band is not obvious in well 7 (the sample after sonication) and well 6 (the bacteria supernatant). Fortunately, after precipitated by 35% of the saturated ammonium sulphate, the STAT3 $_{127\text{-}497}$ band showed up since most of the bacteria protein contaminants were still soluble. A purified and concentrated STAT3 aggregated solution was added in well 2 as a marker to indicate the position of the STAT3 $_{127\text{-}497}$ protein band in the SDS-PAGE.

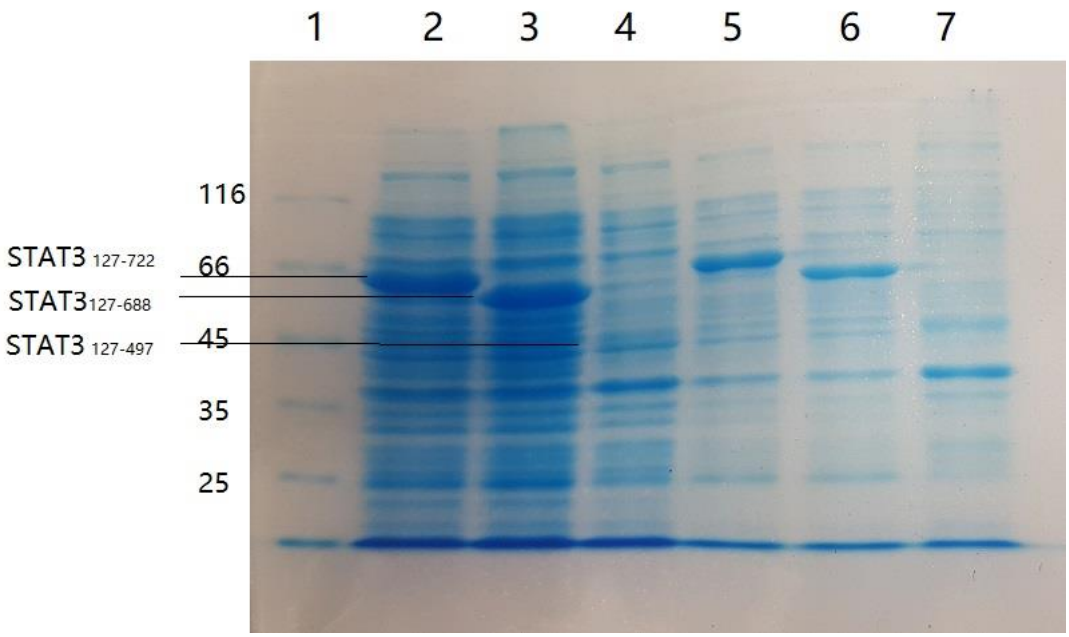


Figure 2.9. A comparison of the three STAT3 mutants. Well 1 contains the molecular weight marker. Well 2 contains the supernatant of the STAT3 $_{127\text{-}722}$. Well 3 contains the supernatant of the STAT3 $_{127\text{-}688}$. Well 4 contains the supernatant of STAT3 $_{127\text{-}497}$. Well 5 contains the ammoniums sulphate precipitated protein sample of the STAT3 $_{127\text{-}722}$. Well 6 contains the ammoniums sulphate precipitated STAT3 $_{127\text{-}688}$. Well 7 contains the ammoniums sulphate precipitated STAT3 $_{127\text{-}497}$.

The three different STAT3 truncated proteins are compared in figure 2.9. By comparing the three unlabelled STAT3 mutants, we noted that the expression of the STAT3 $_{127\text{-}722}$, STAT3 $_{127\text{-}688}$ truncated proteins were clearly visible on the SDS-PAGE gels but the over-expression of STAT3 $_{127\text{-}497}$

truncated protein was not so obvious on the SDS-PAGE gel. Different STAT3 mutants have different expression rate in the same *E. coli* competent cell. Truncated STAT3 proteins with longer amino acid sequence have higher expression rate in the *E. coli* cells. With our production and purification method, 1 litre bacteria culture with OD600 is approximately 1.0 can produce 10g of the STAT3 $_{127\text{-}722}$, 8g of the STAT3 $_{127\text{-}688}$ and 1g of the STAT3 $_{127\text{-}497}$ after ion exchange chromatography.

Since the level of STAT3 $_{127\text{-}497}$ protein expression is very low in Rosetta2 (DE3) competent cells, an experiment comparing the expression rate of STAT3 $_{127\text{-}497}$ in induced and non-induced bacteria culture was conducted.

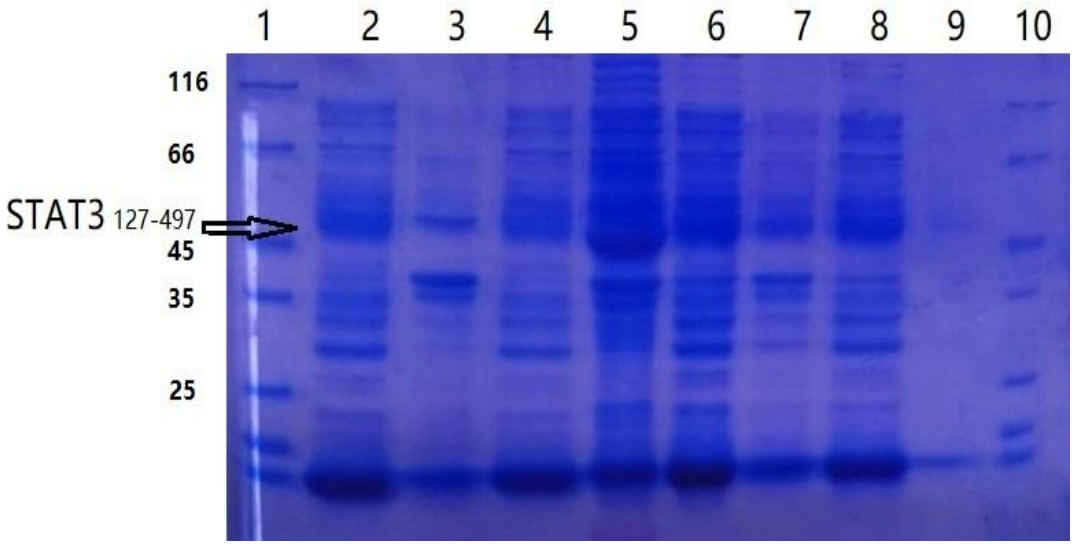


Figure 2.10. SDS-PAGE gel picture comparing the STAT3 $_{127\text{-}497}$ production in induced and non-induced *E. coli* cells. Well 1 and well 10 are unstained protein molecular weight markers. Well 2 contains the supernatant of the sonicated non-induced bacteria. Well 3 contains thepellets of the sonicated non-induced bacteria. Well 4 is the supernatant of the ammoniums sulphate precipitated non-induced bacteria protein. Well 5 contains thepellets of the ammonium sulphate precipitated non induced bacteria protein. Well 6 contains samples from the induced *E. coli*. Well 7 contains the supernatant of the induced bacteria. Well 8 contains the ammonium sulphate precipitate of the induced bacteria. In well 9, the sample was not successfully loaded in this gel.

Shown on figure 2.10, the bands of the STAT3 $_{127\text{-}497}$ in the induced samples are more enhanced compared to the bands of the protein in the non-induced samples. Therefore we confirm that the truncated STAT3 protein- STAT3 $_{127\text{-}497}$ can be expression in Rosetta2 (DE3) competent cells. According to figure 2.10, the level of expression of STAT3 $_{127\text{-}497}$ increased about 50% after induction with IPTG. Although the ammonium sulphate precipitated sample in well 9 was not successfully loaded, the amount of the STAT3 $_{127\text{-}497}$ protein can be calculated from other samples.

All STAT3 truncated proteins were successfully expressed in Rosetta2 (DE3) competent cells with IPTG induction. The molecular structure of the STAT3 $_{127\text{-}722}$ and the STAT3 $_{127\text{-}688}$ proteins were confirmed with X-ray crystallography in previous research [248, 254]. However, the folding of the short STAT3 truncated protein, STAT3 127-497, have not been tested with X-ray crystallography yet.

Fluorescent proteins were fused with the STAT3 mutants to allow the application of different assays. Fused STAT3 proteins with yellow fluorescent protein (YFP) attached to N-terminal of the STAT3 mutants were used in the PEMSA assays. Cyan fluorescent proteins (CFP) were fused to the N-terminal of the STAT3 mutants for the application of FRET assays. C-terminal fluorescent labelled STAT3 mutants were synthesised to optimise the FRET assays. Since there are only a few amino acid differences between CFP and YFP, there is no observed difference between the CFP labelled STAT3s and the YFP labelled STAT3s on an SDS-PAGE gel. Hence only one of the SDS-PAGE photos is displayed in the result section representing both YFP and CFP fused STAT3 truncated proteins.

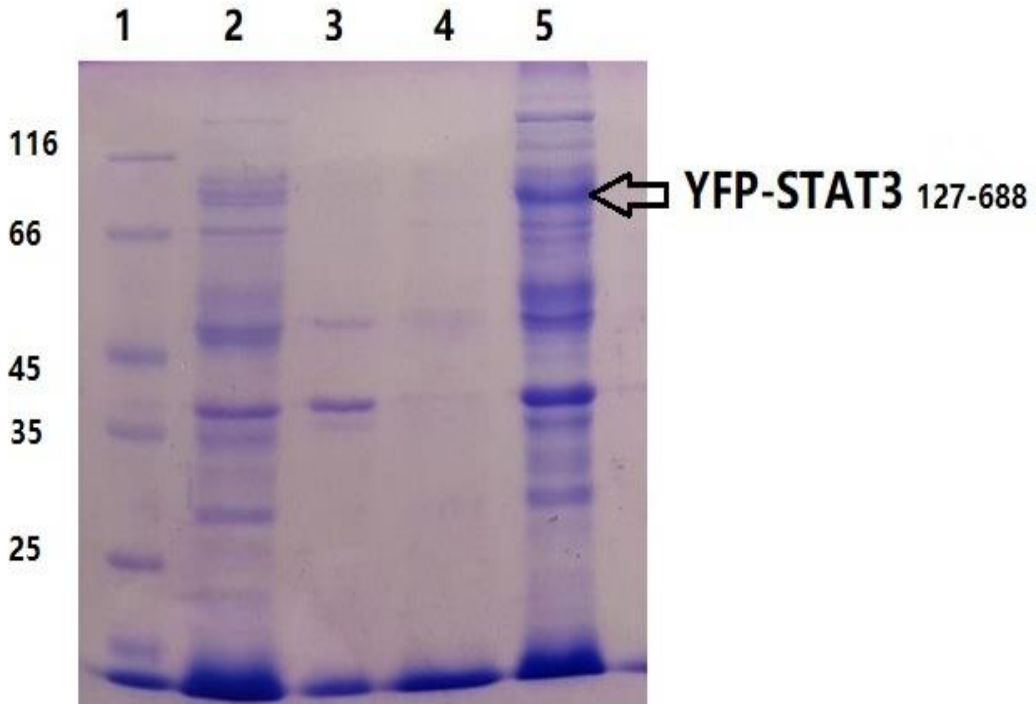


Figure 2.11. SDS-PAGE gel showing the success of extraction of the YFP-STAT3 $_{127\text{-}688}$ mutant. Well 1 contains unstained protein molecular weight marker. Well 2 contains supernatant of the sonicated bacteria. Well 3 is the pellet sample of the bacteria particles. Well 4 is the supernatant sample after adding saturated ammoniums sulphated solution. Well 5 contains samples of the protein precipitated by 45% of the saturated ammonium sulphate.

According to figure 2.11, most of the soluble proteins including the desired YFP-STAT3 $_{127\text{-}688}$ mutant in the bacteria extract was precipitated by 40% of the saturated ammonium sulphate. Comparing the samples in the supernatant of the bacteria extract and ammonium sulphate precipitated pellet, the proportion of YFP-STAT3 $_{127\text{-}688}$ protein of the total protein is higher in the ammonium sulphate pellet sample. Therefore, ammonium sulphate precipitation process can slightly increase the purity of the extracted truncated STAT3.

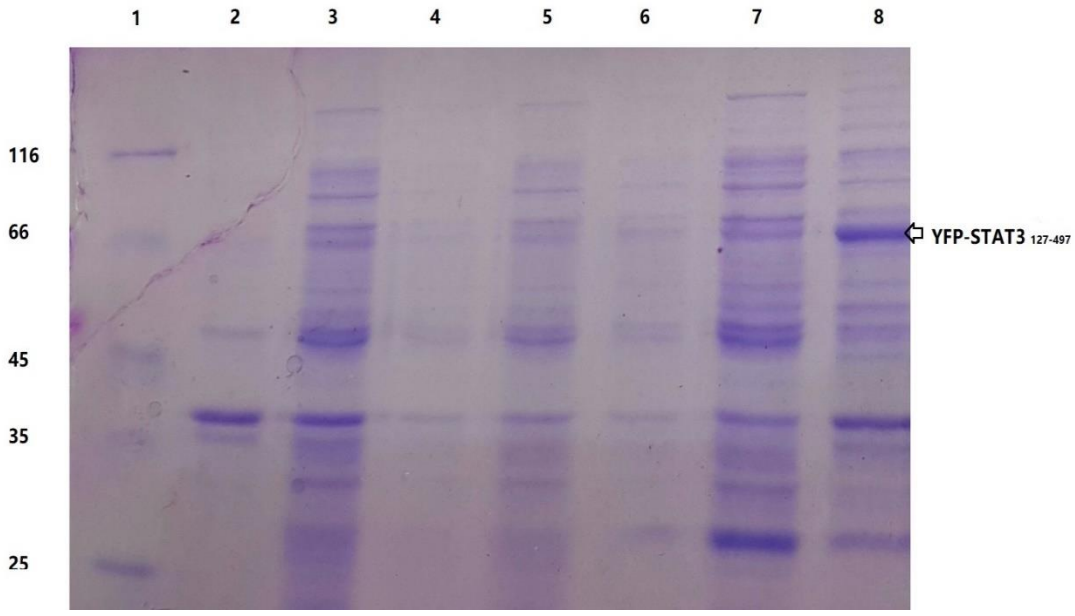


Figure 2.12. SDS-PAGE gel indicating that the YFP-STAT3 127-497 was expressed in *E. coli* cells. Well 1 is the unstained protein molecular weight marker. Well 2 is the pellets of the sonicated bacteria. Well 3 is the supernatant of the sonicated bacteria. Well 4 and 5 are the pellets and the supernatant of the protein precipitated by 20% of the saturated ammonium sulphate. Well 6 and 7 are the pellets and the supernatant of the protein precipitated by 30% of the saturated ammonium sulphate. Well 8 is the pellet of the protein precipitated by 40% of the saturated ammonium sulphate.

Figure 2.12 confirms the success of the YPF-STAT3 $_{127\text{-}497}$ expression in Rosetta2 (DE3) competent cells using the same method as the YFP-STAT3 $_{127\text{-}688}$ mutant. In the protein pellets of 20% and 30% ammonium sulphate precipitations, little STAT3 protein were precipitated. The amount of the YFP-STAT3 127-497 in the 20% and 30% ammoniums sulphate precipitations is too low to form a clear band on the SDS-PAGE. About 90% of the YPF-STAT3 127-497 protein in the bacteria extract supernatant was precipitated with 40% of the saturated ammoniums sulphate. Compared to YFP-STAT3 $_{127\text{-}688}$ protein, less YFP-STAT3 $_{127\text{-}497}$ were expressed in the *E. coli* cells.

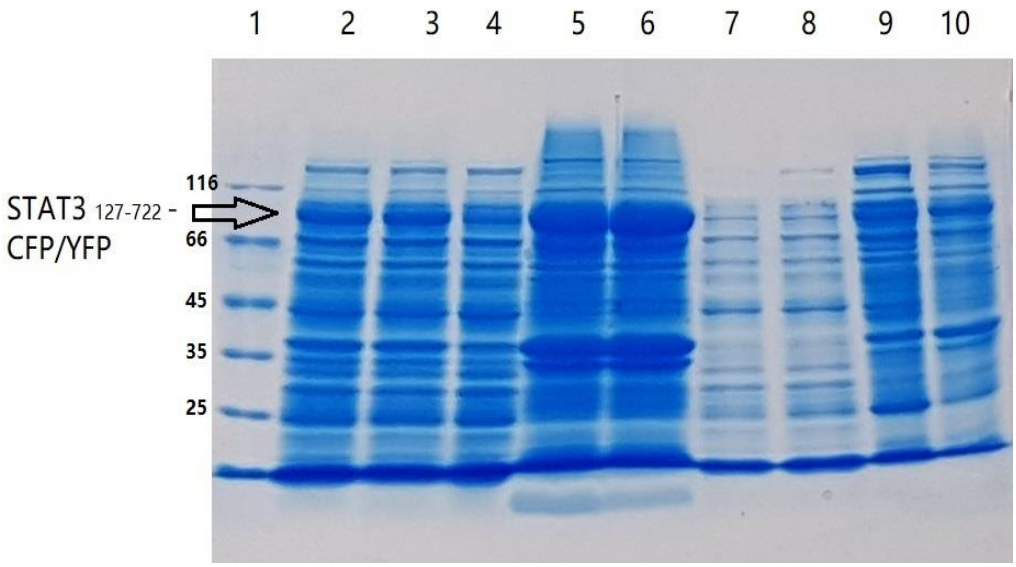


Figure 2.13. The synthesised STAT3 $_{127\text{-}722}$-YFP and STAT3 $_{127\text{-}722}$-CFP were successfully expressed in Rosetta2 (DE3) competent cells. Well 1 is the unstained protein molecular weight marker. Well 2 and 3 contain the samples of the sonicated bacteria culture of the STAT3 $_{127\text{-}722}$-CFP and the STAT3 $_{127\text{-}722}$-YFP respectively. Well 4 is the supernatant of the STAT3 $_{127\text{-}722}$-CFP. Well 5 and Well 6 are the pellets from the centrifuged bacteria culture after sonication containing STAT3 $_{127\text{-}722}$-CFP (in well 5) and STAT3 $_{127\text{-}722}$-YFP (in well 6). Well 7, 8, 9, 10 are samples taken after centrifugation of the ammonium sulphate precipitated protein mixtures, while 7 and 8 are the supernatant of STAT3 $_{127\text{-}722}$-CFP and the STAT3 $_{127\text{-}722}$-YFP and 9 and 10 are the precipitated STAT3 $_{127\text{-}722}$-CFP and the STAT3 $_{127\text{-}722}$-YFP proteins.

As shown in figure 2.13, the amount of the STAT3 mutated proteins produced in the *E. coli* cells is about 13% of the total bacteria protein. The enhanced production of the STAT3 $_{127\text{-}722}$-CFP and the STAT3 $_{127\text{-}722}$-YFP proteins is obvious in the SDS-PAGE gel. However, compared to the N-terminal fluorescent protein fused STAT3 mutants, the C-terminal fluorescent protein fused STAT3 mutants are less soluble. About 90% of the STAT3 127-722 CFP/YFP protein precipitated in the bacteria pellets after sonication. Little STAT3 proteins were still soluble in the supernatant. After adding 40% of the saturated ammoniums sulphate, 98% of the bacteria proteins were precipitated together with the STAT3 proteins. Comparing the sample of the

supernatant and the ammonium sulphate pellet, we conclude that the ammonium sulphate precipitation does not increase any purity of the produced STAT3 mutant. However, the ammonium sulphate precipitation step canbe used to extend the life time of the purified STAT3 proteins under -20℃.

### 2.6.2 Result-Protein purification

All STAT3 mutants were purified in Ion-exchange (IEx) chromatography. After the IEx purification process, the STAT3 proteins can be purified to 80%-99% depending on the different mutations. During the IEx purification, the absorbance at 280nM (A280) of the eluted solution was constantly monitored by the FPLC machine but the exact protein concentration of each fraction was confirmed by the Nanodrop. Samples from the A280 peaks were analysed by SDS-PAGE.

**Protein purification of the STAT3 $_{127\text{-}497}$ truncated protein and its derivatives**

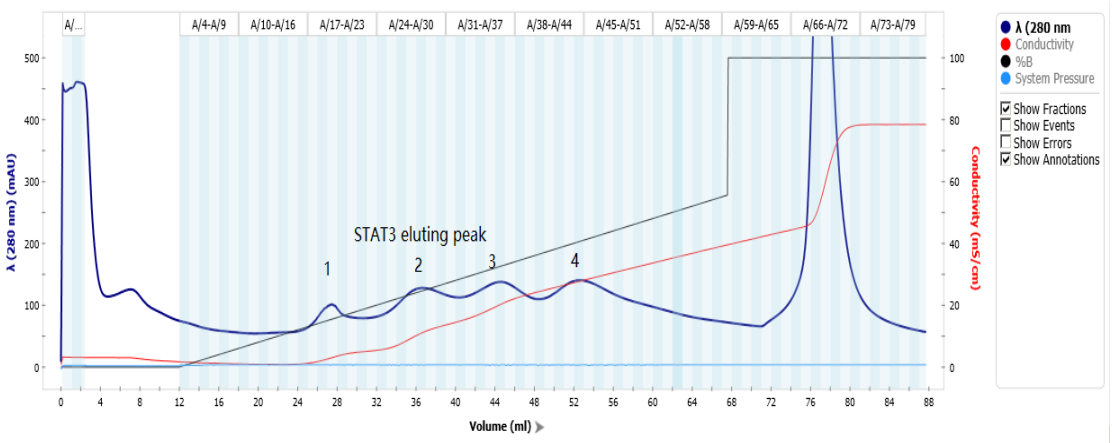


Figure 2.14. An example of the IEx chromatogram of the STAT3 $_{127\text{-}497}$ mutant. Each blue column represent one collection fraction (1 ml). The first three fractions collections were the sample of the loaded protein solution. The %B represent the increasing volume of buffer B (25 mM Tris pH8.5, 1 M NaCl) by the FPLC machine. The %B were set to increase from 0% to 60% in 60mins, and then the columns were washed by 100% buffer B for 20 mins.

Figure 2.14 shows an example of the chromatogram plotted by the FPLC machine. The UV sensor of the machine not only measures the absorbance

at 280nm but there is also a cell that measures the conductivity. The conductivity is usually used to track the actual rather than predicted salt concentration in the current eluting fraction. The samples of the fractions from each peak were analysed with SDS-PAGE. The STAT3 mutants usually elute when the conductivity reach 9 ms/cm, which corresponds to approximately 20% B. Unfortunately, the chromatogram of other purifications can not be provided due to the limited access of the lab during the pandemic.

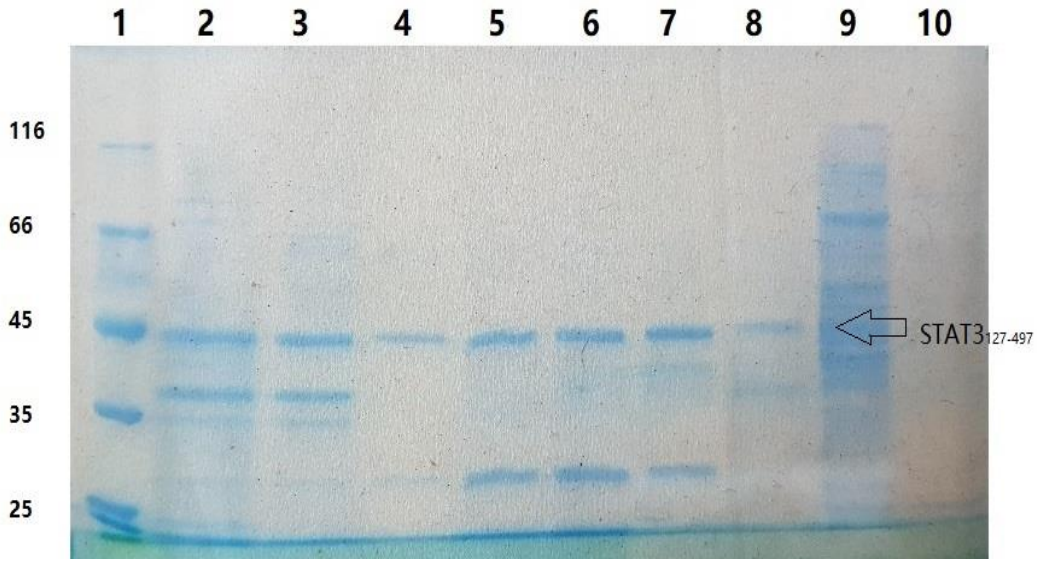


Figure 2.15. Ion exchange purification of the STAT3 $_{127\text{-}497}$ protein samples analysed by SDS-PAGE. Well 1 is the unstained protein molecular weight marker. Well 2 and 3 are samples from peak 1 and refer to fractions 27, 28 in figure 2.14. Well 4, 5, 6, 7 contain samples from peak 2 refer to fractions 35, 36, 37, 38 in figure 2.14. Well 8 is the sample from peak 3, fraction 45 and well 9 is the sample from peak 4, fraction 53. Well 10 is the sample from the wash with 1 M NaCl, 25mM Tris pH8.5 in fraction 78.

According to figure 2.14 and figure 2.15, the STAT3 $_{127\text{-}497}$ protein elutes from several peaks during the IEx purification. In different peaks, the STAT3 $_{127\text{-}497}$ protein elutes with different bacteria protein contaminants at different concentration. In the peak 2, the STAT3 127-497 protein is most concentrated and eluted with a 20kDa contaminant protein which can be easily purified from by size exclusion chromatography. In the peak 1, the

contaminant protein's molecular weight is too close to the STAT3 127-497 mutant therefore hard to be purified from. In the peak 3 and peak 4, the concentration of the desired STAT3 protein is too low thus increased difficulty for further purification. When the column was washed with 1M NaCl, 25mM Tris pH8.5 buffer, there was no STAT3 protein washed off, indicating that the STAT3 elution volume was sufficient to elute all STAT3 bound to the column. There is a band in the SDS-PAGE wash sample because the high absorbance shown in the wash peak was caused by the degraded small peptide and free amino acids. STAT3 $_{127\text{-}497}$ is able to be purified up to 90% by size exclusion chromatography.

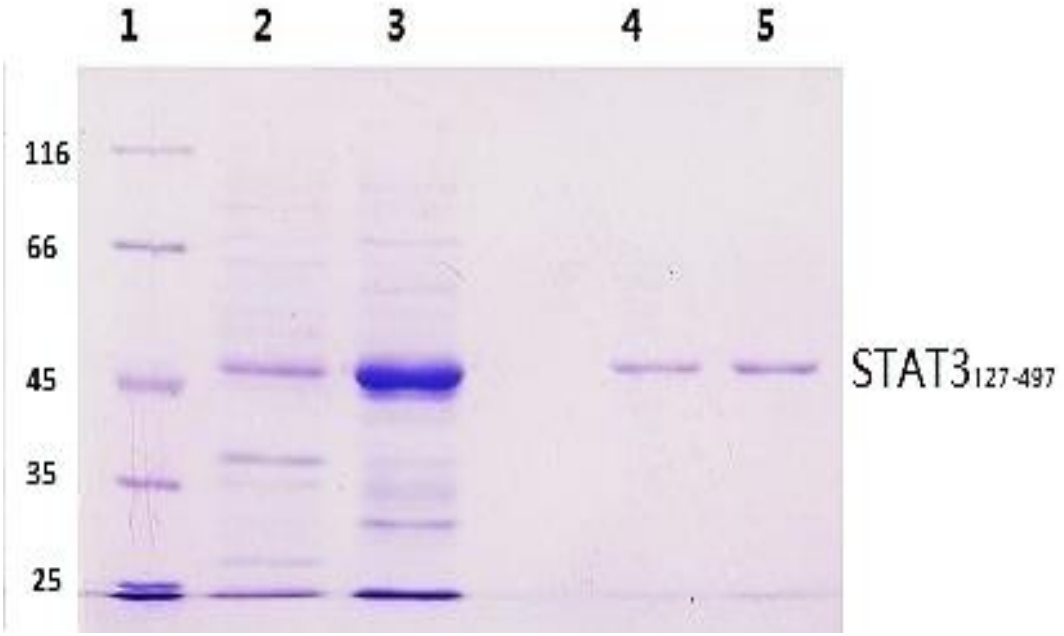


Figure 2.16. SDS-PAGE sample showing the success of the STAT3 $_{127\text{-}497}$ purification by size exclusion after IEx chromatography. Well 1 isprotein molecular weight marker. Well 2 is the loaded protein for IEx purification. Well 3 is the concentrated protein after IEx purification. Well 4, 5 are purified STAT3 $_{127\text{-}497}$ protein by the size exclusion chromatography.

Figure 2.16 indicates that with application of the size exclusion chromatography, the STAT3 $_{127\text{-}497}$ protein can be purified to 90% pure. The purified protein solution only contains STAT3 $_{127\text{-}497}$ protein and small molecular weight (less than 10kDa) protein contaminants. Any small

molecular weight protein contaminant should be able to be purified easily with 10,000 MWCO membrane centrifugation. However, during the experiment, we discovered that the STAT3 truncated proteins aggregate during centrifugation. Over 60% of the purified STAT3 proteins will aggregate and lose their activity especially for the STAT3 $_{127\text{-}497}$ mutant. In this thesis, the STAT3 $_{127\text{-}497}$ protein was used in the fluorescent polarisation assay which would be described in the later chapter. It is not necessary to purify the STAT3 protein to 90% pure in the fluorescent polarisation assay. Therefore, the size exclusion method of purification is only shown as a future improvement method if researchers would like to apply the STAT3 protein in an assay with high protein purity requirement.

Among all STAT3 mutants, the STAT3 $_{127\text{-}497}$, YFP-STAT3 $_{127\text{-}497}$ and CFP-STAT3 $_{127\text{-}497}$ truncated proteins are the most 'problematic' truncated STAT3 proteins. The expression rate of these three proteins are only about 1mg/L in the *E. coli* cells. Therefore, it is also more difficult to be purified from other bacterial proteins.

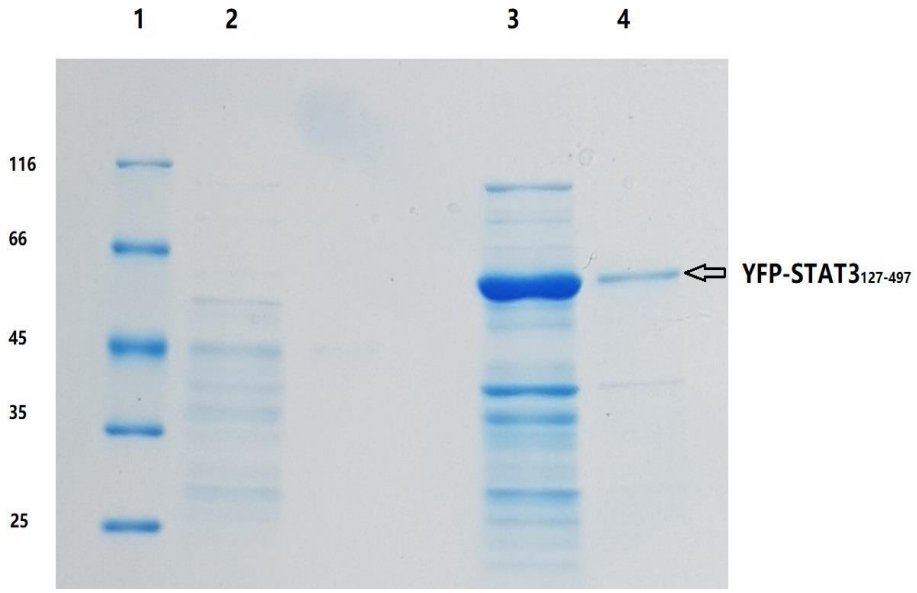


Figure 2.17. SDS-PAGE indicating that the YFP-STAT3 $_{127\text{-}497}$ is successfully purified by IEx purification. Well 1 is the unstained protein molecular weight marker. Well 2 contains proteins washed off the column by 25 mM Tris pH8.5. Well 3 and well 4 are the purified YFP-STAT3 $_{127\text{-}497}$ in two of the observed A280 peaks.

Figure 2.17 confirms that the YFP N-terminal labelled short STAT3 truncated protein can also be purified with IEx chromatography. The purity of the protein increased to 80% after purification. The YPF-STAT3 $_{129-497}$ were eluted in two of the A280 peaks. In peak 1, the YFP-STAT3 $_{127-497}$ was about 70% pure while in peak 2 the YFP-STAT3 127-497 was about 90% pure. However, the YFP-STAT3 127-497 protein eluted in peak 1 was much more concentrated compared to the elution in peak 2. Therefore, proteins from peak 1 was used in PEMSA assays discussed later since the PEMSA assay does not require high protein purity but requires the final protein concentration to be more than 4.5µM. The SDS-PAGE test was conducted after each purification to check the purity of the STAT3 proteins and to select the desired IEx fractions containing STAT3 protein to use in the *in vitro* assays.

**Purification of the fluorescent labelled STAT3 $_{127-722}$ and STAT3 $_{127-688}$**

The STAT3 $_{127-722}$ and STAT3 $_{127-688}$ and their fluorescent protein labelled mutants was purified to 99% pure maximum after the IEx purification step. The IEx purified YFP/CFP-STAT3 $_{127-722}$ and YFP/CFP-STAT3 $_{127-688}$ proteins were used in the PEMSA and FRET assays.

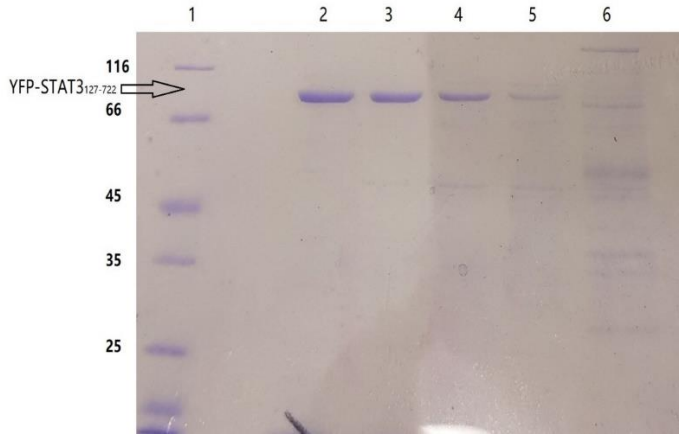


Figure 2.18. SDS gels of the IEx purification of the YFP-STAT3 $_{127-722}$ mutant. Well 2 to 5 contain samples from the STAT3 elution peak. Well 2, 3 contains 99% pure YFP-STAT3 $_{127-722}$ protein. Well 4 contains 90% pure YFP-STAT3 $_{127-722}$ protein. Well 5 only contains 50% of the desired STAT3 mutant. Well 6 is the sample of the protein washed off with 1M NaCl, 25mM Tris pH8.5.

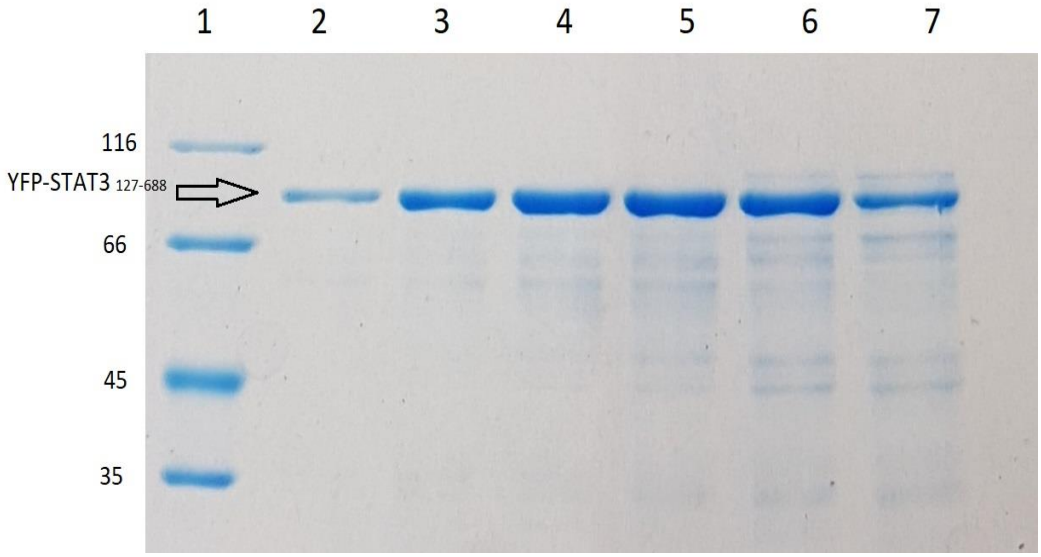


Figure 2.19. SDS-PAGE of the samples from different IEx purification fractions containing purified YFP-STAT3 $_{127\text{-}688}$. In well 1 and well 2, the purity of the YFP-STAT3 $_{127\text{-}688}$ reached 99%. From well 4 to well 7, the purity of the YFP-STAT3 $_{127\text{-}688}$ is decreasing as the contaminant bacteria proteins were eluting with the increasing salt concentration in the liquid phase.

Figure 2.18 and figure 2.19 confirm that the YFP/CFP-STAT3 $_{127\text{-}722}$ and the YFP/CFP-STAT3 $_{127\text{-}688}$ proteins produced in *E. coli* can be purified to 90% pure with IEx chromatography. The purification of the unlabelled STAT3 $_{127\text{-}722}$ and STAT3 $_{127\text{-}688}$ mutants have been optimised by previous research [248, 254]. IEx chromatography is sufficient for purification of the STAT3 truncated proteins for PEMSA, FRET and FP applications.

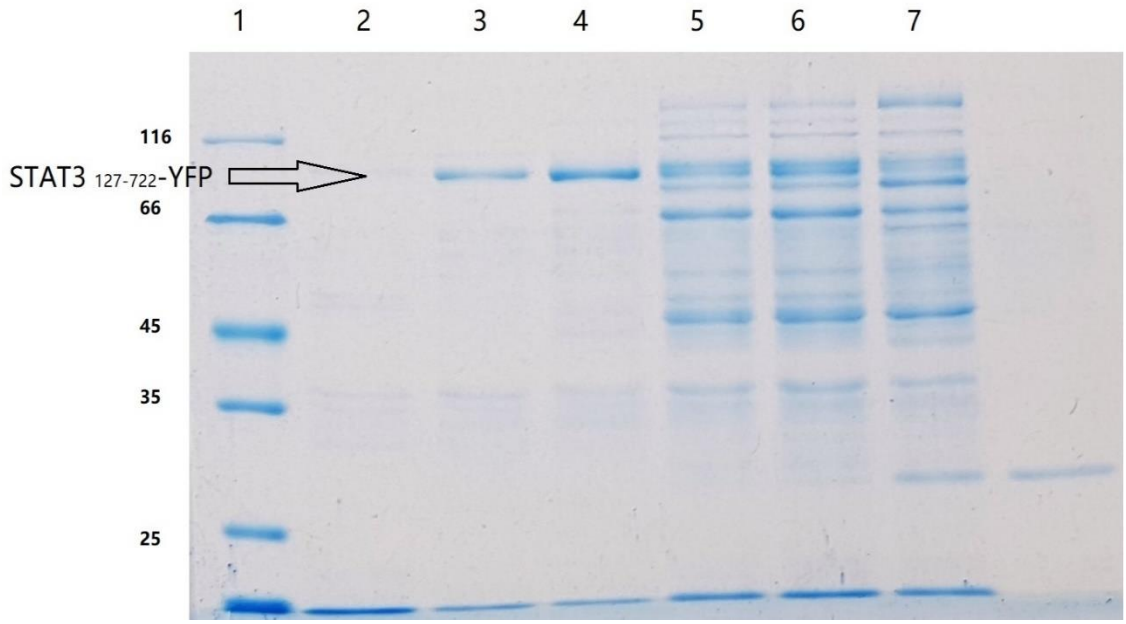


Figure 2.20. SDS-PAGE indicates that the STAT3 $_{127\text{-}722}$-YFP successfully purified in well 3 and well 4. Well 1 is the unstained protein molecular weight marker. Well 2, 5, 6 7 are samples from different A280 peaks from the IEx chromatography.

The newly synthesised STAT3 mutant STAT3 $_{127\text{-}722}$-YFP/CFP were successfully purified by IEx chromatography. The purity is about 80% pure in the best fractions. Comparing to the N-terminal fluorescent protein fused STAT3 truncated proteins, the C-terminal fluorescent protein fused STAT3 truncated proteins are less soluble therefore more difficult to be purified. Although the purity of the STAT3 $_{127\text{-}722}$-YFP/CFP protein is only 80% pure, it can be used in the following FRET assays.

## 2.7 Discussion:

All STAT3 truncated proteins in this thesis were successfully produced in *E. coli* and purified by IEx chromatography. The purified STAT3 proteins were applied in the *in vitro* assays described in chapter 3, 4, and 5. By comparing the differences in the DNA binding activity of different STAT3 truncated proteins, we can understand the STAT3 domain function in detail and predict the mechanisms of the STAT3 transcriptional activation. Furthermore, utilising the different STAT3 truncated proteins, we can screen STAT3 inhibitors targeting different STAT3 domains more specifically. Producing STAT3 proteins in the *E. coli* cells is cost-effective and can be easily

monitored and expanded into large scale production [255]. Therefore, the production and purification of the STAT3 truncated proteins has both important research value and industrial use.

Table 2.1 summarised the basic information of the STAT3 mutants produced in this thesis. Most of the STAT3 mutants were produced in the Rosetta2 (DE3) competent cells with high production level, over 15mg/L of the bacteria culture, except for the short STAT3 truncated proteins and the C-terminal fluorescent protein fused STAT3 proteins. The reason causing the low production level of the STAT3 $_{127\text{-}497}$ protein and its fluorescent fused proteins might be the low stability of the short truncated protein. The low production level of the C-terminal fluorescent protein fused STAT3 mutant is caused by the low solubility of the protein itself. We hypothesis that the low solubility of the STAT3 $_{127\text{-}722}$-YFP/CFP proteins is due to the protein misfolding when over-expressed in *E. coli* cells. The *E. coli* cells do not fold protein exactly as mammalian cells because they lack specific protein involved in protein folding. However, for simple proteins, the protein can fold correctly according to the hydrophobic interaction, hydrophilic interaction and electrostatic between the side chains within the peptides. The crystallisation structure of the *E. coli* folded STAT3 $_{127\text{-}722}$ and STAT3 $_{127\text{-}688}$ proteins were published. This provided confidence for us to believe that other STAT3 mutants can also be folded with full STAT3 biological activity in the *E. coli* cells. To further confirm the structure of the *E. coli* folded STAT3 mutants, X-ray crystallisation can be used. From colleagues experience, the IEx purified STAT3 mutants are not pure enough for crystallisation use. Therefore, size exclusion chromatography purification is essential for the protein preparation step before crystallisation. However, for the STAT3 $_{127\text{-}497}$ mutant, the protein concentration after IEx chromatography is usually too low to be applied to size exclusion chromatography. Therefore even though I also tried to crystallise STAT3 $_{127\text{-}497}$ protein, I did not get any crystal due to the low protein concentration or low protein purity. To increase the purity of the STAT3 $_{127\text{-}497}$ protein after IEx chromatography, increasing its production level in the E. coli cells first is one simple method. We have tried different broth to culture the bacteria however different broth culture does not

influence the STAT3 protein production significantly. Future experiments on increasing the STAT3 $_{127-497}$ production in the *E. coli* cells can be conducted by trying different strains of *E. coli* or different bacterial strains. Besides, based on the huge differences of the STAT3 production ability in different batches of competent cells, single colony producing better STAT3 protein can be selected and stored for long term use.

| STAT3 truncated protein | MW kDa | Extinction coefficient M-1cm-1 | PI | Estimated purity after purification |
|---|---|---|---|---|
| STAT3 $_{127-722}$ | 68.0 | 88975 | 7.2 | 99% |
| STAT3 $_{127-688}$ | 62.3 | 81985 | 8.0 | 99% |
| STAT3 $_{127-497}$ | 42.6 | 31315 | 7.7 | 60% |
| eCFP/eYFP-STAT3 $_{127-722}$ | 96.2 | 110990 | 6.2 | 99% |
| eCFP/eYFP-STAT3 $_{127-688}$ | 92.4 | 104000 | 6.2 | 99% |
| eCFP/eYFP-STAT3 $_{127-497}$ | 70.7 | 53300 | 6.2 | 90% |
| STAT3 $_{127-722}$-eCFP/eYFP | 96.2 | 115000 | 6.2 | 80% |

Table 2.1 A summary of the truncated proteins. The MW, Extinction coefficient and PI of the proteins were calculated according to the amino acid sequences. The purity after purification were estimated according to the SDS-PAGE gels after purification.

# Chapter 3- Protein mobility shift assay for detecting STAT3 DNA binding activity

An multipurpose *in vitro* assay was applied to detect the STAT3 DNA binding activity of the different STAT3 truncated proteins- the protein electrophoresis mobility shift assay (PEMSA) [207]. With application of the PEMSA assay, we can not only make the protein-DNA interaction visible, but also calculate protein-DNA binding coefficients, calculate the stoichiometry and monitor the protein aggregation.  The level of protein aggregation may also be detected in the future development of the PEMSA assay. The principle of the PEMSA assay is the same as the [256](EMSA). Both measure a difference in mobility after the protein-DNA complex formation in gel electrophoresis, but one monitors the protein, whereas the other monitors the DNA.

The EMSA has been regarded as a quick and sensitive method to detect the interaction between protein and DNA since first described [256] In the EMSA assays, the DNA can be labelled with either radioactive or non-radioactive labels. The detection of the protein and DNA interaction is based on the difference of the mobility between the protein/DNA complex and the free DNA in the gels. Usually, the free DNA moves faster than the free protein and the protein-DNA complex. The movement of the compounds in the gels are determined by the shape, temperature, and most importantly, the charge/mass ratio under the current condition [256]. The interaction between the protein and the DNA needs to reach equilibrium before conducting the electrophoresis. During the electrophoresis, the equilibrium may be disturbed and the nuclear-protein complex would dissociate [257].

The EMSA assay has advantages of simple operation, robust performance under a wide range of buffer conditions, straight forward result, and broad applications [258]. The EMSA assay can be designed for very high sensitivity tests by labelling the DNA with radioisotope. The radioisotope labelled DNA can be performed to detect nano-molar range of the protein-DNA interactions[259]. The EMSA assay can be applied to different DNA structure, wide range of DNA lengths and protein concentrations. Therefore,

the EMSA assay is one of the most popular techniques for the detection of protein-DNA interactions.

The EMSA assay has wide application in quality and quantity test, equilibration and kinetics detection of the protein-DNA interactions [260]. Different from the traditional EMSA, the PEMSA assay is performed with labelled protein and non-labelled DNA. The fluorescent labels allow direct observation of the position of the protein and whether the protein is aggregated during gel electrophoresis [261]. In the PEMSA assay, both the free protein and the DNA-bound protein can be observed in the gel since the protein is labelled with fluorescent protein. The aggregated proteins either stay in the wells or form aggregates during the electrophoresis and appears as amorphous fluorescent bands in the gel. Therefore, the PEMSA assay is favoured over the EMSA assay when the modulation of the protein is important in the experiment. In this thesis, the labelled STAT3 proteins were purified before application in the PEMSA assay in order to measure the STAT3 protein concentration using the general protein $A_{280}$ method. However, if a fluorescent standard can be made, it is simple and more sensitive to determine the protein concentration according to the CFP/YFP fluorescent intensity. In that case, high purity of the protein is not required and the steps of the PEMSA assay can be further simplified.

As with the EMSA assay, the PEMSA assay separates the free protein, free DNA and the protein-DNA complex according to the differences of the mobility in the agarose or polyacrylamide gel [256]. Differently, in the PEMSA assays, the protein was labelled to monitor the protein aggregation and detect the quality of the protein during gel electrophoresis. The ability of movement during the gel electrophoresis is positively related to the compound's charge/mass ratio. The STAT3 proteins and the dsDNA were all negatively charged under the electrophoresis condition. The molecular weight of the GAS18 (an 18bp dsDNA containing the GAS sequence) is about 12kDa and the smallest STAT3 mutation applied in the PEMSA assay is about 69kDa. The dsDNA was also more negatively charged than the protein. Thus the GAS18 moves much faster than the protein and the protein/DNA complex in the gels. Since the STAT3 proteins were fused with

yellow fluorescent protein, a fluorescent band shift towards the end of the gel will be observed when the STAT3 proteins bind to the dsDNA.

In previous studies, the PEMSA assay was introduced and applied in the detection of the DNA binding activity of un-phosphorylated STAT3 by Nkansah *et.al.* (2003).The method used in this project is developed from their experiment. Two different eYFP labelled STAT3 truncated proteins: eYFP-STAT3 $_{127\text{-}688}$ and eYFP-STAT3 $_{127\text{-}497}$ were generated by point directed mutagenesis. By testing the DNA binding activity of the two STAT3 mutants, we can understand how SH2 domain influence STAT3 DNA binding activity and therefore speculate on the relationship between STAT3 dimerisation and DNA binding. The PEMSA assay is also developed into a secondary STAT3 inhibitor screening method.

## 3.1 Method

To produce the STAT3 truncated protein with fluorescent labels, point directed mutagenesis was applied to create the plasmids coding for YFP/CFP-STAT3 $_{127\text{-}688}$ and YFP/CFP-STAT3 $_{127\text{-}497}$ proteins. The methods of plasmid preparation and protein purification were described in chapter 2.

### 3.1.1 Buffer preparation:

The PEMSA running buffer (25 mM Tris, 22.5 mM Boric Acid, 2.5 mM EDTA pH 8.3) was prepared and filtered with 0.22μM membrane. The filtered PEMSA buffer was stored at 4℃ before use.

### 3.1.2 Gel preparation:

Two types of gels were used in the PEMSA assay: the agarose gel and the polyacrylamide gel. The agarose gel benefits from shorter running time and simple preparation steps while the polyacrylamide gel has the advantage of higher resolution. The agarose gels were 2% and were used in the PEMSA assay. The weighed solid agarose was added into 0.5x TEB buffer (40 mM Tris-HCl, 45 mM boric acid and 1 mM EDTA) and melted by microwave. The melted agarose gel was set in the gel tray at room temperature for about 30 mins. The polyacrylamide gels were 5% and were prepared with126 mM Tris pH 8.8, 5% polyacrylamide, 0.1% APS and 1% TEMED. The gels were left at room temperature for about 30 mins to allow polymerisation.

### 3.1.3 Sample preparation:

Single stranded DNA (ssDNA) oligoes were purchased from Eurofins and annealed together to form the dsDNA-GAS18. The sequences of the two oligoes were: 5'-TGCATTTCCCGTAAATCT-3' and 5'-AAGATTTACGGGAAATGCA-3'. The oligos were annealed in buffer containing 25 mM Tris pH 8.5, 20 mM NaCl, 10 mM $MgCl_2$ at 95℃ for 5 mins and then cooled down to 10℃ at a rate of 1℃/min in a thermocycler. The annealed GAS18 were stored in -20℃ freezer and thawed on ice before use.

The STAT3 proteins were purified with IEx chromatography as previously described. Buffer exchange was applied using 30kDa MWCO Centrifugal filter centrifuging at 1800 rpm. The buffer was replaced with the PEMSA protein buffer (20 mM NaCl, 25 mM Tris pH8.5) sufficiently as follows: the protein solution from the IEx purification fraction was concentrated to 1/10 of the fraction volume and then topped up to the previous volume, gently mixed and centrifuged again. For example, 10 ml of the IEx protein solution was concentrated to 1ml protein solution and gently mixed with 9ml of the PEMSA protein buffer. This buffer exchange step was usually conducted more than 2 times. The protein concentration was then confirmed with the Nanodrop. If the protein concentration was less than 4.5 µM, the protein was further concentrated by centrifugation at 1800rpm for another 15 mins.

The annealed GAS18, buffer exchanged STAT3 proteins were mixed with 5xPEMSA buffer (125 mM Tris pH8.5, 0.15 mM EDTA, 0.15 mM EGTA, 5 mM $MgCl_2$, 200 mM KCl, 1 mM non-specific oligo, 0.5 mg/ml BSA and 40% glycerol) and $dH_2O$ carefully. The sequence of the non-specific oligo was 5'-GTACCATGGTAC-3'. The aim of adding this oligo is to eliminate non-specific DNA binding of the STAT3 truncated protein to GAS18. The protein DNA mixture was incubated on ice for 1hr before loading to the gel.

Gel electrophoresis was conducted in the cold room at 4 ℃. For the agarose gel PEMSA, the gels were pre-run at 90 V for 1hr before loading the samples and run at 200 V after loading the samples for 2 hrs. For the polyacrylamide gels, the gels were pre-run at 90 V for 2 hrs and then run at 150 V for 2 hrs. After gel electrophoresis, the gels were observed with the blue light Safe Imager.

## 3.2 Result:

### 3.2.1 STAT3 $_{127\text{-}688}$ binding to dsDNA

The STAT3 $_{127\text{-}688}$ PEMSA can be conducted in both agarose and polyacrylamide gels. The electrophoresis were optimised for the separation of the free STAT3 protein and the STAT3/DNA complex. Clear migration differences were observed in both types of the PEMSA gels. With application of the PEMSA assay, we can define the binding coefficient of the STAT3 $_{127\text{-}688}$/DNA interaction, the quality of the STAT3 $_{127\text{-}688}$ protein produced and screen small molecule inhibitors that prevent STAT3 $_{127\text{-}688}$ binding to the dsDNA.

First, the agarose PEMSA was used to detect the $EC_{50}$ of the eYFP-STAT3 $_{127\text{-}688}$ protein binding to GAS18. 2.5µM of the eYFP-STAT3 $_{127\text{-}688}$ protein was applied to increasing concentration of the dsDNA (0-12µM).

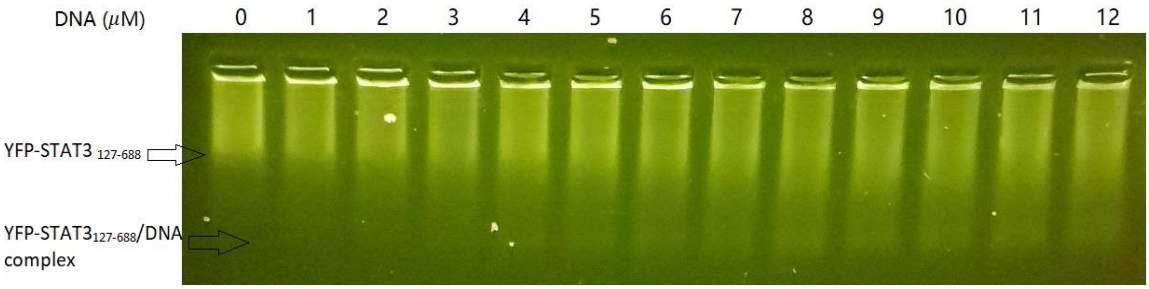


Figure 3.1. Agarose PEMSA gel shows that the eYFP-STAT3 $_{127\text{-}688}$ protein binds to GAS18. The concentration of the dsDNA increases from left to right. The protein concentration applied to this gel was 2.5µM. With the increasing dsDNA concentration, the intensity of the eYFP-STAT3 $_{127\text{-}688}$ and DNA complex band is increasing. In the first well without dsDNA, the protein DNA complex band is completely absence.

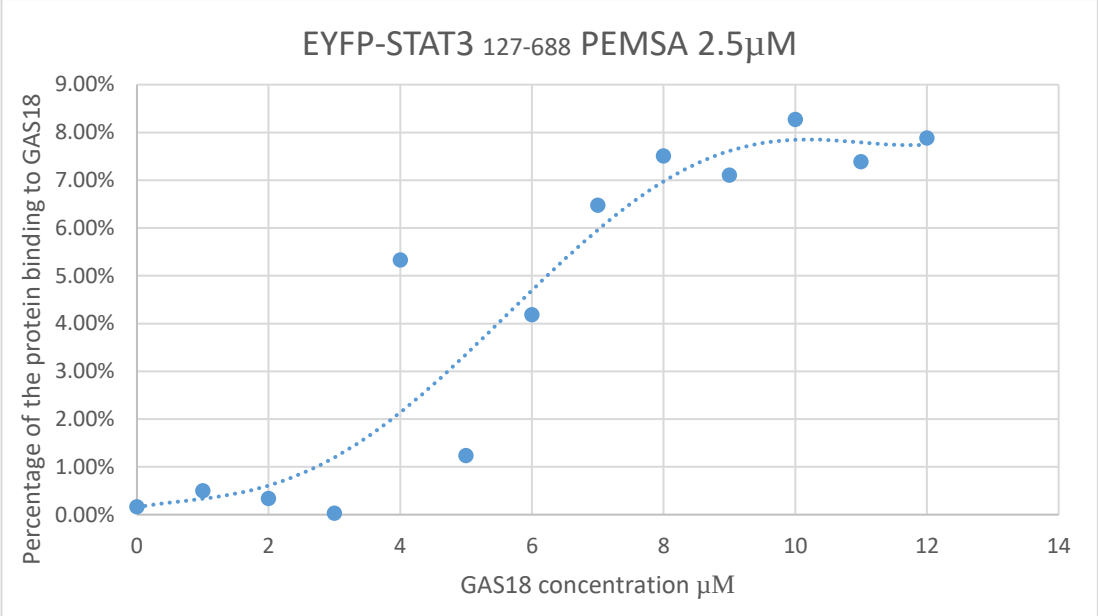


Figure 3.2. eYFP-STAT3 $_{127\text{-}688}$ DNA binding curve generated from the PEMSA result. The percentage of protein bind was calculated according to the intensity of the eYFP-STAT3 $_{127\text{-}688}$ band and the intensity of the eYFP-STAT3 $_{127\text{-}688}$/DNA complex band. The percentage of binding increased from 0 to 8% when the dsDNA concentration increased from 0 to 10µM.

The STAT3 $_{127\text{-}688}$ protein and STAT3 $_{127\text{-}688}$ protein-DNA complex were separated by gel electrophoresis in an agarose gel. In figure 3.1, clear fluorescent band migration in the agarose gel can be observed. Binding curve was generated and shown in figure 3.2. Our result confirms that the STAT3 protein can bind to dsDNA without the Tyr705. The amount of the eYFP-STAT3 127-688 protein-dsDNA complex increases with the increasing GAS18 concentration. The amount of the free protein and the protein/DNA complex is determined by the intensity of the bands in the PEMSA gels. From 0-4µM, the increase of the STAT3/DNA complex amount with the increasing dsDNA concentration is slowly. From 4-8µM, the increase of the STAT3/DNA complex amount is rapid with the increasing GAS18 concentration. The intensity of the protein/DNA complex band increases with the increasing dsDNA concentration while the intensity of the eYFP-STAT3 $_{127\text{-}688}$ protein band decreases. After 10µM, the amount of the protein/DNA complex amount does not increase anymore with the increase DNA concentration. Hence, we assume that the protein-DNA interaction between

the STAT3 mutant and the GAS18 saturates when the DNA concentration was 10 μM and the protein concentration was 2.5 μM. 8% of the YPF-STAT3 $_{127\text{-}688}$ protein was binding to dsDNA when the binding saturates while 92% of the eYFP-STAT3 $_{127\text{-}688}$ protein was free. This indicates that the eYFP-STAT3 $_{127\text{-}688}$ protein is binding to the dsDNA with low affinity. The half maximal effective concentration ($EC_{50}$) of the dsDNA to the STAT3 127-688 protein was about 6μM. The protein: DNA ratio at the $EC_{50}$ point was 1:2.4 while the protein: DNA ratio at the saturation point was about 1:4. In previous researches of the STAT3 $_{127\text{-}722}$ PEMSA, 100% of the STAT3 $_{127\text{-}722}$ protein was able to form the STAT3/DNA complex with excess of the GAS18 concentration. Therefore we conclude that the presence of the sequences after SH2 domain, even without being phosphorylated, can increase the stability of the STAT3 DNA interaction dramatically. Besides, the clear binding shift observed in the PEMSA result also suggests that the lifetime of eYFP-STAT3 127-688 DNA binding activity is longer than 2hrs.

### 3.2.2 eYFP-STAT3 127-497 binding to dsDNA

The eYFP-STAT3 127-497 protein was proved to bind to GAS18 with polyacrylamide gel PEMSA. The eYFP-STAT3 $_{127\text{-}497}$/dsDNA complex band was separated from the free EFYP-STAT3 $_{127\text{-}497}$ band during the gel electrophoresis. The intensity of the fluorescent band is positively related to the protein concentration in the protein-DNA complex and free protein.

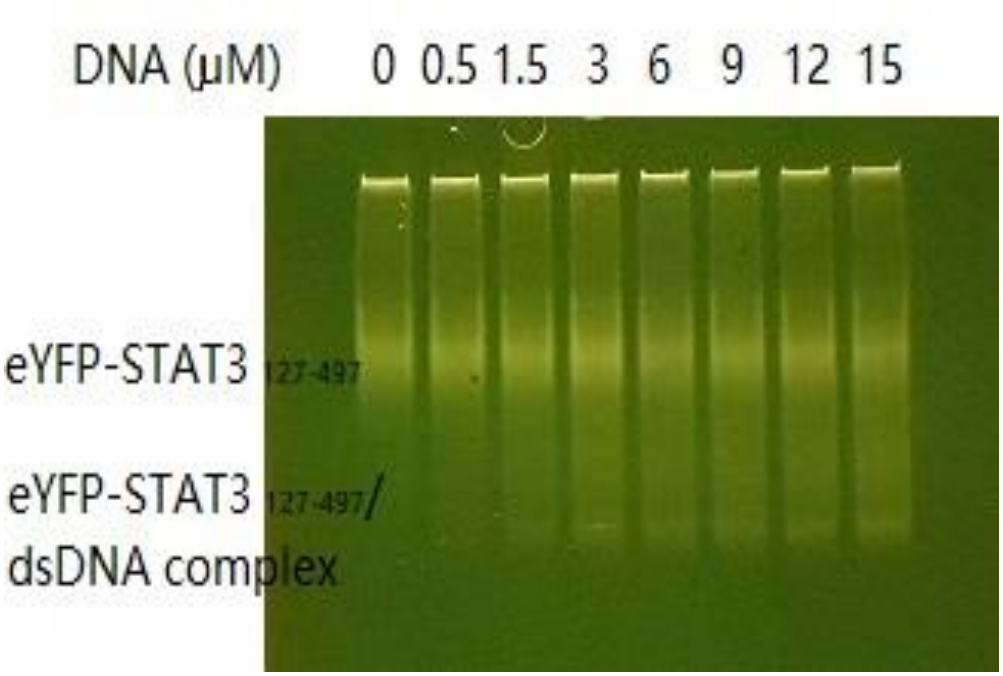


Figure 3.3. Polyacrylamide PEMSA gel showing the DNA binding activity of the eYFP-STAT3 $_{127-497}$ protein. The GAS18 concentration increased from right to left. With the increasing dsDNA concentration, the intensity of the eYFP-STAT3 $_{127-497}$ and DNA complex band is more visible. The protein DNA complex band is completely absence in the 0µM dsDNA well.

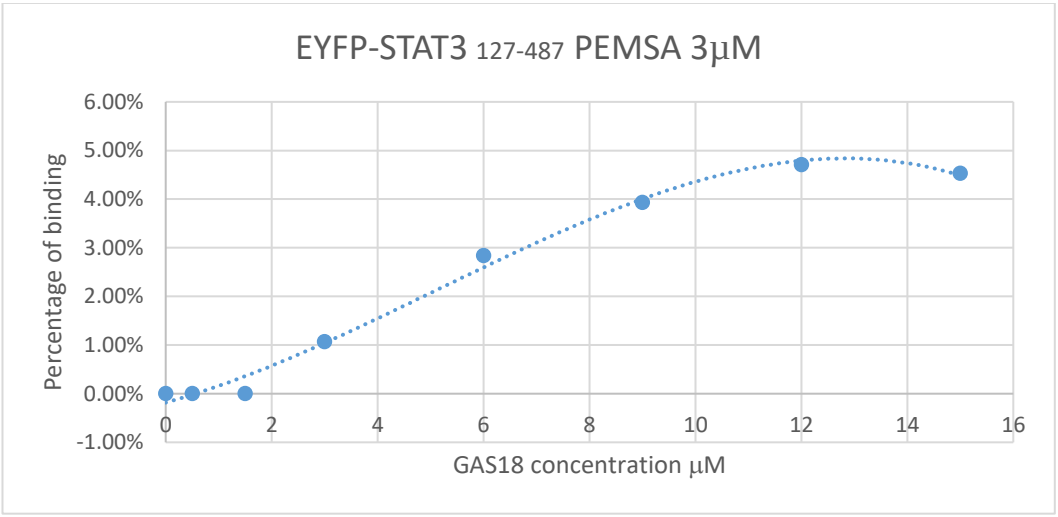


Figure 3.4. The eYFP-STAT3 $_{127-497}$ DNA binding curve generated from the PEMSA result. . The percentage of protein bind was calculated by the proportion of the eYFP-STAT3 $_{127-498}$ band and the intensity of the eYFP-STAT3 $_{127-497}$/DNA complex band.

Our PEMSA results suggests that the eYFP-STAT3 $_{127\text{-}497}$ protein can bind to GAS18. The amount of the free eYFP-STAT3 127-497 protein decreased with the increasing concentration of the GAS18 while the amount of the eYFP-$_{\text{STAT3 127-497}}$-dsDNA complex increased. The 'shift' of the band starts to be obvious at 1.5μM of the dsDNA concentration. From 0 to 1.5μM, the increase of the eYFP-STAT3 $_{127\text{-}497}$-GAS18 complex with the increase of the dsDNA concentration is slowly. When the dsDNA concentration was between 1.5 to 12μM, the increase of the protein-DNA complex proportion was rapid. The formation of the protein-DNA complex was saturated when the GAS18 concentration reached 12μM. At the saturation point, the protein: DNA ratio was 1:4 and the $EC_{50}$ of the dsDNA binding to the eYFP-STAT3 $_{127\text{-}497}$ was about 6μM. According to the PEMSA results of the eYFP-STAT3 $_{127\text{-}497}$ and eYFP-STAT3 $^{127\text{-}688}$, the dsDNA binding to both STAT3 mutations were very similar. This suggests that with integrated CCD and DBD, STAT3 can bind to dsDNA without SH2 domain. However, the binding curve shows that when the dsDNA concentration saturates the protein binding, less than 5% of the STAT3 protein bond to the GAS18. The percentage of the eYFP-STAT3 $_{127\text{-}497}$ that can bind tightly and migrate with the dsDNA when the dsDNA binding was saturated is lower than the percentage of the eYFP-STAT3 $_{127\text{-}688}$ protein. This indicates that the eYFP-STAT3 $_{127\text{-}497}$ protein and the dsDNA association is weaker than the eYFP-STAT3 $_{127\text{-}688}$ protein and the dsDNA interaction.

### 3.2.3 The binding coefficient of the eYFP-STAT3 127-688 and the eYFP-STAT3 127-497 protein-DNA interactions

The association constant of the eYFP-STAT3 $_{127\text{-}688}$ and the eYFP-STAT3 $_{127\text{-}497}$ binding to dsDNA was calculated according to the PEMSA result. The association constant (Ka) of the STAT3-DNA interaction was calculated according to the following equation.

$$Ka = [STAT3{:}\,dsDNA]/([STAT3] * [dsDNA])$$

The STAT3 and dsDNA complex concentration was calculated from the intensity of the YPF-STAT3 truncated protein and the DNA complex band. The STAT3 protein concentration was calculated according to the intensity of

the un-bond STAT3 protein band. The dsDNA concentration was calculated based on the STAT3 proteins bind to dsDNA as dimers. Therefore, the calculated Ka of the eYFP-STAT3 $_{127\text{-}688}$ DNA binding is 0.013 while the Ka of eYFP-STAT3 $_{127\text{-}497}$ DNA binding is 0.0045. This confirms that both STAT3 mutant tested in the PEMSA experiment were weak DNA binders and the eYFP-STAT3 $_{127\text{-}688}$ binds to dsDNA tighter than the eYFP STAT3 $_{127\text{-}497}$. The binding affinity of the YFP fused STAT3 proteins tested by other types of assay might be higher since the protein-DNA complex favours the dissociation form during gel electrophoresis. Even though, the DNA binding of the YFP-STAT3 $_{127\text{-}497}$ protein is still tight enough to form a very obvious fluorescent band. Hence the STAT3 $_{127\text{-}497}$ protein is proved to be the shortest STAT3 truncated protein to date that can accomplish the DNA binding activity. We also conclude that the SH2 domain, LD, TAD stabilises DNA binding of STAT3 but is not pre-requested for STAT3 DNA binding activity.

According to the PEMSA results, the dimerisation of STAT3 may not be the prerequisite for the STAT3 to bind to the dsDNA. The interaction between two STAT3 monomers can be observed in the X-ray crystallisation structure of the STAT3 $_{127\text{-}722}$ protein.

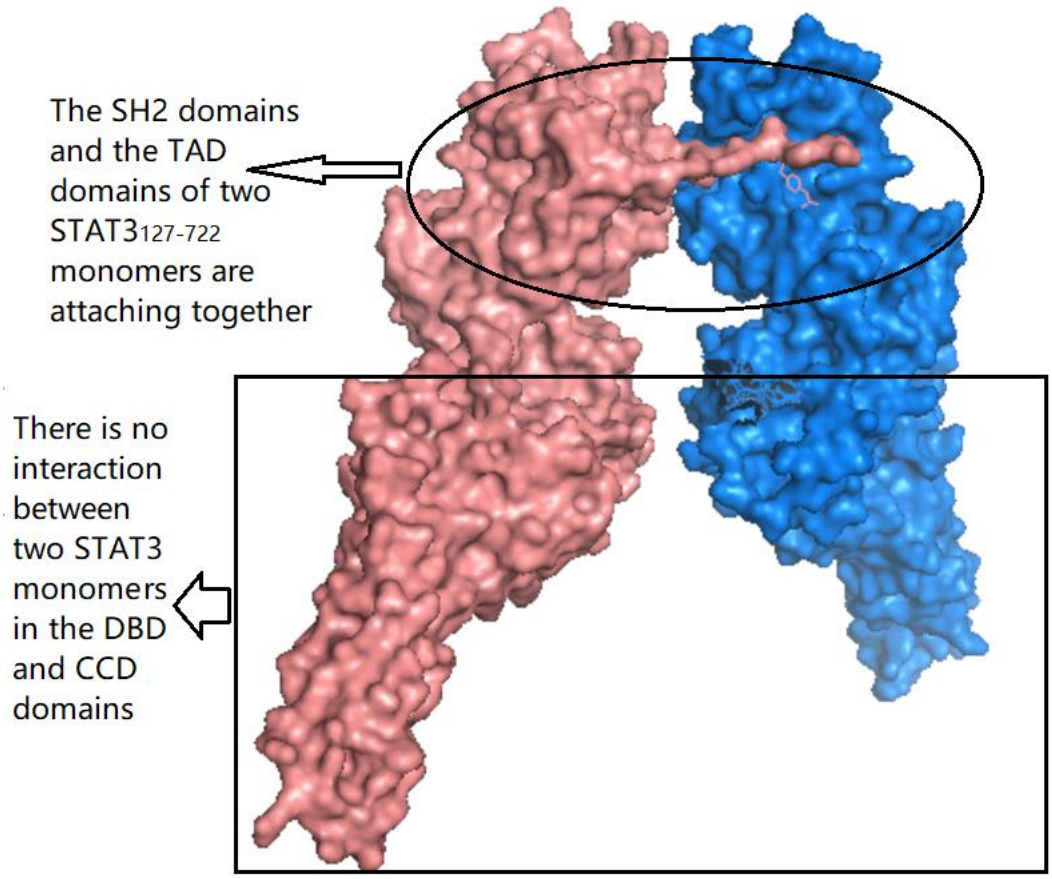


Figure 3.5 shows two STAT3 127-722 monomers forming dimers. The pink and blue molecule represents each STAT3 monomer. The overlapping region circled is the SH2 domain and TAD domain.

The 3D molecular structure clearly indicates that there is no association in the DBD domain between two STAT3 monomers. Therefore, the STAT3 $_{127\text{-}497}$ proteins are unlikely to form dimers without interacting with the dsDNA. We hypothesise that the STAT3 can bind to dsDNA as a monomer and then another STAT3 monomer comes along and to form a dimer.

### 3.2.4 Quality check of the fluorescent protein labelled STAT3 proteins:

The quality of the STAT3 proteins varies with each extraction. The DNA binding activity of the produced STAT3 protein also varies between different batches of bacteria. The differences of the DNA binding affinity were detected by the PEMSA assay.

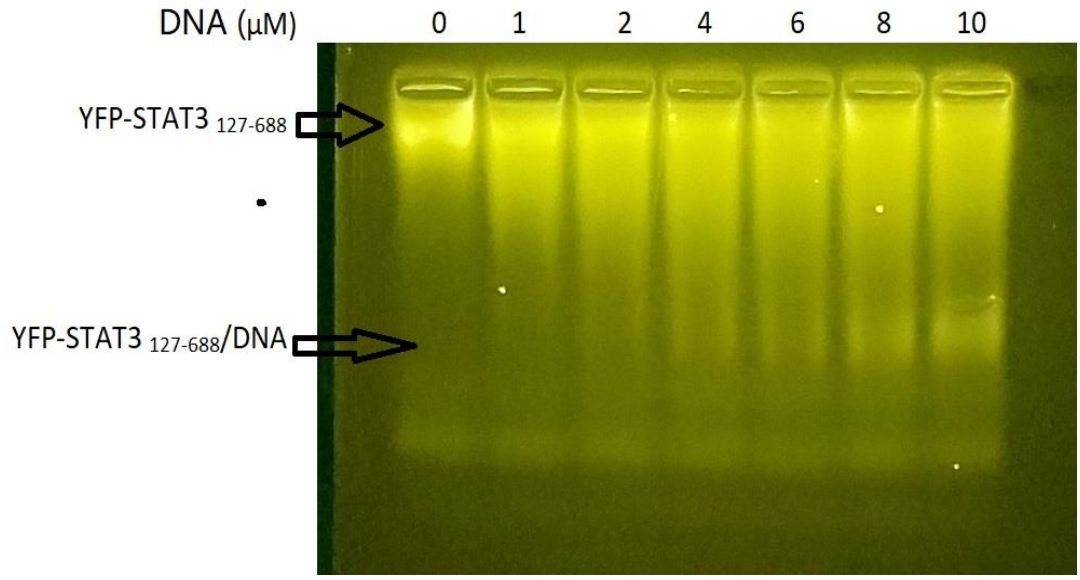


Figure 3.6. An example of the YFP-STAT3 $_{127\text{-}688}$ produced with better DNA binding affinity. The YFP-STAT3 $_{127\text{-}688}$/dsDNA complex band becomes more obvious with the increasing concentration of the GAS18.

Figure 3.6 shows the best YFP-STAT3 $_{127\text{-}688}$ protein produced in the thesis. In this single agarose gel electrophoresis, when the dsDNA concentration reached 10μM, 25% of the purified YFP-STAT3 $_{127\text{-}688}$ protein formed protein-DNA complex with the dsDNA. The differences of the protein quality may be caused by the following reasons: different bacteria colonies have different ability to produce active protein, the STAT3 mutated proteins form variable amounts of inactive aggregates during buffer exchange, the variable oxidation level of the STAT3 proteins affect STAT3 DNA binding activity.

The maximum percentages of different STAT3 truncated proteins binding to dsDNA with excess of the GAS18 concentration were recorded.

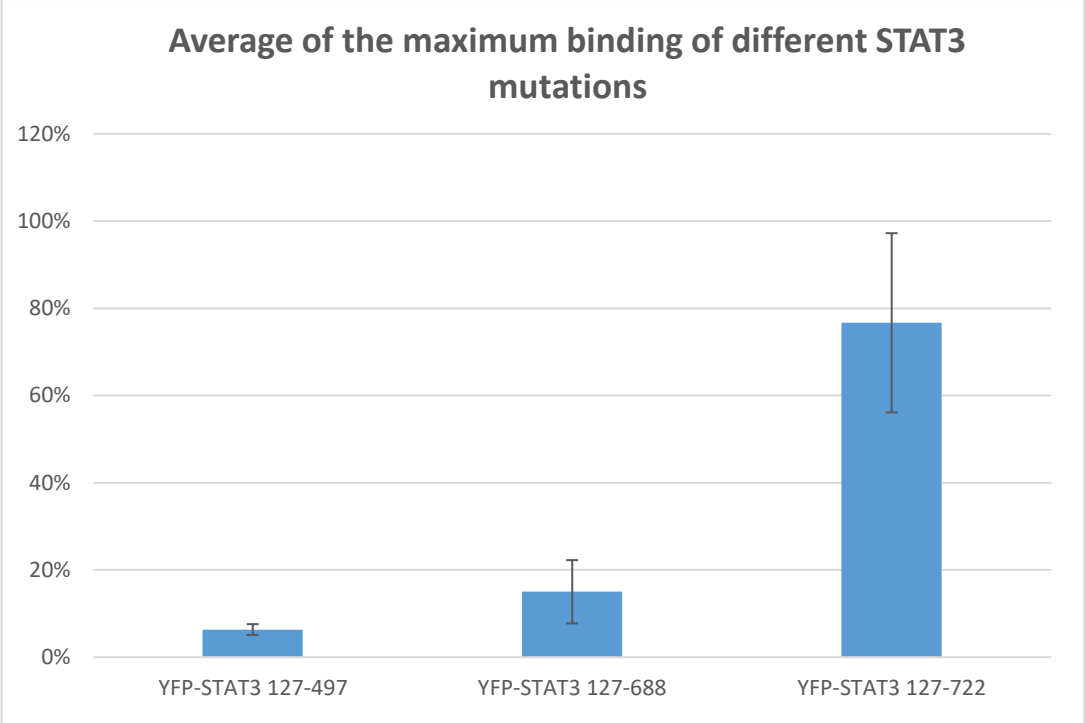


Figure 3.7. The average of the maximum proportion of the STAT3 proteins that can form protein-DNA complex with excess dsDNA: YFP-STAT3 $_{127\text{-}497}$ 6%, YFP-STAT3 $_{127\text{-}688}$ 15% and YFP-STAT3 $_{127\text{-}722}$ 77%. The error bars show the standard deviation of the measurements.

The PEMSA assays were repeated and the maximum percentage of protein binding to the GAS18 were recorded for each STAT3 mutations. As figure 3.7 suggests, the longer the STAT3 truncated protein is, the higher proportion of the protein can bind to the GAS18. This indicates that the length of the STAT3 mutations is positively related to the STAT3 DNA binding affinity. The error bar shows that the quality of the YFP-STAT3 $_{127\text{-}722}$ produced in the *E. coli* cells is the most variable among the three STAT3 truncated proteins. The YFP-STAT3 $_{127\text{-}497}$ protein, in contrast, although with low DNA binding affinity, the quality of the protein produced from each batches of bacteria stays constant.

### 3.2.5 Inhibitor test:

The PEMSA assay was also developed to screen STAT3 inhibitors. The STAT3 inhibitor was synthesised by Dr Po-Chang Shih in the group. With application of the PEMSA assay, we can not only test the $K_D$ of the inhibitor but also visualise the protein aggregation state during the inhibition test.

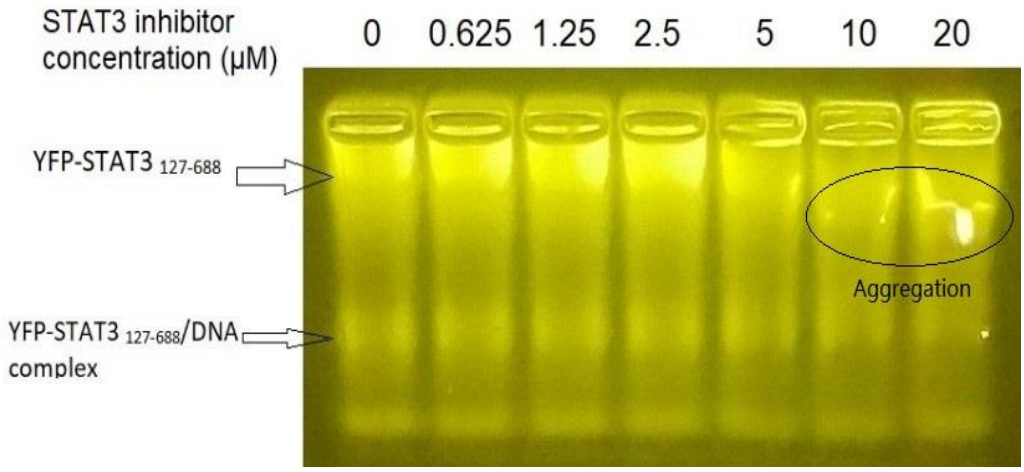


Figure 3.8. A provided STAT3 inhibitor (PS024) tested in an agarose PEMSA gel. In this gel, the dsDNA and STAT3 protein concentrations were stable. The concentration of the small molecule inhibitor increases from left to right.

Figure 3.8 is an example of the STAT3 inhibitor tested by agarose PEMSA. The eYFP-STAT3 $_{127\text{-}688}$ concentration used in this experiment was 3μM. The dsDNA concentration used in this assay was 20μM. The excess dsDNA concentration insure the highest concentration of the protein/DNA complex is formed and a clear shifted band in the PEMSA gel is observed. The inhibitor concentration increased from 0μM to 20μM. With the increasing STAT3 inhibitor concentration, the eYFP-STAT3 $_{127\text{-}688}$ and DNA complex band became fainter. At the same time, the eYFP-STAT3 $_{127\text{-}688}$ band was restoring but with clear aggregation shown in the gel.

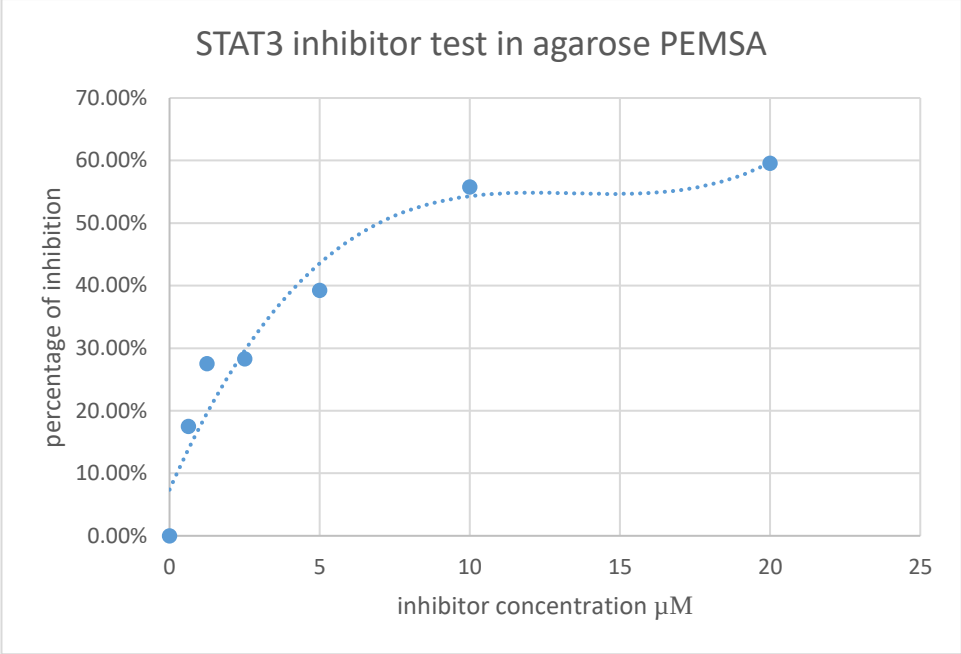


Figure 3.9. Inhibition curve generated from the PEMSA STAT3 inhibitor test. The inhibitor inhibited STAT3 DNA binding activity by 60% with 20μM concentration.

The inhibition curve was generated from the agarose PEMSA gel. As figure 3.9 suggests, with increasing inhibitor concentration, the percentage of inhibition increased. The small molecule inhibitor provided was able to inhibit the STAT3 DNA binding activity by 60% when it reached 20 μM. According to the smoothed trend line predicted by the excel tool according to the provided data, after 20 μM, the percentage of inhibition will increase very slowly with the increasing inhibitor concentration. This suggests that this inhibitor is not very competitive with the dsDNA for the STAT3 truncated protein. Furthermore, the aggregation of the eYFP-STAT3 127-688 protein is more obvious with the increasing inhibitor concentration. Therefore we speculate that this inhibitor inhibits STAT3 DNA binding activity by causing STAT3 protein aggregation.

| Inhibitor name | Inhibition | Aggregation |
|---|---|---|
| PS010 | Yes | Yes |
| PS021 | Yes | Yes |
| PS024 | Yes | Yes |
| PS055 | No | No |
| PS061 | No | No |

Table 3.1 A summary of STAT3 inhibitors tested by the PEMSA assay.

A summary of small molecule inhibitors tested in the PEMSA assay is shown in table 3.1. The inhibitors were synthesised and provided by Dr. Po. All inhibitors shown inhibition of STAT3 caused protein aggregation during the PEMSA assay.

### 3.3 Conclusion and Discussion

The PEMSA experiment confirms that both eYFP-STAT3 $_{127\text{-}688}$ and eYFP-STAT3 $_{127\text{-}497}$ proteins can bind to dsDNA. The DNA binding affinity of both STAT3 mutants are significantly lower than the eYFP-STAT3 $_{127\text{-}722}$ mutant tested in previous experiments. This suggests that although the STAT3 DBD domain is enough to support the STAT3 DNA binding activity the presence of other STAT3 domains stabilises STAT3 DNA binding. The presence of the SH2 domain is not necessary for STAT3 protein DNA interaction. This discovery also brings more confidence that the STAT3 dimerisation is not perquisite for the STAT3 to bind to the dsDNA. One STAT3 may interact with the dsDNA and then the other STAT3 can come to form the dimer. Previous research has proved that un-phosphorylated STAT3 can bind to dsDNA, and the STAT3 nuclear translocation is independent of the STAT3 phosphorylation. Together with our result, we assume that the STAT3 inhibitors targeting Tyr705 and SH2 domain may not completely shut down the STAT3 transcriptional activity. Thus STAT3 inhibitors targeting the STAT3 DBD domain could well be more effective than the STAT3 SH2 inhibitors.

The PEMSA assay can also be applied for the STAT3 inhibitor screening. Both agarose PEMSA and polyacrylamide PEMSA were optimised to test the DNA binding activity of the truncated STAT3. The agarose PEMSA needs less running time since the pre-run is unnecessary. The polyacrylamide gels are more transparent than the agarose gels. The eYFP-STAT3 $_{127\text{-}497}$ PEMSA can only be tested in polyacrylamide gel since the DNA binding is too weak to be observed in agarose gel. Therefore the sensitivity is better in the polyacrylamide gels. The PEMSA assay can not only be used to calculate the $K_D$ of the inhibitor but also allow protein aggregation to be visible. With application of fluorescent protein fused non-STAT3 protein as negative control, it is possible to test the specificity of the STAT3 inhibitor. Furthermore, with application of different STAT3 truncated proteins in the PEMSA assay, we can screen STAT3 inhibitors targeting the DBD domain more specifically. Comparing to the *in vivo* assays, the PEMSA assay cost less. The PEMSA assay contains more information in one experiment compared to other *in vitro* assays. It allows Ka to be calculated. However, the PEMSA assay requires micro molar ranges of materials and hours to run the electrophoresis. These disadvantages make it more suitable as a secondary screen rather than high-throughput for screening large compound libraries for selection of suitable hits.

# Chapter 4- High-throughput FP assay for detecting STAT3 DNA binding method

In order to further confirm the DNA binding activity of the STAT3 truncated proteins and to develop a high-throughput method for selecting STAT3 inhibitors, we developed a fluorescent polarisation (FP) assay. FP assays have been widely developed into high-throughput screening method for detecting an interaction between a large molecule and a small molecule. We have used an FP assay to achieve an efficient and time-saving method for detecting STAT3 DNA binding activity and to screen STAT3 inhibitors targeting DNA binding. In our FP assay, non-labelled STAT3 truncated proteins were used to bind to Bodipy-labelled dsDNA. This method detects the protein-dsDNA interaction directly by the differences between the bound and free FP signals. The FP assay provide more supportive evidence for our results observed from PEMSA assays. Furthermore, by comparing the FP assay and the PEMSA assay, we can be confident that the presence of YFP in the PEMSA assay does not influence the STAT3 DNA interactions. The FP assay has potential to be developed into a high-through put screening method for selecting STAT3 inhibitors. In this chapter, an FP assay using STAT3 $_{127\text{-}497}$ truncated protein is described, which provides a more specific method for screening STAT3 inhibitors targeting the STAT3 DNA binding domain compared to previous FP assays targeting dimerisation.

## 4.1 A brief Introduction of FP assay

Fluorescent polarisation (FP) assay is an *in vitro* assay developed to study the interactions between large molecules and small molecules. The assay was first theoretically introduced by Perrin in 1926 and developed into high throughput screening method in mid 1990s as reviewed by Zhang, Wu and Berizin (2015). Today, the FP assay is widely used in detecting protein-DNA interaction, protein-peptide interaction and protein-small molecular ligand interaction. In this project, it is applied to study the binding activity of STAT3 to DNA.

To conduct an FP assay, a small molecule with fluorescent tag and a large molecule that can bind to the small molecule is required. The principle is

based on Brownian motion. Brownian motion is the random movement of molecules in the solvents and is affected by temperature, viscosity of the molecule and the size of the molecule. In the FP assay, fluorescent tagged small molecules rotate quickly and randomly in the solution and any fluorescence results in a non-polarised signal. Binding to larger molecules significantly decreases its movement due to the increased particle size of the complex, and results in a more polarised signal.

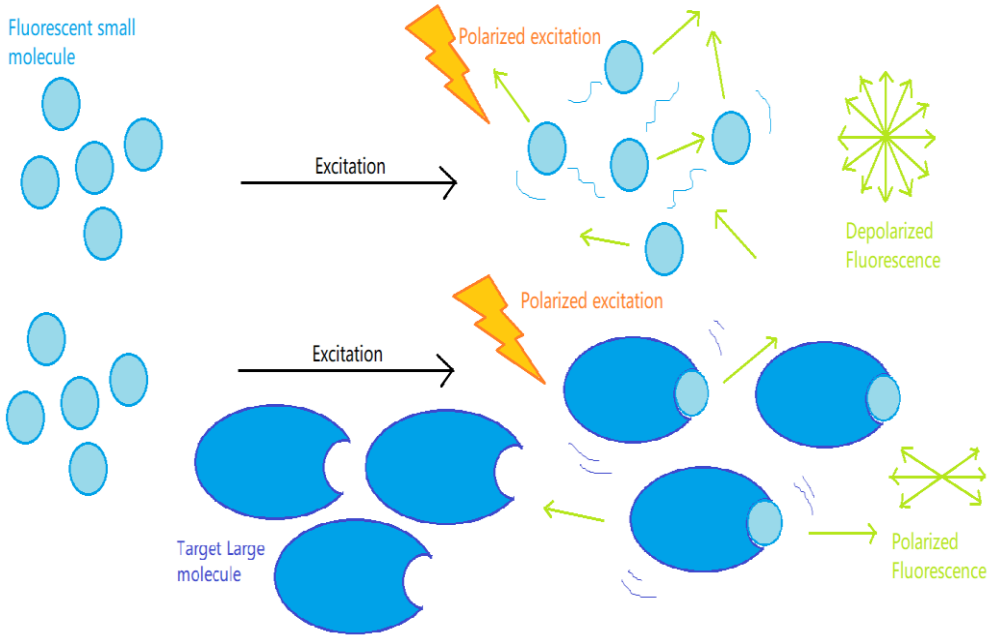


Figure 4.1. The mechanism of florescent polarisation assay. Small fluorescent molecule binding to large protein leads to a polarised fluorescent signal.

The fluorescent polarisation signal (mP) can be calculated by equation 1：

Equation 1 $$\mathrm{mP} = \frac{I\parallel - I\perp}{I\parallel + I\perp}$$

$I \parallel$ refers to the fluorescent intensity measured parallel and the $I \perp$ is the fluorescent intensity measured perpendicular. Upon excitation, the parallel and perpendicular fluorescence emission intensity is measured separately. The calculated FP signal is independent of each absolute emission intensity and thus also independent of the fluorophore concentration. The polarisation is only related to the temperature, the liquid volume and the viscosity of the solvent. With known temperature (T), solvent viscosity ($\eta$) and volume (V),

the rotational relaxation time ($\mu$) can be calculated by the following equation (Equation 2).

Equation 2 $\mu = 3\eta V/RT$

The rotation relaxation time is related to the time that the fluorophore react to the excitation. Perrin *et.al*. define the rotation relaxation time as the time it takes for the molecule to rotate 68.5° after excitation[262]. In the FP assay, the solution volume and viscosity and the temperature are usually constant. Therefore, any change in FP signal is only related to the association of the small molecule with fluorescent tag and the large molecule. Before binding to the large molecule, the small molecule with fluorescent tag moves vigorously in the solvent, so the emission intensity in parallel and perpendicular should be similar. When the small molecule binds to a lager molecule, the perpendicular emission will be decreased dramatically and result in an increase in polarisation of the signal. The polarisation signal is usually increased with the increase of the complex concentration.

## 4.2 Method:

### 4.2.1 Protein preparation:

The STAT3 proteins were purified with Ion Exchange chromatography with HiTrapQFF ion-exchange column and eluted with 200 nM NaCl, 250 mM Tris (pH8.5) and 1 mM DTT. The eluted proteins were buffer exchanged to 250 mM Tris (pH8.5) and 1 mM DTT and diluted to the set concentration in the same buffer before adding the Bodipy labelled dsDNA.

### 4.2.2 DNA preparation:

Single-stranded oligos were purchased from Eurofins. The sequences of the oligonucleotides are shown as follow:

Top: 5’ Bodipy 650/665 -ATT TCC CGT AAA 3’

Bot: 5’ TTT ACG GGA AAT 3’

The purchased oligos were dissolved in dd$H_2O$ and then annealed in the annealing buffer ( 20 mM NaCl, 200 mM HEPES pH7.9) at 95℃ for 5mins and cooled down to room temperature at the speed of 1℃/min. The annealed

Bodipy labelled dsDNA were diluted in 10% DMSO to the required concentration before application to the STAT3 protein. This part of preparation was done by Dr. Po-Chang Shih [263].

### 4.2.3 Fluorescent polarization plate set

The buffer exchanged protein solution were diluted to the desired volume and then mixed with the annealed Bodipy labelled dsDNA solution. The reaction mixture were measured by the plate reader (PHERAstar, BMG Labtech) with module FP 590-675-675.

## 4.3 Result:

From the FP assay results, we confirm that the STAT3 $_{127\text{-}497}$ can bind to dsDNA. This agrees with the PEMSA result. The FP result added evidence to prove that the DBD domain of the STAT3 protein is sufficient to support the STAT3 DNA binding activity. We also compared the influence of different time period incubation on the FP signal. Both STAT3 $_{127\text{-}722}$ and STAT3 $_{127\text{-}497}$ protein were tested in this thesis. Furthermore, the FP assay provide a high-throughput method for screening STAT3 inhibitors. The STAT3 $_{127\text{-}497}$ FP assay allows the screening to target STAT3 DNA binding domain more specifically.

Increasing concentration of the STAT3 127-722 protein was incubated with 20 nM of bodipy-dsDNA for 5mins, 1 hr and overnight (approximately 18hrs) at 4℃. The STAT3 127-722 concentration were detected from 0 nM to 500 nM.

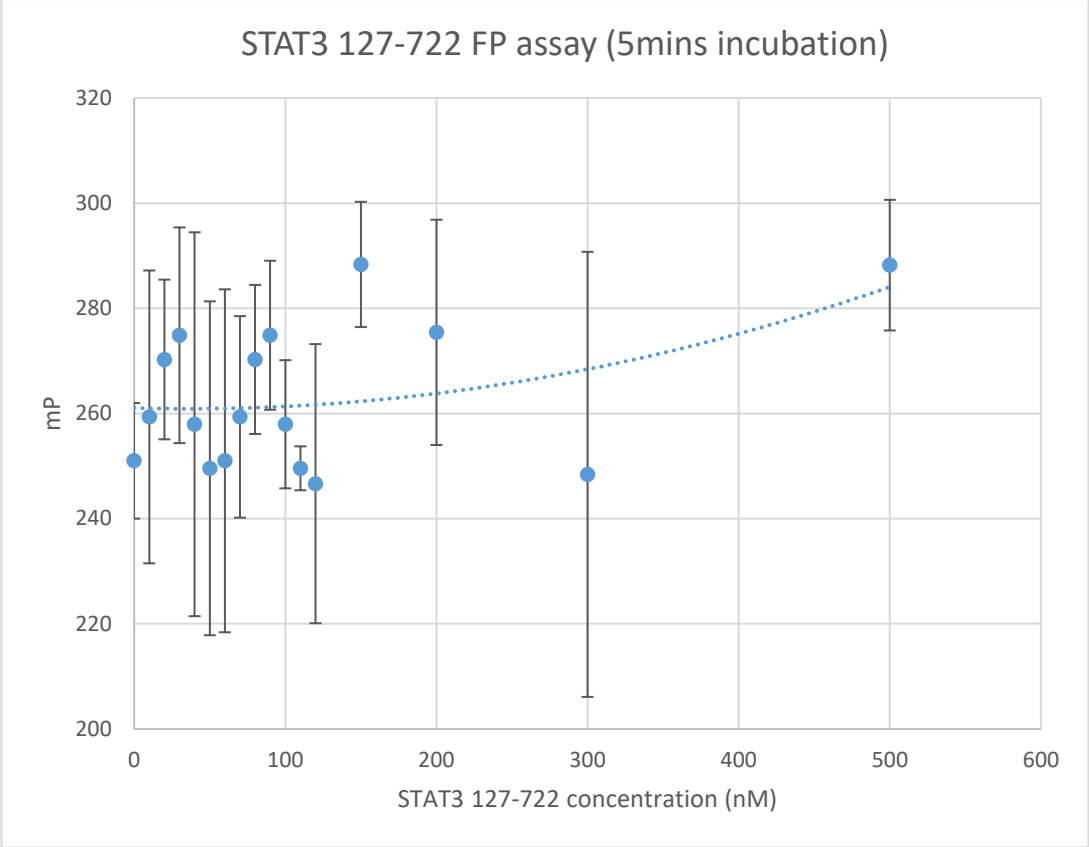


Figure 4.2. STAT3 $_{127\text{-}722}$ fluorescent polarisation assay incubating for 5mins at 4℃. The mP increased slightly with the increased STAT3 127-722 concentration according to the trend line. The error bars show the standard deviation of the measurements of different samples in each concentration.

According to the trend line in figure 4.2, the mP increased slightly with the increasing STAT3 $_{127\text{-}722}$ concentration. The mP increased from 260 to over 280. However, the error bars indicating that there were big differences in the measurements between each sample of the same concentration set. The largest error bar covers mP from 220 to 280. Therefore the increase of the mP is not significant enough to suggest STAT3 $_{127\text{-}722}$ binds to dsDNA after 5mins incubation. The result suggests that the interaction between STAT3 $_{127\text{-}722}$ protein and the Bodipy-dsDNA is not immediate *in vitro*. Longer time incubation will be required to observe binding.

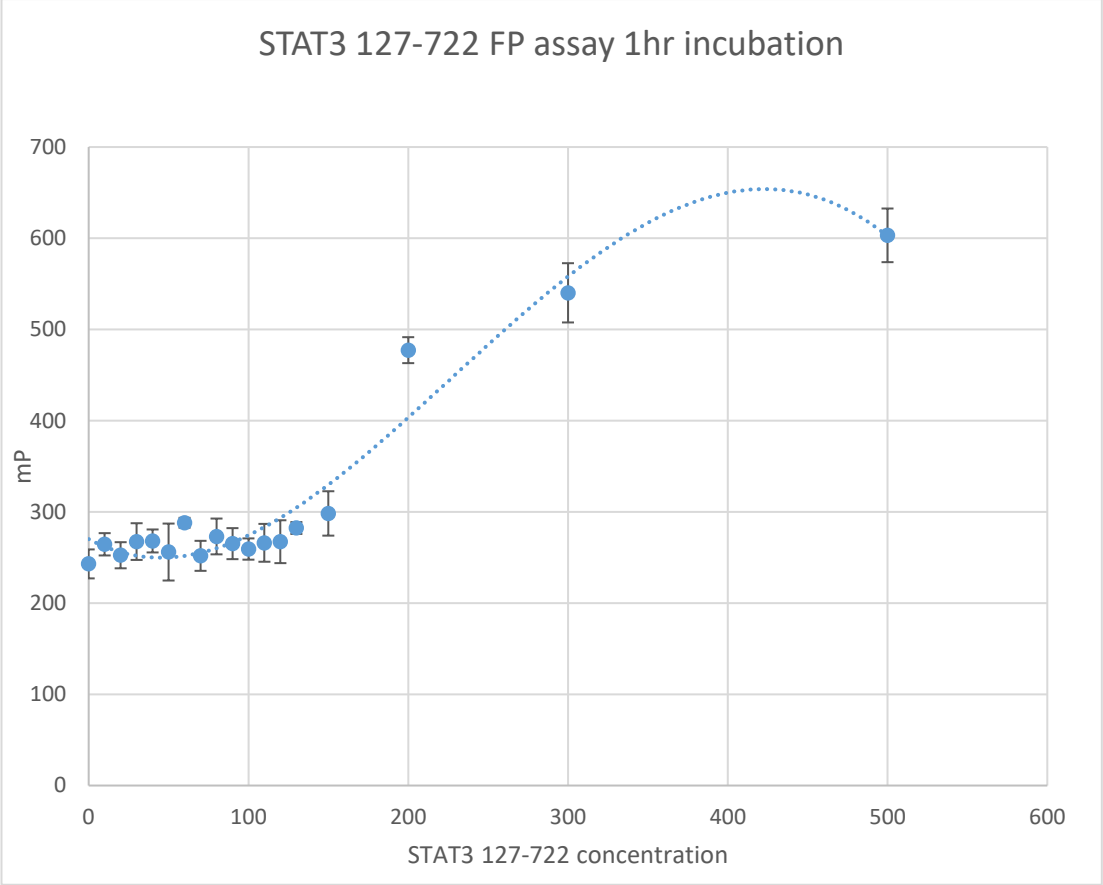


Figure 4.3. STAT3 $_{127\text{-}722}$ FP assay after 1hr incubation. The mP significantly increased with the STAT3 $_{127\text{-}722}$ concentration from about 250 to 600. The error bars show the standard deviation of the measurements for each concentration.

After incubating at 4℃ for 1hr, the mP significantly increased with the increasing STAT3 $_{127\text{-}722}$ concentration. The mP increased from 250 to 600 when the protein concentration increased from 0nM to 400nM. According to the trend line calculated from the obtained data, the mP stopped increasing when the protein concentration reached 400 nM. This indicates that protein-DNA interaction reached saturation with excess of the protein concentration when the protein: dsDNA ratio was 40:1. The EC50 protein concentration was about 250 nM. Comparing to the 5mins incubation, the 1hr incubation samples showed significant differences on FP signal between different protein concentrations. Therefore we conclude that after 1 hr incubation at 4℃ the protein-DNA interaction between the STAT3 $_{127\text{-}722}$ and the Bodipy-dsDNA reached equilibrium.

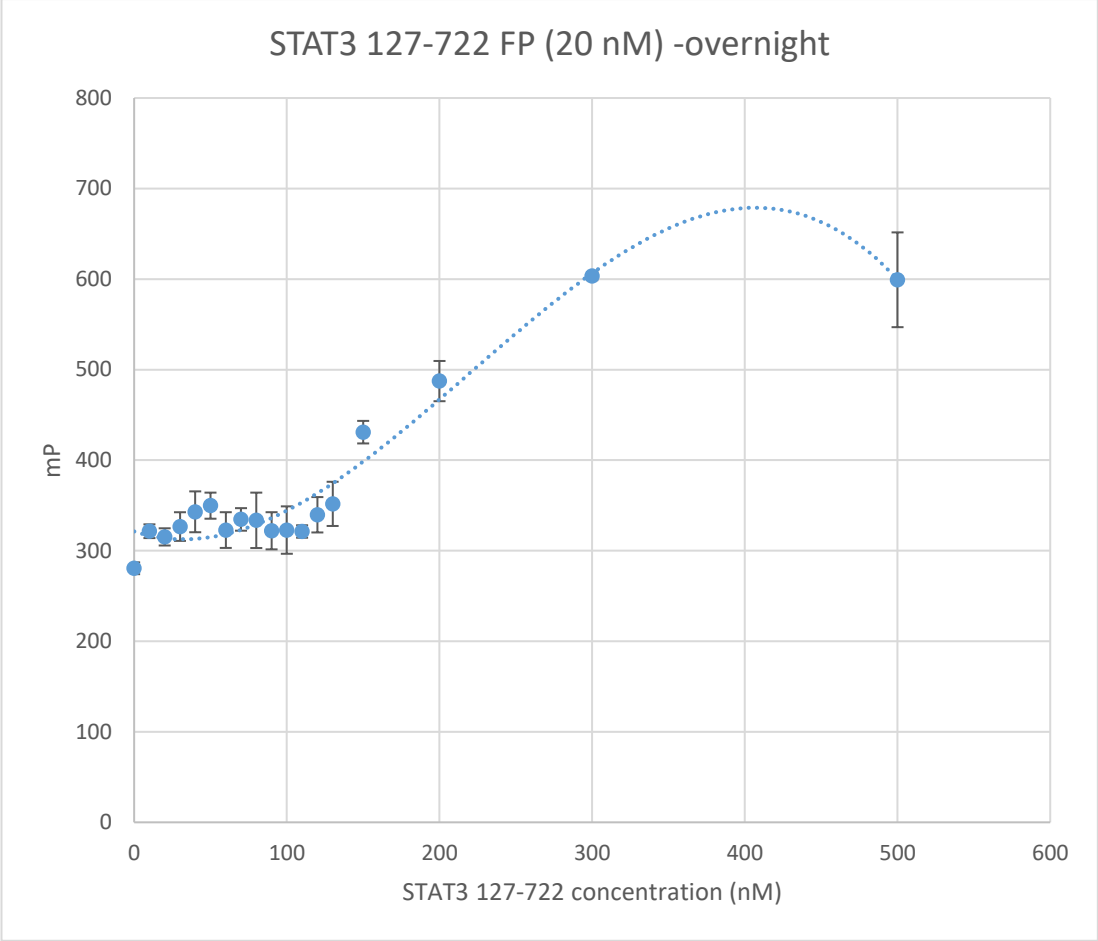


Figure 4.4, the STAT3 $_{127\text{-}722}$ FP assay after overnight incubation. Error bars are the standard deviations.

After incubation overnight for about 18hrs, the mP significantly increased with the increasing STAT3 $_{127\text{-}722}$ concentration. The mP increased from 300 to 600 when the protein concentration increased from 0 nM to 400 nM. The overnight incubation result is similar to the 1hr incubation result, indicating that overnight incubation does not change the equilibrium between the STAT3 $_{127\text{-}722}$ mutant and the Bodipy-dsDNA. Therefore the incubation time to obtain highest mP signal equals or less than 1hr.

STAT3 127-497 protein were incubated with Bodipy-dsDNA for 5mins, 1hr, and overnight (about 18hrs) and the mP was measured both perpendicular and parallel. Increased concentration of STAT3 127-497 protein was tested with 20 nM Bodipy-dsDNA.

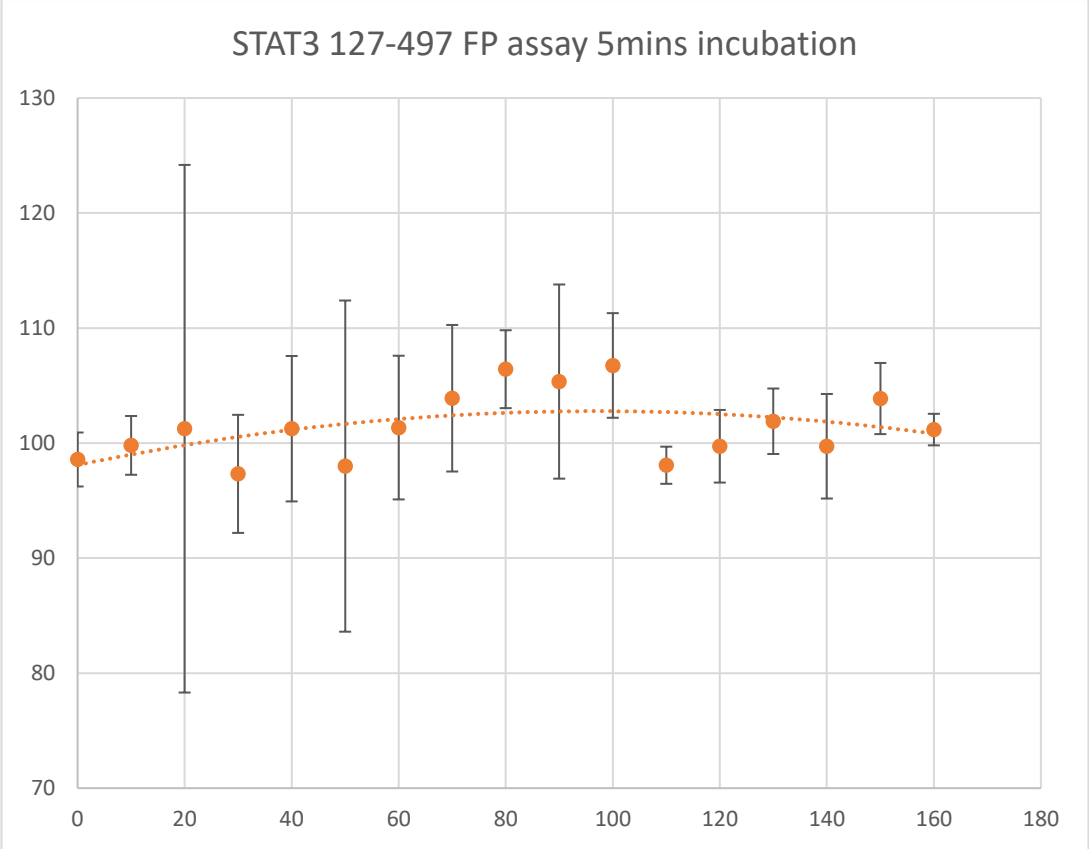


Figure 4.5. FP assay of STAT3 $_{127\text{-}497}$ incubated with Bodipy-dsDNA for 5mins.

Same as the STAT3 $_{127\text{-}722}$ truncated protein, the STAT3 $_{127\text{-}497}$ did not bind to Bodipy-dsDNA without incubation. With the increasing concentration of STAT3 127-497, there is no significant increase on the mP signal. The mP signal is stable around 100.

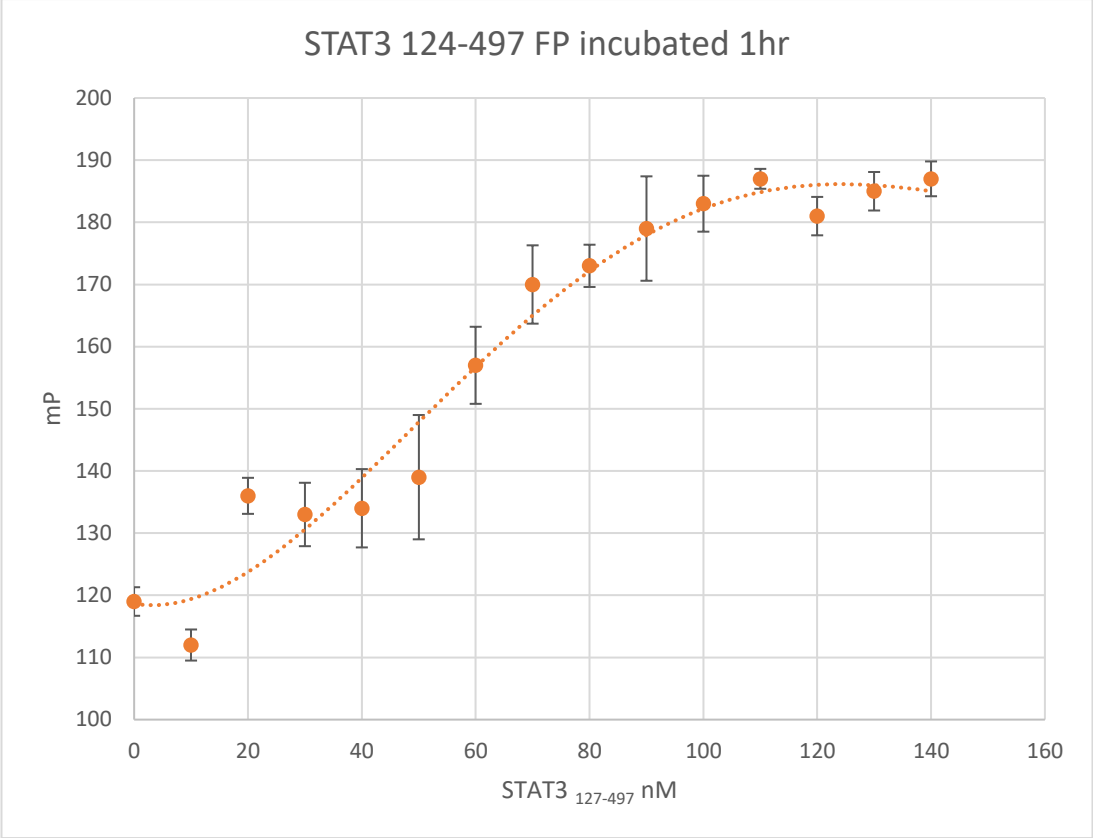


Figure 4.6. STAT3 127-497 FP assay after 1 hr incubation. mP significantly increased with the increase STAT3 127-497 concentration. The error bars show the standard deviations of the measurements for the same concentration.

Figure 4.6 confirms the ability of the STAT3 127-497 truncated protein binding to Bodipy-dsDNA. The mP increased significantly with the increase of the protein concentration from 120 to 190. The mP reached maximum when the protein concentration was 110nM therefore the STAT3 protein saturates the Bodipy-dsDNA at 110 nM with excess of the protein concentration. The protein: dsDNA ratio at the saturation point was about 5.5:1. The $EC_{50}$ was about 70 nM. By comparing the result with STAT3 127-722 FP assays, we conclude that lower STAT3 127-497 protein concentration is required to saturate the dsDNA binding.

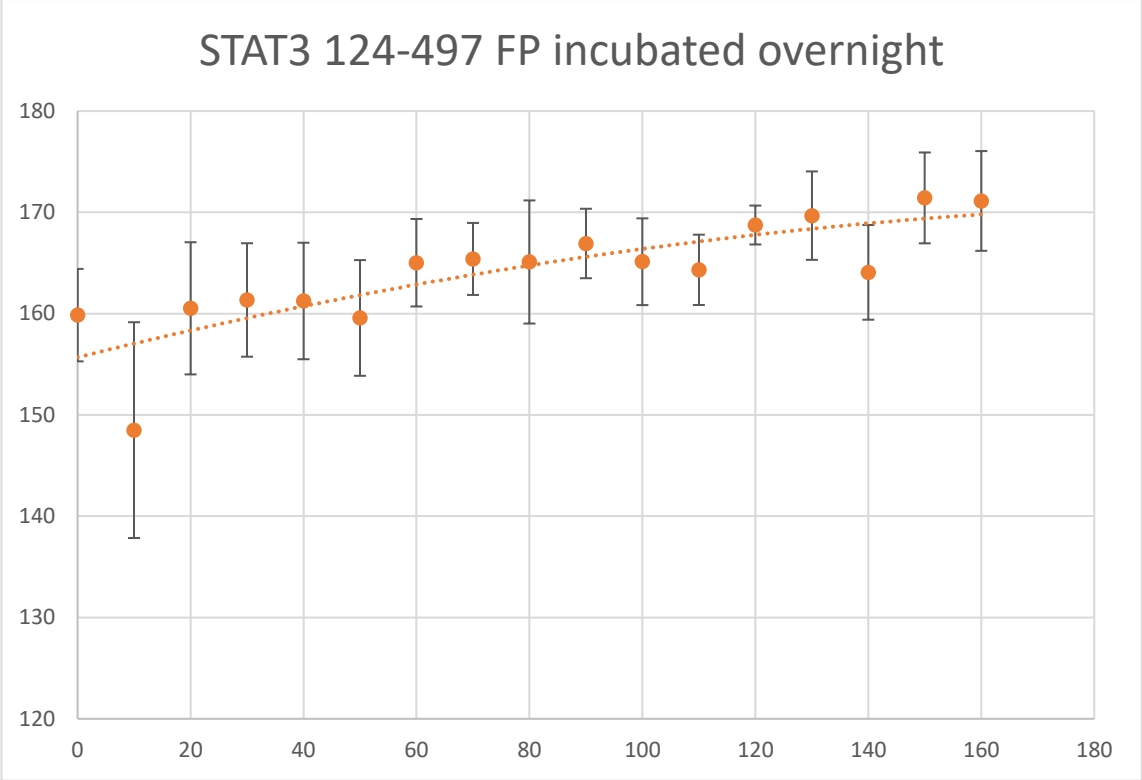


Figure 4.7. STAT3 127-497 FP assay after overnight incubation.

The mP increased slightly with the increasing STAT3 127-497 concentration after overnight incubation. The mP signal ranged from 150 to 170. The increase was significantly less than the 1hr incubation FP assay, indicating the loss of dsDNA binding activity of the STAT3 127-497 after overnight incubation. Therefore we assume that the stability STAT3 127-497 is weaker and loses DNA binding ability after overnight incubation.

In conclusion, we confirmed the DNA binding ability of STAT3 127-497 truncated protein. Interestingly, we discovered that the concentration of STAT3 127-497 protein required to saturate the dsDNA binding is lower than that of the STAT3 127-722 protein. However, the DNA binding activity of STAT3 127-497 protein significantly decreased after overnight incubation. This suggest that the STAT3 127-497 protein is less stable compared to the STAT3 127-722 protein. Furthermore, the FP assay of STAT3 127-497 protein can be used to specifically detect the STAT3 inhibitor targeting the DBD domain and CCD domain.

## 4.5 Discussion

The FP assay provided a high-throughput method for drug screening targeting STAT3. Comparing to the PEMSA assay described in chapter 3, the FP assay is more efficient in detecting small molecule inhibitors that stop STAT3 DNA binding activity. The STAT3 $_{127\text{-}497}$ mutant applied in the FP assay in this thesis lacks the SH2 domain thus can be used to screen STAT3 inhibitors targeting the DNA binding domain more specifically. The FP assay confirmed the DNA binding activity of the STAT3 $_{127\text{-}497}$ mutant again. Therefore the DNA binding activity showed by the YFP-STAT3 $_{127\text{-}497}$ mutant in the PEMSA result was not significantly affected by the YFP. Furthermore, the materials (including the protein, the dsDNA and the small molecule inhibitors) required in the FP assay are in nanomolar range. Same amount of the purified STAT3 protein can be used to detect more inhibitors in the FP assay compared to the PEMSA assay.

# Chapter5- Optimizing FRET assay in detecting STAT3 biological activities

## 5.1 A brief introduction to FRET

Fluorescent resonance energy transfer (FRET), also called Förster resonance energy transfer, is based on the non-radioactive energy transfer that happens between two fluorescent molecules when they are close enough. One of the fluorescent molecules is regarded as the donor while the other is called the acceptor. When the donor is excited, the energy can be transferred to its nearby acceptor if the distance between the donor and acceptor is shorter than 10 nm and suitably oriented. The energy transfer usually results in the decrease fluorescence at the donor's emission wavelength and the increase fluorescence at the acceptor's emission wavelength.

FRET has been a very popular method for detecting protein-protein interaction, peptide and nucleotide folding and fluorescent microscopy imaging *in vivo*. In this thesis, we developed FRET assay to detect STAT3 DNA binding activity *in vitro*.

The proportion of the energy transferred from the donor to the acceptor after excitation is usually referred to as the FRET efficiency. The FRET efficiency is determined by the distance between the donor and the acceptor. The relationship between the FRET efficiency (E) and the distance between the two fluorophores is described according to the following equation:

$$E= 1 / [1+ (r + R_0 )^6]$$

$R_0$ is the distance between the donor and acceptor when E is 50%. According to the mathematics, the FRET efficiency is simply affected by the distance between the donor and the acceptor. However during the real experiment it can also be influenced by various background noise such as the intrinsic fluorescence of the donor and receptor fluorophores, fluorescence quenched by the materials in the solution ($Cl^-$). Therefore

negative controls in the FRET experiments are essential to provide confident results.

The background noises of the FRET assay can be minimised by careful selection of the donor and receptor group. The overlap between the donor's excitation wavelength and the acceptor's excitation wavelength, and the donor's emission wavelength and the acceptor's emission wavelength need to be minimised. In contrast, the donor's emission wavelength is required to be highly overlapped with the acceptor's excitation wavelength.

## 5.2 FRET methods

The FRET assays were conducted in two ways: titration in the cuvette in the scanning fluorimeter (PerkinElmer LS 55 Luminescence Spectrometer) and set reaction in 96-well flat bottom plates using (BMG-Labtech Pherastar fluorescence plate reader). The fluorimeter is able to plot the emission curve for a set range of wavelength while the plate reader has an ultra-high dynamic range and can screen the interaction between wide concentration ranges of the protein and the dsDNA. In the fluorimeter, the emission was recorded at 475nm and 520nm to optimise the differences caused by the energy transfer while in the plate reader the emission was recorded at 480 nm and 530 nm due to the set of the module. Besides, the differences in the instrumental gain lead to the differences of the readings in the two different machines. Therefore, the results of the FRET from the two machines were analysed separately.

The FRET signal can be increased with application of the C-terminal fluorescent protein fused STAT3 mutations since the distance between the STAT3 C-terminal is closer to both the other monomer and the ends of the dsDNA. Therefore, the STAT3 $_{127\text{-}722}$-YFP/CPF proteins were produced to increase the FRET signal and also to detect dimerisation of the STAT3 mutated proteins with FRET. The plasmids were created by PCR cloning and insertion and the proteins were produced and purified with the same methods as other STAT3 proteins. The result of the extraction and

purification of the STAT3 $_{127\text{-}722}$-YFP and STAT3 $_{127\text{-}722}$-CFP protein was described in chapter 2.

To optimise the FRET signal between STAT3 DNA interaction and between the STAT3 dimers, C-terminal fluorescent protein fused to the truncated STAT3 proteins were created. Plasmids producing the STAT3 proteins with C-terminal fluorescent protein labels created from the pET32a (+) plasmid expressing STAT3 $_{127\text{-}722}$ protein. The eYFP and eCFP genes used for insertion were copied from the plasmids expressing YFP-STAT3 127-722 and CFP-STAT3 127-722 proteins using polymerase chain reaction (PCR). Restriction digestion sequences for cloning were designed in the primers used for eYFP and eCFP amplification. The amplified DNA was inserted downstream of the STAT3 gene between the *Eco*R1 and *Sal*1 restriction digestion sites. During the gene cloning, Qiagen PCR purification kits and Qiagen gel purification kits were used to purify the desired insertion sequence and the digested template. The success of insertion was detected by restriction digestion. The modified plasmids were produced and purified by Qiagen Maxiprep kit with the same method as purification of other pET32a (+) plasmids. The processes of creating the plasmids for producing STAT3 $_{127\text{-}722}$-YFP/CFP proteins are shown in figure 5.1.

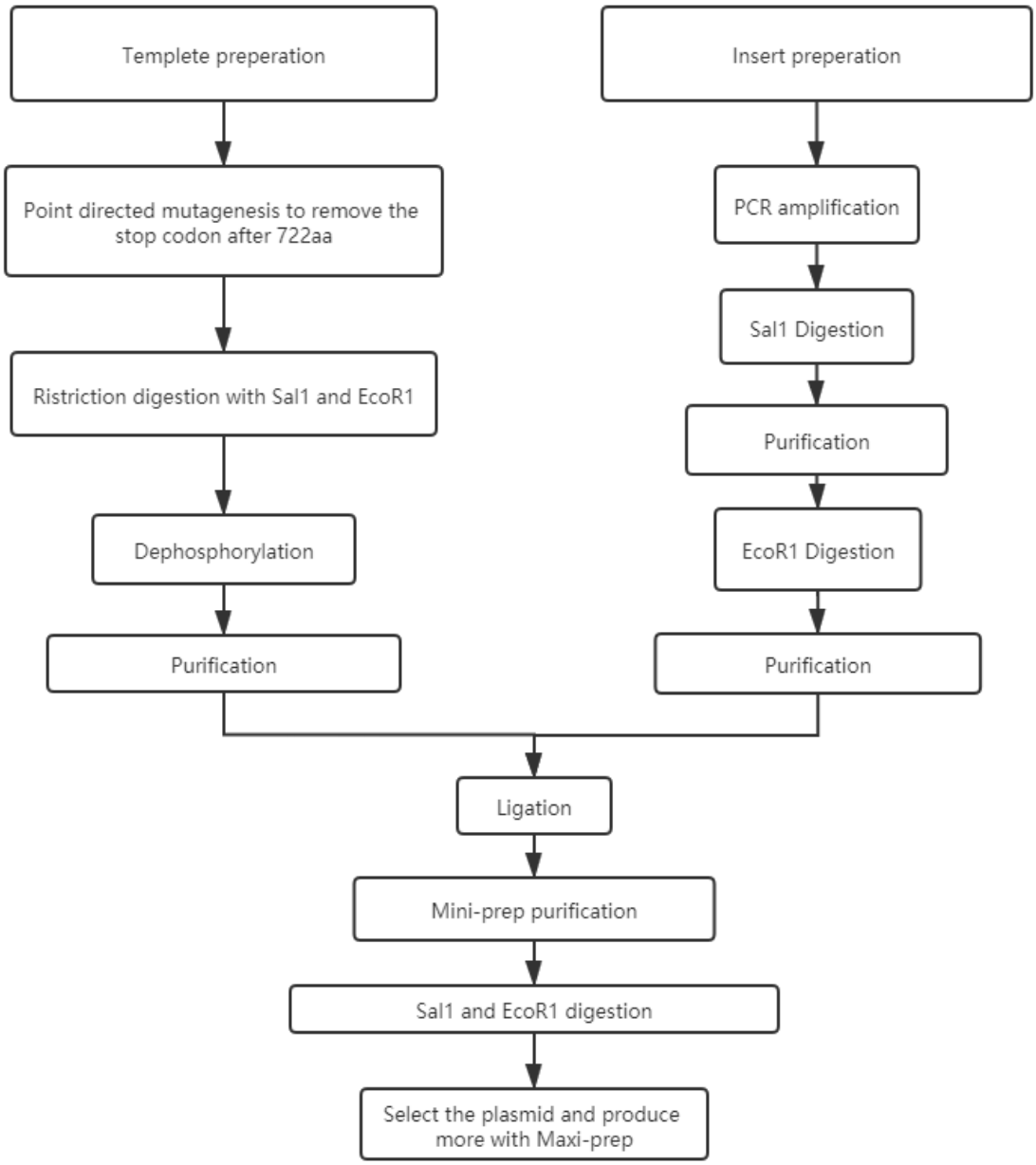


Figure 5.1. The processes of creating C-terminal fluorescent protein fused STAT3 mutations.

### 5.2.1 PCR amplification of the eYFP and eCFP gene

The eYFP and eCFP genes were amplified with PCR using the YFP-STAT3 $_{127\text{-}722}$ and CFP-STAT3 $_{127\text{-}722}$ plasmids as templates. Two designed primers were used to multiply the eYFP and eCFP genes as well as inserting restriction digestion sites to the ends of the genes. The principle of the PCR process were shown in figure 5.2.

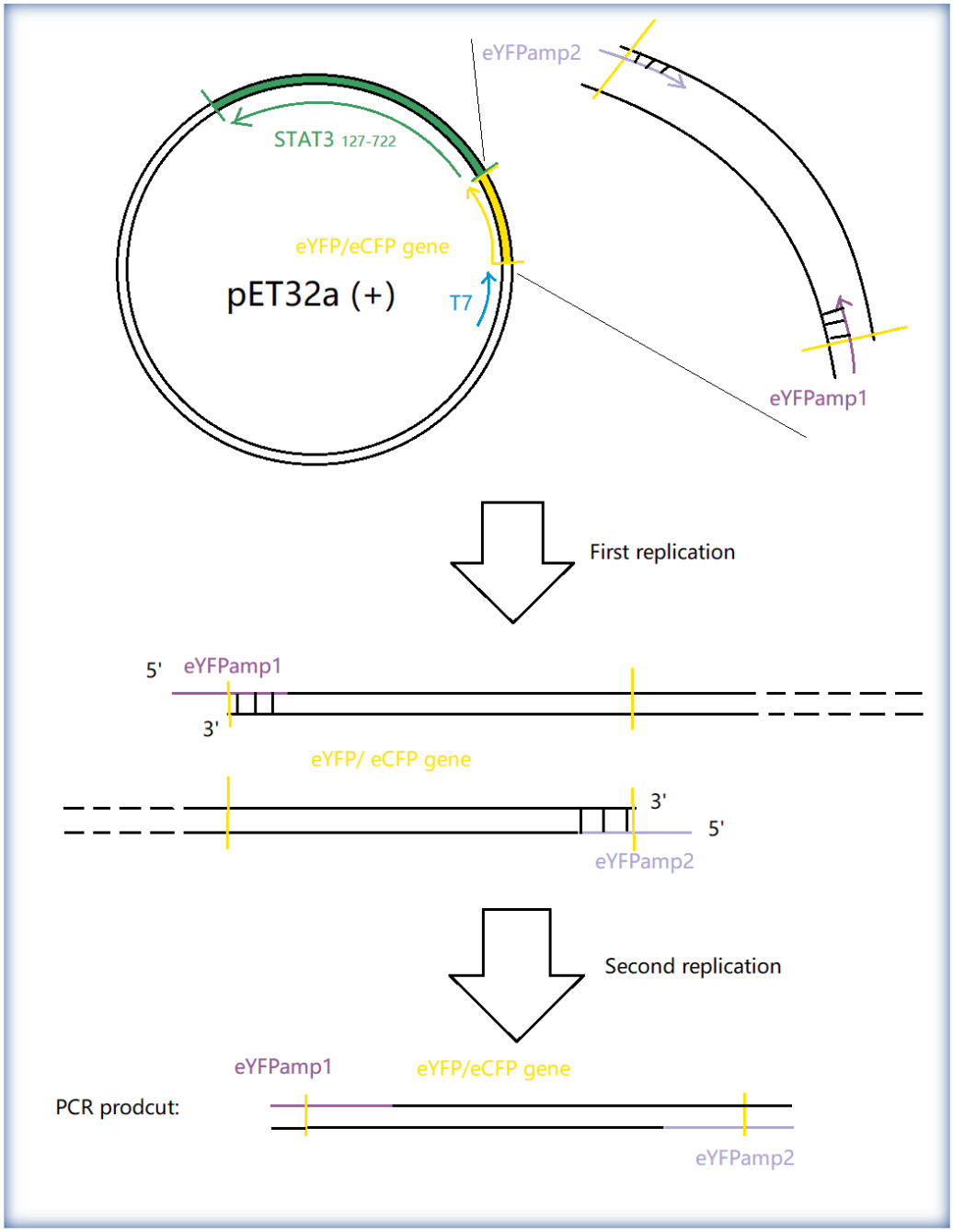


Figure 5.2. PCR amplification of the eYFP and eCFP genes to create insertion sequences that can be further used in the cloning.

The primers were ordered from Eurofins Genomics. The sequences are shown below:

eYFPamp1: 5'- AAA AGA ATT CAT GGT GAG CAA GGG CGA G -3'

eYFPamp2: 5'- ATA TGT CGA CTA CTA TTA CTT GTA CAG CTC GTC CA -3'

The eYFPamp1 is 28 bases with 18bp in the middle that matches the start of the eYFP sequence and 10bp mismatches on 5' end with designed *Eco*R1 digestion site and 4As extension. The un-pairing sequences in the two primers allow the restriction enzyme to bind tightly to the restriction digestion site. The GC% of the matching sequences in the eYFPamp1 is 61% and the Tm calculated is 61.7℃. The length of the eYFPamp2 is 35 bases with 25 bases matches and 10 bases mismatches attached to the 5' end. The mismatches consist of 4 bases overhangs (ATAT) and 6 bases of the *Sal*1 digestion sequence. The GC content of the matching sequence in eYFPamp2 is 40% and the Tm is 60.4℃.

The PCR was performed according to the following chart:

| Stage | Cycles | Temperature | Time |
|---|---|---|---|
| 1 | 1 | 60 | 2mins |
| 2 | 18 | 95 | 20s |
| | | 60 | 10s |
| | | 68 | 240s |
| 3 | 1 | 68 | 5mins |
| 4 | 1 | 4 | 10mins |

### 5.2.2 Agarose gel electrophoresis

The success of amplification was checked with 0.8% agarose gel. 0.48 grams of the agarose were added to 60ml of the 0.5x TBE buffer (22.5 mM Tris-Base, 22.5 mM boric acid, 0.5 mM EDTA) and melted by microwave heating. 24 µl of the 6x SYBR safe dye was added into the melted agarose solution before it solidifies. 10 µl of the PCR sample was mixed with 2 µl of the DNA loading dye and 10 µl of the mixtures were loaded into each well. The electrophoresis were conducted at 80 V for 1hr 20mins.

### 5.2.3 Purification of the PCR products with the Qiagen gel purification kit

The bands of the PCR products in the agarose gel were carefully cut out under the safe imager. The purification steps were performed according to the Qiagen gel purification kit. The final PCR products were eluted in dd$H_2O$ and concentration measured with nanodrop.

### 5.2.4 Preparation of the template

The template used in the cloning was developed from the plasmid coding for the STAT3 127-722 protein. The stop codon after the 722aa was removed by point-directed mutagenesis with the QuickChange Lightning kit. Primers used in the mutation are shown below:

722stopdel1:

5'- GAT GCA GTT TGG AAA ^GAA TTC GAG CTC CG -3'

722stopdel2:

5'- CGG AGC TCG AAT TC^T TTC CAA ACT GCA TC -3'

Both primers are 29bp with 14bp and 15bp matching sequence on both ends of the deletion point. The GC content was 48.3% and the Tm was about 74℃.

The PCR for the point-directed mutagenesis was performed according to the following chart:

| Stage | Cycles | Temperature | Time |
|---|---|---|---|
| 1 | 1 | 60 | 2mins |
| 2 | 18 | 95 | 20s |
| | | 60 | 10s |
| | | 68 | 240s |
| 3 | 1 | 68 | 5mins |
| 4 | 1 | 4 | 10mins |

The original plasmids were removed by *Dpn*1 digestion for 5mins at 37℃. *Dpn*1 recognises and cleaves GATC sequence only when Adenine (A) is methylated. PCR amplified plasmids are not methylated while the original templates were synthesised in bacteria cells and methylated. Therefore *Dpn*1 cleaves the templates selectively. The PCR amplified plasmids were transferred into XL10 competent cells and further purified with Qiagen Maxiprep kit. The purified plasmids were sequenced by Eurofins to ensure the deletion of the stop codons. The purified plasmids were used as stock templates.

### 5.2.5 Restriction digestion with *Eco*R1 and *Sal*1

Both the template and the insertions (eYFP and eCFP cloned genes) were treated with *EcoR1* and *Sal*1 separately. The *Eco*R1 restriction enzyme was purchased from Thermofisher and the *Sal*1 was purchased from New England Biolabs. The template and the insertions were first incubated with *Eco*R1 for 6hrs in the provided *Eco*R1 buffer at 37℃. After incubation, the enzyme was de-activated by heating at 95℃ for 10 mins. Then the treated samples were purified with Qiagen PCR purification kit to remove the enzyme and the buffer. The purified products were treated with *Sal*1 in the provided *Sal*1 buffer. Same purification steps were conducted before insertion. The templates were treated with phosphatase (Quick CIP). The phosphatase treatment removed the phosphate group at the 5' end of the template therefore reduces the chance of template re-close.

### 5.2.6 Insertion

The digested template was purified with Qiagen PCR product purification kit to remove the small fragment of gene between *Sal*1 and *Eco*R1. The ligation (50 ng template, 37.5 ng purified eYFP/eCFP, 1 μl T4 DNA ligase, provided T4 ligase buffer) was performed with T4 DNA ligase purchased from New England Biolabs.

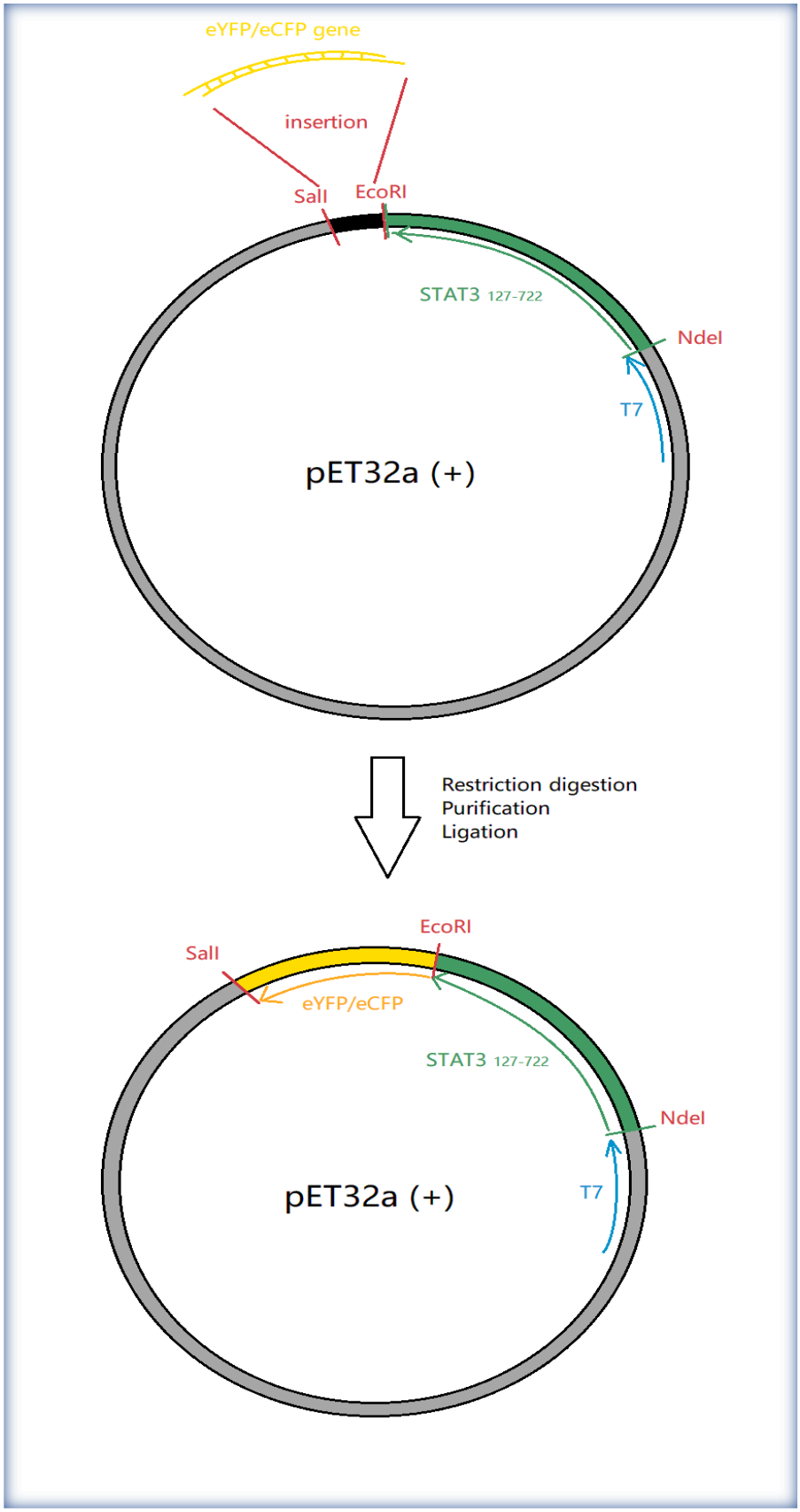


Figure 5.3. The eYFP/eCFP gene was inserted into the template between the *Eco*R1 and *Sal*1 restriction digestion site.

The re-linked plasmids were transferred into XL10 competent cells through the process of heat shock and purified with Qiagen Miniprep kits. The purified plasmids were then treated with *Eco*R1 and *Sal*1 together in the [*Sal*1 buffer] and incubated at 37℃ overnight and the digestion products were screened with 8% agaroses gel using the same method mentioned above. According to the agarose gel, two plasmids were selected for the STAT3 $_{127\text{-}722}$-eYFP and the STAT3 $_{127\text{-}722}$-eCFP and further DNA stocks were produced and purified by Qiagen maxiprep kit. The purified plasmids were eluted in dd$H_2O$ and stored at -20℃.

## 5.3 Result:

### 5.3.1 Success deletion of the 722 stop codons

The samples of the purified plasmids were commercially sequenced by Eurofins. The results obtained are shown in figure 5.4.

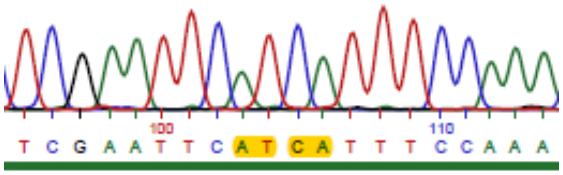


(a)

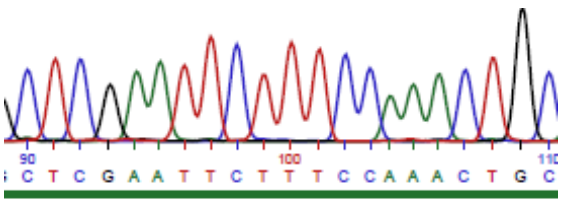


(b)

Figure 5.4. (a) Sequencing result before the stop codon was deleted. (b) Sequencing result after the TCA stop codon was deleted. Both (a) and (b) are the sequence of the complementary strand from 5' to 3'. The yellow labelled nucleotides in (a) are deleted in (b).

The sequencing results confirmed the success of the deletion. The deleted sequences contains two stop codons: TAG, TAA. Deletion of the four nucleotides completely removed the two stop codons after the 722aa. The deletion ensures the transcription of the subsequently inserted sequences.

Therefore, the modified plasmid can be used as a template for both eYFP and eCFP gene to be inserted separately.

### 5.3.2 Replication of the eCFP and eYFP gene

The eYFP and eCFP genes were successfully produced by the PCR. Bright single bands can be observed from agarose gel indicating pure and high concentration DNA products. 1kb plus ladder were purchased from Invitrogen indicating the size of the PCR product.

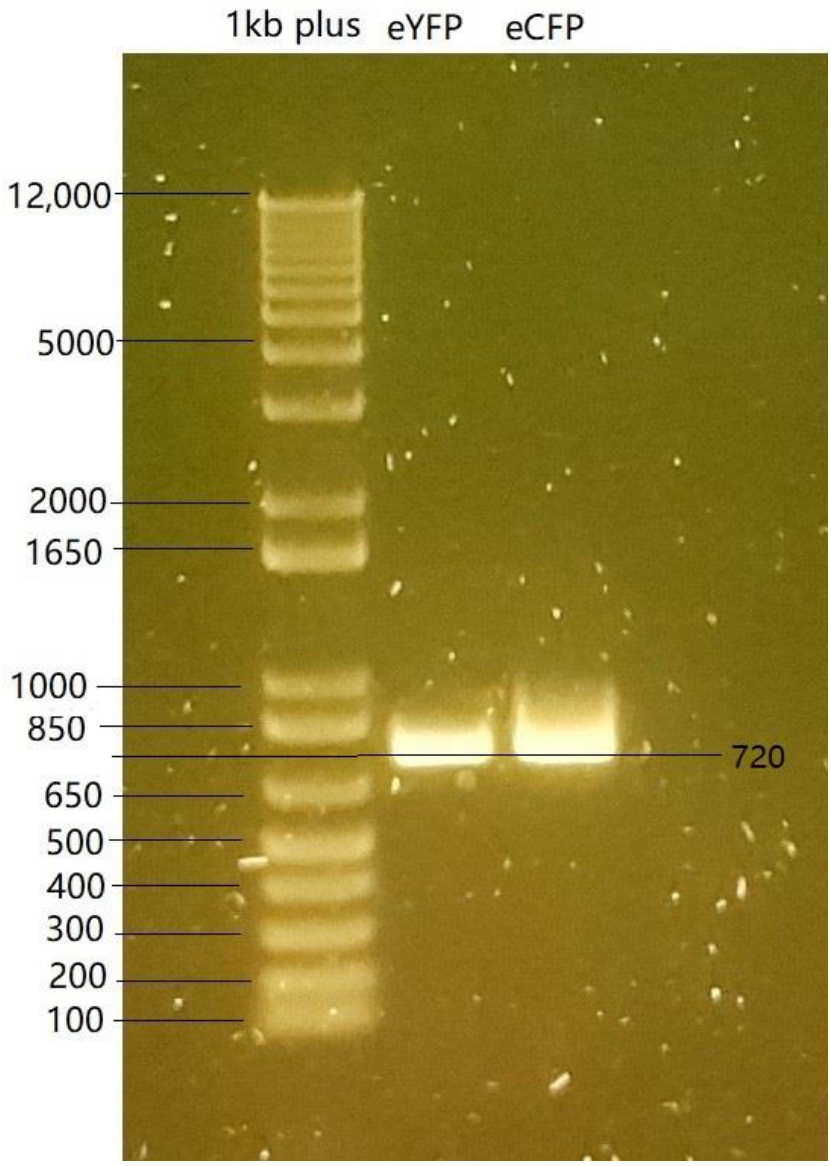


Figure 5.5. eYFP and eCFP were produced with PCR and the PCR products were tested in the agarose gel.

The 1 kb plus ladder shows the molecular weight from 12,000 bp to 100 bp. The size of the two bright bands are about 720 bp. The length of the desired eYFP and eCFP genes are 736 bp. Therefore we assume that the two bands were the desired PCR products.

### 5.3.3 Restriction digestion of the purified plasmids

The digested plasmid samples were screened with agarose gel electrophoresis. The plasmids with a successful insertion should be digested into two bands with *Sal*1 and *Eco*R1. If the digestion was insufficient, there might be three or four bands. The possible bands of a successful cloned plasmid after digestion can include: eYFP/eCFP band about (720 bp), and the rest of the plasmid, pET32a (+) with STAT3 insertion (7200 bp), or once digested plasmids (7950 bp), or uncut circular, or supercoiled plasmids. The supercoiled plasmids of the pET32a (+) with STAT3 insertion usually run slower than the single digested band under the described electrophoresis condition.

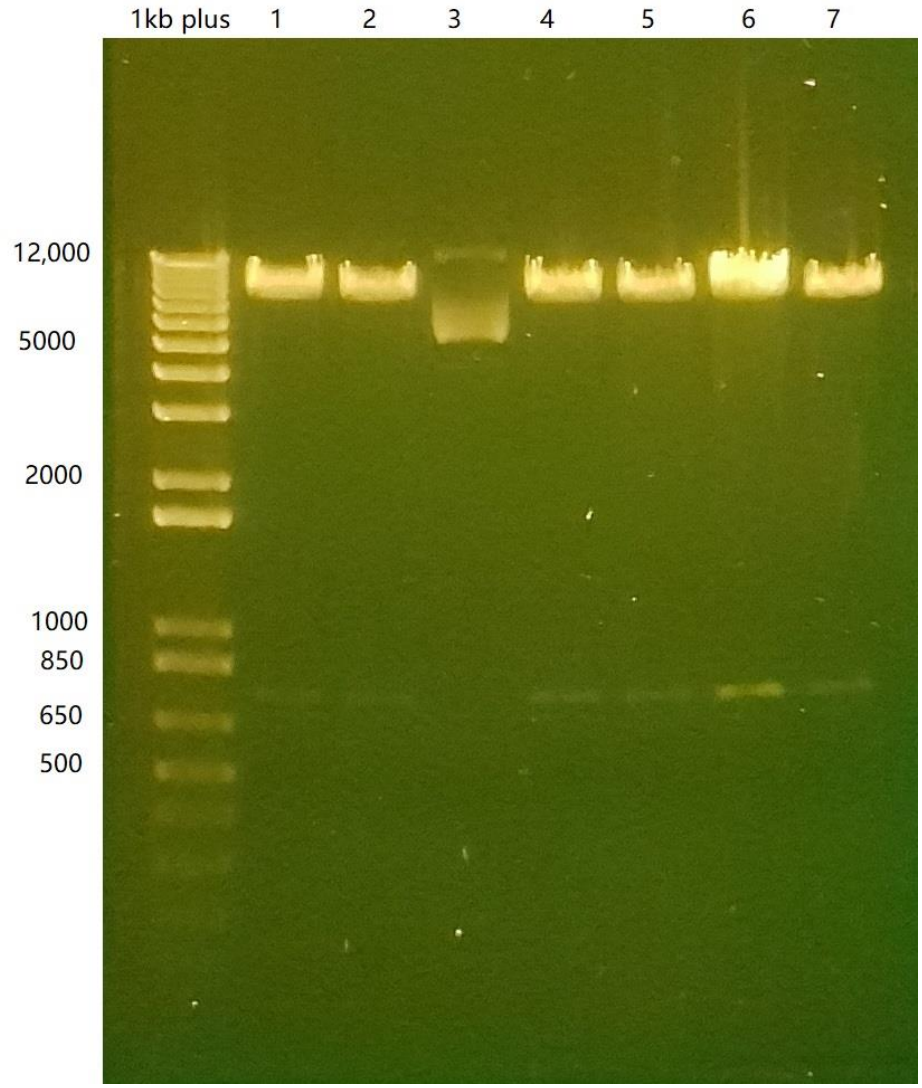


Figure 5.6. Agarose gel of the *Sal*1 and *Eco*RI digested plasmid samples. Wells 1, 2, 3, 4 were the eYFP insertion samples and wells 5, 6, 7 were the eCFP insertion samples.

According to figure 5.6, plasmids in well 1, 2, 4, were successfully eYFP/ 5, 6, 7 were successfully inserted with eCFP genes. In those wells, feint bands at about 720bp can be observed. The *Eco*R1 digestion may not be sufficient in the *Sal*1 buffers therefore there should be three bands: the 720bp insertions, the 7200bp templates, and the 7950bp single digested plasmids. The 720bp insertions can only be created by double digestion with both *Eco*R1 and *Sal*1. Therefore the double digested plasmids contribute to a low proportion of the plasmid samples. The concentration of the single digested plasmid in the samples were high thus the 7950bp bands were extremely

thick and bright that covers the 7200bp bands. No undigested plasmids were observed in the gel indicating that the *Sal*1 digestion is sufficient. Sample 1 and sample 6 were selected from 1, 2, 4 and 5, 6, 7 separately to represent the eYFP and eCFP insertions respectively.

### 5.3.4 Protein preparation:

The STAT3 proteins purified by IEx chromatography (produced and purified in Chapter 2) were buffer exchanged with Centrifugal (30 kDa) centrifugation. The purified proteins were buffer exchanged into buffer contains 25mM Tris pH8.5, 100 mM NaCl. The buffer exchanged proteins were then mixed and diluted with 5xFRET binding buffer (150 nM Tris pH8.5, 1.5 mM EDTA, 1.5 mM EGTA, 5 mM $MgCl_2$, 200 nM KCl, 0.5 mg/ml BSA and 0.2 mg/ml sonicated salmon sperm) and dd$H_2O$.

**DNA annealing:**

Two single stranded DNA oligos were purchased from Eurofins Genomics. The sequences of the two oligoes are shown below:

5'-ATTO488-TGC ATT TCC CGT AAA TCT-3'

5'-AGA TTT ACG GGA AAT GC-3'

The single stranded DNA oligoes were annealed in annealing buffer (15 mM Tris pH 8.3, 20 mM NaCl) at 90℃ for 5mins and cooled down 1 ℃/min to 10℃ in a PCR machine.

**FRET titration and 96-well plates:**

In the FRET titration assay, the STAT3 protein or the dsDNA was first mixed with the 5x FRET buffer and d$H_2O$. The concentrated dsDNA or STAT3 protein was then added into the mixed solution and incubated for 5mins before reading. The reaction solution were excited at 430nm. Fluorescent intensity at 475 nm and 520 nm were recorded as the donor's emission and acceptor's emission.

Besides the titration FRET assay, additional FRET assays were conducted in 96 well plates to simplify and increase through-put for the experiment processes. The STAT3 proteins and the annealed Atto488-GAS18 DNA

were pre-mixed and incubated on ice for 30 mins in the 96-well flat bottom plate before the measurement. With excitation at 430 nm, the fluorescence intensity at 480 nm (donor's emission) and 530 nm (acceptor's emission) were detected by the plate reader.

**FRET ratio and FRET efficiency:**

The FRET energy transfer is usually expressed in two ways: the FRET efficiency and the FRET ratio. The proportion of the non-radioactive energy transferred from the excited donor to the receptor can be defined in both ways.

The FRET efficiency was calculated based on the following equation:

$$FRET\ efficiency = 1 - FDA/FD$$

FDA is the fluorescent intensity measured at donor's emission wavelength with both donor and acceptor while FD is the fluorescent intensity at donor's emission wavelength without acceptor (Atto-DNA). In our case, FDA is the fluorescent intensity measured at FI475 with both protein and Atto-DNA added in the samples while FD is the fluorescent intensity measured at FI475 without Atto-DNA. The result shows that the FRET efficiency is also increasing with the increased concentration of receptor. This indicates that when STAT3 127-722-CFP binds to Atto-DNA, there was signal transfer between the donor and receptor. The FRET efficiency suggests that when the donor's (STAT3 127-722-CFP) concentration is stable, increasing acceptor concentration will increase the FRET signal.

The FRET ratio was calculated based on the following equation:

$$FRET\ ratio = FAD/FA$$

FAD is the fluorescent intensity measured at FI530 with both donor and acceptor while FA is the fluorescent intensity at FI530 when there is no donor (STAT3-CFP). The FRET ratio should be higher than 1 to indicate there is FRET happening.

## 5.4 Result:

### 5.4.1 Donor and Receptor pair: CFP and Atto488

The selected donor-receptor pair in this thesis is CFP and Atto488. The CFP attached to the STAT3 truncated proteins were used as the donor while the Atto488 attached to the dsDNA was used as the receptor. The excitation wavelength of the CFP is 435nm and the emission wavelength is 485nm. The Atto488 is a synthetic water soluble fluorescent label described by ATTO-TEC. Atto488 is characterised with high quantum yield (0.8). The quantum yield stands for the proportion of the proton emitted to the number absorbed. The excitation wavelength of the Atto488 ranges from 480nm to 500nm while the emission wavelength is maximal at 520nm. The excitation for the Atto488 at 430nm is minimal. According to the described excitation and emission wavelength, the CFP and Atto488 can be used as the donor and receptor pair in the FRET assays. 10nM of the CFP-STAT3 127-722 protein and 10nM of the Atto488-GAS18 were excited at 430nm. Emissions were recorded in figure 5.7.

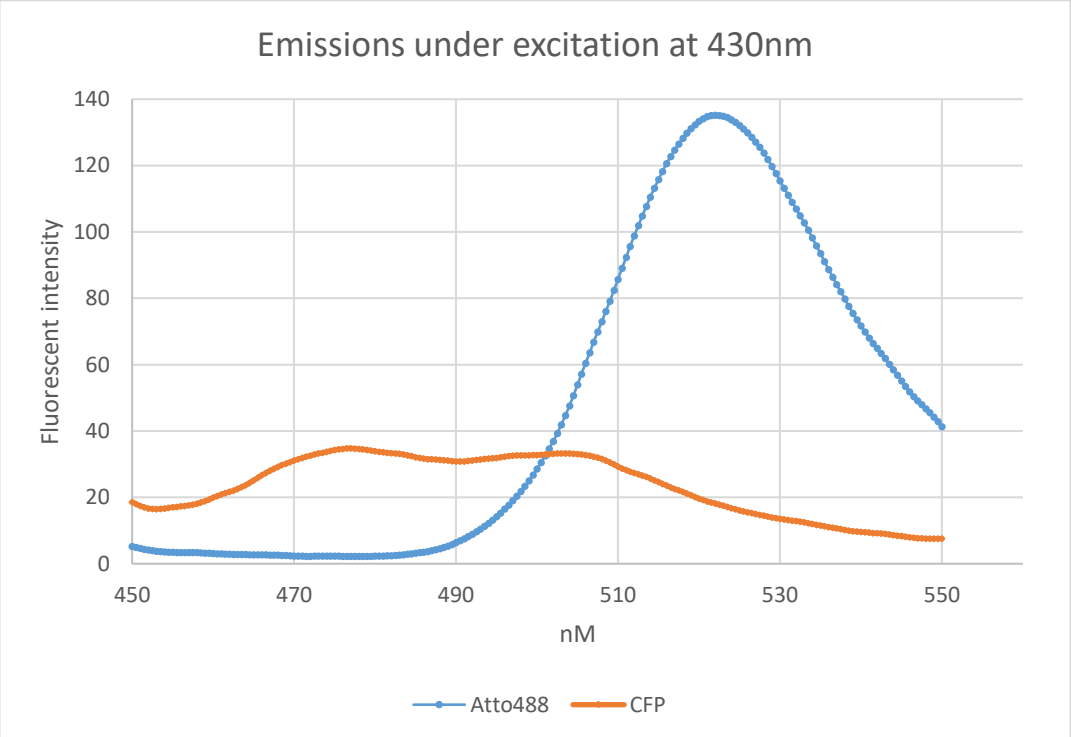


Figure 5.7. Emission from 450 nm to 550 nm of 10 nM CFP-STAT3 $_{127-722}$ protein and 10 nM Atto488-GAS18 with the excitation at 430 nm.

With excitation at 430 nm, the fluorescent emission of 10 nM CFP-STAT3 127-722 and 10 nM Atto488 was measured separately. The fluorescent intensity peak of the CFP-STAT3 127-722 protein ranges from 475-510 nm. The fluorescent intensity of the CFP-STAT3 127-722 truncated protein at 475 nm is about 38 while the fluorescent intensity at 510 nm is about 35. Although the excitation of the Atto488 is minimal at 430 nm, there is still a fluorescent peak with highest reading about 138 at 520 nm. Comparing the fluorescent intensity peaks of the CFP-STAT3 127-722 and Atto488-GAS18, the emission of fluorescence of the acceptor is significantly higher than the donor under the donor's excitation wavelength with the same concentration of the fluorophore. The Atto488 is much more sensitive of the excitation comparing to the CFP. Therefore, high donor (CFP) concentration is recommended in the future experiments. The energy transfer may not contribute to significant fluorescent intensity increase at 520 nm since the receptor's (Atto488) emission is too high at the donor's excitation (430 nm). Besides, the observation of the decrease fluorescent intensity at the donor's emission wavelength (475 nm) with the increase of receptor concentration should be more efficient to measure the FRET ratio for this pair of fluorescent labels.

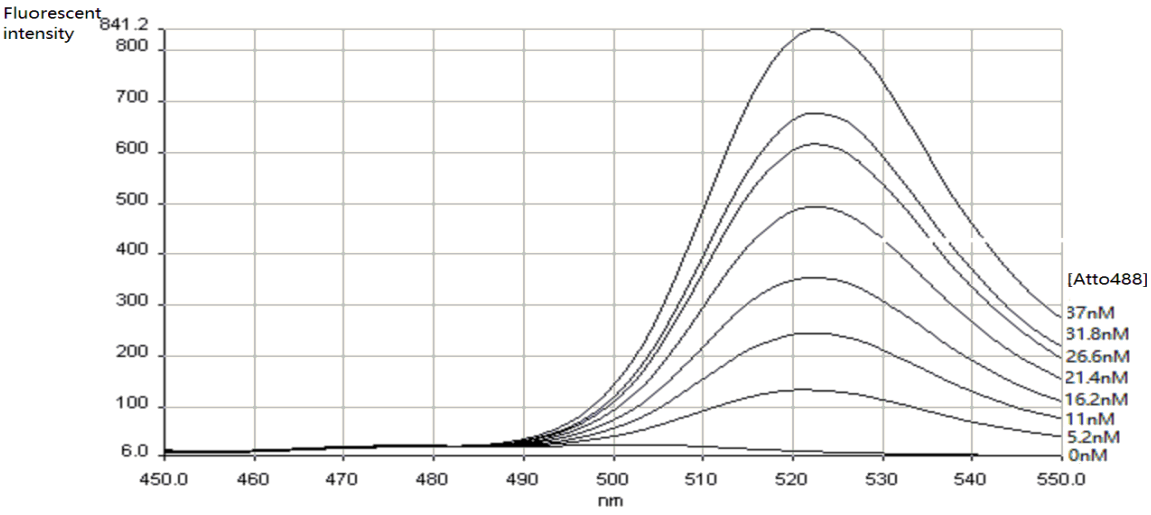


Figure 5.8. Titration of Atto488-GAS18 into the buffers without CFP-STAT3 proteins. The concentration of the Atto488-GAS18 increased from 0nM to 37 nM. The scans are directly obtained from the fluorimeter. The Y-axis is the fluorescent intensity while the x-axis is the emission wavelength.

Figure 5.8 shows the original data obtained from the fluorimeter, in which the fluorescent intensity at FI520 increased with Atto 488 concentration while FI475 did not. Atto488 can be excited at 430nm. Atto488-GAS18 was titrated into the 1xFRET binding buffers (30 mM Tris pH8.5, 0.3 mM EDTA, 0.3 mM EGTA, 1 mM $MgCl_2$, 40 mM KCl, 0.1 mg/ml BSA, 40 ng/ml sonicated salmon sperm and 8% glycerol). The fluorescent intensity was measured from 450 nm to 550 nm. Fluorescent peak can be observed at about 522 nm. No peak at 475 nm was detected. No significant increase of fluorescent intensity at 475 nm was detected with the increase of Atto488-GAS18 concentration. Although no donor was added, the emission at 520 nm still increased with the increase of donor's concentration. Therefore, the increase of fluorescent intensity at 520 nm with the increasing acceptor's concentration cannot be regarded as energy transfer. Negative control to eliminate the influence of the FI520 results from the acceptor excited by the donor's excitation wavelength was found to be necessary.

CFP-STAT3 $_{127\text{-}722}$ was titrated into the 1xFRET binding buffer and the emission curve was plotted in figure 5.9.

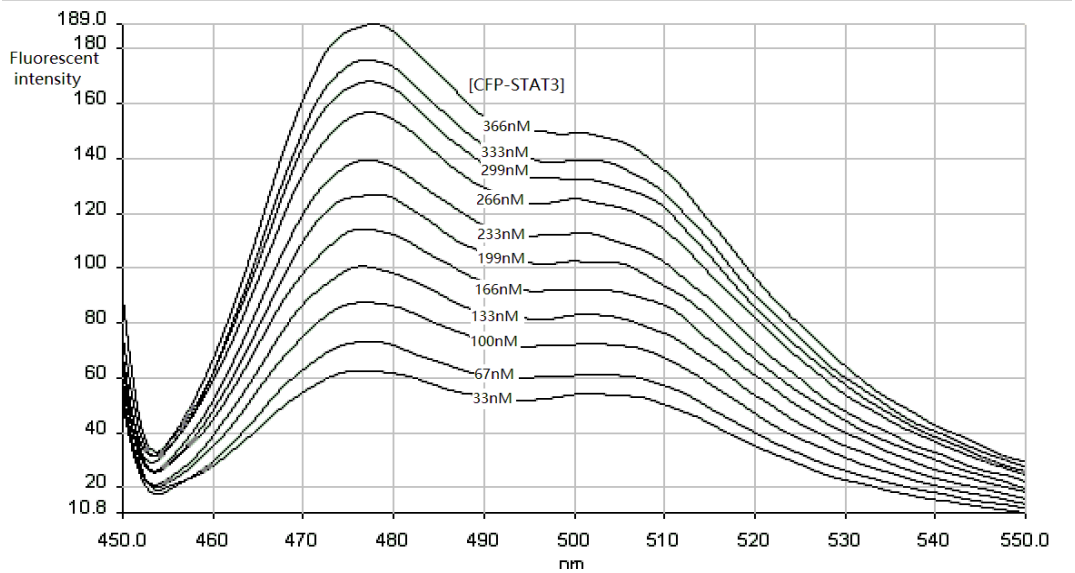


Figure 5.9. The emission curves of the increase concentration of CFP-STAT3 $_{127\text{-}722}$ proteins. Y-axis is the fluorescent intensity while X-axis is the emission wavelength. The CFP-STAT3 127-722 protein increases from 33 nM to 366 nM.

Two peaks were shown in all emission curves: one main peak at about 475 nm and a smaller peak at 500 nm. The two peaks covers a wide range of the emission wavelength from 470 nm to 510 nm. The increase of the CFP-STAT3 127-722 protein concentration significantly influenced not only the fluorescent intensity at 475nm (FI475) but also the fluorescent intensity at 520nm (FI520), which is the receptor's emission wavelength. This indicates that the increase of FI520with the increase of the donor concentration cannot be regarded as the FRET signal. Negative controls are necessary to eliminate the influence of the donor's emission contributing to FI520 readings. Combining the two titration results shown in figure 5.10 and figure 5.10, the decrease of FI475 with the increasing acceptor concentration can be directly used to represent the FRET signal.

### 5.4.2 FRET development using N-terminal fluorescent labelled STAT3

Atto488-GAS18 DNA was titrated in 0 μM, 0.5 μM and 1 μM of the CFP-STAT3 $_{127\text{-}722}$ proteins, FI520 and FI475 were recorded to detect the FRET signal and calculate FRET ratio. With the increase of the Atto488-GAS18 concentration, we were expecting to see the increase of the FI530 in all samples due to the contribution from donor emission while with higher acceptor protein concentration, the increase of the fluorescent intensity should be higher. There should be a decrease of the FI475 with the increase of the Atto488-GAS18 concentration to indicate the success of the FRET energy transfer. However, the hypothesised results were not observed.

The FI520 obtained from the titration assay indicates that the CFP-STAT3 $_{127\text{-}722}$ concentration did not influence the increase of the fluorescent intensity at 520 nm.

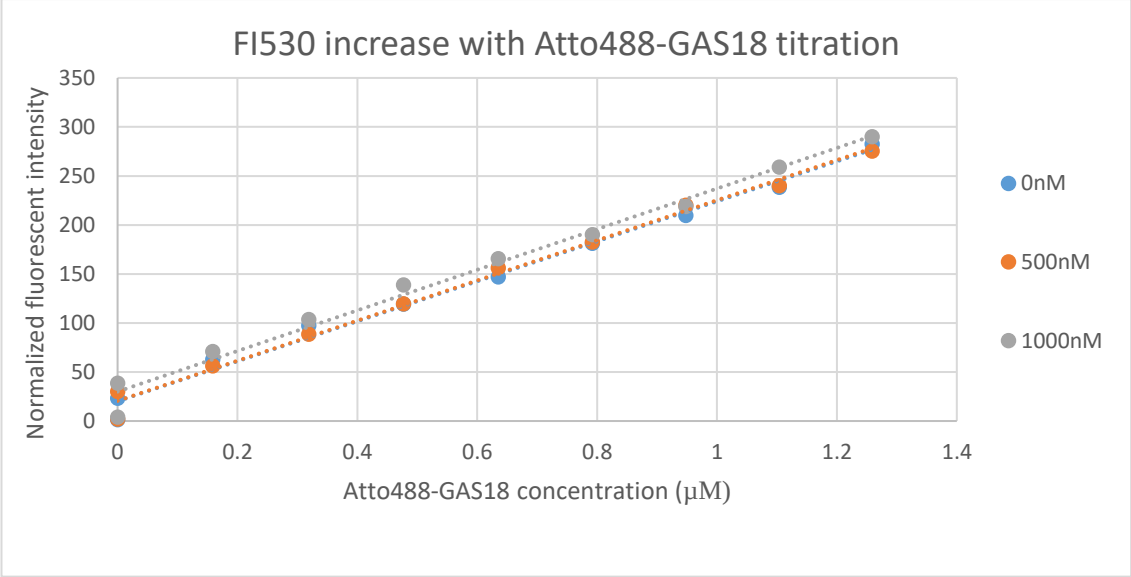


Figure 5.11. The fluorescent intensity at 520nm increase with increasing Atto488-GAS18 concentration. The Atto488-GAS18 was titrated into 0 nM (blue), 500 nM (orange) and 1000nM (grey) of the CFP-STAT3 $_{127\text{-}722}$ separately. 2μl of the 85μM Atto488-GAS18 were added into 1ml of the CFP-STAT3 $_{127\text{-}722}$ protein for each titration point.

The fluorescent intensity at the 520nm increases with the Atto488-GAS18 concentration in all three protein concentrations. After subtracting the intrinsic fluorescent intensity at 520nm caused by the CFP-STAT3 $_{127\text{-}722}$ protein, the FI520 readings at the same Atto488-GAS18 concentration were similar in all protein concentrations. There was no significant difference in the increase of FI520 between different protein concentrations thus no FRET signal was obtained from FI520 increase.

The FI475 decreases slightly with the increase of the Atto488-GAS18 concentration. However, there was no significant differences in the FI475 decrease between the three different protein concentrations.

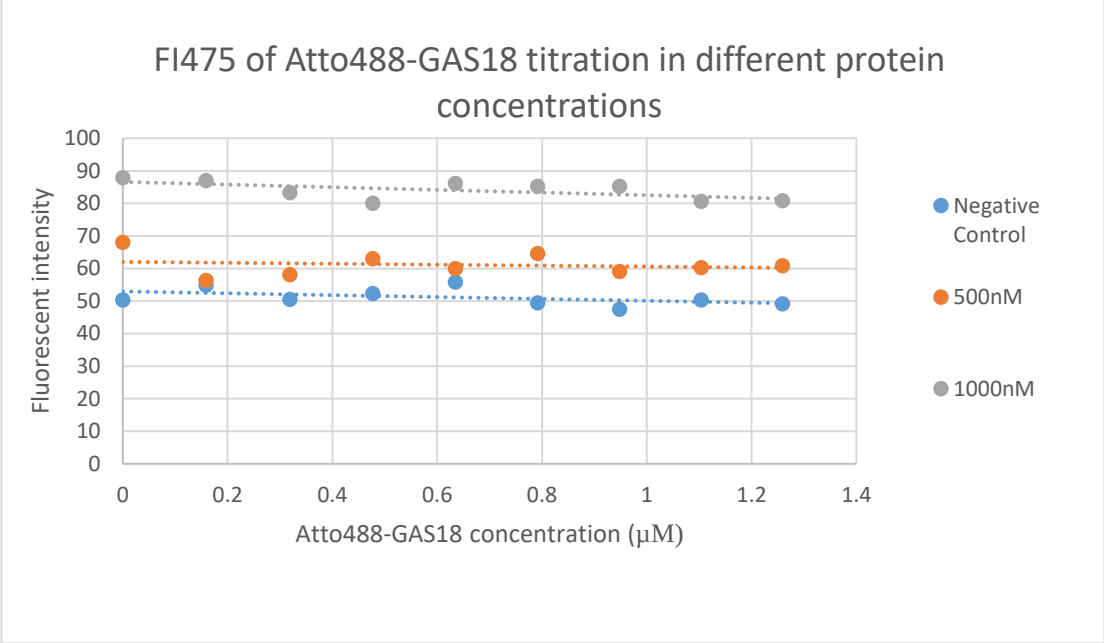


Figure 5.12. The fluorescent intensity at 475nm decreases slowly with the increase of the Atto488-GAS18 concentration. Three CFP-STAT3 127-722 protein concentrations were detected: Negative control (blue), 500 nM (orange) and 1000 nM (grey). 2 μl of the 85 μM Atto488-GAS18 were added into 1ml of the CFP-STAT3 $_{127\text{-}722}$ protein for each titration point.

Figure 5.12 shows that FI475 readings decreased slightly with the increase of the acceptor (Atto488-GAS18) concentration. This observation matches the signal of the energy transfer. However, the negative control (no STAT3 protein added) also showed slight decrease with the increase of the acceptor concentration. During the titration, while adding the 2μl acceptor, the donor's concentration as well as the BSA, salmon sperm and glycerol concentration in the FRET binding buffers were diluted by 0.2% per addition. The fluorescent intensity can not only be affected by both the CFP-STAT3 $_{127\text{-}722}$ concentration but also the content and concentration of the buffers. The decrease of fluorescent intensity with the increase of Atto488 concentration in 1000nM protein sample is slightly greater than the negative control (0nM protein sample). This suggests that there might be FRET happening but the technique may not be very sensitive.

In order to test the influence of different receptor and protein concentrations to the FI480 and FI530 more efficiently, the FRET assay was also conducted

in 96-well plates using the Pherastar plate-reader. In the 96-well plates, different protein and dsDNA concentrations can be detected at the same time. Four CFP-STAT3 127-722 concentrations and six Atto488-GAS18 concentrations were screened to detect the optimal donor/receptor concentration that produces best FRET ratio. The interaction between the protein and the dsDNA were incubated to reach the equilibrium before read by the plate reader.

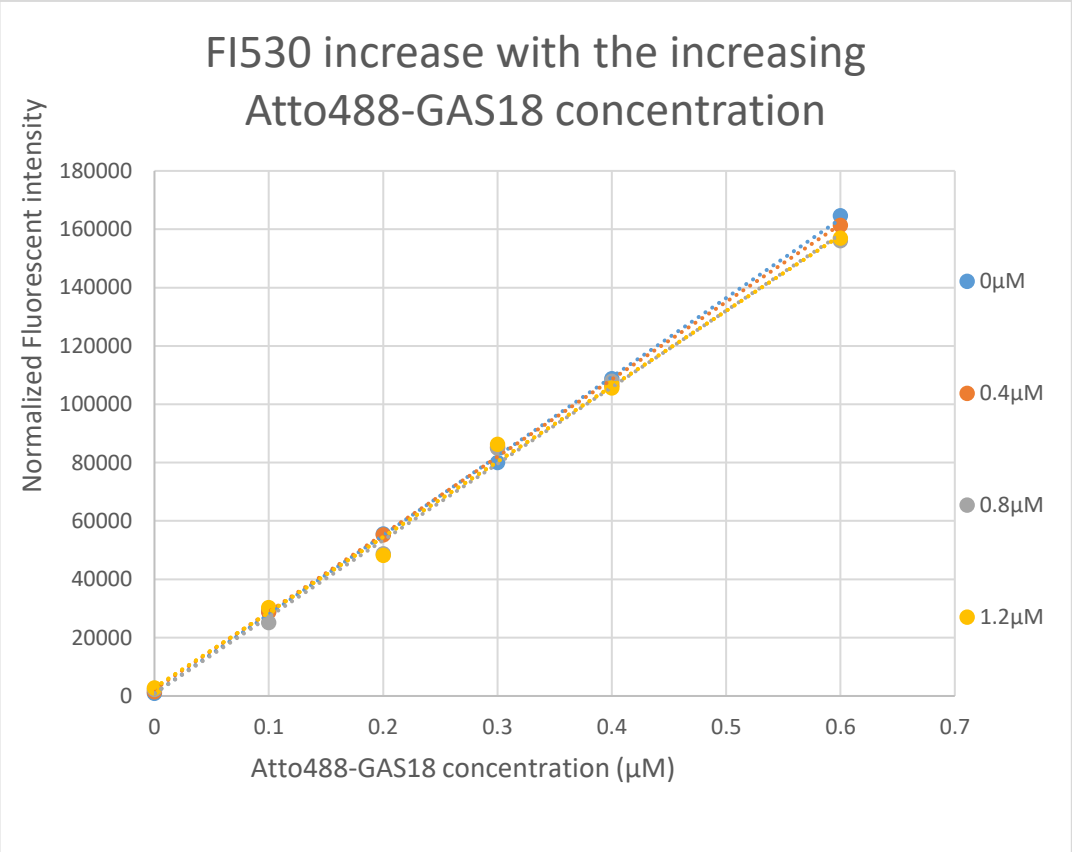


Figure 5.13. Fluorescent intensity at 530nm increasing with the Atto488-GAS18 concentration. The concentrations of the CFP-STAT3 127-722 proteins applied were 0 μM, 0.4 μM, 0.8 μM and 1.2 μM. The increase of fluorescent intensity was normalised.

In figure 5.13, the fluorescent intensity at 530nm increases with the Atto488-GAS18 concentration despite the protein concentration. After normalizing, the trend line of the four protein concentrations overlapped. The slope of the trend lines are the same thus the ratio of the fluorescent intensity increases are the same in the four protein concentrations including the negative control without protein. There is no significant difference in the FI530 increase

between different protein concentrations. Therefore we conclude that in this experiment, the increase of FI530 is caused by the intrinsic fluorescence of Att488-GAS18. No signal of energy transfer was detected in the CFP-STAT3 127-722 and Atto488-GAS18 FRET assay. This result matches the result of the FRET titration assay.

The fluorescent intensity at 480nm did not decrease with the increase of the acceptor concentration.

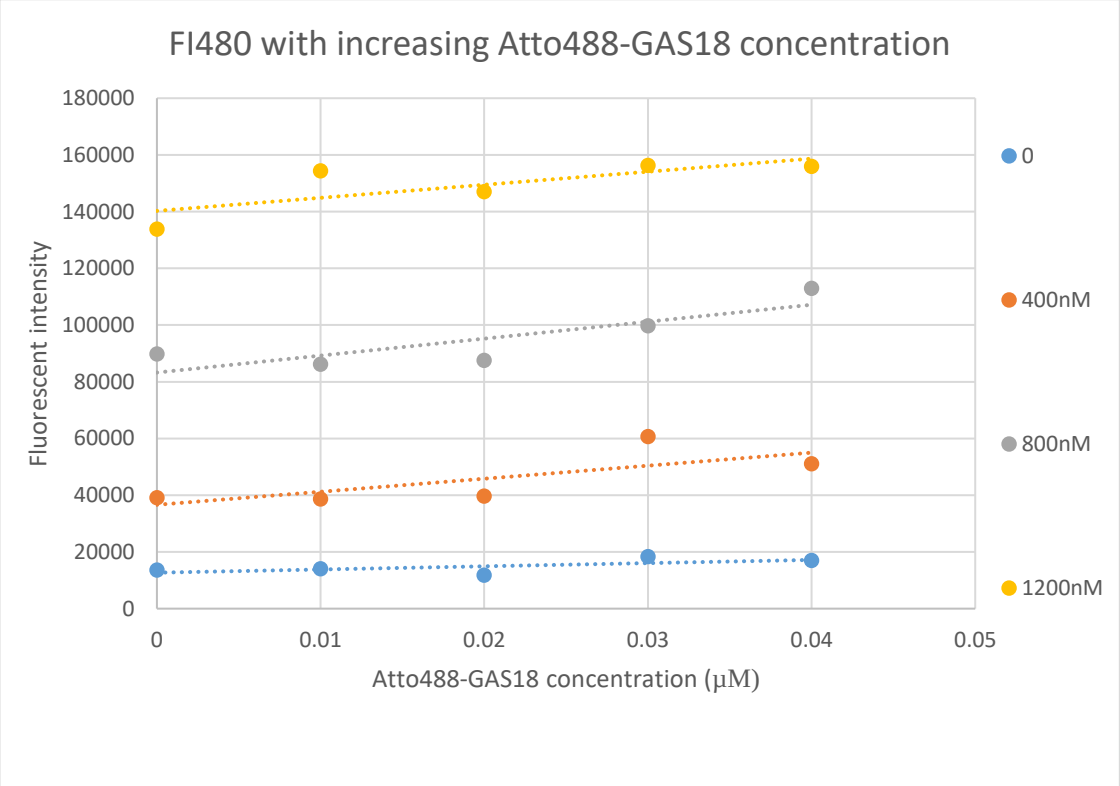


Figure 5.14. The fluorescent intensity at 480nm stays constant with increasing Atto488-GAS18 concentration. CFP-STAT3 127-722 concentration applied were 0 μM (blue), 0.4 μM (orange), 0.8 μM (grey) and 1.2μM (yellow).

According to figure 5.14, FI480 did not decrease with the increasing Atto488-GAS18 concentration for any protein concentration. On contrast, the fluorescent intensity at 480nm increased lightly with the increasing Atto488-GAS18 concentration. No energy transfer was detected. This may be due to the decrease of fluorescent intensity at 475 nm was too small to be dominant from the background noises.

The fluorescent intensity at 530nm was also measured with increase of the protein concentration. The fluorescent intensity at 530nm is influenced by the CFP-STAT3 $_{127-722}$ emission. With no Atto488-GAS18 added, FI530 will increase with the CFP-STAT3 $_{127-722}$ concentration. If FRET happens, the increased fluorescent intensity at 530nm should be higher in the samples with increasing Atto488-GAS18 compared to the negative control.

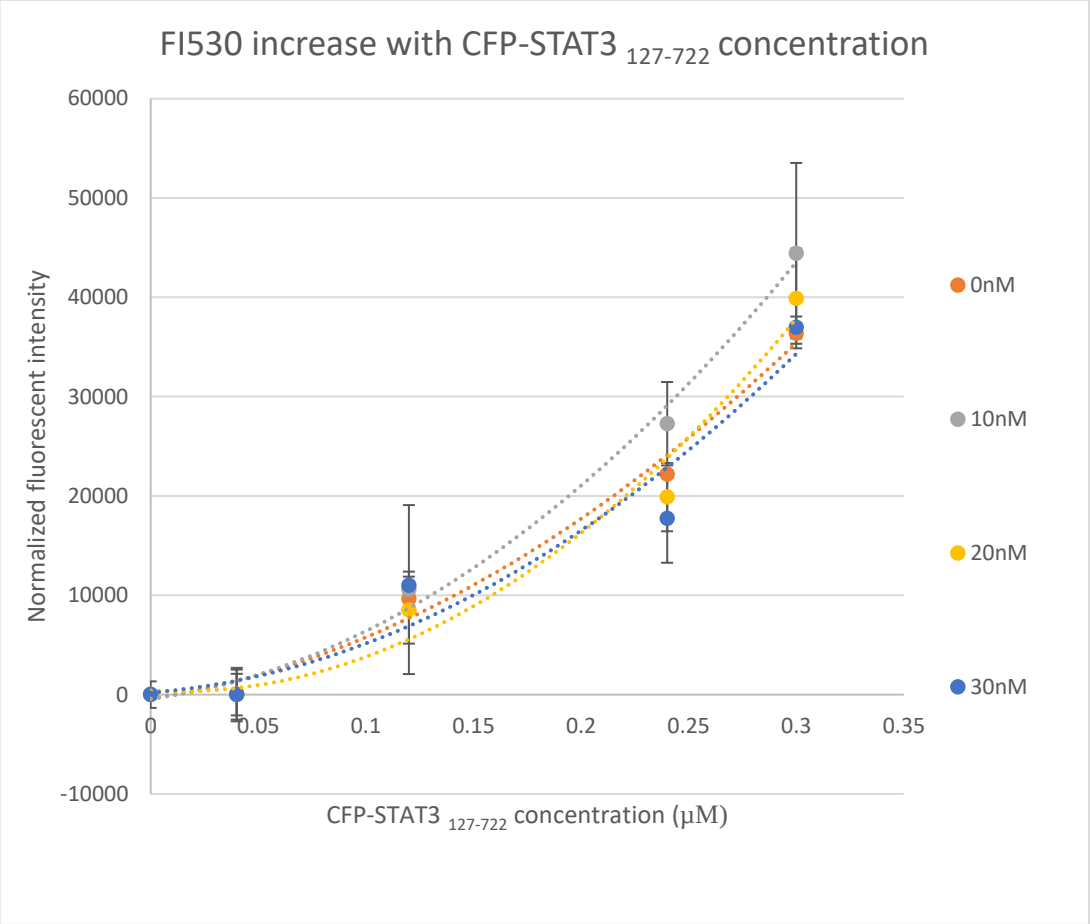


Figure 5.15. The fluorescent intensity increases with the CFP-STAT3 $_{127-722}$ concentration. The Atto488-dsDNA concentration were 0nM (orange), 10nM (grey), 20nM (yellow) and 30nM (blue). The error bars shows the standard diviations.

Figure 5.15 shows FI530 increases with the CFP-STAT3 $_{127-722}$ concentration. The error bars cover the differences of the fluorescent intensity between different Atto488 concentrations. Therefore this figure shows no significant relationship between the increase of fluorescent intensity at 530nm and the increased Atto488 concentration. In the 10nM of

the CFP-STAT3 127-722 Atto488-GAS18 concentration, the FI530 increase is greater than the negative control. However, in the 20nM and 30nM receptor concentrations, the FI530 increase with the protein concentration is still the same with the DNA concentration. Since the error bars of the 10nM dsDNA concentration readings are larger than other concentrations, the increase can not be used as the signal of energy transfer.

In conclusion, no or very weak energy transfer was detected between the CFP-STAT3 $_{127\text{-}722}$ and Atto488-GAS18. The overlap of the donor and the acceptor's emission wavelength can be one reason that contributed the difficulties of measuring the energy transfer. The wide range of CFP emission wavelength decreased the sensitivity of the fluorescent intensity affected by the energy transfer. Moreover, the excitation of the Atto488 at 430nm results in a relatively high emission at 530nm. The increase of emission at 530nm is therefore highly influenced by the Atto488 concentration. Therefore, the increase of FI530 cannot be regarded as the FRET signal without considering the intrinsic fluorescence of the system. Negative controls were tested in each experiment to eliminate those 'noises' but no significant increase of FI530 were observed when adding the donor. Another reason causing the low FRET signal may be the average distance between the donor and the receptor. This will be discussed in detail in the next section. Although the FI520 is not suitable to be used as the FRET signal, the decrease of FI475 with the increase of the acceptor concentration showed some sign of FRET even it may not be very sensitive.

### 5.4.3 Distance measurement

In FRET assays, the efficiency of energy transfer can be increased by shortening the distances between the donor and acceptor fluorophores. The distance between the donor and acceptor fluorophores are required to be within 10nm to allow the energy transfer while efficient energy transfer between the donor and acceptor usually happens when the distance is bellow 5nm. Hence, we measured the distance between the N-terminal of the STAT3 protein and the fluorophore attached DNA.

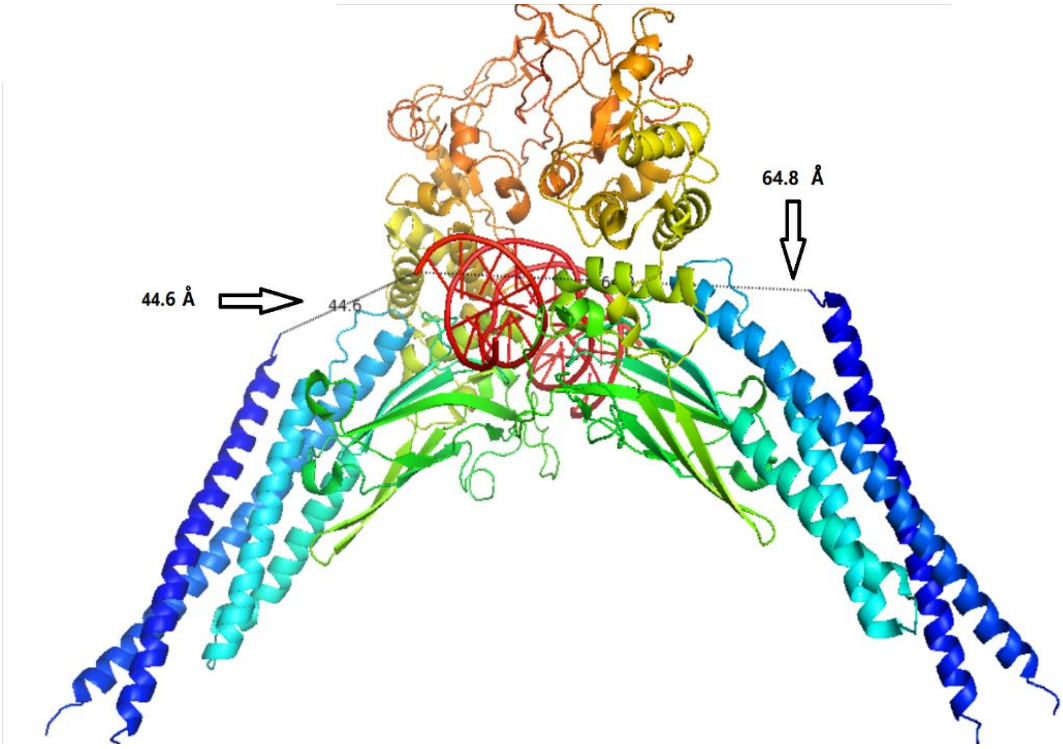


Figure 5.16. Distances measured from N-terminal of the STAT3 dimer binding to dsDNA. The distances between the N-terminals of the STAT3 proteins and the fluorescent labelled DNA end are 4.46nm and 6.48nm. [PDB: 4e68]

The distances from the N-terminals of the STAT3 proteins to the 5' Thymine of the dsDNA, where the Atto488 was attached, were measured with PyMol. The distances between the acceptor fluorophore and the two N-terminal ends of the two STAT3 proteins that form one dimers are 4.46nm to 6.48nm. Residues 127-137 at the N-terminal end disordered in this crystal structure. In this project, the donor fluorophores were attached to the 127aa of the STAT3 N-terminal protein so the distance was measured to amino acid 138. The missing 11aa lead to the uncertainty of the position of the chromophore in CFP. Furthermore, the chromophores of YFP and CFP are protected by the beta-sheet protein structure. Therefore the distance between the two chromophores is at least 1nm further from the measured distance. The distance between the C-terminus attached CFP and the Atto488 fluorophore attached to the dsDNA is estimated to be 7nm. The distance between the donor attached to the N-terminal end of the STAT3 protein and the acceptor

attached to the 5’ Thymine of the dsDNA may not be short enough for efficient FRET energy transfer.

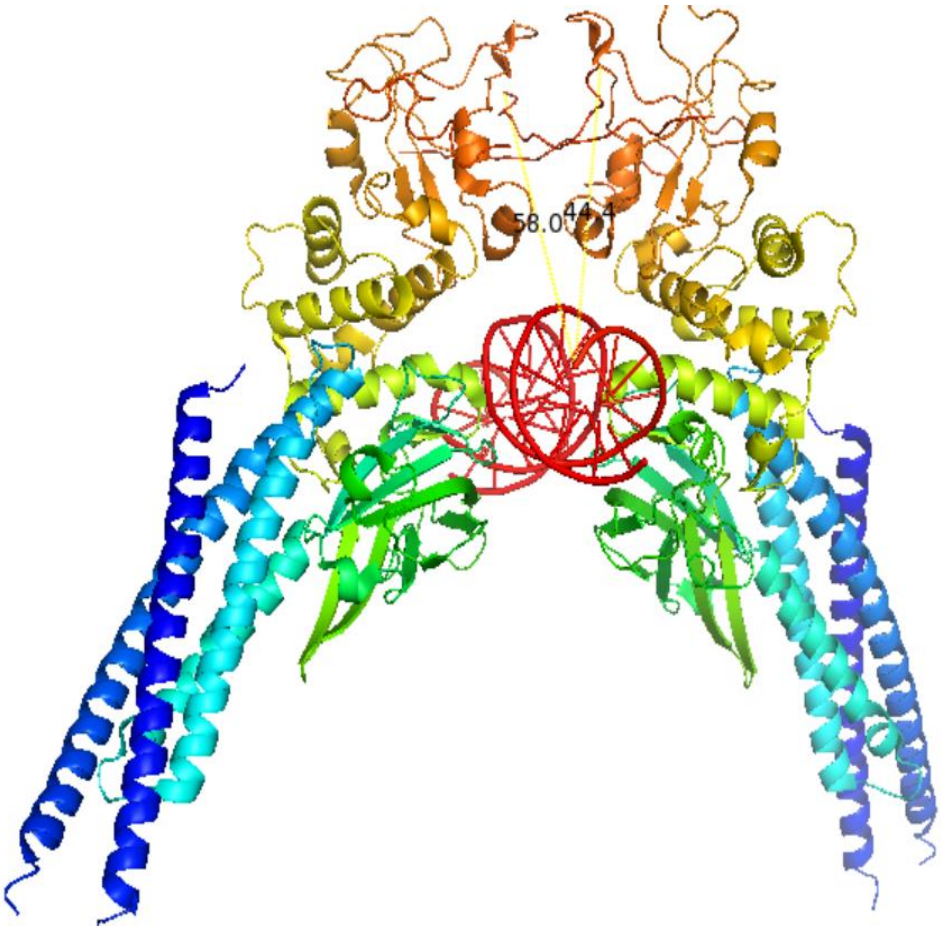


Figure 5.17. Distances measured from C-terminal of the STAT3 dimer binding to dsDNA. The distances between the C-terminals of the STAT3 proteins and the fluorescent labelled DNA end are 4.44nm and 5.08nm. [PDB: 4e68]

On the other hand, the distance between the C-terminal end of the two STAT3 dimers and the 5’-Thymine of the dsDNA is slightly shorter compared to the distance between N-terminal ends and the 5’ Thymine of the dsDNA. According to the distance measurement, the distances are 5.08nm and 4.44nm. In this crystal structure, there are 6 disordered amino acids at the C-terminal end of the STAT3 protein. Although it is still hard to prove that the distance between the C-terminal end of the STAT3 protein and the 5’ thymine of the dsDNA is close enough for FRET energy transfer, the C-

terminal end attached fluorophores are possibly more likely transfer the FRET energy to the acceptor attached to the dsDNA. Therefore, we tried the C-terminal fluorescent STAT3 proteins in the FRET assay to investigate FRET efficiency.

### 5.4.4 C-terminal FRET improvement

A FRET assay with C-terminal fused fluorophores of STAT3 was designed to detect the STAT3 DNA binding activity due to the potentially shorter transfer distance. Cyan fluorescent protein fused to the C-terminal end of STAT3 protein (aa. 127-722) was used in this FRET assay. Atto-488 was attached to on strand of the double stranded DNA. CFP was used as a donor while Atto488 was used as a receptor.

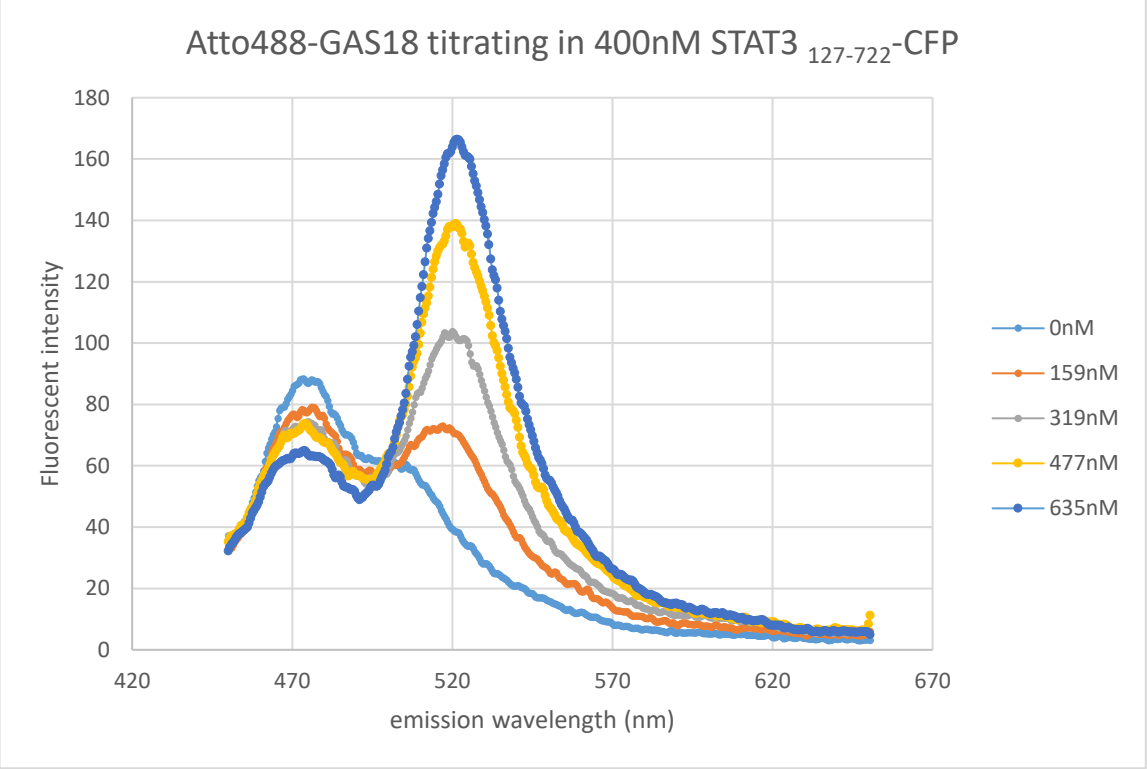


Figure 5.18. Fluorescent intensity changes with the increase of the Atto488-GAS18 concentration in the FRET titration assay. 1μl of the 478μM Atto488-GAS18 were titrated into 3ml of 400nM STAT3 $_{127\text{-}722}$-CFP proteins each time.

The FRET titration assay showed that with the increase of Atto488-GAS18 concentration, the fluorescent intensity at the donor's emission wavelength (FI475) decreased significantly with the increase concentration of the acceptor. The fluorescent intensity at the acceptor's emission wavelength (FI520) was increasing with the increase concentration of the acceptor. 478μM of the Atto488-GAS18 stock were applied in the titration to minimise the influence FI475 by the diluted protein and buffer components. Comparing to previous experiments shown in figure 5.18, the decrease of FI475 in this titration assay is not caused by the concentration changes of the STAT3 $_{127\text{-}722}$-CFP protein. The significant decrease in the FI475 suggests the success of the energy transfer between the CFP and the Atto488. The FRET efficiency was calculated from the titration assay.

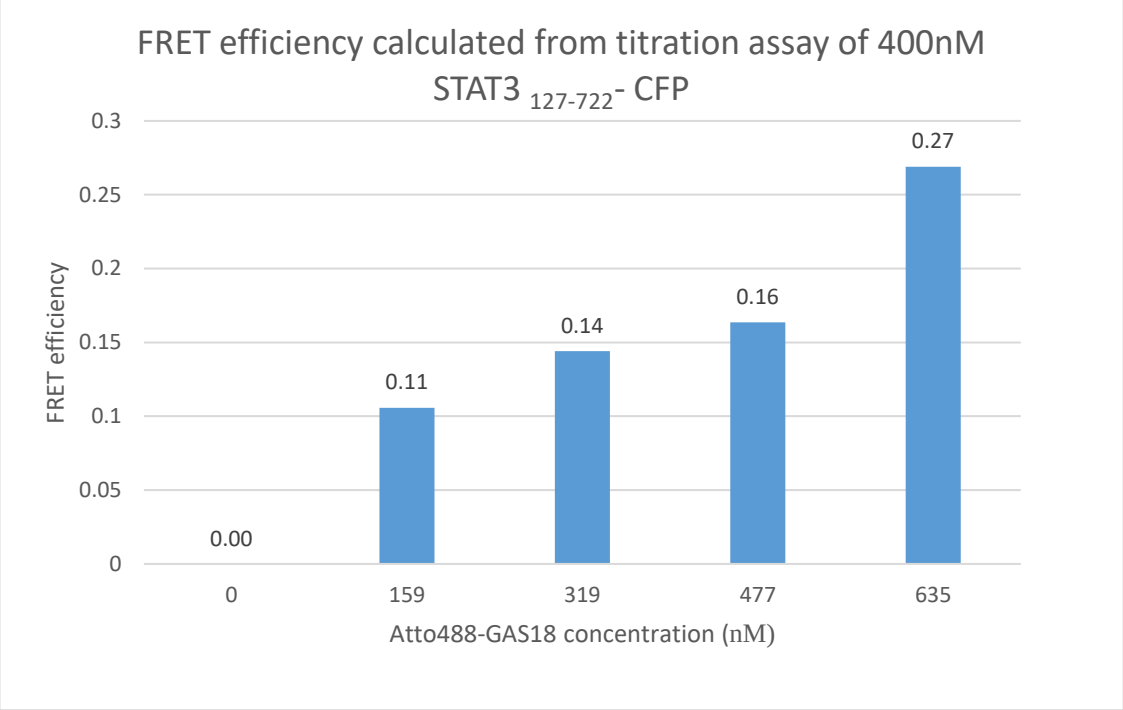


Figure 5.19. FRET efficiency calculated from the STAT3 $_{127\text{-}722}$- CFP titration assay.

The FRET efficiency increases with the Atto488-GAS18 concentration. The FRET efficiency increased from 0.1 to 0.269 when the Atto488-GAS18 concentration increases from 159nM to 536nM. This indicates that the protein-DNA interaction was not saturated. To test higher FRET efficiency,

higher Atto488-GAS18 concentration or alternatively lower STAT3$_{127-722}$-CFP concentration could be used. However, low STAT3 $_{127-722}$-CFP concentration may result in low fluorescent intensity at 475nm therefore limit the sensitivity of the FRET titration assay. Highest STAT3 $_{127-722}$-CFP concentration and a higher Atto-GAS18 concentration were tested in later experiments to optimise the experimental concentration of the protein and the dsDNA.

A series of FRET titration assays were conducted to confirm the success of the FRET energy transfer and to check the FRET efficiency between different donor and receptor concentrations. The Donor/receptor ratio that provide the highest FRET efficiency can then be applied in further experiments for STAT3 inhibitor selection. 85µM Atto488-GAS18 were titrated into 1.2µM, 2µM and 4µM STAT3 $_{127-722}$-CFP proteins. The 1xFRET binding buffer were also titrated with 85µM of the Atto488-GAS18 to be used as negative control. The decrease of FI475 were recorded to calculate the FRET efficiency.

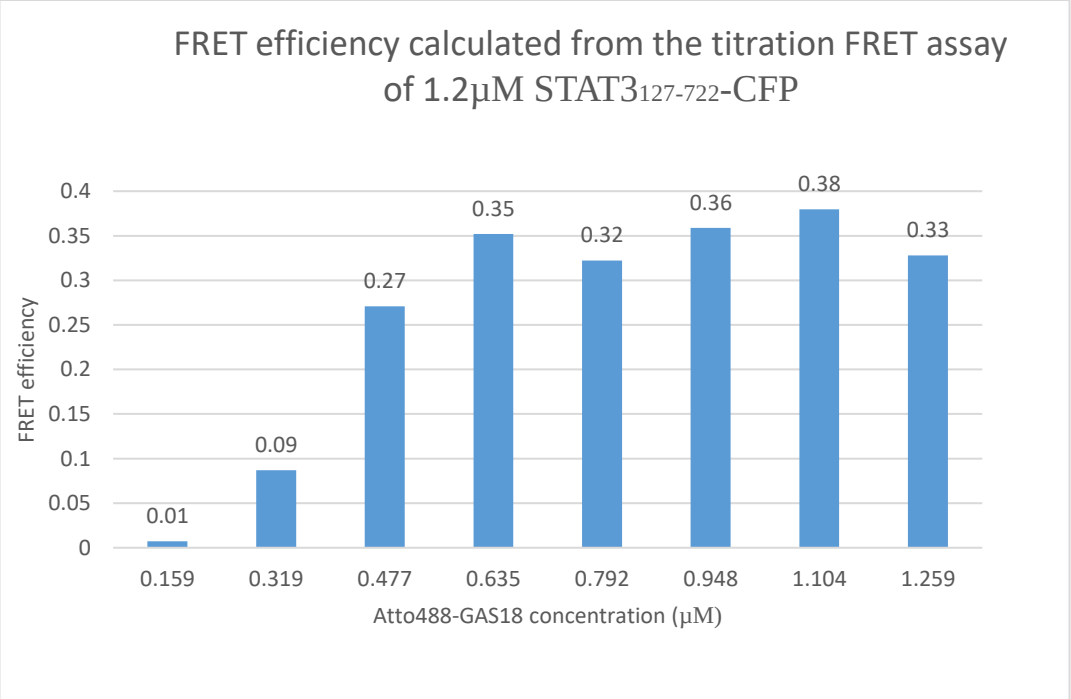


Figure 5.20. FRET efficiency of the different Atto488-GAS18 concentrations in 1.2µM STAT3 $_{127-722}$-CFP. 2µl of the 85µM Atto488-GAS18 were titrated into 1ml of the STAT3 $_{127-722}$-CFP protein each time.

The FRET efficiency increased from 0.007 to 0.352 when the dsDNA concentration increased from 0.159 μM to 0.4635μM. After 0.635 μM of the Atto488-GAS18 concentration, the FRET efficiency stays similar around 0.35. The protein-dsDNA interaction seems to be saturated when the dsDNA concentration reached about 0.6 μM. At this stage, the protein: dsDNA concentration is 2:1. This is an interesting discovery since the interaction ratio between the STAT3 protein and the dsDNA is expected to be 2:1 (2 moles of STAT3 monomer to 1 mole of the double-stranded oligo). It indicates that the produced STAT3 $_{127\text{-}722}$ protein can bind to dsDNA very effectively. The highest FRET efficiency achieved in this titration assay is about 0.38 when the Atto488-GAS18 concentration is about 1.1 μM.

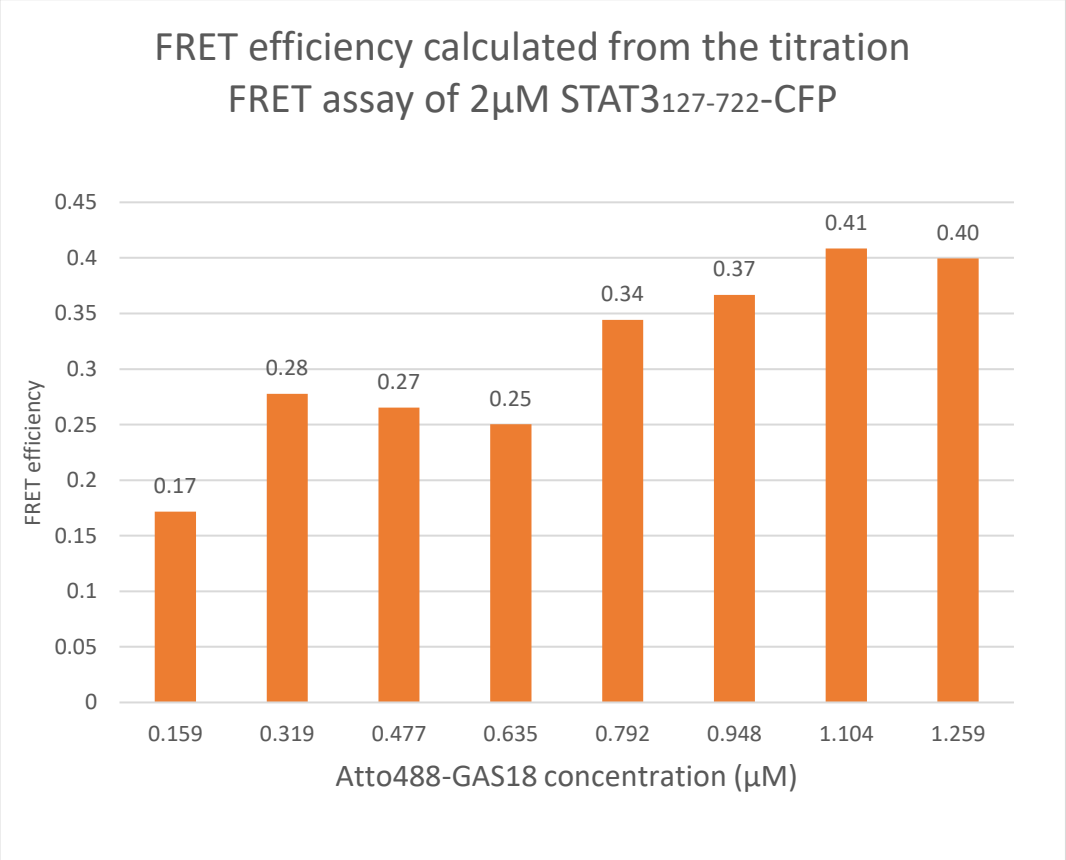


Figure 5.21. 85μM Atto488-GAS18 titrated into 2μM STAT3 $_{127\text{-}722}$-CFP protein. FRET efficiency calculated according to fluorescent intensity changes at 475nm.

When the Atto488-GAS18 were titrated in higher concentration of the STAT3 $_{127\text{-}722}$-CFP protein, the FRET efficiency is higher in general. The FRET

efficiency increased from 0.17 to 0.40 when the Atto488-GAS18 concentration increased from 0.159μM to 1.104μM. The highest FRET efficiency achieved in this titration assay is 0.4. The FRET efficiency stopped increase with the acceptor concentration when the dsDNA concentration reached about 1.1μM. Again, the protein-DNA interaction was saturated when the protein: dsDNA ratio is 2:1. This result again confirms that the STAT3 $_{127\text{-}722}$-CFP protein binds to dsDNA as dimer.

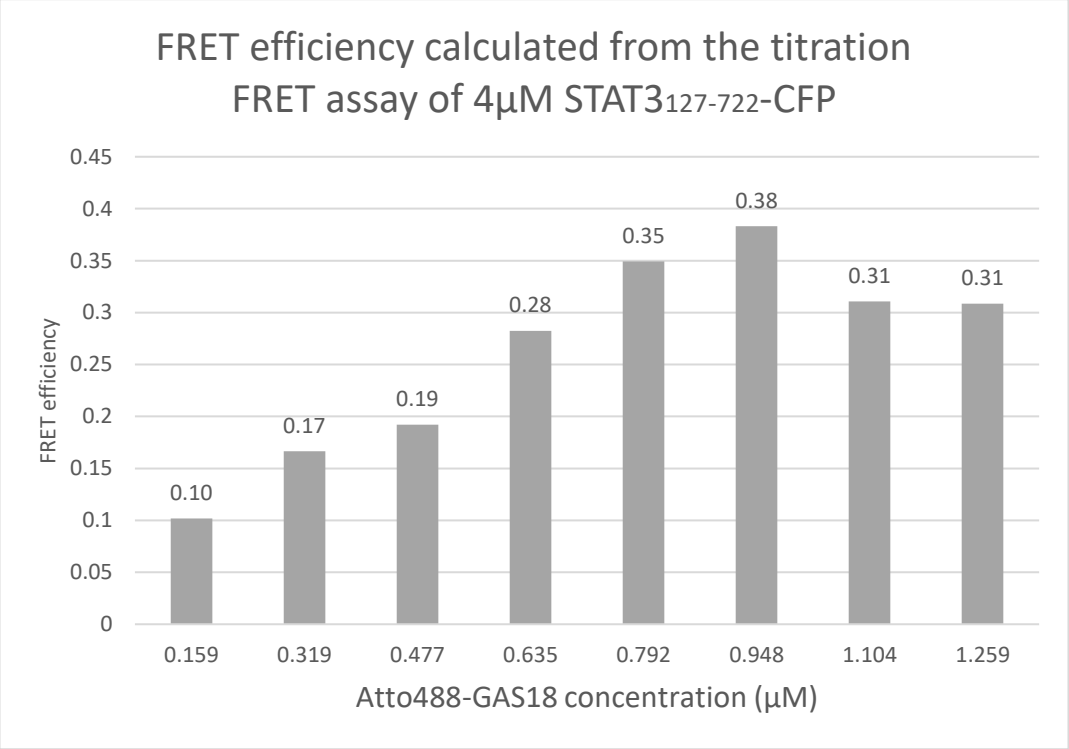


Figure 5.22. 85μM Atto488-GAS18 titrated into 4μM STAT3 $_{127\text{-}722}$-CFP protein. FRET efficiency calculated according to fluorescent intensity changes at 475nm.

The overall FRET efficiency achieved in the titration assay with 4μM STAT3 $_{127\text{-}722}$-CFP is lower than that of the 2μM STAT3 $_{127\text{-}722}$-CFP. The FRET efficiency increased from 0.1 to 0.38 when the Atto488-GAS18 concentration increased from 0.159 μM to 0.948μM. After the dsDNA concentration reached 0.948μM, the FRET efficiency decreased to about 0.3. The protein-DNA interaction appeared to be saturated when the protein: dsDNA ratio was about 4:1. The differences in the results may be caused by the differences of the protein quality. High concentration of the STAT3 $_{127\text{-}722}$-CFP protein is

very difficult to preserve and easy to aggregate. Therefore, protein concentration of 2μM is better than 4μM to be used in the titration assay.

In conclusion, the FRET signal is highly improved with application of the STAT3 $_{127\text{-}722}$-CFP protein compared to the CFP-STAT3 $_{127\text{-}722}$ protein FRET. Significant decreases of fluorescent intensity at the donor's emission wavelength (475nm) can be observed with the increase of the acceptor (Atto488) concentration. After normalizing FI475 with negative control, the decrease of FI475 were used to calculate the FRET efficiency. The FRET efficiency achieved the highest value of 0.40 when protein concentration was about 2μM while the dsDNA concentration was about 1μM. These concentrations of the STAT3 $_{127\text{-}722}$-CFP and the Atto488-GAS18 were suggested to be used in the future for STAT3 inhibitor test.

In order to achieve high-throughput in the FRET assays, the STAT3 $_{127\text{-}722}$-CFP and Atto488-GAS18 were also screened in the 96-well flat bottom plates. The FRET ratio were calculated according to normalised FI530 readings.

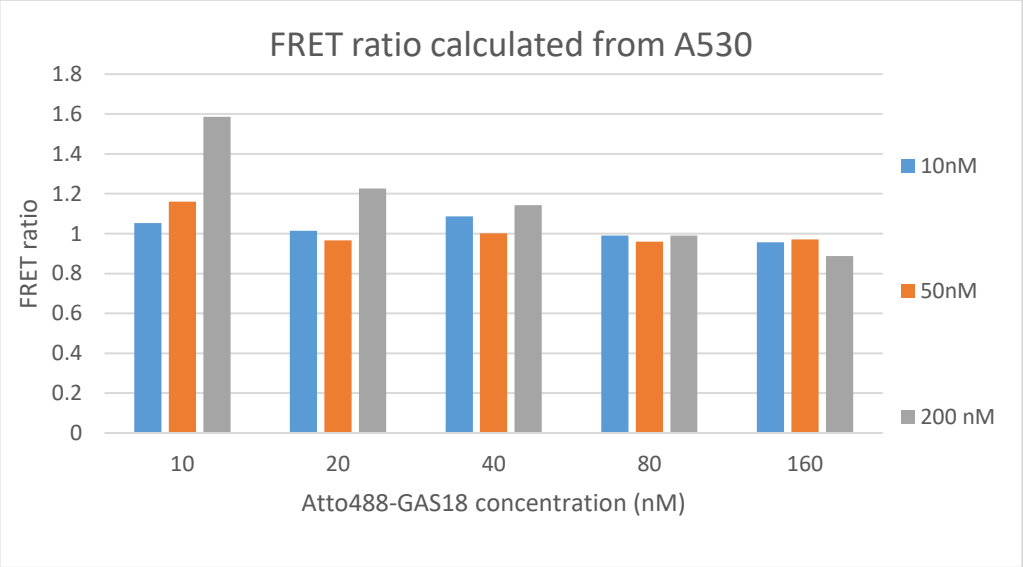


Figure 5.23. FRET ratio tested with different concentration of protein and DNA. Three protein concentrations: 10 nM (blue), 50 nM (orange) and 200 nM (grey) were tested against five dsDNA concentrations: 10 nM, 20 nM, 40 nM, 80 nM and 160 nM.

The result shows that when the STAT3 $_{127\text{-}722}$ -CFP concentration was 200nM and the Atto-DNA concentration was 10nM, the FRET ratio was the highest. If the FRET ratio is above 1, it indicates that there is energy transfer between the donor and acceptor. Therefore, no obvious FRET energy transfer was detected when the Atto488-GAS18 concentration was higher than 80nM. This may be caused by the high fluorescent emission of the Atto488 when excited at 430nm. The 'background' fluorescence is too high for the energy transfer to be detected when the Atto488 concentration was high. At low Atto488 concentrations, higher protein concentration results in higher FRET ratio. According to figure 5.23, high STAT3 $_{127\text{-}722}$-CFP: Atto488-GAS18 concentration result in high FRET ratio.

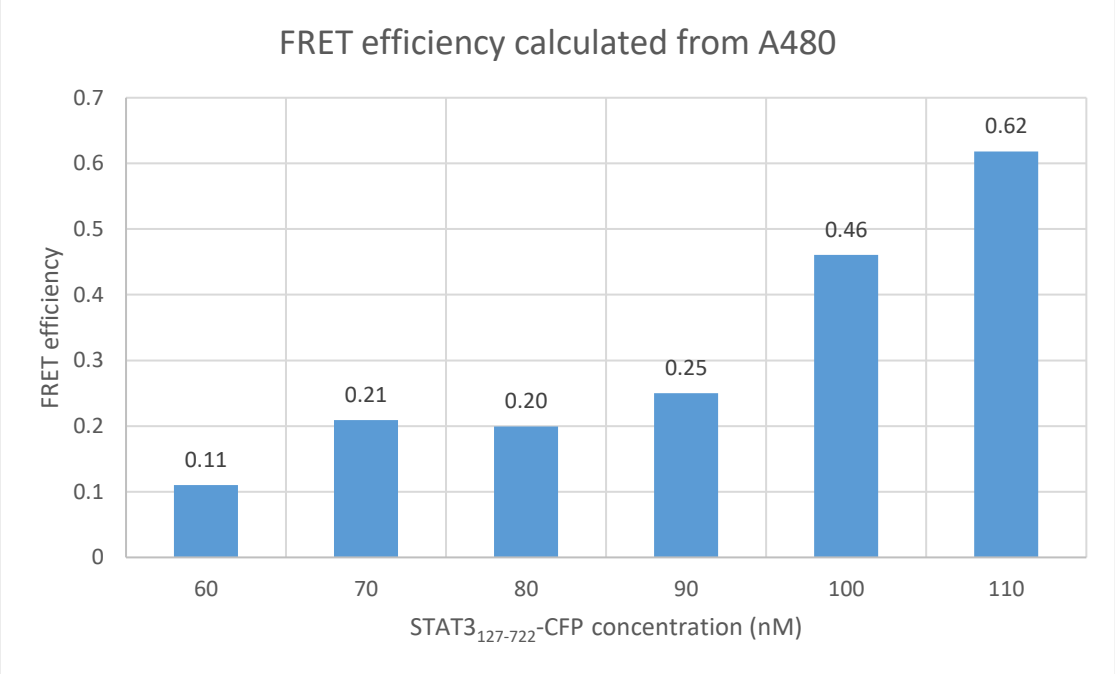


Figure 5.24. FRET efficiency calculated by normalised fluorescent intensity at 480nm. 10nM of the Atto488-concentration were applied with increase of the STAT3 $_{127\text{-}722}$-CFP concentration.

The FRET efficiency increased with the STAT3 $_{127\text{-}722}$-CFP concentration from 60nM to 110nM. When the protein concentration was lower than 60nM, no FRET signal was detected and the FRET efficiency was below 0. This is due to the low reading at FI480. The donor's emission is optimised at FI475 and the FRET signal is not strong enough to dominate the fluorescent intensity peaks. Therefore when reading at FI480, the sensitivity of the FRET

is decreased. Although the FRET efficiency calculated from FI480 was decreased, the FRET signal was strong enough to show the decrease of donor's emission caused by the energy transfer to the acceptor.

In conclusion, the optimised FRET assay can be developed into high-throughput screening method for selecting STAT3 inhibitors. A decreased FRET signal should be detected with the inhibition of STAT3 binding to the DNA. The optimal Atto488-GAS18 concentration to be used is 10nM while the suggested STAT3 127-722-CFP protein concentration is 100nM.

## 5.5 Discussion

FRET assay can be used to detect the interaction between the STAT3 proteins and the dsDNA. A strong fluorophore donating to YFP had been tested previously and there was too much bleed-through from the donor emission into the acceptor emission channel. Therefore the stronger fluorophore was chosen as the acceptor. CFP and Atto488 were chosen to be used as the donor-receptor group since the Atto488 is a stronger fluorophore. The CFP were attached to the STAT3 proteins while the Atto488 were attached to the dsDNA. One difficulty of using fluorescent protein and commercial fluorophores as donor and receptor pairs is that the synthesised fluorophore is much more sensitive to the excitation. Although the excitation of the Atto488 is minimised at 430nm, the resulted emission is still higher than the emission of the CFP, whose excitation is optimised at 430nm. Thus the dominant increase of FI530/FI520 with application of the acceptor is caused by the emission of the Atto488 excited at 430nm. Furthermore, the CFP emission wavelength also covers the 520nm and 530nm. 60% to 70% of the fluorescent emission can be detected from 520nm to 530nm when the CFP is excited at 430nm. Therefore, the FI530 peak does not reflect the energy transfer from the donor to the acceptor. Fortunately, the Atto488 emission spectrum does not cover 480nm. For this fluorophore pairs, the FRET energy transfer can be indicated by the decrease of the FI475/FI480 with the application of the acceptor. In general, the CFP and Atto488 can be used as the donor and receptor pairs in the FRET assay to detect protein-dsDNA interaction.

The CFP-STAT3 127-722 and Atto488-GAS18 FRET assays showed no FRET signal. In the FRET titration assays, no significant increase at FI520/FI530 was observed. Slight decrease of the FI475 was detected with the increase of the acceptor concentration but the decrease was caused by the dilution of the protein and the buffer components. Both the FRET titration assay and 96-well plate assay showed no energy transfer between the CFP and the Atto488. This may be caused by three reasons: the overlap of the donor and acceptor's excitation wavelength, the overlap of the donor and acceptor's emission wavelength and the distance between the CFP and Atto488. To overcome the difficulties that stop FRET being detected, we moved the CFP from the N-terminal end of the STAT3 truncated protein to the C-terminal end. Alternative improvements could have included changing of the fluorophore pairs and using different labelling method to label the STAT3 proteins.

With application of the C-terminal fluorescent labelled STAT3 proteins, the FRET signal was significantly improved in both the titration assay and the plate reader assay. The FRET titration assay was more sensitive since it can measure the emission at 475nm. The 96-well plate FRET method can be developed into a high throughput screening method for selecting STAT3 inhibitors. In the future experiment for inhibitor screening, 10nM of the Atto488-GAS18 and 100nM of the STAT3 $_{127\text{-}722}$-CFP protein were suggested for optimizing the FRET signal.

Besides, the FRET assay can be used to detect the dimerisation of the STAT3 proteins. The STAT3 $_{127\text{-}722}$-YFP protein can be used together with the STAT3 $_{127\text{-}722}$-CFP protein in the FRET assay. A clear FRET signal should be observed since the distance between the C-terminal ends of the two STAT3 monomers in a STAT3 dimer is within 5nm. [248]. However, with limited time and lack of single CFP and YFP for a negative control, such an assay not investigated in this thesis.

# Chapter 6 General conclusions and Future research

## 6.1 General Conclusion

STAT3 is a transcription factor involved in the regulation of many cellular functions including proliferation, differentiation, apoptosis, migration and immune response. The STAT3 protein plays an important role not only in cancer cells but also in normal cells. Firstly, it up-regulates the expression of cyclin D protein that promotes the entry into S phase of the cell cycle and therefore enhances cell proliferation. Secondly, anti-apoptosis factors including Bcl-2, Bcl-XL, and Mcl-1 are all directly activated by STAT3. STAT3 is involved in regulation of many important proteins that retain normal cellular activities. Up- or down- regulation of those proteins due to the abnormal function of STAT3 contribute to different types of diseases. Furthermore, STAT3 is involved in the differentiation of myeloid cells, which also emphasize the importance of STAT3 in normal cell development. Finally, STAT3 up-regulates many inflammatory regulators and plays an important role in many types of T-cells therefore is essential for the control of immune response. STAT3 has great biological value in understanding the regulation system from genes to cellular activities. STAT3, as one transcriptional activator, is involved in multiple cellular activities in different cells. An understanding of the detailed biological activity of STAT3 can lead to the discovery of mechanisms of regulation of different cellular functions.

Since the STAT3 activity is involved in many essential cellular functions, the regulation of STAT3 activities is essential to retain normal cellular functions. Abnormal STAT3 expression and activation is usually related to tumour growth. STAT3 activity contributes to the proliferation, transformation, anti-apoptosis and immune escape of cancer cells. Therefore STAT3 is regarded as an oncogene and potential anticancer drug target. However, the complete STAT3 activation and inhibition pathway is still unknown. STAT3 activity is also reported to be related to the expression of some pro-inflammatory factors and has some anti-cancer activities. The opposite contributions of

STAT3 to different types of cancer cells may due to the different activation mechanisms or different STAT3 sub-isoforms level.

The mechanisms of how STAT3 get involved in regulation of different cellular functions is complex and lacks a systematic review. Currently, the most well studied STAT3 activation mechanism is the JAK-STAT pathway through Tyrosine705 phosphorylation. Other tyrosine phosphates were also reported to phosphorylate STAT3 Tyr705 including Scr. With the development of STAT3 research, more STAT3 activation mechanisms were discovered including: Ser727 phosphorylation and Lys685 acetylation. Different STAT3 activation system may be invoked during different cell development stages, in different cell types or under different environments. Therefore the multiple STAT3 activation pathway may lead to the heterogeneity of the STAT3 cellular functions. Furthermore, since STAT3 activation involves various post transcriptional modifications of STAT3, inhibition of a single pathway may not complete inhibit STAT3 activity. Thus the direct inhibition of STAT3 DNA binding domain is a promising target for STAT3 inhibitors.

In this thesis, we reveal more detailed biological activities of STAT3 with different *in vitro* methods. The development of *in vitro* methods provide more direct visualisation of STAT3 biological functions such as DNA binding activity, dimerisation and aggregation. Furthermore, the *in vitro* methods can be easily developed into inhibitor screening methods and speed up the development of anti-STAT3 drugs. Three different STAT3 truncated proteins were investigated within this thesis. By comparing the biological activities of these different STAT3 mutants, we examine the influence of different STAT3 domains on STAT3 DNA binding activities.

All STAT3 mutations were successfully produced in *E. coli* and purified with simple ion exchange chromatography steps. The methods can instruct future cheap and fast production of sufficiently pure STAT3 proteins, which can be applied in all *in vitro* assays. Furthermore, the methods can also be up-scaled for industrial production of purified STAT3 proteins.

During the production and purification of the STAT3 proteins, protein aggregation and precipitation was the major problem to solve. To increase

the solubility of the STAT3 protein, different additives including: KCl, MgCl2, Arginine, and Glutamine were applied to the purification buffer of the STAT3 proteins. However, none of them made significant difference of the STAT3 solubility. Finally low concentration of the STAT3 proteins (less than 0.6mg/ml) were applied during the purification and storage to maintain the soluble state of the proteins. Besides, reducing reagent DTT also played an important role to stop STAT3 aggregation during purification.

We developed three types of *in vitro* assays in this thesis to test STAT3 biological activities. Firstly, the PEMSA assay provides a visual method to detect STAT3 DNA binding activity. With the developed PEMSA assay, we successfully proved that the shortest STAT3 mutant YFP-STAT3 $_{127\text{-}497}$ protein can bind to the targeted dsDNA without SH2 domain. Therefore we conclude that STAT3 dimerisation is not a perquisite for DNA binding activity. This discovery challenges the traditional hypothesis that STAT3 must bind to dsDNA as a dimer. The observation is that STAT3 can bind to the dsDNA as a monomer and then another STAT3 binds to the same dsDNA and forms the dimer. Secondly, this result is further confirmed with the FP assay. Compared to the PEMSA assay, the FP assay is cheaper and more amenable to high-throughput screening. With application of STAT3 $_{127\text{-}497}$ protein in the FP assay, we developed a STAT3 inhibitor screening method that targets the DNA binding domain only. Moreover, the FP assay can be used to detect the stability of the purified STAT3 proteins. Thirdly, we optimised a previous FRET assay and developed another high-throughput method for detecting STAT3 biological activities. The developed FRET assay can not only be used to study the DNA binding activity of STAT3 but also be used to detect STAT3 dimerisation. However, further work is needed to test dimerisation conditions.

| Assay | Advantage | Disadvantage |
|---|---|---|
| PEMSA | Show the proportion of free protein, protein/DNA complex and aggregated protein | Slower and more expensive compared to the FP and FRET |
| FP | High-throughput | Limited information |
| FRET | High-throughput. Can detect both protein dimerisation and DNA binding | The method of testing protein dimerisation haven't been optimised |

Table 6.1. A summary of the advantages and disadvantages of the three *in vitro* assays developed in this thesis.

Table 6.1 summarises the advantages and disadvantages of the three in vitro assays: PEMSA, FP and FRET. The PEMSA is the only assay that can be used to detect protein/DNA interaction and protein precipitation. However, it is not as high-throughput as the other two assays. FP is the most high-throughput assay. FRET is also high-throughput and can be applied to detect STAT3 dimerisation. All three assays are very useful in small inhibitor tests targeting STAT3.

In conclusion, this thesis first suggested that the STAT3 dimerisation is not a perquisite for DNA binding activity by proving that truncated STAT3 protein can also bind to the GAS18 sequence. This discovery not only revealed the STAT3 DNA binding requirements but also highlighted the importance of the inhibition of DNA binding domain for anti-STAT3 drug design. This thesis also provide details for the experiment design and industrial up-scale of anticancer drug screening targeting STAT3, especially STAT3 DNA binding domains.

## 6.2 Future research

Based on the developed techniques and the discoveries in this thesis, we have suggested future work that continues the research on STAT3 biological activities. Firstly, the optimised PEMSA and the FP assays can be used to select small molecules that have the potential to be developed into novel

anticancer drugs. More small-molecule screening assay can be done based on our developed methods. Secondly, the FRET assay can be used to detect STAT3 dimerisation activity. With this application, it enables comparison of the relationship between STAT3 dimerisation and DNA binding more directly. Thirdly, we suggest a study of the relationship between STAT3 oxidation, multimerisation and STAT3 DNA binding activity. During the experiments we generated the hypothesis that STAT3 may form functional aggregates and the aggregation of STAT3 may be involved in the regulation of its DNA binding activity. The full length STAT3 is never crystallised since it precipitate easily. However, during nature evolution most proteins are developed into a stable and soluble form. It is possible that the multimerisation is involved in the STAT3 activity of regulation. On the other hand, STAT3 expression is up-regulated in many cancer cells, the high level of STAT3 in cell cytoplasm and nucleus may result the formation of STAT3 multimers and therefore regulate the STAT3 activity. However, there is little research relating the level of STAT3 association to the biological activity.

# References:

**Uncategorized References**


[1] C.V. Clevenger, Roles and regulation of stat family transcription factors in human breast cancer, Am J Pathol 165(5) (2004) 1449-60.
[2] K. Onishi, P.W. Zandstra, LIF signaling in stem cells and development, 142(13) (2015) 2230-2236.
[3] A.V. Villarino, Y. Kanno, J.R. Ferdinand, J.J. O'Shea, Mechanisms of Jak/STAT signaling in immunity and disease, Journal of immunology (Baltimore, Md. : 1950) 194(1) (2015) 21-27.
[4] K. Sugimoto, Role of STAT3 in inflammatory bowel disease, World J Gastroenterol 14(33) (2008) 5110-5114.
[5] K. Blaszczyk, H. Nowicka, K. Kostyrko, A. Antonczyk, J. Wesoly, H.A.R. Bluyssen, The unique role of STAT2 in constitutive and IFN-induced transcription and antiviral responses, Cytokine & Growth Factor Reviews 29 (2016) 71-81.
[6] K. Mowen, M. David, Role of the STAT1-SH2 Domain and STAT2 in the Activation and Nuclear Translocation of STAT1, 273(46) (1998) 30073-30076.
[7] J.F. Ma, B.J. Sanchez, D.T. Hall, A.-M.K. Tremblay, S. Di Marco, I.-E. Gallouzi, STAT3 promotes IFNγ/TNFα-induced muscle wasting in an NF-κB-dependent and IL-6-independent manner, 9(5) (2017) 622-637.
[8] V. Sanchez-Guajardo, J.A.M. Borghans, M.-E. Marquez, S. Garcia, A.A. Freitas, Different Competitive Capacities of Stat4- and Stat6-Deficient CD4<sup>+</sup> T Cells during Lymphophenia-Driven Proliferation, The Journal of Immunology 174(3) (2005) 1178.
[9] C.E. Egwuagu, STAT3 in CD4+ T helper cell differentiation and inflammatory diseases, Cytokine 47(3) (2009) 149-156.
[10] L.M. Heltemes-Harris, M.J.L. Willette, K.B. Vang, M.A. Farrar, The role of STAT5 in the development, function, and transformation of B and T lymphocytes, 1217(1) (2011) 18-31.
[11] S. Akira, Functional Roles of STAT Family Proteins: Lessons from Knockout Mice, STEM CELLS 17(3) (1999) 138-146.
[12] T.J. Mitchell, S. John, Signal transducer and activator of transcription (STAT) signalling and T-cell lymphomas, Immunology 114(3) (2005) 301-12.
[13] S. John, U. Vinkemeier, E. Soldaini, J.E. Darnell, Jr., W.J. Leonard, The significance of tetramerization in promoter recruitment by Stat5, Mol Cell Biol 19(3) (1999) 1910-1918.
[14] X. Zhang, J.E. Darnell, Functional Importance of Stat3 Tetramerization in Activation of the α2-Macroglobulin Gene, 276(36) (2001) 33576-33581.
[15] J.E. Durbin, R. Hackenmiller, M.C. Simon, D.E. Levy, Targeted Disruption of the Mouse Stat1 Gene Results in Compromised Innate Immunity to Viral Disease, Cell 84(3) (1996) 443-450.
[16] B.J. Tierney, G.A. McCann, S. Naidu, K.S. Rath, U. Saini, R. Wanner, P. Kuppusamy, A. Suarez, P.J. Goodfellow, D.E. Cohn, K. Selvendiran, Aberrantly activated pSTAT3-Ser727 in human endometrial cancer is suppressed by HO-3867, a novel STAT3 inhibitor, Gynecol Oncol 135(1) (2014) 133-141.
[17] J.I. Song, J.R. Grandis, STAT signaling in head and neck cancer, Oncogene 19(21) (2000) 2489-2495.
[18] X. Zhang, P. Yue, B.D.G. Page, T. Li, W. Zhao, A.T. Namanja, D. Paladino, J. Zhao, Y. Chen, P.T. Gunning, J. Turkson, Orally bioavailable small-molecule inhibitor of transcription factor Stat3 regresses human breast and lung cancer xenografts, Proc Natl Acad Sci U S A 109(24) (2012) 9623-9628.
[19] N. Don-Doncow, Z. Escobar, M. Johansson, S. Kjellström, V. Garcia, E. Munoz, O. Sterner, A. Bjartell, R. Hellsten, Galiellalactone Is a Direct Inhibitor of the Transcription Factor STAT3 in Prostate Cancer Cells, 289(23) (2014) 15969-15978.

[20] I. Kelesidis, T. Kelesidis, C.S. Mantzoros, Adiponectin and cancer: a systematic review, Br J Cancer 94(9) (2006) 1221-1225.
[21] P. Wang, S.M. Henning, D. Heber, J.V. Vadgama, Sensitization to docetaxel in prostate cancer cells by green tea and quercetin, J Nutr Biochem 26(4) (2015) 408-415.
[22] M.A. Bill, C. Nicholas, T.A. Mace, J.P. Etter, C. Li, E.B. Schwartz, J.R. Fuchs, G.S. Young, L. Lin, J. Lin, L. He, M. Phelps, P.K. Li, G.B. Lesinski, Structurally modified curcumin analogs inhibit STAT3 phosphorylation and promote apoptosis of human renal cell carcinoma and melanoma cell lines, PLoS One 7(8) (2012).
[23] J. Wang, S. Chen, S. Xu, X. Yu, D. Ma, X. Hu, X. Cao, In vivo induction of apoptosis by fucoxanthin, a marine carotenoid, associated with down-regulating STAT3/EGFR signaling in sarcoma 180 (S180) xenografts-bearing mice, Mar Drugs 10(9) (2012) 2055-2068.
[24] E. El-Habr, Implication of the JAK-STAT Pathway in Gliomagenesis: A Target for Therapy?, Journal of Neurological Disorders 01 (2013).
[25] F.M. Corvinus, C. Orth, R. Moriggl, S.A. Tsareva, S. Wagner, E.B. Pfitzner, D. Baus, R. Kaufmann, L.A. Huber, K. Zatloukal, H. Beug, P. Ohlschläger, A. Schütz, K.-J. Halbhuber, K. Friedrich, Persistent STAT3 activation in colon cancer is associated with enhanced cell proliferation and tumor growth, Neoplasia 7(6) (2005) 545-555.
[26] J. Darnell, I. Kerr, G. Stark, Jak-STAT pathways and transcriptional activation in response to IFNs and other extracellular signaling proteins, 264(5164) (1994) 1415-1421.
[27] F. Seif, M. Khoshmirsafa, H. Aazami, M. Mohsenzadegan, G. Sedighi, M. Bahar, The role of JAK-STAT signaling pathway and its regulators in the fate of T helper cells, Cell Commun Signal 15(1) (2017) 23-23.
[28] C. Rebe, F. Vegran, H. Berger, F. Ghiringhelli, STAT3 activation: A key factor in tumor immunoescape, JAKSTAT 2(1) (2013) e23010.
[29] Z.-l. Yuan, Y.-j. Guan, D. Chatterjee, Y.E. Chin, Stat3 Dimerization Regulated by Reversible Acetylation of a Single Lysine Residue, 307(5707) (2005) 269-273.
[30] T. Kisseleva, S. Bhattacharya, J. Braunstein, C.W. Schindler, Signaling through the JAK/STAT pathway, recent advances and future challenges, Gene 285(1) (2002) 1-24.
[31] A. Giraud, T. Menheniott, L. Judd, Targeting STAT3 in gastric cancer, Expert opinion on therapeutic targets 16 (2012) 889-901.
[32] Z. Wang, X. Si, A. Xu, X. Meng, S. Gao, Y. Qi, L. Zhu, T. Li, W. Li, L. Dong, Activation of STAT3 in human gastric cancer cells via interleukin (IL)-6-type cytokine signaling correlates with clinical implications, PloS one 8(10) (2013) e75788-e75788.
[33] W. Gong, L. Wang, J.C. Yao, J.A. Ajani, D. Wei, K.D. Aldape, K. Xie, R. Sawaya, S. Huang, Expression of Activated Signal Transducer and Activator of Transcription 3 Predicts Expression of Vascular Endothelial Growth Factor in and Angiogenic Phenotype of Human Gastric Cancer, Clinical Cancer Research 11(4) (2005) 1386.
[34] N. Kanda, H. Seno, Y. Konda, H. Marusawa, M. Kanai, T. Nakajima, T. Kawashima, A. Nanakin, T. Sawabu, Y. Uenoyama, A. Sekikawa, M. Kawada, K. Suzuki, T. Kayahara, H. Fukui, M. Sawada, T. Chiba, STAT3 is constitutively activated and supports cell survival in association with survivin expression in gastric cancer cells, Oncogene 23(28) (2004) 4921-9.
[35] S.J. Thomas, J.A. Snowden, M.P. Zeidler, S.J. Danson, The role of JAK/STAT signalling in the pathogenesis, prognosis and treatment of solid tumours, Br J Cancer 113(3) (2015) 365-71.
[36] D.A. Harrison, The JAK/STAT Pathway, 4(3) (2012).
[37] H. Kiu, S.E. Nicholson, Biology and significance of the JAK/STAT signalling pathways, Growth Factors 30(2) (2012) 88-106.
[38] C. Dethlefsen, G. Højfeldt, P. Hojman, The role of intratumoral and systemic IL-6 in breast cancer, Breast Cancer Research and Treatment 138(3) (2013) 657-664.
[39] J. Yang, G.R. Stark, Roles of unphosphorylated STATs in signaling, Cell research 18(4) (2008) 443-51.

[40] Z. Wen, Z. Zhong, J.E. Darnell, Jr., Maximal activation of transcription by Stat1 and Stat3 requires both tyrosine and serine phosphorylation, Cell 82(2) (1995) 241-50.
[41] C.P. Lim, X. Cao, Serine phosphorylation and negative regulation of Stat3 by JNK, J Biol Chem 274(43) (1999) 31055-61.
[42] M. Sakaguchi, M. Oka, T. Iwasaki, Y. Fukami, C. Nishigori, Role and regulation of STAT3 phosphorylation at Ser727 in melanocytes and melanoma cells, J Invest Dermatol 132(7) (2012) 1877-85.
[43] S. Courapied, H. Sellier, S. de Carné Trécesson, A. Vigneron, A.-C. Bernard, E. Gamelin, B. Barré, O. Coqueret, The cdk5 kinase regulates the STAT3 transcription factor to prevent DNA damage upon topoisomerase I inhibition, The Journal of biological chemistry 285(35) (2010) 26765-26778.
[44] R. Wakahara, H. Kunimoto, K. Tanino, H. Kojima, A. Inoue, H. Shintaku, K. Nakajima, Phospho-Ser727 of STAT3 regulates STAT3 activity by enhancing dephosphorylation of phospho-Tyr705 largely through TC45, Genes to cells : devoted to molecular & cellular mechanisms 17(2) (2012) 132-45.
[45] S.F. Yang, S.S. Yuan, Y.T. Yeh, M.T. Wu, J.H. Su, S.C. Hung, C.Y. Chai, The role of p-STAT3 (ser727) revealed by its association with Ki-67 in cervical intraepithelial neoplasia, Gynecol Oncol 98(3) (2005) 446-52.
[46] I. Hazan-Halevy, D. Harris, Z. Liu, J. Liu, P. Li, X. Chen, S. Shanker, A. Ferrajoli, M.J. Keating, Z. Estrov, STAT3 is constitutively phosphorylated on serine 727 residues, binds DNA, and activates transcription in CLL cells, Blood 115(14) (2010) 2852-2863.
[47] P. Yue, J. Turkson, Targeting STAT3 in cancer: how successful are we?, Expert Opinion on Investigational Drugs 18(1) (2009) 45-56.
[48] R. Wang, P. Cherukuri, J. Luo, Activation of Stat3 sequence-specific DNA binding and transcription by p300/CREB-binding protein-mediated acetylation, J Biol Chem 280(12) (2005) 11528-34.
[49] U. Rozovski, D.M. Harris, P. Li, Z. Liu, P. Jain, I. Veletic, A. Ferrajoli, J. Burger, S. O'Brien, P. Bose, P. Thompson, N. Jain, W. Wierda, M.J. Keating, Z. Estrov, Constitutive Phosphorylation of STAT3 by the CK2–BLNK–CD5 Complex, 15(5) (2017) 610-618.
[50] J. Yang, M. Chatterjee-Kishore, S.M. Staugaitis, H. Nguyen, K. Schlessinger, D.E. Levy, G.R. Stark, Novel Roles of Unphosphorylated STAT3 in Oncogenesis and Transcriptional Regulation, 65(3) (2005) 939-947.
[51] M. Dasgupta, H. Unal, B. Willard, J. Yang, S.S. Karnik, G.R. Stark, Critical role for lysine 685 in gene expression mediated by transcription factor unphosphorylated STAT3, J Biol Chem 289(44) (2014) 30763-71.
[52] J.L. Lee, M.J. Wang, J.Y. Chen, Acetylation and activation of STAT3 mediated by nuclear translocation of CD44, J Cell Biol 185(6) (2009) 949-57.
[53] Q.-R. Qi, Z.-M. Yang, Regulation and function of signal transducer and activator of transcription 3, World J Biol Chem 5(2) (2014) 231-239.
[54] T. Hu, Y. Chong, B. Cai, Y. Liu, S. Lu, J.K. Cowell, DNA methyltransferase 1-mediated CpG methylation of the miR-150-5p promoter contributes to fibroblast growth factor receptor 1-driven leukemogenesis, (2019).
[55] G. Sethi, S. Chatterjee, P. Rajendran, F. Li, M.K. Shanmugam, K.F. Wong, A.P. Kumar, P. Senapati, A.K. Behera, K.M. Hui, J. Basha, N. Natesh, J.M. Luk, T.K. Kundu, Inhibition of STAT3 dimerization and acetylation by garcinol suppresses the growth of human hepatocellular carcinoma in vitro and in vivo, Molecular Cancer 13(1) (2014) 66.
[56] S. Ray, I. Boldogh, A.R. Brasier, STAT3 NH2-Terminal Acetylation Is Activated by the Hepatic Acute-Phase Response and Required for IL-6 Induction of Angiotensinogen, Gastroenterology 129(5) (2005) 1616-1632.

[57] S. Ray, Y. Zhao, M. Jamaluddin, C.B. Edeh, C. Lee, A.R. Brasier, Inducible STAT3 NH2 terminal mono-ubiquitination promotes BRD4 complex formation to regulate apoptosis, Cell Signal 26(7) (2014) 1445-55.
[58] Y. Nie, D.M. Erion, Z. Yuan, M. Dietrich, G.I. Shulman, T.L. Horvath, Q. Gao, STAT3 inhibition of gluconeogenesis is downregulated by SirT1, Nat Cell Biol 11(4) (2009) 492-500.
[59] J. Yang, J. Huang, M. Dasgupta, N. Sears, M. Miyagi, B. Wang, M.R. Chance, X. Chen, Y. Du, Y. Wang, L. An, Q. Wang, T. Lu, X. Zhang, Z. Wang, G.R. Stark, Reversible methylation of promoter-bound STAT3 by histone-modifying enzymes, Proc Natl Acad Sci U S A 107(50) (2010) 21499-504.
[60] E. Kim, M. Kim, D.H. Woo, Y. Shin, J. Shin, N. Chang, Y.T. Oh, H. Kim, J. Rheey, I. Nakano, C. Lee, K.M. Joo, J.N. Rich, D.H. Nam, J. Lee, Phosphorylation of EZH2 activates STAT3 signaling via STAT3 methylation and promotes tumorigenicity of glioblastoma stem-like cells, Cancer Cell 23(6) (2013) 839-52.
[61] M. Dasgupta, J.K. Dermawan, B. Willard, G.R. Stark, STAT3-driven transcription depends upon the dimethylation of K49 by EZH2, Proc Natl Acad Sci U S A 112(13) (2015) 3985-90.
[62] J. Yang, J. Huang, M. Dasgupta, N. Sears, M. Miyagi, B. Wang, M.R. Chance, X. Chen, Y. Du, Y. Wang, L. An, Q. Wang, T. Lu, X. Zhang, Z. Wang, G.R. Stark, Reversible methylation of promoter-bound STAT3 by histone-modifying enzymes, 107(50) (2010) 21499-21504.
[63] S.-C. Chen, Y.-L. Chang, D.L. Wang, J.-J. Cheng, Herbal remedy magnolol suppresses IL-6-induced STAT3 activation and gene expression in endothelial cells, 148(2) (2006) 226-232.
[64] R. Wakahara, H. Kunimoto, K. Tanino, H. Kojima, A. Inoue, H. Shintaku, K. Nakajima, Phospho-Ser727 of STAT3 regulates STAT3 activity by enhancing dephosphorylation of phospho-Tyr705 largely through TC45, 17(2) (2012) 132-145.
[65] G. Huang, H. Yan, S. Ye, C. Tong, Q.-L. Ying, STAT3 phosphorylation at tyrosine 705 and serine 727 differentially regulates mouse ESC fates, Stem cells (Dayton, Ohio) 32(5) (2014) 1149-1160.
[66] L. Valentino, J. Pierre, JAK/STAT signal transduction: regulators and implication in hematological malignancies, Biochemical pharmacology 71(6) (2006) 713-21.
[67] L. Espert, I. Dusanter-Fourt, M.K. Chelbi-Alix, [Negative regulation of the JAK/STAT: pathway implication in tumorigenesis], Bulletin du cancer 92(10) (2005) 845-57.
[68] T. Tanaka, Y. Yamamoto, R. Muromoto, O. Ikeda, Y. Sekine, M.J. Grusby, T. Kaisho, T. Matsuda, PDLIM2 Inhibits T Helper 17 Cell Development and Granulomatous Inflammation Through Degradation of STAT3, 4(202) (2011) ra85-ra85.
[69] C.-S. Wu, L. Zou, The SUMO (Small Ubiquitin-like Modifier) Ligase PIAS3 Primes ATR for Checkpoint Activation, 291(1) (2016) 279-290.
[70] E. Perry, R. Tsruya, P. Levitsky, O. Pomp, M. Taller, S. Weisberg, W. Parris, S. Kulkarni, H. Malovani, T. Pawson, S. Shpungin, U. Nir, TMF/ARA160 is a BC-box-containing protein that mediates the degradation of Stat3, Oncogene 23(55) (2004) 8908-8919.
[71] B. Cai, J. Li, J. Wang, X. Luo, J. Ai, Y. Liu, N. Wang, H. Liang, M. Zhang, N. Chen, G. Wang, S. Xing, X. Zhou, B. Yang, X. Wang, Y. Lu, microRNA-124 regulates cardiomyocyte differentiation of bone marrow-derived mesenchymal stem cells via targeting STAT3 signaling, Stem Cells 30(8) (2012) 1746-55.
[72] J. Jiang, Z. Li, C. Yu, M. Chen, S. Tian, C. Sun, MiR-1181 inhibits stem cell-like phenotypes and suppresses SOX2 and STAT3 in human pancreatic cancer, Cancer Letters 356(2, Part B) (2015) 962-970.
[73] H. Zhang, K. Cai, J. Wang, X. Wang, K. Cheng, F. Shi, L. Jiang, Y. Zhang, J. Dou, MiR-7, inhibited indirectly by lincRNA HOTAIR, directly inhibits SETDB1 and reverses the EMT of breast cancer stem cells by downregulating the STAT3 pathway, Stem Cells 32(11) (2014) 2858-68.

[74] D.M. Schwartz, Y. Kanno, A. Villarino, M. Ward, M. Gadina, J.J. O'Shea, JAK inhibition as a therapeutic strategy for immune and inflammatory diseases, Nat Rev Drug Discov 17(1) (2017) 78.
[75] A. Kontzias, A. Kotlyar, A. Laurence, P. Changelian, J.J. O'Shea, Jakinibs: a new class of kinase inhibitors in cancer and autoimmune disease, Curr Opin Pharmacol 12(4) (2012) 464-70.
[76] O.A. Timofeeva, S. Chasovskikh, I. Lonskaya, N.I. Tarasova, L. Khavrutskii, S.G. Tarasov, X. Zhang, V.R. Korostyshevskiy, A. Cheema, L. Zhang, S. Dakshanamurthy, M.L. Brown, A. Dritschilo, Mechanisms of unphosphorylated STAT3 transcription factor binding to DNA, J Biol Chem 287(17) (2012) 14192-200.
[77] L. Pedranzini, A. Leitch, J. Bromberg, Stat3 is required for the development of skin cancer, J Clin Invest 114(5) (2004) 619-622.
[78] N. de la Iglesia, G. Konopka, S.V. Puram, J.A. Chan, R.M. Bachoo, M.J. You, D.E. Levy, R.A. Depinho, A. Bonni, Identification of a PTEN-regulated STAT3 brain tumor suppressor pathway, Genes Dev 22(4) (2008) 449-462.
[79] K. Leslie, C. Lang, G. Devgan, J. Azare, M. Berishaj, W. Gerald, Y.B. Kim, K. Paz, J.E. Darnell, C. Albanese, T. Sakamaki, R. Pestell, J. Bromberg, Cyclin D1 Is Transcriptionally Regulated by and Required for Transformation by Activated Signal Transducer and Activator of Transcription 3, 66(5) (2006) 2544-2552.
[80] L. Wang, T. Yi, M. Kortylewski, D.M. Pardoll, D. Zeng, H. Yu, IL-17 can promote tumor growth through an IL-6-Stat3 signaling pathway, J Exp Med 206(7) (2009) 1457-1464.
[81] M.M. Sherry, A. Reeves, J.K. Wu, B.H. Cochran, STAT3 Is Required for Proliferation and Maintenance of Multipotency in Glioblastoma Stem Cells, 27(10) (2009) 2383-2392.
[82] F.M. Corvinus, C. Orth, R. Moriggl, S.A. Tsareva, S. Wagner, E.B. Pfitzner, D. Baus, R. Kaufmann, L.A. Huber, K. Zatloukal, H. Beug, P. Ohlschlager, A. Schutz, K.J. Halbhuber, K. Friedrich, Persistent STAT3 activation in colon cancer is associated with enhanced cell proliferation and tumor growth, Neoplasia 7(6) (2005) 545-55.
[83] R. Haviland, S. Eschrich, G. Bloom, Y. Ma, S. Minton, R. Jove, W.D. Cress, Necdin, a negative growth regulator, is a novel STAT3 target gene down-regulated in human cancer, PLoS One 6(10) (2011) e24923.
[84] H.J. Choi, J.S. Han, Overexpression of phospholipase D enhances Bcl-2 expression by activating STAT3 through independent activation of ERK and p38MAPK in HeLa cells, Biochimica et biophysica acta 1823(6) (2012) 1082-91.
[85] D. Puthier, R. Bataille, M. Amiot, IL-6 up-regulates mcl-1 in human myeloma cells through JAK / STAT rather than ras / MAP kinase pathway, European journal of immunology 29(12) (1999) 3945-50.
[86] J.M. Wang, J.R. Chao, W. Chen, M.L. Kuo, J.J. Yen, H.F. Yang-Yen, The antiapoptotic gene mcl-1 is up-regulated by the phosphatidylinositol 3-kinase/Akt signaling pathway through a transcription factor complex containing CREB, Mol Cell Biol 19(9) (1999) 6195-6206.
[87] L. Zhuang, C.S. Lee, R.A. Scolyer, S.W. McCarthy, X.D. Zhang, J.F. Thompson, P. Hersey, Mcl-1, Bcl-XL and Stat3 expression are associated with progression of melanoma whereas Bcl-2, AP-2 and MITF levels decrease during progression of melanoma, Modern pathology : an official journal of the United States and Canadian Academy of Pathology, Inc 20(4) (2007) 416-26.
[88] A. Zaanan, K. Okamoto, H. Kawakami, K. Khazaie, S. Huang, F.A. Sinicrope, The Mutant KRAS Gene Up-regulates BCL-XL Protein via STAT3 to Confer Apoptosis Resistance That Is Reversed by BIM Protein Induction and BCL-XL Antagonism, J Biol Chem 290(39) (2015) 23838-49.
[89] T. Gritsko, A. Williams, J. Turkson, S. Kaneko, T. Bowman, M. Huang, S. Nam, I. Eweis, N. Diaz, D. Sullivan, S. Yoder, S. Enkemann, S. Eschrich, J.-H. Lee, C.A. Beam, J. Cheng, S.

Minton, C.A. Muro-Cacho, R. Jove, Persistent Activation of Stat3 Signaling Induces Survivin Gene Expression and Confers Resistance to Apoptosis in Human Breast Cancer Cells, 12(1) (2006) 11-19.
[90] V.N. Ivanov, M. Krasilnikov, Z.e. Ronai, Regulation of Fas Expression by STAT3 and c-Jun Is Mediated by Phosphatidylinositol 3-Kinase-AKT Signaling, 277(7) (2002) 4932-4944.
[91] A.P. See, J.E. Han, J. Phallen, Z. Binder, G. Gallia, F. Pan, D. Jinasena, C. Jackson, Z. Belcaid, S.J. Jeong, C. Gottschalk, J. Zeng, J. Ruzevick, S. Nicholas, Y. Kim, E. Albesiano, D.M. Pardoll, M. Lim, The role of STAT3 activation in modulating the immune microenvironment of GBM, J Neurooncol 110(3) (2012) 359-68.
[92] L. Ouaguia, D. Mrizak, S. Renaud, O. Moralès, N. Delhem, Control of the inflammatory response mechanisms mediated by natural and induced regulatory T-cells in HCV-, HTLV-1-, and EBV-associated cancers, Mediators Inflamm 2014 (2014) 564296-564296.
[93] A. Schaefer, C. Unterberger, M. Frankenberger, M. Lohrum, K.J. Staples, T. Werner, H. Stunnenberg, L. Ziegler-Heitbrock, Mechanism of Interferon-gamma mediated down-regulation of Interleukin-10 gene expression, Molecular Immunology 46(7) (2009) 1351-1359.
[94] J.L. Langowski, X. Zhang, L. Wu, J.D. Mattson, T. Chen, K. Smith, B. Basham, T. McClanahan, R.A. Kastelein, M. Oft, IL-23 promotes tumour incidence and growth, Nature 442(7101) (2006) 461-465.
[95] M. Kortylewski, H. Xin, M. Kujawski, H. Lee, Y. Liu, T. Harris, C. Drake, D. Pardoll, H. Yu, Regulation of the IL-23 and IL-12 balance by Stat3 signaling in the tumor microenvironment, Cancer cell 15(2) (2009) 114-123.
[96] S.L. Gaffen, R. Jain, A.V. Garg, D.J. Cua, The IL-23–IL-17 immune axis: from mechanisms to therapeutic testing, Nature Reviews Immunology 14(9) (2014) 585-600.
[97] S. Okada, S. Han, E.S. Patel, L.-J. Yang, L.-J. Chang, STAT3 signaling contributes to the high effector activities of interleukin-15-derived dendritic cells, Immunol Cell Biol 93(5) (2015) 461-471.
[98] Y. Li, X. Yu, Y. Ma, S. Hua, IL-23 and dendritic cells: What are the roles of their mutual attachment in immune response and immunotherapy?, Cytokine 120 (2019) 78-84.
[99] D.A. Braun, M. Fribourg, S.C. Sealfon, Cytokine response is determined by duration of receptor and signal transducers and activators of transcription 3 (STAT3) activation, The Journal of biological chemistry 288(5) (2013) 2986-2993.
[100] T. Wang, G. Niu, M. Kortylewski, L. Burdelya, K. Shain, S. Zhang, R. Bhattacharya, D. Gabrilovich, R. Heller, D. Coppola, W. Dalton, R. Jove, A.M. Pardoll, H. Yu, Regulation of the innate and adaptive immune responses by Stat-3 signaling in tumor cells, Nature Medicine 10(1) (2004) 48-54.
[101] J. Cheng, X.-M. Fan, Role of cyclooxygenase-2 in gastric cancer development and progression, World J Gastroenterol 19(42) (2013) 7361-7368.
[102] X.-L. Yuan, L. Chen, M.-X. Li, P. Dong, J. Xue, J. Wang, T.-t. Zhang, X.-a. Wang, F.-M. Zhang, H.-L. Ge, L.-S. Shen, D. Xu, Elevated expression of Foxp3 in tumor-infiltrating Treg cells suppresses T-cell proliferation and contributes to gastric cancer progression in a COX-2-dependent manner, Clinical Immunology 134(3) (2010) 277-288.
[103] T.H. Chen, K. Fukuhara, M. Mandai, N. Matsumura, M. Kariya, K. Takakura, S. Fujii, Increased cyclooxygenase-2 expression is correlated with suppressed antitumor immunity in cervical adenocarcinomas, International journal of gynecological cancer : official journal of the International Gynecological Cancer Society 16 (2006) 772-9.
[104] H.W. Lo, X. Cao, H. Zhu, F. Ali-Osman, Cyclooxygenase-2 is a novel transcriptional target of the nuclear EGFR-STAT3 and EGFRvIII-STAT3 signaling axes, Molecular cancer research : MCR 8(2) (2010) 232-45.

[105] K. Takeda, B.E. Clausen, T. Kaisho, T. Tsujimura, N. Terada, I. Förster, S. Akira, Enhanced Th1 Activity and Development of Chronic Enterocolitis in Mice Devoid of Stat3 in Macrophages and Neutrophils, Immunity 10(1) (1999) 39-49.
[106] M. Kortylewski, M. Kujawski, T. Wang, S. Wei, S. Zhang, S. Pilon-Thomas, G. Niu, H. Kay, J. Mulé, W.G. Kerr, R. Jove, D. Pardoll, H. Yu, Inhibiting Stat3 signaling in the hematopoietic system elicits multicomponent antitumor immunity, Nature Medicine 11(12) (2005) 1314-1321.
[107] W. Zou, Immunosuppressive networks in the tumour environment and their therapeutic relevance, Nature Reviews Cancer 5(4) (2005) 263-274.
[108] S.J. Park, T. Nakagawa, H. Kitamura, T. Atsumi, H. Kamon, S. Sawa, D. Kamimura, N. Ueda, Y. Iwakura, K. Ishihara, M. Murakami, T. Hirano, IL-6 regulates in vivo dendritic cell differentiation through STAT3 activation, J Immunol 173(6) (2004) 3844-54.
[109] Y. Kawakami, N. Inagaki, S. Salek-Ardakani, J. Kitaura, H. Tanaka, K. Nagao, Y. Kawakami, W. Xiao, H. Nagai, M. Croft, T. Kawakami, Regulation of dendritic cell maturation and function by Bruton's tyrosine kinase via IL-10 and Stat3, 103(1) (2006) 153-158.
[110] A. Mantovani, T. Schioppa, C. Porta, P. Allavena, A. Sica, Role of tumor-associated macrophages in tumor progression and invasion, Cancer and Metastasis Reviews 25(3) (2006) 315-322.
[111] Q. Al-Ismaeel, C.P. Neal, H. Al-Mahmoodi, Z. Almutairi, I. Al-Shamarti, K. Straatman, N. Jaunbocus, A. Irvine, E. Issa, C. Moreman, A.R. Dennison, A. Emre Sayan, J. McDearmid, P. Greaves, E. Tulchinsky, M. Kriajevska, ZEB1 and IL-6/11-STAT3 signalling cooperate to define invasive potential of pancreatic cancer cells via differential regulation of the expression of S100 proteins, Br J Cancer 121(1) (2019) 65-75.
[112] C. Zhang, F. Guo, G. Xu, J. Ma, F. Shao, STAT3 cooperates with Twist to mediate epithelial-mesenchymal transition in human hepatocellular carcinoma cells, Oncol Rep 33(4) (2015) 1872-82.
[113] Y. Cui, Y.-Y. Li, J. Li, H.-Y. Zhang, F. Wang, X. Bai, S.-S. Li, STAT3 regulates hypoxia-induced epithelial mesenchymal transition in oesophageal squamous cell cancer, Oncology reports 36(1) (2016) 108-116.
[114] M.K. Wendt, N. Balanis, C.R. Carlin, W.P. Schiemann, STAT3 and epithelial–mesenchymal transitions in carcinomas, JAK-STAT 3(2) (2014) e28975.
[115] E. Macias, D. Rao, J. Digiovanni, Role of Stat3 in Skin Carcinogenesis: Insights Gained from Relevant Mouse Models, Journal of skin cancer 2013 (2013) 684050.
[116] J. Turkson, T. Bowman, R. Garcia, E. Caldenhoven, R.P. De Groot, R. Jove, Stat3 activation by Src induces specific gene regulation and is required for cell transformation, Mol Cell Biol 18(5) (1998) 2545-52.
[117] C. Suiqing, Z. Min, C. Lirong, Overexpression of Phosphorylated-STAT3 Correlated with the Invasion and Metastasis of Cutaneous Squamous Cell Carcinoma, 32(5) (2005) 354-360.
[118] H.d. Li, C. Huang, K.j. Huang, W.d. Wu, T. Jiang, J. Cao, Z.z. Feng, Z.j. Qiu, STAT3 knockdown reduces pancreatic cancer cell invasiveness and matrix metalloproteinase-7 expression in nude mice, PloS one 6(10) (2011) e25941-e25941.
[119] M. Itoh, T. Murata, T. Suzuki, M. Shindoh, K. Nakajima, K. Imai, K. Yoshida, Requirement of STAT3 activation for maximal collagenase-1 (MMP-1) induction by epidermal growth factor and malignant characteristics in T24 bladder cancer cells, Oncogene 25(8) (2006) 1195-1204.
[120] T.-x. Xie, D. Wei, M. Liu, A.C. Gao, F. Ali-Osman, R. Sawaya, S. Huang, Stat3 activation regulates the expression of matrix metalloproteinase-2 and tumor invasion and metastasis, Oncogene 23(20) (2004) 3550-3560.

[121] T.N. Dechow, L. Pedranzini, A. Leitch, K. Leslie, W.L. Gerald, I. Linkov, J.F. Bromberg, Requirement of matrix metalloproteinase-9 for the transformation of human mammary epithelial cells by Stat3-C, Proc Natl Acad Sci U S A 101(29) (2004) 10602-10607.
[122] S. Chakraborty, S. Kaur, S. Guha, S.K. Batra, The multifaceted roles of neutrophil gelatinase associated lipocalin (NGAL) in inflammation and cancer, Biochimica et biophysica acta 1826(1) (2012) 129-69.
[123] D. Silver, H. Naora, J. Liu, W. Cheng, D. Montell, Activated signal transducer and activator of transcription (STAT) 3: Localization in focal adhesions and function in ovarian cancer cell motility, Cancer research 64 (2004) 3550-8.
[124] D.C.H. Ng, B.H. Lin, C.P. Lim, G. Huang, T. Zhang, V. Poli, X. Cao, Stat3 regulates microtubules by antagonizing the depolymerization activity of stathmin, The Journal of cell biology 172(2) (2006) 245-257.
[125] T.S. Teng, B. Lin, E. Manser, D.C. Ng, X. Cao, Stat3 promotes directional cell migration by regulating Rac1 activity via its activator betaPIX, Journal of cell science 122(Pt 22) (2009) 4150-9.
[126] Z. Chen, Z.C. Han, STAT3: a critical transcription activator in angiogenesis, Medicinal research reviews 28(2) (2008) 185-200.
[127] G. Niu, K.L. Wright, M. Huang, L. Song, E. Haura, J. Turkson, S. Zhang, T. Wang, D. Sinibaldi, D. Coppola, R. Heller, L.M. Ellis, J. Karras, J. Bromberg, D. Pardoll, R. Jove, H. Yu, Constitutive Stat3 activity up-regulates VEGF expression and tumor angiogenesis, Oncogene 21(13) (2002) 2000-8.
[128] D. Wei, X. Le, L. Zheng, L. Wang, J.A. Frey, A.C. Gao, Z. Peng, S. Huang, H.Q. Xiong, J.L. Abbruzzese, K. Xie, Stat3 activation regulates the expression of vascular endothelial growth factor and human pancreatic cancer angiogenesis and metastasis, Oncogene 22(3) (2003) 319-329.
[129] G.L. Semenza, Targeting HIF-1 for cancer therapy, Nature reviews. Cancer 3(10) (2003) 721-32.
[130] M.K. Oh, H.J. Park, N.H. Kim, S.J. Park, I.Y. Park, I.S. Kim, Hypoxia-inducible factor-1alpha enhances haptoglobin gene expression by improving binding of STAT3 to the promoter, J Biol Chem 286(11) (2011) 8857-65.
[131] N.R. Madamanchi, S. Li, C. Patterson, M.S. Runge, Thrombin regulates vascular smooth muscle cell growth and heat shock proteins via the JAK-STAT pathway, J Biol Chem 276(22) (2001) 18915-24.
[132] X.-s. Chen, Y. Zhang, J.-s. Wang, X.-y. Li, X.-k. Cheng, Y. Zhang, N.-h. Wu, Y.-f. Shen, Diverse effects of Stat1 on the regulation of hsp90α gene under heat shock, 102(4) (2007) 1059-1066.
[133] H.-M. Oh, C.-R. Yu, N. Golestaneh, A. Amadi-Obi, Y.S. Lee, A. Eseonu, R.M. Mahdi, C.E. Egwuagu, STAT3 protein promotes T-cell survival and inhibits interleukin-2 production through up-regulation of Class O Forkhead transcription factors, The Journal of biological chemistry 286(35) (2011) 30888-30897.
[134] P.K. Vogt, J.R. Hart, PI3K and STAT3: a new alliance, Cancer Discov 1(6) (2011) 481-486.
[135] K. Abell, A. Bilancio, R.W.E. Clarkson, P.G. Tiffen, A.I. Altaparmakov, T.G. Burdon, T. Asano, B. Vanhaesebroeck, C.J. Watson, Stat3-induced apoptosis requires a molecular switch in PI(3)K subunit composition, Nature Cell Biology 7(4) (2005) 392-398.
[136] S. Pensa, B. Lloyd-Lewis, T.J. Sargeant, H.K. Resemann, C.R. Kahn, C.J. Watson, Signal transducer and activator of transcription 3 and the phosphatidylinositol 3-kinase regulatory subunits p55α and p50α regulate autophagy in vivo, The FEBS journal 281(20) (2014) 4557-4567.
[137] R. Fagard, V. Metelev, I. Souissi, F. Baran-Marszak, STAT3 inhibitors for cancer therapy: Have all roads been explored?, JAKSTAT 2(1) (2013) e22882.

[138] J.-H. CHOI, M.-J. AHN, C.-K. PARK, H.-X. HAN, S.-J. KWON, Y.-Y. LEE, I.-S. KIM, Phospho-Stat3 expression and correlation with VEGF, p53, and Bcl-2 in gastric carcinoma using tissue microarray, 114(9) (2006) 619-625.
[139] D. Sinibaldi, W. Wharton, J. Turkson, T. Bowman, W.J. Pledger, R. Jove, Induction of p21WAF1/CIP1 and cyclin D1 expression by the Src oncoprotein in mouse fibroblasts: role of activated STAT3 signaling, Oncogene 19(48) (2000) 5419-27.
[140] A. Wincewicz, M. Baltaziak, L. Kanczuga-Koda, M. Koda, U. Sulkowska, W. Famulski, S. Sulkowski, STAT3 and apoptosis regulators: Bak and Bcl-xL in endometrioid adenocarcinomas of different estrogen receptor-alpha immunoprofile, Gynecological endocrinology : the official journal of the International Society of Gynecological Endocrinology 27(8) (2011) 536-40.
[141] S.W. Lee, Y.Y. Ahn, Y.S. Kim, S.B. Kang, S.W. Nam, D.S. Lee, H.Y. Jeong, J.M. Kim, The Immunohistochemical Expression of STAT3, Bcl-xL, and MMP-2 Proteins in Colon Adenoma and Adenocarcinoma, Gut Liver 6(1) (2012) 45-51.
[142] Y. Sehara, K. Sawicka, J.-Y. Hwang, A. Latuszek-Barrantes, A.M. Etgen, R.S. Zukin, Survivin Is a transcriptional target of STAT3 critical to estradiol neuroprotection in global ischemia, J Neurosci 33(30) (2013) 12364-12374.
[143] S.-H. Chen, D.A. Murphy, W. Lassoued, G. Thurston, M.D. Feldman, W.M.F. Lee, Activated STAT3 is a mediator and biomarker of VEGF endothelial activation, Cancer Biol Ther 7(12) (2008) 1994-2003.
[144] Y.-W. Zhang, L.-M. Wang, R. Jove, G.F. Vande Woude, Requirement of Stat3 signaling for HGF/SF-Met mediated tumorigenesis, Oncogene 21(2) (2002) 217-226.
[145] Y. Liu, J. Lv, J. Liu, X. Liang, X. Jin, J. Xie, L. Zhang, D. Chen, R. Fiskesund, K. Tang, J. Ma, H. Zhang, W. Dong, S. Mo, T. Zhang, F. Cheng, Y. Zhou, Q. Jia, B. Zhu, Y. Kong, J. Guo, H. Zhang, Z.-W. Hu, X. Cao, F.X.-F. Qin, B. Huang, STAT3/p53 pathway activation disrupts IFN-β–induced dormancy in tumor-repopulating cells, J Clin Invest 128(3) (2018) 1057-1073.
[146] M. Kortylewski, M. Kujawski, T. Wang, S. Wei, S. Zhang, S. Pilon-Thomas, G. Niu, H. Kay, J. Mule, W.G. Kerr, R. Jove, D. Pardoll, H. Yu, Inhibiting Stat3 signaling in the hematopoietic system elicits multicomponent antitumor immunity, Nat Med 11(12) (2005) 1314-21.
[147] F. Zhang, Z. Wang, Y. Fan, Q. Xu, W. Ji, R. Tian, R. Niu, Elevated STAT3 Signaling-Mediated Upregulation of MMP-2/9 Confers Enhanced Invasion Ability in Multidrug-Resistant Breast Cancer Cells, Int J Mol Sci 16(10) (2015) 24772-24790.
[148] J. Chen, X. Liu, H. Jiao, L. Peng, Z. Huo, W. Yang, Q. Shen, T. Li, Q. Liu, Prognostic and clinical significance of STAT3 and MMP9 in patients with gastric cancer: a meta-analysis of a Chinese cohort, Int J Clin Exp Med 8(1) (2015) 546-557.
[149] Y. Wang, A.H.H. van Boxel-Dezaire, H. Cheon, J. Yang, G.R. Stark, STAT3 activation in response to IL-6 is prolonged by the binding of IL-6 receptor to EGF receptor, Proc Natl Acad Sci U S A 110(42) (2013) 16975-16980.
[150] I. Kinjyo, M. Ohishi, T. Shouda, T. Kobayashi, A. Yoshimura, Positive and negative roles of IL-6, STAT3, and SOCS3 in inflammatory arthritis, Advances in experimental medicine and biology 602 (2007) 113-24.
[151] J.D. Peda, S.M. Salah, D.P. Wallace, P.E. Fields, C.J. Grantham, T.A. Fields, K.I. Swenson-Fields, Autocrine IL-10 activation of the STAT3 pathway is required for pathological macrophage differentiation in polycystic kidney disease, Dis Model Mech 9(9) (2016) 1051-1061.
[152] R.L. Carpenter, H.-W. Lo, STAT3 Target Genes Relevant to Human Cancers, Cancers 6(2) (2014) 897-925.
[153] G. Niu, K.L. Wright, M. Huang, L. Song, E. Haura, J. Turkson, S. Zhang, T. Wang, D. Sinibaldi, D. Coppola, R. Heller, L.M. Ellis, J. Karras, J. Bromberg, D. Pardoll, R. Jove, H. Yu,

Constitutive Stat3 activity up-regulates VEGF expression and tumor angiogenesis, Oncogene 21(13) (2002) 2000-2008.
[154] J.E. Jung, H.G. Lee, I.H. Cho, D.H. Chung, S.H. Yoon, Y.M. Yang, J.W. Lee, S. Choi, J.W. Park, S.K. Ye, M.H. Chung, STAT3 is a potential modulator of HIF-1-mediated VEGF expression in human renal carcinoma cells, FASEB journal : official publication of the Federation of American Societies for Experimental Biology 19(10) (2005) 1296-8.
[155] L. Giovannini-Chami, T.P. Vogel, L.R. Forbes, A. Fabre, M.-C. Trojani, S. Leroy, O. Antunes, N. Vincent-Mefitiot, S. Hiéronimus, M. Baque-Juston, C. Roux, N. Tieulié, STAT3 gain of function: a new aetiology of severe rheumatic disease, Rheumatology 58(2) (2018) 365-367.
[156] S. Nabhani, C. Schipp, H. Miskin, C. Levin, S. Postovsky, T. Dujovny, A. Koren, D. Harlev, A.M. Bis, F. Auer, B. Keller, K. Warnatz, M. Gombert, S. Ginzel, A. Borkhardt, P. Stepensky, U. Fischer, STAT3 gain-of-function mutations associated with autoimmune lymphoproliferative syndrome like disease deregulate lymphocyte apoptosis and can be targeted by BH3 mimetic compounds, Clin Immunol 181 (2017) 32-42.
[157] A. Jerez, M.J. Clemente, H. Makishima, H. Rajala, I. Gómez-Seguí, T. Olson, K. McGraw, B. Przychodzen, A. Kulasekararaj, M. Afable, H.D. Husseinzadeh, N. Hosono, F. LeBlanc, S. Lagström, D. Zhang, P. Ellonen, A. Tichelli, C. Nissen, A.E. Lichtin, A. Wodnar-Filipowicz, G.J. Mufti, A.F. List, S. Mustjoki, T.P. Loughran, Jr., J.P. Maciejewski, STAT3 mutations indicate the presence of subclinical T-cell clones in a subset of aplastic anemia and myelodysplastic syndrome patients, Blood 122(14) (2013) 2453-2459.
[158] G.H. Fisher, F.J. Rosenberg, S.E. Straus, J.K. Dale, L.A. Middelton, A.Y. Lin, W. Strober, M.J. Lenardo, J.M. Puck, Dominant interfering fas gene mutations impair apoptosis in a human autoimmune lymphoproliferative syndrome, Cell 81(6) (1995) 935-946.
[159] T. Tanaka, T. Bai, H. Utsunomiya, T. Fukumoto, K. Yukawa, STAT3 enhances intracellular Fas-mediated apoptotic signals in HHUA human endometrial epithelial cells, Mol Med Rep 4(2) (2011) 307-12.
[160] S.E. Flanagan, E. Haapaniemi, M.A. Russell, R. Caswell, H.L. Allen, E. De Franco, T.J. McDonald, H. Rajala, A. Ramelius, J. Barton, K. Heiskanen, T. Heiskanen-Kosma, M. Kajosaari, N.P. Murphy, T. Milenkovic, M. Seppänen, Å. Lernmark, S. Mustjoki, T. Otonkoski, J. Kere, N.G. Morgan, S. Ellard, A.T. Hattersley, Activating germline mutations in STAT3 cause early-onset multi-organ autoimmune disease, Nature genetics 46(8) (2014) 812.
[161] E.M. Haapaniemi, M. Kaustio, H.L.M. Rajala, A.J. van Adrichem, L. Kainulainen, V. Glumoff, R. Doffinger, H. Kuusanmäki, T. Heiskanen-Kosma, L. Trotta, S. Chiang, P. Kulmala, S. Eldfors, R. Katainen, S. Siitonen, M.-L. Karjalainen-Lindsberg, P.E. Kovanen, T. Otonkoski, K. Porkka, K. Heiskanen, A. Hänninen, Y.T. Bryceson, R. Uusitalo-Seppälä, J. Saarela, M. Seppänen, S. Mustjoki, J. Kere, Autoimmunity, hypogammaglobulinemia, lymphoproliferation, and mycobacterial disease in patients with activating mutations in STAT3, Blood 125(4) (2015) 639-648.
[162] S. Davis, J. Schaller, R. Wedgwood, M.D. Harvard, JOB'S SYNDROME: Recurrent, " Cold ", Staphylococcal Abscesses, The Lancet 287(7445) (1966) 1013-1015.
[163] K.J. Sowerwine, S.M. Holland, A.F. Freeman, Hyper-IgE syndrome update, Annals of the New York Academy of Sciences 1250 (2012) 25-32.
[164] Y. Minegishi, M. Saito, S. Tsuchiya, I. Tsuge, H. Takada, T. Hara, N. Kawamura, T. Ariga, S. Pasic, O. Stojkovic, A. Metin, H. Karasuyama, Dominant-negative mutations in the DNA-binding domain of STAT3 cause hyper-IgE syndrome, Nature 448(7157) (2007) 1058-62.
[165] S.M. Holland, F.R. DeLeo, H.Z. Elloumi, A.P. Hsu, G. Uzel, N. Brodsky, A.F. Freeman, A. Demidowich, J. Davis, M.L. Turner, V.L. Anderson, D.N. Darnell, P.A. Welch, D.B. Kuhns, D.M. Frucht, H.L. Malech, J.I. Gallin, S.D. Kobayashi, A.R. Whitney, J.M. Voyich, J.M. Musser, C. Woellner, A.A. Schaffer, J.M. Puck, B. Grimbacher, STAT3 mutations in the hyper-IgE syndrome, The New England journal of medicine 357(16) (2007) 1608-19.

[166] J.-Z. Tang, X.-J. Kong, A. Banerjee, N. Muniraj, V. Pandey, M. Steiner, J.K. Perry, T. Zhu, D.-X. Liu, P.E. Lobie, STAT3α Is Oncogenic for Endometrial Carcinoma Cells and Mediates the Oncogenic Effects of Autocrine Human Growth Hormone, Endocrinology 151(9) (2010) 4133-4145.
[167] E. Caldenhoven, T.B. van Dijk, R. Solari, J. Armstrong, J.A. Raaijmakers, J.W. Lammers, L. Koenderman, R.P. de Groot, STAT3beta, a splice variant of transcription factor STAT3, is a dominant negative regulator of transcription, J Biol Chem 271(22) (1996) 13221-7.
[168] U. Bharadwaj, M.M. Kasembeli, T.K. Eckols, M. Kolosov, P. Lang, K. Christensen, D.P. Edwards, D.J. Tweardy, Monoclonal Antibodies Specific for STAT3β Reveal Its Contribution to Constitutive STAT3 Phosphorylation in Breast Cancer, Cancers 6(4) (2014) 2012-2034.
[169] H. Shao, A.J. Quintero, D.J. Tweardy, Identification and characterization of cis elements in the STAT3 gene regulating STAT3α and STAT3β messenger RNA splicing, Blood 98(13) (2001) 3853-3856.
[170] S. Biethahn, F. Alves, S. Wilde, W. Hiddemann, K. Spiekermann, Expression of granulocyte colony-stimulating factor– and granulocyte-macrophage colony-stimulating factor–associated signal transduction proteins of the JAK/STAT pathway in normal granulopoiesis and in blast cells of acute myelogenous leukemia, Experimental Hematology 27(5) (1999) 885-894.
[171] S. Dewilde, A. Vercelli, R. Chiarle, V. Poli, Of alphas and betas: distinct and overlapping functions of STAT3 isoforms, Frontiers in bioscience : a journal and virtual library 13 (2008) 6501-14.
[172] D.L. Hevehan, W.M. Miller, E.T. Papoutsakis, Differential expression and phosphorylation of distinct STAT3 proteins during granulocytic differentiation, Blood 99(5) (2002) 1627-1637.
[173] J.-Y. Yoo, D.L. Huso, D. Nathans, S. Desiderio, Specific Ablation of Stat3β Distorts the Pattern of Stat3-Responsive Gene Expression and Impairs Recovery from Endotoxic Shock, Cell 108(3) (2002) 331-344.
[174] P. Aigner, V. Just, D. Stoiber, STAT3 isoforms: Alternative fates in cancer?, Cytokine 118 (2019) 27-34.
[175] D. Maritano, M.L. Sugrue, S. Tininini, S. Dewilde, B. Strobl, X. Fu, V. Murray-Tait, R. Chiarle, V. Poli, The STAT3 isoforms alpha and beta have unique and specific functions, Nature immunology 5(4) (2004) 401-9.
[176] R. Catlett-Falcone, T.H. Landowski, M.M. Oshiro, J. Turkson, A. Levitzki, R. Savino, G. Ciliberto, L. Moscinski, J.L. Fernández-Luna, G. Nuñez, W.S. Dalton, R. Jove, Constitutive Activation of Stat3 Signaling Confers Resistance to Apoptosis in Human U266 Myeloma Cells, Immunity 10(1) (1999) 105-115.
[177] J. Lin, R. Buettner, Y.-C. Yuan, R. Yip, D. Horne, R. Jove, N. Vaidehi, Molecular dynamics simulations of the conformational changes in signal transducers and activators of transcription, Stat1 and Stat3, Journal of Molecular Graphics and Modelling 28(4) (2009) 347-356.
[178] I.H.W. Ng, M.A. Bogoyevitch, D.A. Jans, Cytokine-Induced Slowing of STAT3 Nuclear Import; Faster Basal Trafficking of the STAT3β Isoform, Traffic 15(9) (2014) 946-960.
[179] H.-F. Zhang, Y. Chen, C. Wu, Z.-Y. Wu, D.J. Tweardy, A. Alshareef, L.-D. Liao, Y.-J. Xue, J.-Y. Wu, B. Chen, X.-E. Xu, K. Gopal, N. Gupta, E.-M. Li, L.-Y. Xu, R. Lai, The Opposing Function of STAT3 as an Oncoprotein and Tumor Suppressor Is Dictated by the Expression Status of STAT3β in Esophageal Squamous Cell Carcinoma, 22(3) (2016) 691-703.
[180] A.S. Banerjee, A.D. Pal, S. Banerjee, Epstein–Barr virus-encoded small non-coding RNAs induce cancer cell chemoresistance and migration, Virology 443(2) (2013) 294-305.
[181] X. Zhang, K.-W. Min, J. Wimalasena, S.J. Baek, Cyclin D1 degradation and p21 induction contribute to growth inhibition of colorectal cancer cells induced by epigallocatechin-3-gallate, J Cancer Res Clin Oncol 138(12) (2012) 2051-2060.

[182] Z. Xia, S.N.J. Sait, M.R. Baer, M. Barcos, K.A. Donohue, D. Lawrence, L.A. Ford, A.M.W. Block, H. Baumann, M. Wetzler, Truncated STAT proteins are prevalent at relapse of acute myeloid leukemia, Leukemia Research 25(6) (2001) 473-482.
[183] F. Marino, V. Orecchia, G. Regis, M. Musteanu, B. Tassone, C. Jon, M. Forni, E. Calautti, R. Chiarle, R. Eferl, V. Poli, STAT3β controls inflammatory responses and early tumor onset in skin and colon experimental cancer models, Am J Cancer Res 4(5) (2014) 484-494.
[184] A. Chakraborty, D.J. Tweardyabc, Stat3 and G-CSF-Induced Myeloid Differentiation, Leukemia & Lymphoma 30(5-6) (1998) 433-442.
[185] O.A. Timofeeva, S. Chasovskikh, I. Lonskaya, N.I. Tarasova, L. Khavrutskii, S.G. Tarasov, X. Zhang, V.R. Korostyshevskiy, A. Cheema, L. Zhang, S. Dakshanamurthy, M.L. Brown, A. Dritschilo, Mechanisms of unphosphorylated STAT3 transcription factor binding to DNA, The Journal of biological chemistry 287(17) (2012) 14192-14200.
[186] H.L. Ramos, J.J. O'Shea, W.T. Watford, STAT5 isoforms: controversies and clarifications, The Biochemical journal 404(1) (2007) e1-e2.
[187] C.F. Zheng, G.J. Jones, M. Shi, J.C. Wiseman, K.J. Marr, B.M. Berenger, S.M. Huston, M.J. Gill, A.M. Krensky, P. Kubes, C.H. Mody, Late expression of granulysin by microbicidal CD4+ T cells requires PI3K- and STAT5-dependent expression of IL-2Rbeta that is defective in HIV-infected patients, J Immunol 180(11) (2008) 7221-9.
[188] M.S. Redell, M.J. Ruiz, T.A. Alonzo, R.B. Gerbing, D.J. Tweardy, Stat3 signaling in acute myeloid leukemia: ligand-dependent and -independent activation and induction of apoptosis by a novel small-molecule Stat3 inhibitor, Blood 117(21) (2011) 5701-5709.
[189] T. Hu, J.E. Yeh, L. Pinello, J. Jacob, S. Chakravarthy, G.-C. Yuan, R. Chopra, D.A. Frank, Impact of the N-Terminal Domain of STAT3 in STAT3-Dependent Transcriptional Activity, Mol Cell Biol 35(19) (2015) 3284-3300.
[190] T. Hu, J.E. Yeh, L. Pinello, J. Jacob, S. Chakravarthy, G.C. Yuan, R. Chopra, D.A. Frank, Impact of the N-Terminal Domain of STAT3 in STAT3-Dependent Transcriptional Activity, Mol Cell Biol 35(19) (2015) 3284-300.
[191] L. Lerner, M.A. Henriksen, X. Zhang, J.E. Darnell, Jr., STAT3-dependent enhanceosome assembly and disassembly: synergy with GR for full transcriptional increase of the alpha 2-macroglobulin gene, Genes Dev 17(20) (2003) 2564-77.
[192] J. Sgrignani, M. Garofalo, M. Matkovic, J. Merulla, C.V. Catapano, A. Cavalli, Structural Biology of STAT3 and Its Implications for Anticancer Therapies Development, Int J Mol Sci 19(6) (2018) 1591.
[193] V. Cimica, H.-C. Chen, J.K. Iyer, N.C. Reich, Dynamics of the STAT3 transcription factor: nuclear import dependent on Ran and importin-β1, PloS one 6(5) (2011) e20188-e20188.
[194] T. Domoszlai, A. Martincuks, D. Fahrenkamp, H. Schmitz-Van de Leur, A. Küster, G. Müller-Newen, Consequences of the disease-related L78R mutation for dimerization and activity of STAT3, 127(9) (2014) 1899-1910.
[195] A. Pranada, S. Metz, A. Herrmann, P. Heinrich, G. Müller-Newen, Real Time Analysis of STAT3 Nucleocytoplasmic Shuttling, The Journal of biological chemistry 279 (2004) 15114-23.
[196] O.A. Timofeeva, N.I. Tarasova, X. Zhang, S. Chasovskikh, A.K. Cheema, H. Wang, M.L. Brown, A. Dritschilo, STAT3 suppresses transcription of proapoptotic genes in cancer cells with the involvement of its N-terminal domain, Proc Natl Acad Sci U S A 110(4) (2013) 1267-1272.
[197] T. Zhang, W.H. Kee, K.T. Seow, W. Fung, X. Cao, The coiled-coil domain of Stat3 is essential for its SH2 domain-mediated receptor binding and subsequent activation induced by epidermal growth factor and interleukin-6, Mol Cell Biol 20(19) (2000) 7132-7139.

[198] N. Sato, R. Tsuruma, S. Imoto, Y. Sekine, R. Muromoto, K. Sugiyama, T. Matsuda, Nuclear retention of STAT3 through the coiled-coil domain regulates its activity, Biochemical and Biophysical Research Communications 336(2) (2005) 617-624.
[199] J. Ma, T. Zhang, V. Novotny-Diermayr, A.L.C. Tan, X. Cao, A Novel Sequence in the Coiled-coil Domain of Stat3 Essential for Its Nuclear Translocation, 278(31) (2003) 29252-29260.
[200] P. Filippakopoulos, S. Muller, S. Knapp, SH2 domains: modulators of nonreceptor tyrosine kinase activity, Curr Opin Struct Biol 19(6) (2009) 643-9.
[201] X. Zhang, P. Yue, S. Fletcher, W. Zhao, P.T. Gunning, J. Turkson, A novel small-molecule disrupts Stat3 SH2 domain-phosphotyrosine interactions and Stat3-dependent tumor processes, Biochemical pharmacology 79(10) (2010) 1398-1409.
[202] M.S. Wake, C.J. Watson, STAT3 the oncogene - still eluding therapy?, The FEBS journal 282(14) (2015) 2600-11.
[203] A. Tao, Y. Huang, Y. Shinohara, M.L. Caylor, S. Pashikanti, D. Xu, ezCADD: A Rapid 2D/3D Visualization-Enabled Web Modeling Environment for Democratizing Computer-Aided Drug Design, J Chem Inf Model 59(1) (2019) 18-24.
[204] S. Becker, B. Groner, C.W. Müller, Three-dimensional structure of the Stat3β homodimer bound to DNA, Nature 394(6689) (1998) 145-151.
[205] T. Decker, P. Kovarik, Transcription factor activity of STAT proteins: structural requirements and regulation by phosphorylation and interacting proteins, Cellular and Molecular Life Sciences CMLS 55(12) (1999) 1535-1546.
[206] Z. Yu, B.C. Kone, The STAT3 DNA-binding domain mediates interaction with NF-kappaB p65 and inducible nitric oxide synthase transrepression in mesangial cells, Journal of the American Society of Nephrology : JASN 15(3) (2004) 585-91.
[207] E. Nkansah, R. Shah, G.W. Collie, G.N. Parkinson, J. Palmer, K.M. Rahman, T.T. Bui, A.F. Drake, J. Husby, S. Neidle, G. Zinzalla, D.E. Thurston, A.F. Wilderspin, Observation of unphosphorylated STAT3 core protein binding to target dsDNA by PEMSA and X-ray crystallography, FEBS Lett 587(7) (2013) 833-9.
[208] N. Wei, J. Li, C. Fang, J. Chang, V. Xirou, N.K. Syrigos, B.J. Marks, E. Chu, J.C. Schmitz, Targeting colon cancer with the novel STAT3 inhibitor bruceantinol, Oncogene 38(10) (2019) 1676-1687.
[209] Y. Tsujita, A. Horiguchi, S. Tasaki, M. Isono, T. Asano, K. Ito, T. Asano, Y. Mayumi, T. Kushibiki, STAT3 inhibition by WP1066 suppresses the growth and invasiveness of bladder cancer cells, Oncol Rep 38(4) (2017) 2197-2204.
[210] T.J. Han, E.J. Choi, B.J. Cho, S.H. Song, S.H. Paik, I.A. Kim, ATPS-42: INHIBITION OF STAT3 ENHANCES THE RADIOSENSITIZING EFFECT OF TEMOZOLOMIDE IN MALIGNANT GLIOMA CELLS IN VITRO AND IN VIVO, Neuro Oncol 17(Suppl 5) (2015) v27-v27.
[211] Y. Pan, F. Zhou, R. Zhang, F.X. Claret, Stat3 inhibitor Stattic exhibits potent antitumor activity and induces chemo- and radio-sensitivity in nasopharyngeal carcinoma, PLoS One 8(1) (2013) e54565-e54565.
[212] M. Pang, L. Ma, R. Gong, E. Tolbert, H. Mao, M. Ponnusamy, Y.E. Chin, H. Yan, L.D. Dworkin, S. Zhuang, A novel STAT3 inhibitor, S3I-201, attenuates renal interstitial fibroblast activation and interstitial fibrosis in obstructive nephropathy, Kidney International 78(3) (2010) 257-268.
[213] Z. Wang, J.a. Li, W.a. Xiao, J. Long, H. Zhang, The STAT3 inhibitor S3I-201 suppresses fibrogenesis and angiogenesis in liver fibrosis, Laboratory Investigation 98(12) (2018) 1600-1613.
[214] R. Kong, G. Sun, X. Li, L. Wu, L. Li, Y. Li, F. Wang, P. Xuan, S. Yang, B. Sun, J. Hu, Small Molecule Inhibitor C188-9 Synergistically Enhances the Demethylated Activity of Low-Dose 5-Aza-2′-Deoxycytidine Against Pancreatic Cancer, Frontiers in Oncology 10(612) (2020).

[215] J.F. Longo, S.N. Brosius, L. Black, S.H. Worley, R.C. Wilson, K.A. Roth, S.L. Carroll, ErbB4 promotes malignant peripheral nerve sheath tumor pathogenesis via Ras-independent mechanisms, Cell Commun Signal 17(1) (2019) 74-74.
[216] S. Choi, H.J. Jung, M.W. Kim, J.H. Kang, D. Shin, Y.S. Jang, Y.S. Yoon, S.H. Oh, A novel STAT3 inhibitor, STX-0119, attenuates liver fibrosis by inactivating hepatic stellate cells in mice, Biochem Biophys Res Commun 513(1) (2019) 49-55.
[217] R. Zhang, X. Chen, S. Fu, L. Xu, J. Lin, A small molecule STAT3 inhibitor, LLL12, enhances cisplatin- and paclitaxel-mediated inhibition of cell growth and migration in human ovarian cancer cells, Oncol Rep 44(3) (2020) 1224-1232.
[218] Q.-y. Wu, Z. Cheng, Y.-z. Zhou, Y. Zhao, J.-m. Li, X.-m. Zhou, H.-l. Peng, G.-s. Zhang, X.-b. Liao, X.-m. Fu, A novel STAT3 inhibitor attenuates angiotensin II-induced abdominal aortic aneurysm progression in mice through modulating vascular inflammation and autophagy, Cell Death & Disease 11(2) (2020) 131.
[219] D.S. Shin, H.N. Kim, K.D. Shin, Y.J. Yoon, S.J. Kim, D.C. Han, B.M. Kwon, Cryptotanshinone inhibits constitutive signal transducer and activator of transcription 3 function through blocking the dimerization in DU145 prostate cancer cells, Cancer Res 69(1) (2009) 193-202.
[220] W. Zhang, W. Yu, G. Cai, J. Zhu, C. Zhang, S. Li, J. Guo, G. Yin, C. Chen, L. Kong, A new synthetic derivative of cryptotanshinone KYZ3 as STAT3 inhibitor for triple-negative breast cancer therapy, Cell Death & Disease 9(11) (2018) 1098.
[221] S.F. Ahmad, M.A. Ansari, A. Nadeem, K.M.A. Zoheir, S.A. Bakheet, A.M.S. Alsaad, O.A. Al-Shabanah, S.M. Attia, STA-21, a STAT-3 inhibitor, attenuates the development and progression of inflammation in collagen antibody-induced arthritis, Immunobiology 222(2) (2017) 206-217.
[222] S. You, R. Li, D. Park, M. Xie, G.L. Sica, Y. Cao, Z.Q. Xiao, X. Deng, Disruption of STAT3 by niclosamide reverses radioresistance of human lung cancer, Molecular cancer therapeutics 13(3) (2014) 606-16.
[223] W. Zhang, T. Ma, S. Li, Y. Yang, J. Guo, W. Yu, L. Kong, Antagonizing STAT3 activation with benzo[b]thiophene 1, 1-dioxide based small molecules, European Journal of Medicinal Chemistry 125 (2017) 538-550.
[224] M. Bar-Natan, E.A. Nelson, M. Xiang, D.A. Frank, STAT signaling in the pathogenesis and treatment of myeloid malignancies, JAKSTAT 1(2) (2012) 55-64.
[225] Y. Chen, M. Ji, S. Zhang, N. Xue, H. Xu, S. Lin, X. Chen, Bt354 as a new STAT3 signaling pathway inhibitor against triple negative breast cancer, Journal of drug targeting 26(10) (2018) 920-930.
[226] Y. He, Q. Fan, T. Cai, W. Huang, X. Xie, Y. Wen, Z. Shi, Molecular mechanisms of the action of Arctigenin in cancer, Biomedicine & pharmacotherapy = Biomedecine & pharmacotherapie 108 (2018) 403-407.
[227] Y.R. Liu, Q.Y. Cai, Y.G. Gao, X. Luan, Y.Y. Guan, Q. Lu, P. Sun, M. Zhao, C. Fang, Alantolactone, a sesquiterpene lactone, inhibits breast cancer growth by antiangiogenic activity via blocking VEGFR2 signaling, Phytotherapy research : PTR 32(4) (2018) 643-650.
[228] M. Ogura, T. Uchida, Y. Terui, F. Hayakawa, Y. Kobayashi, M. Taniwaki, Y. Takamatsu, T. Naoe, K. Tobinai, W. Munakata, T. Yamauchi, A. Kageyama, M. Yuasa, M. Motoyama, T. Tsunoda, K. Hatake, Phase I study of OPB-51602, an oral inhibitor of signal transducer and activator of transcription 3, in patients with relapsed/refractory hematological malignancies, Cancer Sci 106(7) (2015) 896-901.
[229] T.S. Bekaii-Saab, A. Starodub, B.F. El-Rayes, B.H. O'Neil, S. Shahda, K.K. Ciombor, A.M. Noonan, W.T. Hanna, A. Sehdev, W.L. Shaib, S. Mikhail, A.S. Neki, C. Oh, Y. Li, W. Li, L. Borodyansky, C. Li, A phase Ib/II study of cancer stemness inhibitor napabucasin (BBI-608) in combination with gemcitabine (gem) and nab-paclitaxel (nabPTX) in metastatic pancreatic adenocarcinoma (mPDAC) patients (pts), 35(15_suppl) (2017) 4106-4106.

[230] A. Tolcher, K. Flaherty, G.I. Shapiro, J. Berlin, T. Witzig, T. Habermann, A. Bullock, E. Rock, A. Elekes, C. Lin, D. Kostic, N. Ohi, D. Rasco, K.P. Papadopoulos, A. Patnaik, L. Smith, G.M. Cote, A First-in-Human Phase I Study of OPB-111077, a Small-Molecule STAT3 and Oxidative Phosphorylation Inhibitor, in Patients with Advanced Cancers, The oncologist 23(6) (2018) 658-e72.
[231] J. Bosch-Barrera, J.A. Menendez, Silibinin and STAT3: A natural way of targeting transcription factors for cancer therapy, Cancer treatment reviews 41(6) (2015) 540-6.
[232] D. Hong, R. Kurzrock, Y. Kim, R. Woessner, A. Younes, J. Nemunaitis, N. Fowler, T. Zhou, J. Schmidt, M. Jo, S.J. Lee, M. Yamashita, S.G. Hughes, L. Fayad, S. Piha-Paul, M.V. Nadella, M. Mohseni, D. Lawson, C. Reimer, D.C. Blakey, X. Xiao, J. Hsu, A. Revenko, B.P. Monia, A.R. MacLeod, AZD9150, a next-generation antisense oligonucleotide inhibitor of STAT3 with early evidence of clinical activity in lymphoma and lung cancer, Science translational medicine 7(314) (2015) 314ra185.
[233] G. Devkate, S. Hardikar, R. Patil, Protein Aggregation A Review, International Journal of Biochemistry Research & Review 14 (2016) 1-14.
[234] C. Frieden, Protein aggregation processes: In search of the mechanism, Protein Sci 16(11) (2007) 2334-2344.
[235] S.-M. Huang, H. Zhao, J.-I. Lee, K. Reynolds, L. Zhang, R. Temple, L.J. Lesko, Therapeutic Protein–Drug Interactions and Implications for Drug Development, 87(4) (2010) 497-503.
[236] A. Karshikoff, Non-Covalent Interactions in Proteins, 2006.
[237] V. Sluzky, A.M. Klibanov, R. Langer, Mechanism of insulin aggregation and stabilization in agitated aqueous solutions, Biotechnology and Bioengineering 40(8) (1992) 895-903.
[238] R.T. Darrington, B.D. Anderson, Evidence for a common intermediate in insulin deamidation and covalent dimer formation: effects of pH and aniline trapping in dilute acidic solutions, Journal of pharmaceutical sciences 84(3) (1995) 275-82.
[239] C.J. Roberts, Therapeutic protein aggregation: mechanisms, design, and control, Trends Biotechnol 32(7) (2014) 372-80.
[240] M.R. Dyson, Selection of soluble protein expression constructs: the experimental determination of protein domain boundaries, Biochemical Society transactions 38(4) (2010) 908-13.
[241] A. Schrodel, A. de Marco, Characterization of the aggregates formed during recombinant protein expression in bacteria, BMC Biochem 6 (2005) 10.
[242] G. Walsh, Biopharmaceuticals: recent approvals and likely directions, Trends in Biotechnology 23(11) (2005) 553-558.
[243] A.S. Rosenberg, Effects of protein aggregates: an immunologic perspective, AAPS J 8(3) (2006) E501-E507.
[244] W. Wang, Protein aggregation and its inhibition in biopharmaceutics, International Journal of Pharmaceutics 289(1) (2005) 1-30.
[245] Aggregation of Recombinant Proteins, Protein Aggregation in Bacteria, pp. 221-245.
[246] H.C. Mahler, W. Friess, U. Grauschopf, S. Kiese, Protein aggregation: pathways, induction factors and analysis, Journal of pharmaceutical sciences 98(9) (2009) 2909-34.
[247] M. Manno, E.F. Craparo, A. Podestà, D. Bulone, R. Carrotta, V. Martorana, G. Tiana, P.L. San Biagio, Kinetics of Different Processes in Human Insulin Amyloid Formation, Journal of molecular biology 366(1) (2007) 258-274.
[248] E. Nkansah, R. Shah, G.W. Collie, G.N. Parkinson, J. Palmer, K.M. Rahman, T.T. Bui, A.F. Drake, J. Husby, S. Neidle, G. Zinzalla, D.E. Thurston, A.F. Wilderspin, Observation of unphosphorylated STAT3 core protein binding to target dsDNA by PEMSA and X-ray crystallography, FEBS Letters 587(7) (2013) 833-839.

[249] E.O. Melo, A.M. Canavessi, M.M. Franco, R. Rumpf, Animal transgenesis: state of the art and applications, Journal of applied genetics 48(1) (2007) 47-61.
[250] G.L. Rosano, E.A. Ceccarelli, Recombinant protein expression in Escherichia coli: advances and challenges, Front Microbiol 5 (2014) 172-172.
[251] A.L. Demain, P. Vaishnav, Production of recombinant proteins by microbes and higher organisms, Biotechnology Advances 27(3) (2009) 297-306.
[252] E.R. LaVallie, E.A. DiBlasio, S. Kovacic, K.L. Grant, P.F. Schendel, J.M. McCoy, A Thioredoxin Gene Fusion Expression System That Circumvents Inclusion Body Formation in the E. coli Cytoplasm, Bio/Technology 11(2) (1993) 187-193.
[253] F.W. Studier, B.A. Moffatt, Use of bacteriophage T7 RNA polymerase to direct selective high-level expression of cloned genes, Journal of molecular biology 189(1) (1986) 113-30.
[254] Z. Ren, X. Mao, C. Mertens, R. Krishnaraj, J. Qin, P.K. Mandal, M.J. Romanowski, J.S. McMurray, X. Chen, Crystal structure of unphosphorylated STAT3 core fragment, Biochemical and Biophysical Research Communications 374(1) (2008) 1-5.
[255] G.L. Rosano, E.A. Ceccarelli, Recombinant protein expression in Escherichia coli: advances and challenges, Frontiers in Microbiology 5(172) (2014).
[256] L.M. Hellman, M.G. Fried, Electrophoretic mobility shift assay (EMSA) for detecting protein–nucleic acid interactions, Nature Protocols 2(8) (2007) 1849-1861.
[257] L. Blanc, M. Salomao, X. Guo, X. An, W. Gratzer, N. Mohandas, Control of erythrocyte membrane-skeletal cohesion by the spectrin-membrane linkage, Biochemistry 49(21) (2010) 4516-4523.
[258] L.M. Hellman, M.G. Fried, Electrophoretic mobility shift assay (EMSA) for detecting protein-nucleic acid interactions, Nat Protoc 2(8) (2007) 1849-1861.
[259] P. Tijssen, Laboratory Techniques in Biochemistry and Molecular Biology: Hybridization with Nucleic Acid Probes. Probe Labeling and Hybridization Techniques, Elsevier1993.
[260] G.M.M. Fried M.G., The Electrophoretic Mobility Shift Assay (EMSA) for Detection and Analysis of Protein-DNA Interactions. , in: T. D. (Ed.), Nucleic Acid Electrophoresis. , Springer Lab Manual, Springer, Berlin, Heidelberg, 1998.
[261] S.E. Bondos, A. Bicknell, Detection and prevention of protein aggregation before, during, and after purification, Anal Biochem 316(2) (2003) 223-31.
[262] P. F., Polarization of light of fluorescence, average life of molecules., J Phys Radium 7 (1926) 390-401.
[263] P.C. Shih, Y. Yang, G.N. Parkinson, A. Wilderspin, G. Wells, A high-throughput fluorescence polarization assay for discovering inhibitors targeting the DNA-binding domain of signal transducer and activator of transcription 3 (STAT3), Oncotarget 9(66) (2018) 32690-32701.

## Abbreviations

| | |
|---|---|
| ALPS | autoimmune lymphoproliferative syndrome |
| AML | acute myeloid leukaemia |
| Amp | ampicillin |
| bp | base pairs |
| BRD4 | bromodomain containing protein 4 |
| CASP10 | caspase-10 |
| CCD | Coil-coild domain |
| CDK4/6 | cyclin-dependent kinases 4/6 |

| | |
|---|---|
| CDKN2A | cyclin-dependent kinase inhibitor 2A |
| CFP | cyan fluorescent protein |
| Chl | chloramphenicol |
| COX-2 | cyclooxigenase-2 |
| CSF-1 | colony stimulating factor-1 |
| DBD | DNA binding domain |
| DC | dendritic cells |
| DNMT1 | DNA methyltransferase 1 |
| dsDNA | double stranded DNA |
| E.C. | extinction coefficient |
| E.coli | *Escherichia coli* |
| EC50 | half maximal effective concentration |
| EGF | epidermal growth factor |
| EGFR | epidermal growth factor receptor |
| ERK | Extracellular regulated protein kinase |
| EZH2 | Enhancer of Zeste Homolog 2 |
| FAS | Fas receptor |
| FASLG | Fas ligand |
| FOXP3 | forkhead box P3 |
| FP | fluorescent polarization |
| FRET | fluorescent resonance energy transfer |
| GMOs | Genetically modified microorganisms |
| HCC | hepatocellular carcinoma |
| HDAC | histone deacetylase |
| HIES | hyper-IgE syndrome |
| HIF1α | hypoxia-inducible factor 1α |
| HIF-1α | ypoxia-induced factor 1α |
| HSPs | heat shock proteins |
| Iex | Ion-exchange |
| IFN | interferon |
| IHCA | inflammatory hepatocellular adenoma |
| IL | interlukin |
| IPTG | Isopropyl β-D-1-thiogalactopyranoside |
| JAK | Janus Kinases |
| JNK | C-Jun N-terminal kinase |
| Ka | The association constant |
| LD | Linking domain |
| mAbs | monoclonal antibodies |
| MAPK | mitogen-activated protein kinases |
| MCS | multiple cloning site |
| MMPs | matrix metalloproteinase |
| MW | molecular weight |
| ND | N-terminal domain |
| NFκB | nuclear factor κB |
| NGAL | neutrophil gelatinase associated lipocalin |

| | |
|---|---|
| PCR | polymerase chain reaction |
| PDGFR | platelet-derived growth factor receptor |
| PEMSA | protein electrophoresis mobility shift assay |
| PIAS | protein inhibitor of activated STAT |
| PKC | protein-kinase C |
| PPI | protein-protein interactions |
| P-TEFb | positive transcriptional elongation factor |
| PTP | namely protein tyrosine phosphate |
| RBS | ribosome binding site |
| SDS-PAGE | SDS polyacrylamide gel electrophoresis |
| SET9 | SET domain containing methyl transferase 9 |
| SH2 | Src homologous 2 domain |
| SOCS | suppressor of cytokine signalling |
| ssDNA | Single stranded DNA |
| STAT | Signal transducer and activator of transcription |
| STAT3 DN | STAT3 dominant negative disease |
| STAT3 Gof | STAT3 gain of function diseases |
| SUMO | small ubiquitin-like modifier |
| TAD | Transactivation domain |
| Tet | tetracycline |
| TGF-β1 | transforming growth factor β1 |
| Th | helper T cells |
| Treg | regulatory T cells |
| Tyk2 | Tyrosine Kinase 2 |
| uSTAT3 | un-phosphorylated STAT3 |
| VEGFR | vesicular endothelial growth factor receptor |
| YFP | yellow fluorescent protein |